Element recovery from acidic waste streams

Inauguraldissertation

zur
Erlangung der Würde eines Doktors der Philosophie

vorgelegt der
Philosophisch-Naturwissenschaftlichen Fakultät
der Universität Basel

von

Sebastian Hedwig

2023

Genehmigt von der Philosophisch-Naturwissenschaftlichen Fakultät
auf Antrag von

Erstbetreuer: Prof. Dr. Edwin C. Constable und Dr. Markus Lenz

Zweitbetreuer: Prof. Dr. Moritz F. Lehmann

Externer Experte: Prof. Dr. Eric D. van Hullebusch

Basel, den 28.03.2023

Prof. Dr. Marcel Mayor
Dekan

'Es ist nicht genug, zu wissen, man muss auch anwenden.

Es ist nicht genug, zu wollen, man muss auch tun.'

— JOHANN WOLFGANG VON GOETHE

This page is intentionally left blank

Abstract

The world is facing a rising demand for resources, as a result of both the expanding human population and increasing affluence across the globe. Consequently, some nations have started to declare specific resources as critical due to their economic importance, while being at risk of supply shortage. One such critical raw material is scandium (Sc), a light-weight rare earth metal. Although not widely used yet, its unique physicochemical properties offer advantages for the transport and energy sectors that could lead to disruptive changes. For instance, Sc could foster large scale additive manufacturing of ultra-light car bodies for aircraft or other vehicles. Furthermore, it is crucial for commercial solid oxide fuel cells, which represent one of the best available technologies for hydrogen-based electricity supply. Unfortunately, the production of Sc is limited by the availability of concentrated ores. Hence, although an estimated 6 Mt of Sc could be available, the annual production is only about $\sim$20 t. Notably, Sc was found in comparably high concentrations in bulk industrial wastes, such as bauxite residues and white pigment acid waste from production of aluminium and titanium oxides respectively. Overall, this makes Sc a prime example for the development of novel hydrometallurgical strategies that allow for sustainable element recovery. Membrane processes are an attractive option for this purpose, as they can provide ion-selective separation that complements established procedures, while generally having a low material footprint. In this thesis, two advanced membrane procedures were selected to investigate their potential for Sc recovery in a real-world scenario. Therefore, based on European TiO_2 acid waste, acid resistant nanofiltration and liquid membrane extraction using polymer inclusion membranes were extensively researched. The conducted studies included the manufacturing and optimisation of tailor-made nanofiltration and polymer inclusion membranes, culminating in the development of a process cascade for Sc recovery, that was eventually piloted on cubic metre scale. The results presented here may contribute to the establishment of future Sc supply from secondary streams. However, they are also expected to have broader implications beyond Sc recovery, potentially extending to other critical raw materials. Thus, this work advances the role of membranes in hydrometallurgy and may ultimately facilitate strategies for a more sustainable supply of resources.

Table of Contents

Table of Contents

Acknowledgements

The work presented is a cocktail of fruits that could not have been harvested without the help of experienced and diligent gardeners, who ensured the plants would receive all the nutrients they needed to grow to their full potential. At this point I want to thank everyone, who accompanied me on this journey and enabled me to reach this goal.

First of all, I would like to thank Prof. Dr. Edwin. C. Constable for becoming my doctoral supervisor. The constellation allowing me to pursue my PhD at the University of Basel, while being able to work and research externally at the FHNW was only made possible by you. You were always open for the application-oriented research ideas that I brought with me and I received your support wherever I needed it, thank you!

Together with you, I would like to thank Prof. Dr. Catherine Housecroft for welcoming me so warmheartedly into the Constable/Housecroft research group. You both made clear from day one that this arrangement is not just on paper, but a full invitation to participate in research and work group activities, which I still appreciate very much.

I would like to thank Prof. Dr. Moritz F. Lehmann for being my second examiner. I enjoyed the discussions we had during the regular meetings and am looking forward to further input in the future.

I would like to thank Prof. Dr. Eric D. van Hullebusch for becoming the external expert of my committee without hesitation.

Last but not least, I would like to thank my *second first* supervisor, without whom my committee would not be complete: Dr. Markus Lenz. Sticking to the initial metaphor, it was Markus who found and ploughed the field and who eventually chose me as the farmer in charge of growing the plants. You became my mentor and I honestly couldn't have wished for a better one taking over this role. Regardless of the circumstances, you were always extremely supportive and understanding in scientific but also in personal matters. I want to thank you for the time and the patience you have invested into this PhD project and in me and I am looking forward to fruitful future collaborations with you!

A big shoutout to everyone who worked together with me in the presented projects. I would like to thank Dr. Kirsten Remmen and Roman Schäfer for introducing me to the field of nanofiltration and lbl-membranes and involving me in their research, leading to an article presented here. Further, I want to express my gratitude to Prof. Dr. Bengi Yagmurlu for the excellent collaboration in SCALE, on the two research articles presented in this work and also beyond. I am looking forward to future proposals and projects together. Additionally, I would like to thank Dr. Edward M. Peters for the collaboration in SCALE and your contribution of antisolvent crystallisation to the pilot research article that is presented here. I would also like to thank my fellow FHNW colleagues, Viktor Misev and Dirk Hengevoss for the collaboration in SCALE, the fantastic trips, and the additions on material

and energy flow analyses that is part of the pilot research article. I would like to thank some of the most diligent gardeners for whom I have been fortunate enough to supervise them during their internships or during their MSc theses: Meret Amrein, Danyu Huang, Manuel Kraus, Johannes Stiehm and Oliver von Arx. I appreciated the time as your advisor and am thankful for the effort you all have put into the projects. I would also like to express my gratitude to Meret and Dr. Felix Schmidt for allowing me to be a part of your research projects, which resulted in a fantastic publication. Furthermore, I want to thank Ying Liu, Dr. Mathieu Martinez, Dr. Anna Potysz, and Dr. Ildiko Fekete-Kertész for all the collaborations that were already published or will (hopefully) be published soon.

Next, I would like to thank all the staff at FHNW, who keep the infrastructure running and assist with technical support and craftmanship. A big shoutout to Pavel Dagorov, Georg Hasler and Theo Walser from the workshop, you are truly enablers of our research! I would also like to thank Irena Brzak, Nicolas Furler, Erik Ammann and Patrik Eckert for taking care of the labs. Another thanks goes to Theodor Bühler for always helping with all kinds of optical methods.

Furthermore, I want to thank the entire Institute for Ecopreneurship. Particularly, I want to thank Prof. Dr. Michael Thomann, for providing an excellent atmosphere in the group and giving me the flexibility to finish my papers and this thesis in parallel to working. I further want to thank Prof. Dr. Christoph Hugi for being an excellent and generous (interims) head of the institute. You are considerably contributing to a good working climate. Additionally, I want to thank my fellow corner office colleagues, Meret, Dr. Luca Loreggian, Dr. Manupriyam Dubey and Michael Pulfer. It's always fun with you guys! I would also like to express my thanks to Luca and Oli for their fantastic collaboration and steady support during the writing process.

I also want to thank some former colleagues, especially Dr. Robin Wünsch, Dr. Nadja Schillinger, Lara Da Costa and Ying Liu.

Eventually, I would like to express my gratitude to Riccardo Perri, my oldest fellow sufferer and good friend since the beginning of our PhD journey. While many people came and went, we walked this path together and I am sincerely grateful for his constant support and companionship.

Acknowledgements

Abbreviations

μ-XRF	Micro X-ray fluorescence (spectroscopy)		EI	Economic importance
arNF	Acid resistant nanofiltration		ENP	Extended Nernst-Planck equation
ASC	Antisolvent crystallisation		EU	European Union
ATR	Attenuated total reflectance		FC	Filter Cake from TiO_2 Production
ATR-FTIR	Attenuated total reflectance Fourier-transform infrared spectroscopy		FTIR	Fourier-transform infrared (spectroscopy)
BCE	Before the Common Era		HDPE	High-density polyethylene
BR	Bauxite Residue from the Bayer Process (also called red mud)		HSAB	Hard-Soft-Acid-Base
CAPEX	Capital expenditure		IBC	Intermediate bulk container
CE	Circular economy		ICP	Inductively coupled plasma
CL	Crosslinked/-ing		IEX	Ion exchange
CP	Concentration polarisation		IUPAC	International Union of Pure and Applied Chemistry
CRM	Critical raw material		lbl	Layer-by-layer
CTA	Cellulose triacetate		LCA	Life cycle analysis
Cyanex 272	Bis(2,4,4-trimethylpentyl)phosphinic acid		LOD	Limit of detection
Cyanex 923	Mixture of octyl-/hexylphosphine oxides		LOQ	Limit of quantification
DE	Dielectric exclusion		MF	Microfiltration
DEHPA/D2EHPA	Di-(2-ethylhexyl)phosphoric acid		MFA	Material flow analysis
DLaTGS	Deuterated L-alanine-doped TriGlycine Sulfate		MS	Mass spectrometry
DMPA	2,2-Dimethoxy-2-phenylacetophenone		MWCO	Molecular weight cut off
DOA	Dioctyl adipate		NF	Nanofiltration
DoE	Design of experiments		NORM	Naturally Occurring Radioactive Material
DOP	Dioctyl phthalate		NPOE	2-Nitrophenyl octyl ether
DSPM-DE	Donnan steric partitioning model with dielectric exclusion model		OECD	Organisation for Economic Co-operation and Development
EC	European Commission		OPEX	Operational expenditure

Abbreviations

P&I	Piping & instrumentation	S/L	Solid-liquid
PA	Phosphoric acid	SCALE	Production of Scandium Compounds and Scandium Aluminum Alloys from European Metallurgical By-Products, project acronym
PC-88A	2-Ethylhexyl hydrogen-2-ethylhexylphosphonate	SDEM	Solution diffusion electromigration model
PDADMAC	Poly(diallyldimethylammonium chloride)	SDG	Sustainable development goal
PE	Polyelectrolyte	SEM	Scanning electron microscopy
PEG-DMA	Polyethylene glycol dimethacrylate	SIR	Solvent Impregnated Resins
PES	Polyethersulfone	SOFC	Solid oxide fuel cell
PET	Polyethylene terephthalate	SR	Supply risk
PIM	Polymer inclusion membrane	SSZ	Scandia stabilised zirconia
PLS	Pregnant Leach Solution	SX	Solvent extraction
PP	Polypropylene	TBP	Tributyl phosphate
PSS	Poly(sodiumstyrenesulfonate)	TFC	Thin-film composite
PVC	Polyvinyl chloride	THF	Tetrahydrofuran
PVDF-HFP	Poly(vinylidene fluoride-co-hexafluoropropylene)	TMP	Transmembrane pressure
PWP	Pure water permeability	TOPO	Trioctylphosphine oxide
QQQ	Triple quadrupole	UF	Ultrafiltration
R&D	Research & development	UNEP	United Nations Environment Programme
REE	Rare Earth Elements	UN-IRP	United Nations International Resource Panel
RM	Raw material	WGI	Worldwide governance indicators
RO	Reverse osmosis	WW	Wastewater
RP	Receiving phase	XRD	Powder X-ray diffraction

1 Utilisation of natural resources

Since the dawn of mankind, natural resources have been used to make tools, clothing or shelter. The amount and type of materials processed increased with the development of human society. Epochs of human prehistory were titled after the primary tool-making materials (Stone Age, Bronze Age, Iron Age).[1] Innovation and technological development have allowed humanity to steadily increase its productivity and population. In the last two centuries, however, growth has accelerated dramatically: It took thousands of years to reach 1 billion people, but only from 1800-2022 to reach a population of ~8 billion (Figure 1.1). Alone in the last half century, the world population doubled and grew on average by ~1 billion per 12 years. Projections expect the growth rate to decline but a world population in the range of ~11 billion by 2100.[2]
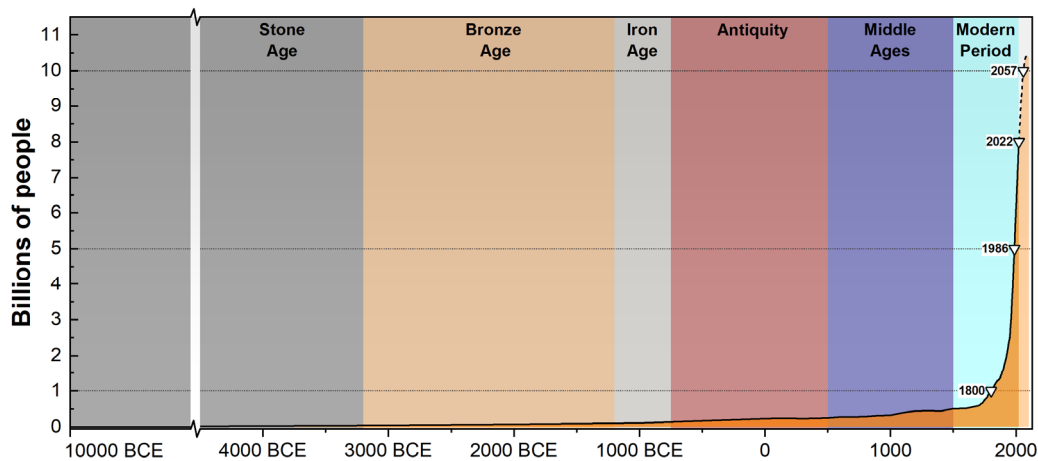
Figure 1.1 Global Population development from 10 000 BCE to 2100[2–4] and simplified indication of periods in human history[5]. Predictions until 2100 are based on medium-fertility scenario.[2]

The increasing number of people is challenging the capacities of Earth. Additionally, rising living standards are a key factor, driving the extraction of resources. Affluence is directly linked to environmental impact.[6,7] The wealthiest 10% were responsible for 50% of the global CO_2 emissions in 2019.[7] Still, prosperity is unequally distributed. In fact, high-income countries in North America and Europe are living at higher standards than the world for many decades.[8] However, the transitioning and developing countries, home to the majority of the global population, are on the rise. In this regard, an adoption of Western living standards holds enormous potential to accelerate material extraction and use.[8,9]

Today, exploitation of natural resources mobilises more material than the natural forces combined and alters the face of the planet.[10] In response to the unprecedented impact of humankind on the Earth, the transition to a new geological period, the *Anthropocene*, is officially being discussed.[11–16] Today's generations are witnesses of climate change, environmental pollution and substantial loss of biodiversity.[17–20] The United Nations International Resource Panel (UN-IRP) estimated that 90%

1

of biodiversity loss and water scarcity are associated with resource use.[21] Notably, many trends observed today were predicted already in 1972 by Meadows et al. in their seminal work 'The limits to growth'.[22–24] Ultimately, the report concluded that continued growth in population and resource consumption would result in a collapse of the global system in the 21st century.[22] Being updated in 2004, the simulation model still shows high agreement with empirical data.[24] Rockström et al. took the approach further and investigated on planetary boundaries for a safe operation range of humanity.[25] They proposed a total of nine different natural systems with estimated thresholds for control variables. In this regard, the chosen limits did not represent inflection points for a system collapse but were intended to provide a margin for safe operation. However, the further a boundary is exceeded, the higher the risk of dangerous environmental changes would be.[25] During a follow-up study in 2015, the research group found, that four systems boundaries were already drastically overstepped (P- and N-cycles, Biosphere integrity, Land-system change and climate change).[19]

In view of the already visible and possibly upcoming effects of human actions, urgent and profound measures are needed to prevent the collapse of the system. Within its agenda 2030, the UN declared 17 sustainable development goals (SDGs; Figure 1.1).[26]

Figure 1.2 Overview of the 17 sustainable development goals.[27]

While many of the SDGs indirectly addressed or included sustainable resource management, Goal 12, 'Responsible Consumption and Production' was especially devoted to the topic.[26,28] According to target 12.2, 'sustainable management and efficient use of natural resources' should be achieved by 2030.[26]

The agenda itself lacks a set limit for a sustainable consumption.[26] Nonetheless, the UN-IRP specified earlier, that a target of 6-8 t per capita per year should be reached by 2050 for resource sustainability.[29]

To achieve this goal, comprehensive understanding of the discrepancy between the envisaged and the actual situation is crucial.

1.1 Natural resource flows in the global economy

For visualisation of global material flows, the UN-IRP database was used, listing data from 1970 to 2019.[30] Global regions were classified according to Schandl et al. (Figure 1.3).[31] Materials were categorised in five groups: 1) fossil fuels, 2) metallic ores, 3) non-metallic ores, 4) biomass, 5) products. The first four groups were defined by UN-IRP. The term 'products' was introduced here to summarise all manufactured goods as well as 'mixed' and 'complex' products listed in the UN-IRP database.[30]
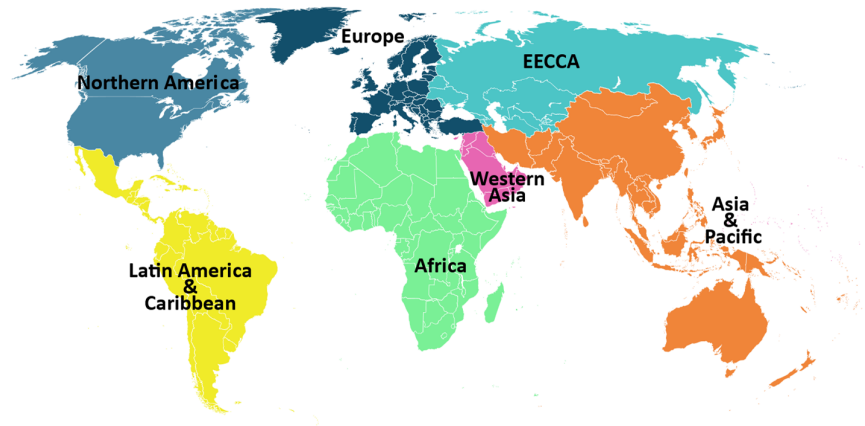
Figure 1.3 Regional classification according to Schandl et al..[31]

In 2019, a total of ~96 Gt of materials was extracted from Earth, meaning a triplication of total annual extraction since 1970 (+210%; Figure 1.4). Most materials were extracted in Asia & Pacific (53%), followed with some distance by the other regions (Figure 1.4A). Within the available period, Asia-Pacific outperformed the rest of the world in terms of growth: while in 1970 the region extracted only 14% more than the number two (North America), in 2019 extraction in Asia & Pacific was 465% higher than in the second-placed region (Latin America & the Caribbean). China had overall the highest share to extraction in the Asia-Pacific region (~60% of total).[32] The extraction curve for Asia-Pacific started to flatten slightly since 2014. This can be explained through China's domestic extraction contracting (on average -0.5% year^{-1} from 2014-2019).

In regard of material groups extracted, the majority was made up by non-metallic minerals, followed by biomass, fossil fuels and metal ores (Figure 1.4B). Non-metallic materials, used mainly in construction, were mined 4.7 times more in 2019 than in 1970.

A **B**
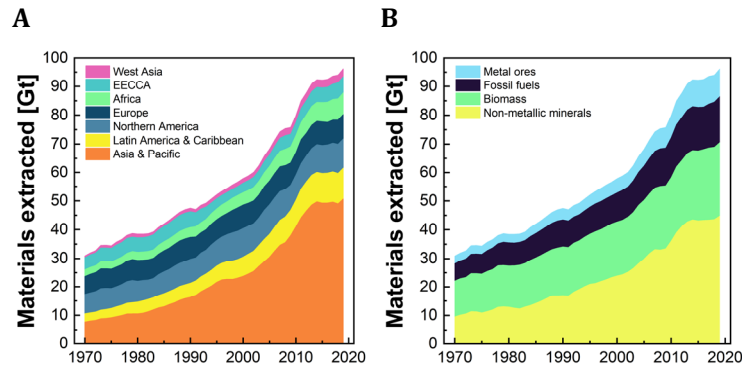
Figure 1.4 Stacked diagrams for globally extracted materials by region of origin (A) and by material group (B).

On global average 12 t per capita of materials were extracted in 2019, being > 40% higher than in 1970 (8.4 t per capita). In this regard, major factors were investments in infrastructure and rising living standards, especially in developing and transitioning countries.[21,33]

In 2019, the reported globally traded raw materials (i.e. w/o 'products') represented ~10% of the total extracted (Figure 1.5). Relatively seen, this share was similar to 1970 (7%). Considering also 'products', the absolute amount of traded goods reached 16 Gt in 2019, being six times higher than in the 1970s (Figure 1.5). However, it should be noted that the reported values underestimate the real material input. Schandl. et al. described that in 2010 the material demand of goods traded was about 2.5 times higher than the actual quantity reported.[31] Thus, in 2017 about 50% of all raw materials extracted were indirectly or directly associated with global trading.[34]

Recently, Asia & Pacific had the highest share by region for both imported and exported materials, followed by Europe (Figure 1.5A and C). At least since 1970, both regions were net importers, with rising tendency.[33] Especially, in Asia & Pacific imports rose substantially.[33] All, other regions were net exporting. Since 2015, 'products' have been the most important traded material group (Figure 1.5B and D). Previously, for > 40 years (except 2005 and 2007), fossil fuels were the most traded commodity globally (Figure 1.5B and D).
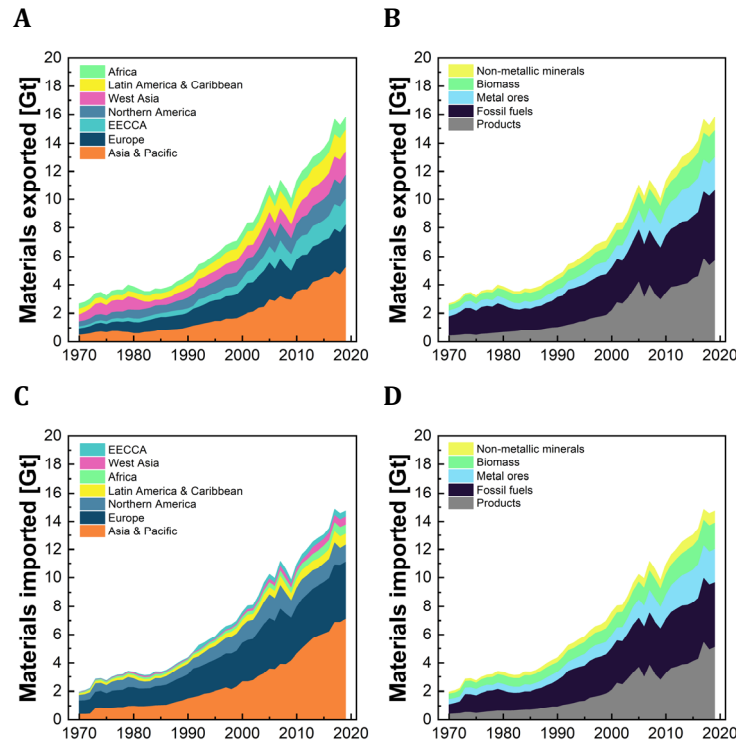
Figure 1.5 Stacked diagrams for global material exports by region (A) and group (B) and global imports by region (C) and group (D).

Based on the UN-IRP year 2050 target, an extraction of 54-73 Gt would be sustainable for a projected world population of 9.1 billion people.[29] Other sources assume an even lower sustainability threshold of 25-50 Gt per year.[35] Thus, the current data of the UN-IRP provides a worrying picture. Although the extraction pace has slowed marginally in recent years, the current per capita extraction of 12 t a^{-1} is well above the goal for 2050. While 1970's values were only merely higher than the UN-IRP's conception, in the last five decades material extraction increased about 50% faster than the global population. Projections by the United Nations Environment Programme (UNEP) assume a material extraction of about 140 Gt in 2050.[36] However, this estimate is low compared to other studies, anticipating 180 Gt (Schandl et al.) or 218 Gt (Krausmann et al.) in 2050.[9,31] In case of the latter, the UN-IRP sustainability target would be exceeded three to four times.

Given the link between affluence and wasteful spending, highly industrialised countries are particularly required to develop strategies to reduce their consumption.[6,8] Hickel et al. reported that the USA, UK and the EU-27 alone accounted for more than half of the material consumption overshoot since 1970.[8] This is not due to a drastic increase in material demand, but due to cumulated overconsumption over decades.[8]

1.1.1   EU-27 resource use

Material extraction in the EU-27 states was relatively constant from 1970-2019 with 5.6 ± 0.3 Gt a^{-1} (Figure 1.6A). Mostly non-metallic minerals and biomass were extracted. Fossil fuels and metal ores were mined considerably less (Figure 1.6A). While biomass, non-metallic and metal ores were ex-

tracted slightly more in 2019 than in 1970 (+24%, +21% and +4%), fossil fuels were mined considerably less (-42%). Consumption of materials has been always slightly higher than extraction, with an average of 6.2 ± 0.5 Gt a^{-1} between 1970-2019 (Figure 1.6B).

A

B

C

D
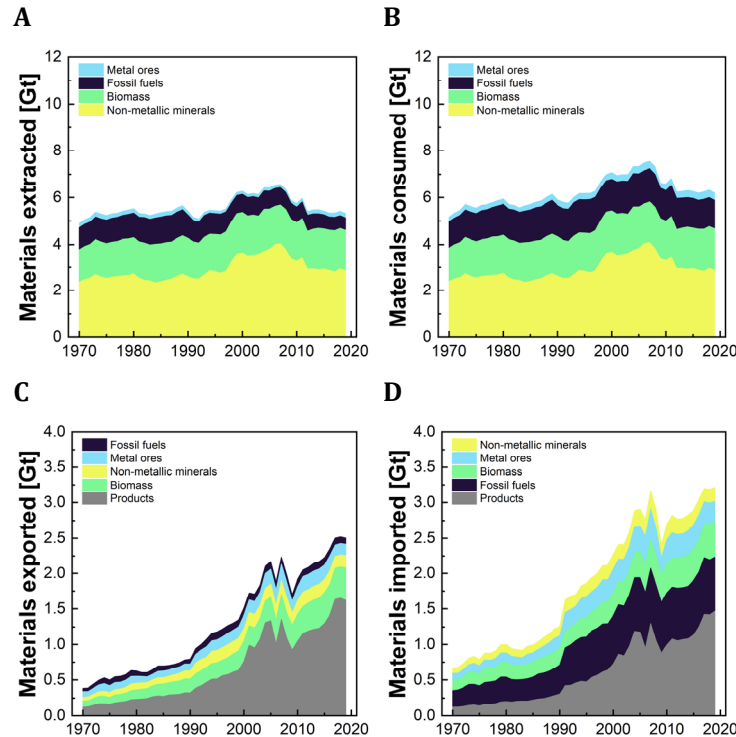
Figure 1.6 Stacked diagrams for materials extracted (A), consumed (B), exported (C) and imported (D) in the EU-27 states, categorised by type of material.

From 1970 to 2019, export of materials showed a steep increase, especially for products (+1200%), biomass (+420%) and non-metallic ores (+250%) (Figure 1.6C). Metal ore exports doubled (+100%). Relatively to the other, fossil fuel exports increased only merely (+45%).

From 1970-2019 considerably more goods were imported (products: +1100%, fossil fuels: +230%, biomass: +260%, metal ores: +190%, non-metallic ores: +150%; Figure 1.6D). In 2019, the EU-27 showed a high trade deficit for fossil fuels (-679 Mt) and metal ores (-117 Mt). Between 1970 and 2019, the import dependency increased considerably (trade deficit growth: +610% for metal ores, +260% for fossil fuels).

Both commodity groups are finite. In difference to renewable resources, these materials are not replenished in the course of a (human) lifetime. Hence, to comply with the demand, finite resources have to be mined. However, without sufficient mineable reserves (primary or secondary), resource-poor countries are dependent on imports or have to search for alternatives. Thus, these countries are tied to the market and to compliant trading partners. This dependency inherently poses risks such as supply chain disruptions, economic damage and political fallout.

Compared to its other business sectors, the mining and quarrying sector in the EU-27 is small and contributed only 0.3% of the total gross value added in 2019.[37] Many European mines closed due

to low ore grades.[38] This explains to some extend the high import dependency of the EU-27 (Figure 1.6).

1.2   Critical raw materials

From a strategic perspective, the raw material groups differ considerably. The sustainable use of finite resources is especially intricate and requires proper management in order to prevent supply chain disruptions and accessibility for future generations. The EU created a methodology for the assessment of raw materials being especially vital for its own economy but are at risk of supply.[39] Such commodities are called critical raw materials (CRMs).
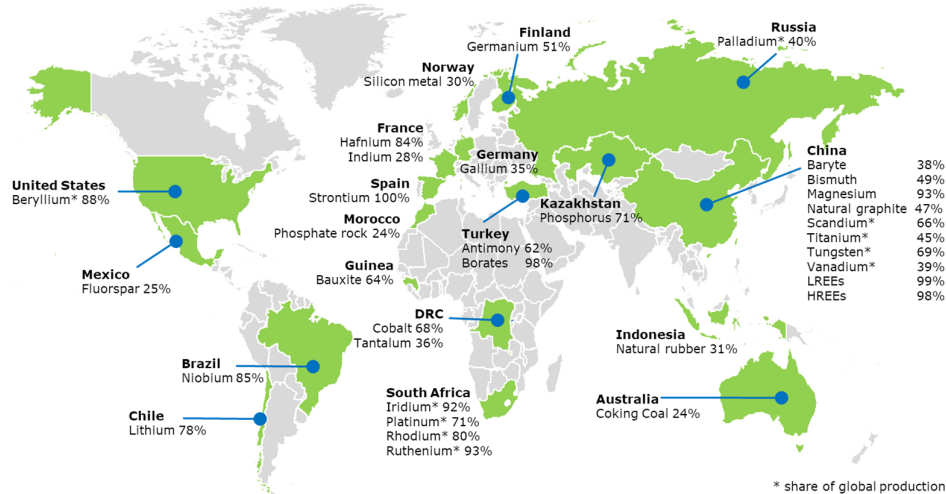
Figure 1.7 Major supplier countries of critical raw materials to the EU in 2020. Image from European Commission (2020).[40]

The EU-27 sources several commodities to high extend from single countries (Figure 1.7).[40,41] For instance, China alone provided the most of at least ten different economically important raw materials, resp. groups of raw materials.[40] Some of these (Mg, light and heavy rare earth elements) to even more than 90%.[41] This monopoly situation leaves supply chains in the recipient economy particularly vulnerable to disruption.

In 2008, the EU launched their raw material initiative.[42] Since then, every three years, a dedicated commission reviews raw materials (RMs) and ranks their criticality based on economic importance (EI) and supply risk (SR). In this regard, different factors and indicators are considered to calculate the EI and the SR of each commodity (Figure 1.8). The calculation of the EI of an RM is based on the economic value added of the respective economic sector (NACE[1]) and the RM's contribution to it. Furthermore, the substitutability of the RM is evaluated and considered.

_____

[1] NACE (French: *nomenclature statistique des activités économiques dans la Communauté européenne*) is the 'Statistical Classification of Economic Activities in the European Community'.[43].

For calculating SR a more complex routine was developed. Firstly, the substitutability of the RM is taken into account. Secondly, recycling options and rates for the RM are evaluated. Lastly, the global market and the EU demand are reviewed. This market assessment comprises different aspects, such as a screening for (production) bottlenecks, the worldwide governance indicators[2] (WGI), the import reliance, trade restrictions, and supply and sourcing concentrations based on the HERFINDAHL-HIRSCHMAN Indices[3].[39] Ultimately, EI and SR are normalised (scale: 0-10). For CRM classification, an SR of ≥ 1.0 and an EI of ≥ 2.8 were defined as critical thresholds, i.e. any commodity exceeding both thresholds simultaneously is considered a CRM.[39]
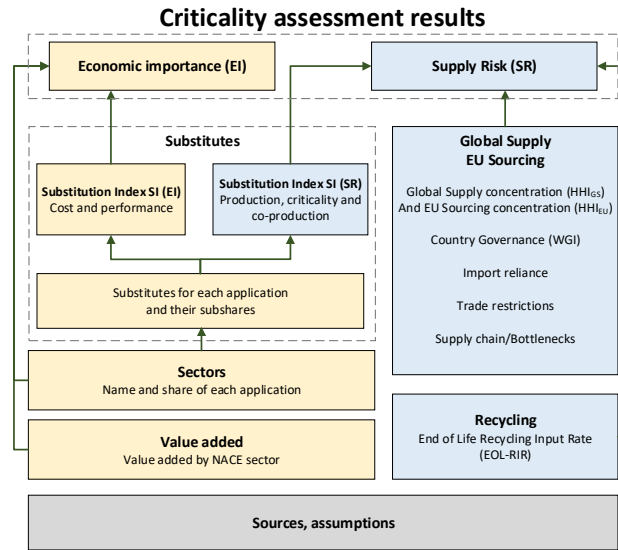
Figure 1.8 Structure of the critical raw material assessment. Adapted from Blengini et al. (2020).[40]

Based on the described review procedure, the EU commission declared 30 of 66 raw materials, resp. raw material groups as critical (Figure 1.9).[40,41] The highest EI value was determined for tungsten (EI = 8.1).

The highest supply risk was calculated for light rare earth elements (LREE; SR = 6.0), followed by heavy rare earth elements (HREE; SR = 5.6). In the EU assessment, LREE and HREE comprised all group III metals and lanthanides, except scandium (Sc).[41] Listed separately, Sc was considered a CRM since 2017, scoring a SR of 3.1 and an EI of 4.4 in 2020.[41]

---

[2] The Worldwide Governance Indicator expresses a country's governance based on six criteria: Voice and Accountability, Political Stability and Violence, Government Effectiveness, Rule of Law, Regulatory Quality, and Control of Corruption[44].

[3] The HERFINDAHL-HIRSCHMAN Index is an expression for market concentration on companies within industrial sectors[45].
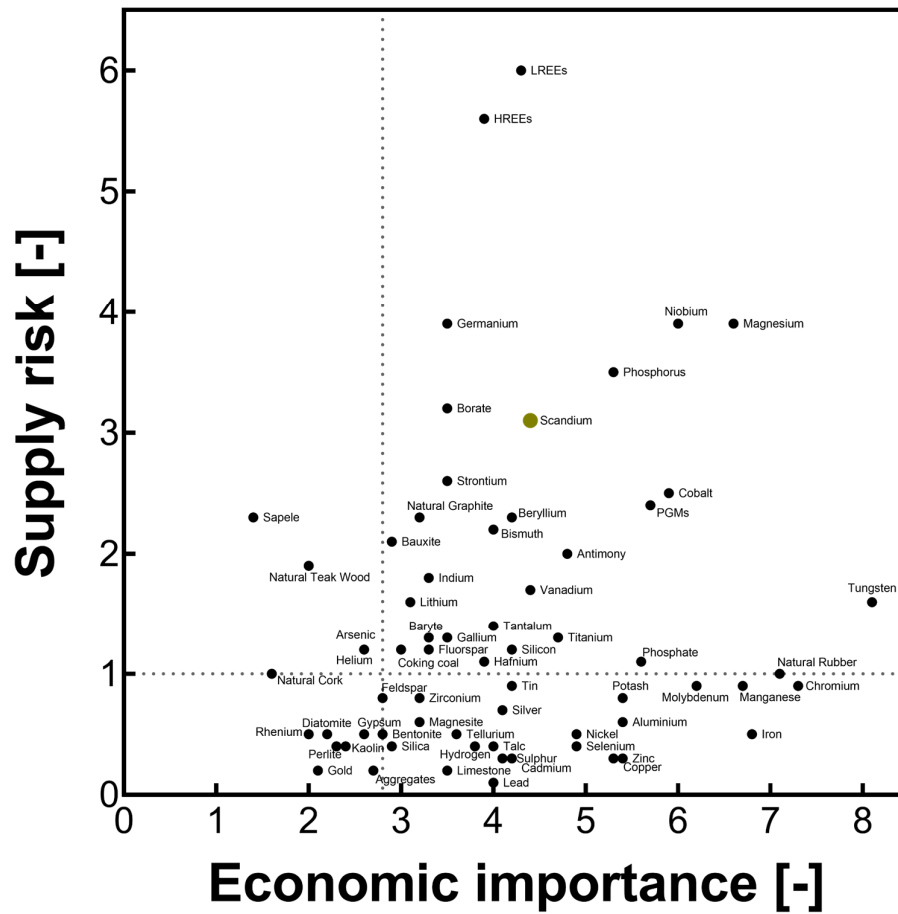
Figure 1.9 Supply risk and economic importance of raw materials reviewed by EU commission in 2020. The hashed lines indicate the thresholds for SR and EI. Scandium was highlighted in red. Adapted from Blengini et al. (2020).[41]

Following the example of the EU's assessment further nations have launched CRM programs, such as the USA, Japan and China.[46–48] The recognition of raw material criticality by leading industrial nations may result in a race for resources in the future.[49] In light of the transition to carbon neutrality, demand for CRMs, such as Co, Li and REEs will further increase.[50,51] Consequently, mining will become even more important in the upcoming decades.[51,52]

1.3 Strategies for sustainable resource use

Population growth, changing living standards and management of critical raw materials will drive future material extraction.[53] Notably, The current material consumption already exceeds UN sustainability limits.

A major concern is the link between economic growth and natural resource use. Hence, economic activities are often entailed by environmental impacts. Nonetheless, growth was declared a probate measure to achieve social development goals.[26] Hence, the UNEP fosters the concept of *decoupling*, aiming to separate economic growth from unsustainable resource use and environmental degrada-

tion.[36] This envisages minimising resource input per product output (resource efficiency) and maximising value generation per resource input (resource productivity).

According to the UN, the World Bank and the OECD, decoupling is a prerequisite for *green growth*, i.e. the combination of economic development with environmental sustainability.[26,54,55] In this regard the importance of so-called *eco-innovation* is emphasised.[36,56] While innovation refers to the implementation and commercialisation of a new knowledge (invention), eco-innovation focuses in particular on technologies and concepts having a direct or indirect benefit for the environment. Moreover, this approach is not limited to the technosphere, but also encompasses marketing strategies, organisational structures, and institutional arrangements.[56,57] Generally, investments into environmental protection are not seen as a cost, but as an opportunity for economic expansion.[58] Some successful examples for decoupling and green growth include the promotion of renewable energies, waste recycling strategies or plant-based alternatives to animal-derived food.[57,59–62] The allure of green growth, lies in the promise of not jeopardising the prosperity of industrialised countries, while developing countries could achieve the same level of well-being.

On the contrary, the concept of enabling (green) growth through decoupling is also perceived as insufficient and misleading, whereas economic expansion and sustainability are considered as incompatible.[63,64] Given the prevailing exploitation of natural capital and the associated emissions, rapid realisation of absolute decoupling would be required, i.e. additional growth is achieved while environmental impact stagnates or decreases.[63–66] However, if at all, regionally a relative decoupling can be observed, i.e. faster economic growth than increasing environmental impact.[63–65] Moreover, in view of the globalised economy local positive effects mostly diminish, as regional decoupling builds often onto external environmental damage.[23,64,67] Realistically, economic activities can be optimised but not absolutely decoupled from physical resource use.[23] Based on the measurable impact of previous decoupling and green growth efforts, avoiding economic expansion, i.e. *degrowth*, was argued to be the more plausible option for achieving the sustainability goals.[63,65,68] Nonetheless, so far the UN does not consider degrowth as a strategy to reach their SDGs.[58] The opposition of scientific plausibility and political action is argued to be based on a political impossibility of renouncing growth in favour of environmental protection.[58,63]

Aside of green growth and degrowth the so-called *circular economy* (CE) is discussed as a sustainable alternative to the linear 'take-make-dispose' economy. The CE aims to maximise resource efficiency by closing material cycles through avoidance of wastes ('reduce-recycle-reuse').[58] Thus, by-products could be used as starting materials for downstream processes, reducing the need for pristine raw materials. In addition, circular product design aims to preserve value, i.e. design concepts should pursue primarily longevity, secondly reusability (in whole or in part) and ultimately recyclability of the base materials. Additionally to technological solutions, business models supporting waste avoidance were conceptualised. For instance the so-called 'Product Service Systems' ap-

proach. In brief, customers pay for the functionality and not for the product. The companies retain ownership and take responsibility for maintenance and end-of-life management.[69]

However, although 'zero-waste' is the standard in nature, realising CE within the anthroposphere will require drastic changes in socio-economic behaviour.[70] The current economic system widely thrives on consumerism.[70] Consumption is central to the society, and the production of waste is the accepted normality. Companies strive to design saleable, short-lived products that ensure maximum profit margins and long-term sales opportunities.[70] Moreover, creating habitual patterns of consumption and suppressing a sense of sufficiency became a common marketing practice. Apparently, typical business models and practices of a linear economy oppose CE concepts (Table 1.1) and would need to be eradicated in the transition to a CE.

Table 1.1 Characteristics of a linear and a circular economy. Based on ING Economics Department (2015) and FinanCE (2016).[71,72]

	Linear economy	Circular economy
Attitude towards nature	Coercing nature for maximum output	Optimising output based on given natural production
Attitude towards production	Take, make, dispose	Reduce, recycle, reuse
Material life cycle	Single lifetime use of products, components, materials and energy	Materials and energy are infinitely cycled in economy
Product end of life	Products become obsolete while still usable	Product life extension, direct by repurposing or indirect by providing inputs for other products
Consumer approach	Ownership economy: consumers buy products	Performance economy: consumers invest in access and performance rather than ownership and increasingly share products
Earnings model	Producers charge for product sale	Producers charge for product use
Values and principles	Monetary interest determines business models	Business models are based on multiple values (financial, environmental and social values)
Supply chain	Companies improve efficiencies in isolation of each other	Companies work together to increase value along the supply chain. Risk and benefits are shared upstream and downstream

The concept and goals of CE are constantly discussed and developed. Hence, also different use case scenarios were derived. For instance, the EU fosters the adoption of a CE for reconciling sustainability with economic growth.[73] Others argue CE concepts should emphasise sufficiency and serve a sustainability-oriented 'post-growth economy'.[74] However, despite a general recognition of the ecological potential, CE adoption fell well behind the increase in resource consumption. Thus, the 'circularity' of the global economy reportedly declined from 9.1% in 2018 to currently 7.2%.[75] In order to accelerate CE, the EU has presented a circular economy action plan in 2020.[73]

In summary, the concepts of green growth, degrowth and circular economy, promise to improve the sustainability of economic activities. In regard of their demand to change the current economic system, their progressivity could be ordered as degrowth > CE > green growth. To manage resources more sustainably, degrowth avoids finding an eco-economical trade-off and targets the reduction of

the economy. The CE approach focusses on maximum resource efficiency through recirculation concepts for products and materials as the solution to the end-of-life question for waste. Lastly, the green growth strategy aims to decouple growth from environmental impact through innovation. Nonetheless, as pre-conditions are multidimensional and non-uniform in global comparison, a single solution appears unlikely. The feasibility of any strategy depends on social, political, technological and ecological aspects. The corresponding tension field can be seen within the 17 SDGs. With respect to the currently chased policies, technologies facilitating higher resource efficiency and productivity, i.e. bearing eco-innovation potential, are urgently sought for.

1.4 Scandium – a metal for eco-innovation?

1.4.1 Properties and uses

Sc is a light transition metal named after Scandinavia, where it was first isolated in the 19th century.[76,77] The IUPAC considers Sc a REE, accounting for its occurrence in ores together with Y and the lanthanides.[78] Nonetheless, the chemistry of Sc deviates from other REEs. As the first d-block element, its ionic radius is much smaller than of all other REEs (0.75 Å in sixfold coordination).[76,79] Sc occurs naturally only in the oxidation state +3. Thus, Sc^{3+} is a relatively hard LEWIS acid, wherefore it finds use as catalyst in organic chemistry.[79]

Metallic Sc is the most effective reinforcement additive to aluminium alloys.[80] Minute amounts of Sc (e.g. ~0.2% w/w) improve strength, fatigue behaviour, corrosion resistance and weldability of high-performance aluminium alloys typically used for aircraft construction.[80–82] In this regard, Airbus developed a 3D printable alloy (Scalmalloy®).[81] Overall, by means of additive manufacturing and sophisticated redesigning, Sc may allow for production of 15-20% lighter aircraft.[83,84] The first plane comprising AlSc alloys was the Russian MIG-29, produced in the 1980's. However, this application is not limited to aircraft construction, but could well extend to the entire transport sector. Obviously, a substantial weight reduction of vehicles, could render mobility more resource efficient, saving on fuel and GHG emissions. Moreover, light-weight construction is highly desirable for e-mobility, compensating for battery weight and extending the range.

Ultimately, since ScAl alloys enable the production of filigree structures without sacrificing strength, other branches could benefit, such as the heat exchanger industry.[85–87] In case of adoption, a Sc demand of approx. 100 t for aircraft and of 3000 t for automotive industries was projected for 2032.[88]

Aside of Sc metal, its oxide (Sc_2O_3) is a vital component of commercial solid oxide fuel cells (SOFCs).[89,90] SOFCs enable efficient electric energy generation from the reaction of a fuel (e.g. H_2) with O_2.[91] Thereby, Sc_2O_3 enhances the O^{2-} conductivity of the solid electrolyte, allowing for operation below 1000 °C.[90,92,93] The biggest supplier of commercial SOFCs (Bloom energy®), uses scandia stabilised zirconia (SSZ) in their products.[86,94] Bloom energy has designed a modular fuel cell

system, that can reach conversion efficiencies > 50% relatively to the fuel energy (lower heating value). Theoretically, SOFCs could even reach up to 70% efficiency.[95] Aside of fuel cells, Bloom energy's current portfolio includes hydrogen generators, either by water electrolysis or by steam reforming natural gas or biogas.[96] According to Bloom energy® their technological solutions are in alignment with six SDGs (6: clean water and sanitation, 7: affordable and clean energy, 9: industry, innovation and infrastructure, 11: sustainable cities and communities, 12: responsible consumption and production, and 13: climate action).[97]

Certainly, fuel cells pose a complementary addition to conventional renewable energy technologies such as photovoltaics, wind and hydro power. SOFCs offer outstanding efficiencies, being virtually decoupled from scale.[95] Aside of hydrogen, different fuels can be used, such as (small) hydrocarbons, hydrazine or ammonia.[95] When used with carbonaceous fuel, CO_2 emissions per kWh are generally lower than for combustion systems (e.g. ~40% lower than for systems fuelled with gas).[95] Overall, plants are relatively compact. For instance, Bloom energy's system in the size of a shipping container (30 ft) could generate an output of 400 - 600 kW.[98] Principally, units can be operated almost everywhere, while being silent with rel. low maintenance.[95] Therefore, also mobile SOFCs exist.[95] Ultimately, commercial systems excel in reliability, hence they have already found a niche market in the data centre operator sector.[99]

On the downside, SOFCs still require considerable investment cost.[99] Secondly, the high operating temperatures lead to relatively long start-up times and faster degradation of components.[99,100] Furthermore, without the availability of green hydrogen, the environmental benefits of SOFCs are limited, as upstream GHG emissions remain.

So far, Sc applications are not very numerous. Nonetheless, owing to its complementary physico-chemical properties, Sc already has substantial improvement potential for the transport and energy sectors.[101] Utilisation of Sc could directly boost resource efficiency and considerably cut GHG emissions. Notably, lighter vehicle bodies are also of great interest for the transition to e-mobility.[101]

However, despite the beneficial aspects of Sc application, only a few companies in the market have dared to realise Sc-containing products. The major concern is the insufficient Sc supply, being the bottleneck for potential actors.

1.4.2   Sources and supply

Contrary to the name *rare* earth metal, Sc is relatively widespread on Earth, with an average concentration of 22 ppm. Sc is the 32nd most common element in the Earth's crust and more abundant than e.g. lead or lithium.[102] Currently only ~20 t a^{-1} of Sc are produced globally.[103] For comparison, rhenium, one of the rarest elements on Earth (0.7 ppb in Earth's crust), has an annual production volume of ~60 t.[102,104]

Sc minerals containing high concentrations of Sc, such as thortveitite ($Sc_2Si_2O_7$), pretulite ($ScPO_4$) or kolbeckite ($ScPO_4 \cdot 2H_2O$), are rare. This phenomenon is explained by a low affinity of Sc for com-

mon ore forming anions (O^{2-}, S^{2-}, CO_3^{2-}).[105] Consequently, Sc is found widely dispersed in the lithosphere, accompanying some hundreds of minerals.[105] Hence, virtually all Sc originates from by-production. The primary product is scandium oxide (Sc_2O_3). Sc metal is not directly obtained from Sc_2O_3 but from ScF_3 as after metallothermic reduction with elemental calcium. High purity Sc metal is obtained from sublimation (e.g. 1350 °C, ~10^{-12} bar).[76] Scandium is not traded on official markets and quoted prices for Sc metal and compounds show a wide range but are generally very high (e.g. in 2021: ~2200 USD kg^{-1} of Sc_2O_3).[103]

So far, knowledge about Sc as an economic resource is still limited. For instance, there is no global Sc resource inventory, wherefore also information on reserves is missing.[103,106] However, based on the available data, Wang et al. estimated the cumulative Sc resources at over 6 Mt.[107]

While this quantity suggests a promising supply future for Sc, the rarity of concentrated Sc deposits remains a constraint, wherefore any source with Sc concentrations > 20 mg kg^{-1} can be designated as an ore.[108,109] Currently, the major source for Sc is the Bayan Obo mine in China, being the largest known REE deposit on Earth.[110] Here, Sc is mostly hosted by aegirine ($NaFe^{3+}[Si_2O_6]$), containing approx. 210 mg kg^{-1}.[111] The total Sc resource of the Bayan Obo deposit has been estimated at 140 kt.[111]

Another potential primary source for Sc are laterites, emerging from the intense weathering of ultramafic and mafic rocks. Laterites found in Australia and Brazil may contain Sc concentrated > 400 mg kg^{-1}.[109] According to Geoscience Australia, although currently not mined, more than 26 kt of Sc resources are economically accessible.[106] Several projects in Queensland, New South Wales and Western Australia have targeted Sc-rich laterites and may substantially contribute to future Sc supply.[106] For instance in Owendale a deposit containing a total of ~13 kt of Sc at ~400 mg kg^{-1} has been identified.[109] In Nyngan up to 4 kt of Sc at concentrations > 200 mg kg^{-1} could be mined in the future.[109]

Moreover, numerous projects targeting primary production of Sc were announced worldwide. A few of these are the Crater Lake Project in Canada[112], the Makuutu Project in Uganda[113] and the Kiviniemi Project in Finland[114].

While the interest in Sc extraction is certainly positive with regard to its application and the attributed ecological benefits, the need for a Sc primary production can be questioned. Sc is an accompanying element of many raw materials processed in the mineral industry, including bauxites[115] (alumina/aluminium), ilmenites & rutiles[111] (titania/titanium) and phosphate rocks[116] (phosphorous). Therefore, Sc may be present highly enriched in secondary streams (wastes), emerging from established processes, extracting the primary components. Consequently, waste may feature comparable concentrations to identified primary sources, with no additional mining costs and the ability to eliminate disposal expenditures. This approach would also be in line with the SDGs, respectively sustainable resource use strategies (section 1.3). Thus, as long as the Sc de-

mand could be covered by by-production, this option should be preferred over potential primary production.

So far, various waste materials have been reviewed for their Sc content.[117] Bauxite residues (also called red mud) might be the most frequently studied alternative Sc resource.[117] The caustic material arises as the side product of the BAYER-process during alumina production. The process exploits the solubility of hydroxo aluminate complexes, allowing to leach Al from bauxites under high pressure, temperature and alkaline pH. After S/L separation and crystallisation pure Al_2O_3 can be obtained. For decades, about two tonnes of red mud have been landfilled for every tonne of aluminium produced. Thus, over 120 Mt of red mud are added every year. Globally, more than 4 Gt of red mud is already being deposited.[118,119] In terms of Sc, Gentzmann et al. found concentrations of 50-100 mg kg^{-1} in bauxite residues from various European processors.[115] Thus, Botelho Junior et al. assumed 200 kt of Sc being accumulated in red mud.[117] Furthermore, regarding the annual red mud production, more than 6 kt of Sc could be additionally salvaged every year. Currently, Sc makes up approx. 95% of the economic value in red mud.[120] In conclusion, Sc extraction from red mud alone has the potential to ensure the long-term supply of Sc.

Aside from bauxite residues, white pigment (TiO_2) industry generates considerable quantities of waste containing Sc. In fact, TiO_2 represents the main titanium product and is valued for its superior refractive index and tinting strength over alternative pigments.[121] Therefore, white pigment has a wide range of application, being added to most paints, in plastics, textiles, paper, cosmetics, pharmaceuticals and food.[121] According to USGS, the production capacity for white pigment had reached about 9.4 Mt in 2022.[122]

Two main processes for TiO_2 production exist: the sulfate route and the chloride route. Both processes aim to extract and purify TiO_2 from its major ores (ilmenite and rutile). For this purpose, within the older sulfate route ilmenite ($FeTiO_3$) is dissolved in concentrated H_2SO_4 (98%) under formation of titanyl sulfate and iron sulfate. After partial hydrolysation, crude TiO_2 precipitates and can be separated via filtration from the Fe-rich sulfuric acid. Eventually, the crude pigment is refined (calcinated, coated etc.) to yield a saleable white pigment.[123] Per tonne of TiO_2 an estimated ~6-8 t of sulfuric acid waste (20%) is generated.[124] The waste acid can contain dissolved Sc in the range of 15-20 mg L^{-1}.[125] In 2017, approx. 3.7 Mt of TiO_2 was produced via the sulfate route.[126] Therefore, an estimated 300 – 500 t Sc per year could be available from wastes of the sulfate route.

Within the chloride route, pure TiO_2 is produced via $TiCl_4$ as an intermediate. Principally, TiO_2-rich starting materials (natural and synthetic rutile or Fe-depleted ilmenite) are mixed with elemental chlorine in the presence of coke (as a reducing agent) in a fluidized bed reactor at 900 – 1000 °C. Metal chlorides are formed, whereby the volatile $TiCl_4$ evaporates from the reactor and is separated in purified liquid form after cooling. Afterwards, $TiCl_4$ is converted at high temperatures with elemental O_2 to yield pure TiO_2 and Cl_2, which can be recycled into the ore digestion step.[123] Unreacted ore, overblown coke and chlorides of accompanying impurity elements end up in an acidic waste

slurry. This stream is usually neutralised, filtered and disposed of (i.e. the aqueous phase is sent to the treatment plant and the solid phase to a landfill). Gentzmann reported for the wastes of a European TiO_2 manufacturer > 100 mg L^{-1} of Sc in the (pre-neutralised) liquid phase and > 250 mg kg^{-1} of Sc in the filter cake.[109] Other sources reported less Sc, reaching ~130 mg kg^{-1} in the filter cake.[125] The chloride route is considered advantageous in terms of product quality, waste generation and energy consumption over the sulfate route. However, the starting materials need more control and should have high initial TiO_2 concentrations (90-95%) to avoid chlorine losses during the process.[123] Depending on the used raw materials a range of 0.2-1.4 t waste chlorides per tonne TiO_2 was reported.[124] In 2017, a total of 3.3 Mt of TiO_2 was produced via the chloride route.[126] Thus, an estimated 100-1000 t of Sc per year could be available from wastes of the chloride route.

Overall, several opportunities exist to ensure consistent and scalable future Sc supply. As briefly demonstrated on the examples of alumina and titania production, sufficient quantities to meet current and projected Sc demand could be obtained from secondary streams. However, regardless of primary or secondary production, effective strategies capable of handling traces of Sc in complex and challenging media are urgently sought.

1.5 State of the art Sc extraction

Sc can be found in various sources, but its low concentrations of 10^{-1}-10^{-2} g kg^{-1} render recovery processes challenging and expensive. Nevertheless, increasingly effective processes are being developed allowing for the isolation of even minute traces of the metal. Essentially, all of these processes belong to the field of hydrometallurgy.[127]

Notably, one of the earliest reported scandium production is linked to one of the first examples of modern hydrometallurgy, the extraction of uranium.[128] In the 1960's, uranium was produced by leaching of respective ores with H_2SO_4 and subsequent solvent extraction (SX) with 0.1 M dodecyl phosphoric acid in kerosene. During stripping with HCl uranium was recovered, but some metals such as Sc, Ti and Th remained in the organic phase. For removal of the aforementioned elements, hydrofluoric acid was needed. The precipitated Sc-Ti-Th fluoride was purified in an eight-stage cascade of dissolution and precipitation, yielding 99.5% pure Sc_2O_3.[128] The process described by Lash & Ross was published more than 60 years ago, but the combination of leaching, SX, stripping and downstream purification still represents the blueprint for hydrometallurgical recovery of many metals, such as REEs incl. Sc.[117,125] Nonetheless, Sc extraction during uranium production was done unintentionally. The enrichment of Sc had a negative impact on the main process by poisoning the organic extractant. During regeneration of the extraction agent, the Sc-concentrate emerged as a waste product. Hence, waste valorisation by monetisation of Sc_2O_3 was a logical step. However, it is doubtful that the recovery of Sc would have been sought without its concentration in the organic phase. Most likely, the Sc (co-)extraction was also not optimised in terms of yield and material effi-

ciency. In this respect, modern approaches that directly target Sc recovery differ, striving to optimise every stage of the recovery process.[125]

The first step in virtually all processes starting from solid raw materials, is the dissolution of Sc (leaching). Parameters for process adjustment include the choice of lixiviant, pulp concentration, particle size, temperature, and agitation.[129] Importantly, these have to be determined on a case-by-case basis, as the Sc binding phases depend on the starting material, entailing different reactivities. As a more concrete example, the exploration of Sc leaching conditions from red mud are discussed in the following. In this regard, some of the major challenges were relatively low Sc yields, high alkalinity, high iron concentrations and the formation of silica gels.[117,120,130–132] According to Gentzmann et al., Sc is hosted on different mineral phases in bauxite residues.[132] Among these easily and hardly leachable fractions were identified, explaining the occurrence of Sc yield plateaus during operation.[109,132] Sc distribution in these phases depends on the bauxite residue, i.e. its origin and processing conditions. In the hardly leachable phases 50-80% of the total Sc was found, being mainly associated with Fe.[132] Therefore, high Sc leaching yields are likely bound to intensive leaching conditions (e.g. high temperatures, pressure, acid concentrations). Inevitably, this also entails the dissolution of iron, causing problems in downstream stages. Nonetheless, co-leaching of Fe, was found to be partially supressed using alternative lixiviants, such as nitric acid.[131]

Aside of the constrained Sc yield, the high alkalinity increases the acid consumption during red mud leaching. Hence, attempts have been made to separate residual NaOH or lower the alkalinity by addition of CO_2, prior to the addition of lixiviant.[117] In regard of the problematic formation of silica gel, the use of H_2O_2 was demonstrated to act suppressing, presumably by promoting quartz generation.[117,133]

While several strategies for the challenges of bauxite leaching were developed, many might be neither economically nor ecologically viable, generating problematic wastes themselves (e.g. when using HNO_3) or consuming excessive amounts of resources.[117,131] Hence, successful Sc leaching should represent the best trade-off between effort and outcome. This means, even low Sc yields could be attractive, if guaranteeing easier processing and downstream operation. Currently, pilot plants for Sc leaching from bauxite residues are operated in Greece and Russia, while further may come in the future.[109,127]

Aside of red mud, few studies also dealt with leaching of Sc from solid chloride wastes of white pigment production.[134,135] However, as a major advantage for Sc recovery, the element is already dissolved during TiO_2 production, wherefore leaching can also be entirely omitted. Thus, by-production of Sc has already been realised in some white pigment production plants.[103]

Once dissolved, Sc has to be separated from surrounding impurities. This means to remove ~99.99% of matrix, while preserving the ~0.01% (100 ppm) of desired compound. The prevailing industrial process for this purpose is SX, although alternatives using ionic liquids, ion exchange resins (IEX) or solvent impregnated resins (SIR) have also been reported.[117,125,136–138] The basic

principle of these approaches is to selectively enrich scandium using extractants in a non-miscible secondary phase, which is typically a hydrophobic organic solvent in the case of SX, or a polymer substrate in the case of SIR. This allows the majority of the surrounding matrix to be removed by phase separation. The remaining residues can be washed off, and co-extracted impurities can be scrubbed.[139,140] Ultimately, the targeted Sc can be stripped from the secondary phase, yielding a purified concentrate.[125] One of the major advantages of SX and related methods is that the organic phase, including the extractants, can be regenerated and recycled, which helps to keep emissions and costs low.

In the past, a variety of extraction agents, such as carboxylic acids, amines, and ionic liquids, have been tested for Sc SX.[136,141] However, the most commonly used reagents are organophosphorus compounds (Figure 1.10).[125,141–143] Structurally, many extractants have an amphiphilic character, as they comprise relatively polar or ionic moieties and long apolar aliphatic chains. This allows for the coordination of dissolved metals while creating a hydrophobic shell around them. Consequently, the metal transfer into the secondary phase is promoted. Notably, only charge-neutral complexes can enter the hydrophobic secondary phase. Therefore, metal speciation should be considered in the choice of extractant to allow extraction of metal cations, metalate anions or metal salts.[140] Furthermore, it is important to also account for extractant speciation under the projected using conditions. For instance, SX at low pH might impair dissociation of the weaker acidic extractants (e.g. phosphinic acids like Cyanex 272), directly affecting their extraction ability. Neutral extractants (e.g. TOPO) on the other hand can be protonated under highly acidic conditions, allowing the formation of ion assemblies that promote the extraction of metalate anions.[140]

Base structure	X	R^1	R^2	R^3	Commercial name
$R^1-\overset{\overset{X}{\|}}{\underset{\underset{R^2}{\|}}{P}}-R^3$	O				TBP
					TOPO (Main component of Cyanex 923)
				OH	DEHPA
					PC-88A
					Cyanex 272
	S			SH	Cyanex 302
					Cyanex 301

Figure 1.10 Structural comparison of commonly used organophosphorus extraction agents.[141,144]

18

Organophosphorus extractants have gained special attention for their ability to improve metal selectivity by fine-tuning their binding properties. For instance, their ligand 'hardness' can be adjusted by sulfurization/desulfurization. Thio-analogous organophosphorus extractants may be advantageous for recovering softer metals, while their oxygenated equivalents might be more suitable for harder metals. By tailoring an extractant's properties to the targeted metal species, extraction efficiency and selectivity can be improved.[140]

In terms of Sc recovery, the origin (e.g. from TiO_2 sulfate or chloride route) can have a considerable influence on Sc speciation, hence extraction behaviour.[141,143,145] Often Sc can be extracted in cationic form from acidic media with strong cation exchanging extractants, such as DEHPA or PC-88A.[125,141] However, it was also reported that anionic Sc species can be extracted from sulfuric and malonic acid media, using amine extractants.[141] Furthermore, $ScCl_3$ could be extracted from chloride-rich media using solvating neutral extractants similar to TBP - although TBP itself showed inferior selectivity compared to alternatives.[141] Some of the reportedly most efficient extractants for Sc from TiO_2 wastes so far were synergistic mixtures of cation exchangers, such as DEHPA, with primary amines or neutral extractants, such as TBP.[146–148] Under the right conditions, SX can separate Sc from challenging impurities such as Fe^{III}, Ti^{IV}, Zr^{IV} and other REEs. However, as Sc is typically present at much lower concentrations than many impurities, even minute co-extraction of major elements can lead to underwhelming purities in the organic phase. Hence, either some of the most concerning impurities have to be removed *a priori*, e.g. by precipitation or need to be scrubbed from the loaded organic phase before Sc stripping. Fortunately, when strong cation exchangers are used in SX, Sc is typically well bound to the organic phase, allowing to strip impurities while preserving most of the Sc. Thus, HCl (> 3M), H_2SO_4 or even H_2O_2 /H_2SO_4 are commonly reported scrubbing agents.[125,127,141,148] On the downside, the strong affinity of organophosphorus extractants for Sc impedes its stripping. Default stripping agents are strong bases (e.g. NaOH, KOH) and fluorides (e.g. HF, NH_4F).[125,149] Their use, however, might directly cause precipitation of Sc salts, entailing phase separation problems and the co-precipitation of residual impurities from the organic. In that regard, the use of NH_4F was reported beneficial, keeping Sc dissolved as $(NH_4)_3ScF_6$. The complex can be crystallised for higher product purities by means of the antisolvent crystallisation method.[150]

1.5.1 Membrane processes for Sc recovery

Aside of classical hydrometallurgical approaches, membranes for element recovery have gained increasing interest in recent years.[151–153] Membranes may offer complementary separation abilities, rendering them as useful addition to the portfolio of existing extraction methods. The possibilities for membranes are versatile, such as the different modes they are typically operated in, comprising advanced filtration techniques, (electro-)dialysis and liquid membrane extraction, amongst others.[151,154] For instance Zimmermann et al. used nanofiltration (NF) for the recovery of indium

from wasted photovoltaic cells.[155] Moreover, NF was reported for the separation of REE from secondary streams in the past.[156] On the other hand, different kind of liquid membranes were demonstrated to enable REE extraction from various media.[157,158] In view of their promising future application[159], the membrane technologies of nanofiltration and the so-called polymer inclusion membranes (PIMs) are presented in more detail in the following.

1.5.1.1 Nanofiltration

The term nanofiltration was proposed by P. Eriksson in the 1980's for filtration with membranes that retained solutes in the nanometre range, lying between porous ultrafiltration (UF) and non-porous reverse osmosis (RO) membranes.[160] The definition of NF by the International Union of Pure and Applied Chemistry (IUPAC) is *a pressure-driven membrane-based separation process in which particles and dissolved molecules smaller than about 2 nm are rejected*.[161] Typical molecular weight cut-offs (MWCOs) reported in literature are between 200 – 1000 Da corresponding to pore diameters of 0.5 – 2 nm.[162]

NF membranes are typically constructed asymmetrically, i.e. a very thin active layer (~10-200 nm) is placed on top of much thicker highly porous support structures (~200 μm; Figure 1.11). These fabricates are also called thin-film composite (TFC) membranes.[163]

Active layer, ~0.01-0.2 μm
(e.g. polyamide)

Microporous support, ~50 μm
(e.g. polysulfone)

Carrier material, ~100-150 μm
(e.g. non-woven PET)
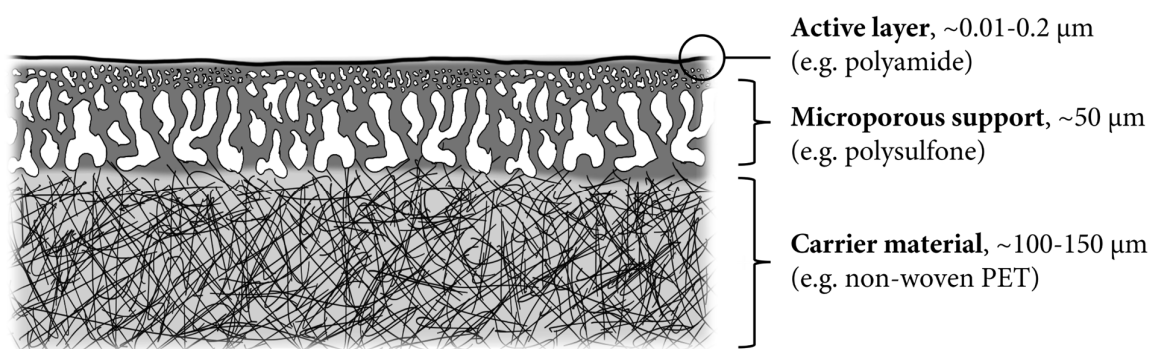
Figure 1.11 Scheme of a thin-film composite membrane. Illusatration based on Bhaskar et al. (2022) and Shimura (2022).[163,164]

Normally, TFC-NF membranes are produced in a stepwise process. Firstly, the microporous support layer is coated onto a carrier material (e.g. non-woven PET) via the phase inversion method. For this purpose, a polymer is dissolved in a suitable solvent and applied to the carrier. Afterwards, the polymer is precipitated by immersion in an antisolvent, through solvent evaporation or by cooling (thermal induction). Secondly, the thin active layer is prepared by interfacial polymerisation directly on top of the microporous support. For instance, commonly found polyamides layers can be crafted by soaking the support material in an aqueous solution of a polyamine monomer (e.g. piperazine) and subsequently covering it with a hydrophobic poly-acyl chloride solution

(e.g. trimesoyl chloride in hexane). Thus, the amide building blocks can polymerise, forming the thin active layer of the NF membrane.[165]

While this represents the standard production procedure for various commercially available membranes, novel membrane manufacturing strategies are being developed. One successful example is the assembly of alternatingly charged polyelectrolytes in a layer-by-layer (lbl) fashion on suitable substrates (mainly UF-membranes). This procedure allows relatively easy adjustment and tailoring of the active layer and its properties. Lbl-membranes comprise outstanding water permeabilities, while showing high metal retentions, behaving in that regard like NF membranes. Moreover, in difference to standard TFC membranes some lbl-specimen were demonstrated to offer backwashability. Due to their high separation potential at low pressures, lbl-membranes are promising candidates for future NF applications, such as in the field of element recovery.

From mechanistical point of view, the fundamental principle of any filtration is the use of a barrier, such as a membrane, to impede the movement of certain components within a fluid stream and selectively separate them from the rest of the stream. This retention (R_M) of a component (M) can be calculated based on its concentrations in permeate and feed ($c_{M,permeate}$, $c_{M,feed}$):

$$R_M = 1 - \frac{c_{M,permeate}}{c_{M,feed}} \tag{1.1}$$

Compared to filtration with classical porous membranes (such as UF) NF membrane permeability is more complex and not solely determined by sieving/steric effects. On the other hand, NF membranes are also not completely dense as many RO membranes. Therefore, different approaches for modelling transport (and thus retentions) in NF exist, some of which treat NF membranes as porous (e.g. DONNAN steric partitioning model) and others as dense (e.g. solution diffusion model).[166]

Typically solute transport in NF is described by the extended NERNST-PLANCK equation (ENP; equation 1.2). In its most common form, the ENP explains the flow of solutes as a combination of diffusion, convection and electromigration (Figure 1.12A).[167,168] Consequently, three major driving forces are considered: 1) concentration gradient across the membrane (diffusion), 2) solvent flux (convection), 3) electric potential gradient across the membrane (electromigration). For completely dense membranes, convection will tend towards zero. Similarly, for uncharged solutes, the electromigration term is zero.

$$J_i = -D_{i,p} \frac{dc_i}{dx} + K_{i,c}c_i J_s - z_i c_i D_{i,p} \frac{d\phi}{dx} \frac{F}{RT}$$

(1.2)

where:

J_i = flux of an ion, i

$D_{i,p}$ = pore diffusion coefficient $\qquad$ z_i = charge of ion, i

c_i = concentration of an ion, i $\qquad$ R = ideal gas constant

$K_{i,c}$ = convective hindrance factor $\qquad$ T = temperature

J_s = solvent permeate flux $\qquad$ F = FARADAY constant

$\frac{dc_i}{dx}$ = concentration gradient across the membrane profile $\qquad$ $\frac{d\phi}{dx}$ = electric potential gradient across the membrane profile

The ENP has been used for multiple NF modelling approaches.[168] One of the most prominent NF models is the so-called DONNAN steric partitioning model with dielectric exclusion (DSPM-DE).[168] As described by Wang et al., the DSPM-DE is based on the following assumptions[168]:

1) For transport, only the thin active layer is considered, i.e. the support structures are disregarded.

2) The active layer is a porous structure with uniform parallel cylindrical pores.

3) The transport is modelled only one-dimensional, i.e. no back diffusion or concentration gradients tangentially to the membrane are considered.

4) Solutes are modelled as spheres, whereas their size is based on the STOKES-radius.

5) Solute-solute interactions are neglected, i.e. low solute concentrations are assumed.

6) Dielectric exclusion is based on the BORN model.

7) The volumetric charge density is assumed uniform in the membrane.

8) Electro-neutrality has to be maintained.

9) The NF process is in steady state.

The water flux in DSPM-DE can be calculated through the HAGEN-POISEUILLE equation (equation 1.3).[168]

$$J_s = \frac{r_p^2 (\Delta p - \Delta \pi)}{8 \eta L_e}$$

(1.3)

where:

J_s = solvent permeate flux

r_p = average pore radius

Δp = hydraulic pressure difference across membrane

$\Delta \pi$ = osmotic pressure difference (feed vs. permeate)

η = dynamic viscosity of the solvent

L_e = effective membrane thickness

According to equation 1.3, the solvent flux in NF is mainly controlled by the pressure difference across the membrane. Typical applied pressures in NF are between 5-40 bar.

Aside from the transport phenomena explained by the ENP, the DSPM-DE provides three main mechanisms for solute exclusion, resp. partitioning (Figure 1.12B).
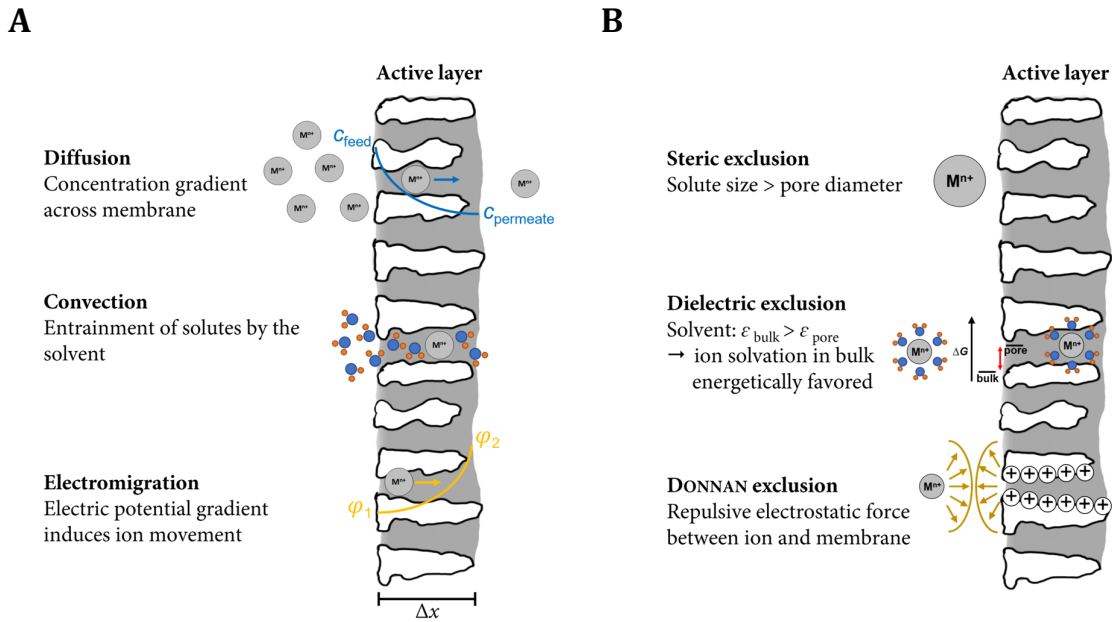
Figure 1.12 Solute transport (A) and exclusion (B) mechanisms occurring in NF according to the DSPM-DE. Illusatration based on Roy et al. (2017) and Lu et al. (2022).[169,170]

Steric exclusion occurs when the solute size exceeds the pore diameter. This sieving effect is often translated into the MWCO, as a membrane specific parameter. The MWCO of a membrane is the molecular weight of the lightest neutral test solute that is at least 90% retained under given filtration conditions.[171]

Secondly, dielectric exclusion (DE) plays a role in NF. This effect is based on different dielectric properties of the solvent in bulk and in the confined space of a NF membrane pore. Typically, the dielectric constant, ε_s, in the bulk is higher than in the pore. Therefore, solvation of ions in the feed is energetically favoured compared to solvation in the membrane pores. Consequently, when entering the pore, solvated ions have to overcome an energetic barrier. Additionally, the solvation shell may be partially shed during the entrance (i.e. dehydration in case of water), affecting the partitioning energy during NF. The energetical difference causing DE can be expressed through the BORN model. The pore dielectric constants can be empirically determined and used for exclusion calculations in the DSPM-DE.[168]

Lastly, NF membranes are often charged during operation, thus electrostatic interactions play an important role in NF. The so-called DONNAN exclusion occurs when an ion with the same charge as the membrane surface tries to enter the membrane. The respective ion is repelled, whereas the higher the charge, the higher the repulsion. Therefore NF provides an ion permselectivity: as a rule, multivalent ions are retained in NF, while monovalent ions can still permeate.[168] This makes NF attractive for applications where differently charged substances should be separated in solution. Some examples are the purification of sulphuric or phosphoric acid, in which the speciation of the multi-proton acids is exploited.[172,173] By keeping the pH very low, monovalent (HSO_4^- and $H_2PO_4^-$) or neutral species (H_2SO_4 and H_3PO_4) can be generated as the predominant forms of the acids. All of these are well permeable in NF, while multivalent impurities, such as heavy metals, can be retained and thus removed from the acids.[173] The permselectivity of NF facilitates working at lower filtration pressures (e.g. in water desalination and purification), as monovalent species contribute little to nothing to the osmotic pressure.

The DSPM-DE has been successfully used to predict and explain electrolyte transport in the past.[174–177]

For instance, Fang and Deng could well predict the behaviour of two commercial NF membranes during filtration of an As(V) and Na containing solution.[176] The model has also been used for NF of REE containing streams. Léniz-Pizarro et al. used the DSPM-DE to model observed retentions of $LaCl_3$, $NdCl_3$ and NaCl. Good accuracy was found for positively charged NF membranes. However, when negatively charged membranes were used, the DSPM-DE deviated from the observations, whereas the authors concluded that adsorption of La^{3+} might have altered the membrane surface charge and hence caused the differences.[175]

The latter example emphasises, how complex phenomena may affect the predictability of membrane behaviour. In this context, long-term effects that usually occur during NF operation should also be considered. For instance, fouling (deposition of material on the active surface) presents a major challenge in membrane processes, such as NF.[171] Due to the asymmetric construction, most NF membranes are not backwashable, as this would lead to delamination / irreversible damage of the active layer.[171] Hence, chemical cleaning protocols were developed based on oxidising, alkaline

and acidic cleansers.[178] However, Process engineering, which includes the operation mode and construction of the membrane module, can significantly aid in maintaining membrane permeability during filtration. Typically, NF is conducted in cross-flow mode, in which the feed solution flows tangentially over the active side of the membrane and perpendicular to the permeate.[171] This approach inhibits the built-up of solids, by creating a 'dynamic gel layer' rather than a filter cake.[179] To prevent the deposition of foulants on the membrane surface, a sufficiently high cross-flow velocity is used to induce turbulence and improve mixing of the feed. Furthermore, this reduces concentration polarisation (CP), which could otherwise decrease solute retention. CP occurs due to a non-uniform spatial distribution of solutes during filtration, with solutes accumulating in a boundary layer proximally to the membrane surface (feed side) while solvent is removed. As a result, the concentration gradient across the membrane ($\frac{dc_i}{dx}$) is virtually higher than between bulk feed and permeate, driving the solute diffusion (equation 1.2). Vigorous mixing, i.e. turbulence, is beneficial to disrupt the boundary layer and prevent CP. Typically, for a turbulent flow Reynolds numbers of >2000 should be reached (equation 1.4).

$$Re = \frac{\rho \, v \, D_H}{\eta} \tag{1.4}$$

where:

Re	= Reynolds number
ρ	= density
v	= cross-flow velocity (feed)
D_H	= hydraulic diameter
η	= dynamic viscosity of the solvent

The Reynolds number (Equation 1.4) allows conclusions on the flow regime based on the ratio between inertial forces (numerator) and viscous forces (denominator). Thus, higher cross-flow velocities promote turbulent flow, by increasing the shear stress.[180] While this approach suppresses CP, high velocities also lead to pressure drop through the membrane module and higher energy consumption, i.e. higher operational expenditure (OPEX).[180] Additionally, too high flow rates might damage/delaminate the membrane, being an inherent limit of the approach. To overcome this problem, membrane spacers are typically used. Spacers are grids that are placed on top of the membrane, causing improved mixing of the fluid stream, promoting turbulent flows at relatively low Re.[180,181] Layering membrane flat-sheets and spacers alternatingly allows for the build of highly packed membrane modules, such as pillow or spiral wound elements (Figure 1.13).
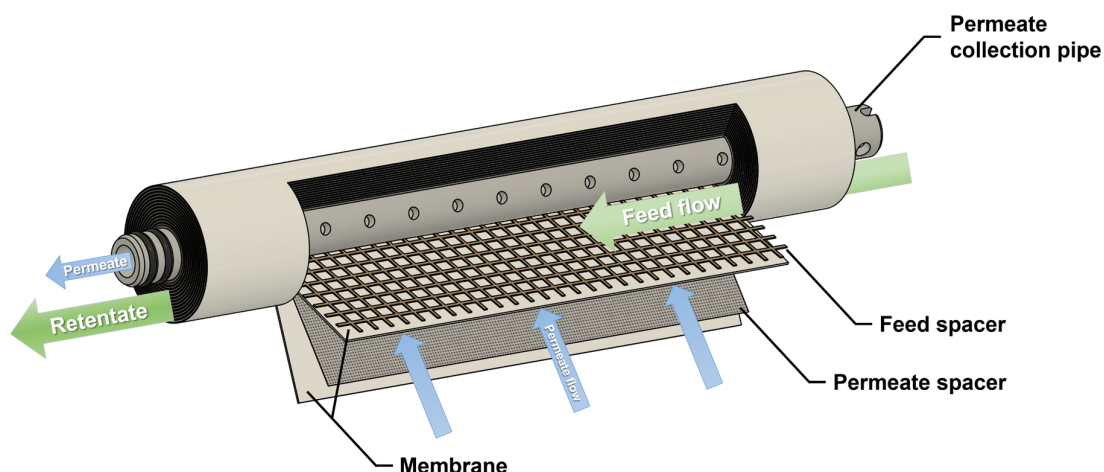
Figure 1.13 Schematic of a spiral wound element with cut-out section, indicating components and streams. Illusatration based on Tan et al. (2012).[182]

In the past NF has found application mostly in the desalination/water softening and dairy industries.[183] Nonetheless, due to improved material engineering, membranes for organic solvent nanofiltration and extreme pH range have become increasingly available. Aside of the use for acid purification, acid resistant nanofiltration (arNF) has been applied on the recovery of valuable elements form acidic waste streams. For instance, López et al. successfully tested a commercial polysulfonamide NF membrane (Duracid, GE®) for the recovery of sulfuric acid and the concentration of metals, such as Cu, Fe, Ni.[184] Kose Mutlu et al. reported on the recovery of REE from coal fly ash leachate using different commercial NF membranes.[185] Also Zhao et al. investigated on NF for the separation of REE from synthetic REE leaching solutions.[186] Overall, NF can be described as a mature technology for instance in desalination and wastewater treatment, but applications for element recovery are relatively scarce, yet. Nevertheless, developments in materials science, novel production possibilities and a steadily increasing demand for improved element separation processes are driving the testing of NF in the field of element recovery.

1.5.1.2 Polymer inclusion membranes

NF may offer ion separation. However, its permselectivity mainly enables to discriminate between neutral solutes and monovalent and multivalent ionic species. As described before, the hydrometallurgical recovery of (precious) elements requires the handling of complex streams with minute concentrations of targeted components surrounded by various impurities. In this regard, NF may facilitate a pre-selection and -concentration but is generally insufficient to achieve element concentration factors $>>10^1$. SX, on the other hand, may offer outstanding selectivity for targeted solute, based on the underlying chemical reactions, wherefore easily separation factors $>10^3$ can be reached. Nonetheless, in terms of process engineering SX can be challenging. Operation requires permanent mixing and multiple stages of phase separations. In the past, attempts have been made

to mimic SX by membrane processes, resulting in the development of the class of the so-called liquid membranes.[187] The fundamental concept is the utilisation of membranes to separate two otherwise miscible phases, eliminating the need for constant mixing and separation required by SX. In this case, the liquid membrane itself serves as the aforementioned secondary phase, employing organic extractants that facilitate solute uptake by complexation. Proper reagents can subsequently cleave the solute-extractant complexes and release (elute) the solutes from the membrane, comparable to the stripping process in SX. Unlike in SX, liquid membranes enable simultaneous extraction and elution. Thus, solutes can be transported from a feed to a receiving solution by a liquid membrane. During solute transport, the extractant undergoes a cycle of complexation, diffusion, regeneration and back-diffusion (Figure 1.14). As the extractant 'carries' solutes across the membrane it is conventionally called *carrier*. Nonetheless, the mobility of the solute within the membrane during carrier-mediated transport is still debated.[188] The prevailing concepts are: 1) free diffusion of solute-carrier complexes as a whole, and 2) a 'hopping mechanism', in which the solute can travel between (fixed) carrier sites within the membrane.[188] Another aspect is that, as explained for SX, only uncharged species can enter the secondary phase (i.e. membrane). Thus, for transport of ionic species, counterions, either from the bulk feed phase (Figure 1.14A) or oppositely charged ionic carriers are required for charge compensation (Figure 1.14B). In case of the latter, after solute elution the charge of the carrier-ion has to be accordingly compensated during contact with the receiving phase (typically by protonation). Consequently, ionic carriers transport counterions in opposing direction to solutes (Figure 1.14B). The counterions' concentration gradient between feed and receiving phase can serve as a driving force for the entire process. Hence, in many cases, a proton gradient between the two aqueous phases is maintained during liquid membrane operation.[153,189]
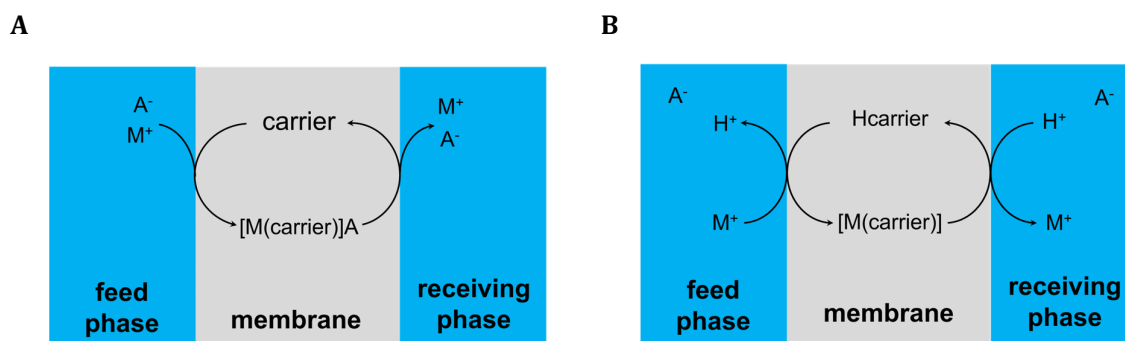
Figure 1.14 Schematic of two mechanisms for transport of cationic solutes (M^+) from feed to receiving phase using liquid membranes. The transport can be facilitated together with a co-ion, A^- (A) or in exchange for a counterion, such as H^+ (B).

Different liquid membrane concepts have been developed so far. For instance, bulk liquid membranes in which a liquid organic phase is entrapped between membranes or emulsion liquid membranes, in which the receiving phase is shielded from the feed by an emulsified organic phase, creating a double emulsion. Furthermore, an organic phase can also be adsorbed by a porous membranes substrate, leading to so-called supported liquid membranes.[189] Another type are polymer

inclusion membranes (PIMs). PIMs are thin-films of a blend of polymers and organic extractants, usually obtained by the solvent-casting method (Figure 1.10 and Figure 1.15). In brief, the components (polymer, extractant, and optionally plasticisers/additives) are dissolved in a solvent and the solution is cast onto a flat surface. Afterwards, the solvent is evaporated slowly, leaving behind the PIM (Figure 1.15B).[153]

A

B
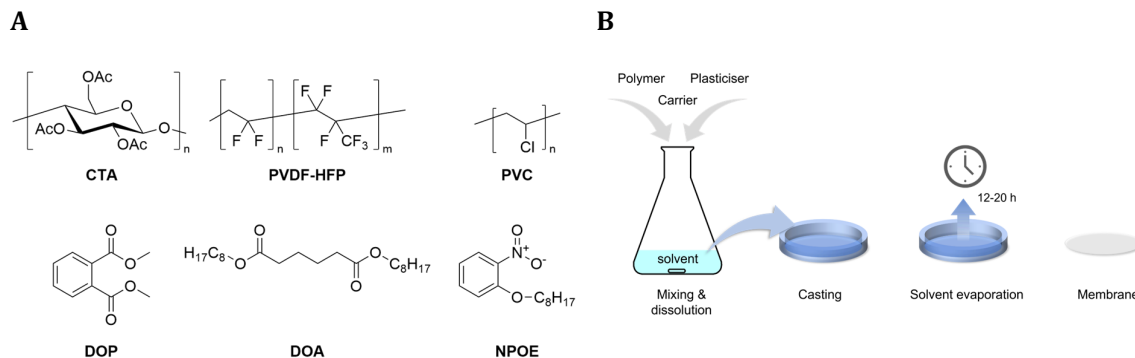
Figure 1.15 Structures of polymers and plasticisers commonly used for PIMs[144,153] (A) and schematic of the solvent casting method for preparation of polymer inclusion membranes (B).[153]

The solvent casting method, gives access to a wide range of PIMs, allowing to tailor membranes for a specific application. Some of the most widely used polymers for PIMs are cellulose triacetate (CTA) and polyvinyl chloride (PVC), because they are relatively cheap, compatible with many carriers and mechanically resistant (Figure 1.15A).[144,153] CTA, however, offers limited chemical resistance and for instance tends to hydrolyse in acidic environment.[153] In that regard, perfluorinated polymers offer outstanding inertness, wherefore poly(vinylidene fluoride-co-hexafluoropropylene) (PVDF-HFP) has gained attraction for the preparation of PIMs (Figure 1.15A). Such membranes were successfully tested in strong acidic environments and even aqua regia, without compromising its structural integrity.[190,191]

When selecting carriers for PIMs, experience with SX and therein utilized organic extractants can be leveraged. Therefore, numerous PIM studies made also use of aforementioned extraction agents, such as organophosphorus compounds (Figure 1.10).[144] However, unlike SX only small amounts of extractants are required for PIM experiments. Hence, also relatively expensive and/or tailor-made compounds can be readily incorporated into PIMs.[192,193]

Besides these two basic components of a PIM, in many cases a plasticiser is added to improve the properties of the polymer matrix (Figure 1.15A). Generally, plasticisers can intercalate between polymer chains, thus enlarge the free volume and increase the mobility of polymer chains, making the material overall more flexible.[194–196] In regard of PIMs higher solute fluxes, presumably through enhanced carrier mobility, and more homogeneous blends have been achieved, when using plasticisers.[153] Notably, carriers themselves may already have plasticising effects. However, the most commonly added plasticisers for PIMs are phthalates, such as dioctyl phthalate (DOP), dioctyl

adipate (DOA) and 2-nitrophenyl octyl ether (NPOE; Figure 1.15A).[144] On the other hand, increasing the malleability may impair the mechanical stability and integrity of the membrane, causing its components to leach into the process solutions during operation. Nonetheless, compared to other liquid membranes, PIMs were demonstrated to show reduced carrier losses and higher reusability potential even when used in harsh conditions.[153,193]

However, many PIM processes indeed suffer from limited membrane reusability, for which the aforementioned disintegration is a possible reason.[190,197] Several solutions have been proposed, including the addition of carrier to the aqueous phases or improving the hydrophobicity of the membrane.[198–200] Recently, Hoque et al. were able to improve the long-term stability of their PIMs by polymer crosslinking. Therefore, polyethylene glycol dimethacrylate (PEG-DMA) was added to the membrane cast solution, to replace a part of the base polymer. After casting, the blend was photopolymerised for crosslinking, resulting in a PIM with increased stability and moreover permeability (Figure 1.16).[197]
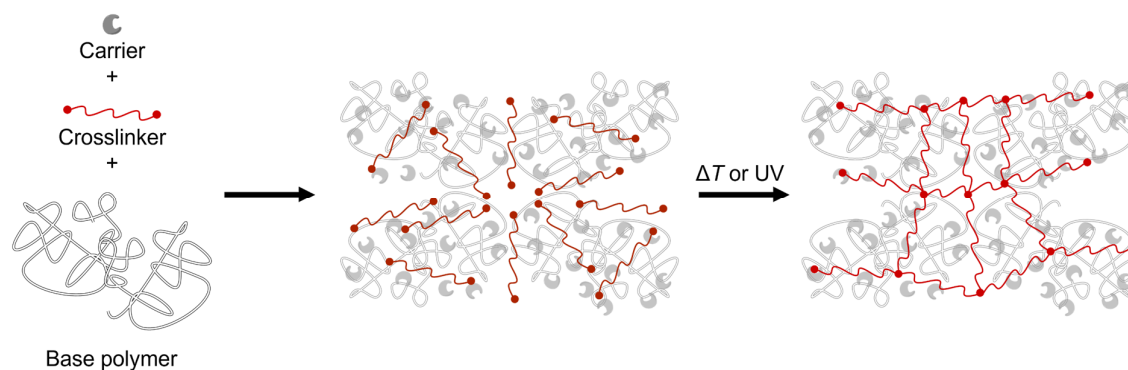
Figure 1.16 Schematic principle of PIM crosslinking. Illusatration based on O'Bryan et al. (2017).[201]

Aside of the membrane-centric optimisation, a PIM process can be further adjusted based on further system parameters. For-instance by changing the composition of the receiving solution, the temperature or the pH gradient. While this variety of options promises high adaptability for a specific task, developing a functioning PIM process from scratch can be challenging due to the complexity and interdependence of these variables.[153]

So far, PIMs have been used for analytical applications for decades, where the thin films serve as diaphragms for ion/solute selective electrodes.[202] In the last 15-20 years PIMs have received increasing interest in the field of element recovery, as an alternative to SX.[144,188,203,204] For instance, Croft et al. reported on PIMs for the separation of some lanthanides from sulfuric acid solutions.[205] Regarding Sc recovery, Yoshida et al. thoroughly demonstrated the suitability of PIMs in several studies.[192,193,206] Thereby, commercial PC-88A, but also novel amic acid[4] carriers were shown to offer high selectivity and efficiency for Sc transport from multielement feed solutions.

---

[4] According to IUPAC, amic acids are compounds containing a carboxy and a carboxamide group.[207].

Overall, PIMs may offer a complementary approach to conventional techniques, particularly SX. PIM-based solute transport can be tuned in several ways, either by adjusting the membrane position and properties or by changing some of the environmental conditions. While the preparation of membranes and the necessary process technology are readily accessible, PIMs have showed great potential to become a tool for more environmentally friendly strategies to conventional processes in the future.

1.6   Scope of the thesis

Identified as a critical raw material, attempts have been made to recover Sc from secondary sources, such as bauxite residues or the white pigment acid waste. Until recently, practically no Sc was recovered in Europe. Due to its rating as a CRM, the EU incentivised domestic Sc extraction. The SCALE project, launched in December 2016 within the Horizon 2020 funding programme, aimed to build a European Sc supply chain using industrial by-products.[109,208] In the framework of SCALE, energy and resource efficient technologies were targeted for Sc recovery. These included advanced leaching, novel SX strategies and also membrane-based technologies, such as nanofiltration, which became the subject of the present work. As described previously, membrane processes can complement conventional separation methods and result in significant energy and material savings.[159,209] Over the past 50 years, membranes have been widely adopted in various industries, such as desalination, wastewater treatment, and the dairy industry.[171,209] However, their use in challenging environments and for element recovery represents a relatively recent development.[151,186,210] Consequently, research into membrane technology for these applications is still in its early stages, with limited studies available and few that have been tested at pilot scale or beyond.[211,212] This stands in contrast to conventional hydrometallurgical processes, which have been more extensively researched and applied in these areas.

This thesis was devoted to the development of membrane-based recovery strategies for Sc from industrial waste generated by European chloride-route TiO_2 production. To showcase the capabilities of membrane technology for Sc extraction, two approaches were focused:

1) Acid resistant nanofiltration for pre-sorting and concentrating Sc.
2) Polymer inclusion membranes as an alternative to solvent extraction.

To the best of our knowledge, NF-based Sc recovery had not been explicitly explored before SCALE. Moreover, PIMs have rarely been tested in a real scenario and most definitely not for Sc recovery under such conditions. For the assessment of applicability and relevance of NF and PIM approaches for TiO_2 acid waste, several challenges were considered, including:

1) Chemical aggressiveness: acid waste generated by the chloride-route is a relatively concentrated corrosive dispersion containing HCl ($\sim$15%), unreacted ore, coke particles and several percent of dissolved metal salts, including naturally occurring radioactive material (NORM).[123,213]

2) Complex Sc matrix: chloride-route acid wastes can contain some 30 elements, whereas Sc represents only a minute fraction of the total metal content.[109]

3) Industrial scale: the TiO$_2$ industry has substantial production capacities (over 9 Mt a^{-1}) and generates correspondingly several million tonnes of waste per year.[122]

4) Knowledge bias: although accounting for approximately half of the TiO$_2$ production[126], less studies are available for wastes of the chloride route compared to those of the sulfate route.

5) Lacking coherence: both technologies would only represent a single stage in the recovery process, rendering the evaluation of implications for upstream and downstream operations difficult when reviewing the membrane-processes isolated.

Therefore, this thesis strived to investigate the effectiveness of NF and PIM-based membrane technologies for Sc recovery from TiO$_2$ acid waste under relevant conditions. In the process, bottlenecks of the two membrane separation strategies should be identified and, if applicable, eliminated or mitigated. In addition, this thesis aimed to assess NF and PIMs in combination with complementary processes. Collaboration was pursued to develop a viable recovery route for Sc. With respect to this, also the demonstration of scalability of membrane-based approaches was targeted, in order to bridge the gap between laboratory tests and industrial-scale implementation. This should also ensure the collection of more relevant data for potential operating costs and on process implications. The aim of this work was to increase the technology readiness of NF and PIMs for Sc recovery and to contribute to the development of complementary hydrometallurgical solutions for the valorisation of secondary raw materials.

At the beginning of this work, NF membranes created by the layer-by-layer method were examined (Chapter 2). This new class of NF membranes can be tailored for a specific application through a precisely controllable and readily accessible manufacturing process.[214] Lbl-membranes were described as suitable for harsh environments, while providing superior stability and permeability over conventional commercial membranes. Hence, they were deemed to be of particular interest for Sc recovery from TiO$_2$ acid waste. Membranes were custom-made and evaluated for their Sc separation potential from model solutions and real TiO$_2$ acid waste, targeting the first proof of principle for NF-based Sc recovery. Aside of the lbl-approach, several commercial acid-resistant membranes were assessed (Chapter 3). A process for Sc recovery based on NF was schemed, including upstream impurity removal by precipitation and downstream SX. Thus, the filtration treatment could be reviewed in regard of implications for a logical subsequent stage. Ultimately, the optimised NF-SX process was piloted and augmented by antisolvent crystallisation for synthesis of a close-to-market Sc product (Chapter 4). Here, the aim was to achieve a cubic metre scale that would allow operation for more than 100 hours and provide relevant data for the evaluation of the overall process. Secondly, with respect to PIMs for Sc recovery, existing studies delivered a proof, that liquid membranes are suitable for Sc recovery. However, as virtually all experiments so far were carried out with diluted model solutions, the applicability for concentrated (acidic) wastes remained ques-

tionable. Moreover, strong organic extractants viable for the SX of Sc, were reported unusable as carriers in PIMs, due to crucially impaired Sc elution. Commonly used stripping agents (HF, NaOH) are no options for PIM-based transport systems. Therefore, a holistic approach was chosen to systematically screen membrane compositions and process parameters to enable selective PIM-based Sc recovery from real TiO_2 acid waste (Chapter 5). Eventually, the PIM process was examined deeper with respect to membrane reusability, alternative carriers and additional membrane optimisation potential. Furthermore, work-up and recycling of the receiving phase was investigated by combining PIMs and NF. This approach would allow to minimise the material footprint of the overall process (Chapter 6). To conclude the thesis, the entirety of developed membranes and procedures is reviewed with respect to their potential for Sc recovery and implications for sustainable hydrometallurgy. Eventually, possible directions for future research are outlined (Chapter 7).

2 Nanofiltration for scandium recovery with tailor-made lbl-membranes

This chapter was published as

K. Remmen[†], R. Schäfer[†], S. Hedwig, T. Wintgens, M. Wessling, and M. Lenz, Layer-by-layer membrane modification allows scandium recovery by nanofiltration, *Environ. Sci.: Water Res. Technol.*, 2019, **5**, 1683-1688; DOI: 10.1039/C9EW00509A
[†]Both authors contributed equally to the publication.

Contribution of Sebastian Hedwig: Investigation, Validation, Writing – original draft, Writing – review & editing.

2.1 Abstract

Aluminium scandium (Sc) alloys are stronger, more corrosion resistant and heat tolerant than classical aluminium alloys and allow for 3D printing. In particular, the aerospace industry benefits from better fuel efficiency due to lighter materials as well as the advantages of additive manufacturing. However, Sc is currently not available in sufficient quantities and has recently been identified as a raw material critical to the economy. Due to the recentness of the demand, technologies for recovery of Sc from secondary sources are in their infancy. In this study, Sc recovery from titanium dioxide pigment production waste by nanofiltration was investigated. Custom-made layer-by-layer (LbL) modified membranes were optimized with regards to their elemental retention (i.e., selectivity towards Sc) as well as their acid resistance. In model solutions, the optimized membrane retained up to 64% ± 4% Sc, removing the major impurity, iron (Fe), efficiently (12% ± 7% retention) while achieving high flux [32 L m^{-2} h^{-1}] at a low transmembrane pressure of 5 bar. Acid resistance was shown down to a pH of 0.1, which could be even further increased (up to ≤ 3M HCl) by adding more bi-layers and changing the coating conditions. In real wastes, the optimized LbL membrane showed higher Sc retention (60% vs. 50%) compared to a commercial acid resistant membrane, while achieving considerably higher fluxes [27 L m^{-2} h^{-1} versus 1 L m^{-2} h^{-1}, respectively at 5 bar]. It was possible to operate filtration at low transmembrane pressure with up to 70% permeate recovery and flux that was still high [~10 L m^{-2} h^{-1}]. In a nutshell, titanium dioxide pigment wastes contained sufficient amounts to satisfy the growing demand for Sc and can be exploited to their full extent by LbL nanofiltration due to the proven advantages of acid stability, Sc retention and selectivity and high achievable fluxes at low pressures.

2.2 Introduction

Recovery of resources from waste streams is essential in moving towards a circular economy.[84,215–217] Critical raw materials have an above average economic importance as well as a supply risk. Amongst 27 materials recently identified by the European Commission (similar lists exist for other major economies[218]), scandium (Sc) is exceptional in terms of complete import reliance and zero end-of-life recycling rates.[219] A main interest of Sc is its application in aluminium (Al) alloys, in which its unique properties lead to stronger, weldable, more corrosion resistant, and more heat tolerant Al products.[84] Al-Sc alloys may decrease an aircraft weight by as much as 15–20%, making Sc particularly interesting for the aerospace industry. In addition, 3D printable alloys are now available (e.g. Scalmalloy©) that allow for additive manufacturing.

Some attempts have been made to recover Sc from secondary sources; in particular, recovery from bauxite residues (so-called red mud) has been found promising.[84,125,215,220–222] Apart from red mud, there are further stockpiled waste materials that may help satisfy the growing global Sc demand, in particular residues from titanium dioxide (TiO_2) production. These are available on a millions-of-

tonnes-per-annum scale. Currently, an estimated 5,400,000 metric tons of ilmenite and 750,000 metric tons of rutile are mined globally.[223] From these, TiO_2 is extracted/purified through either the traditional 'sulfate' or the 'chloride' route.[224] However, very few attempts have been made for Sc recovery via the sulphate route,[225,226] and to the authors' best knowledge, none via the chloride route.

Briefly, during TiO_2 pigment production via the chloride route, ore is processed with coke and gaseous chlorine in a fluidized bed reactor at high temperatures of 900°C–1,000°C.[121,125,227] The process produces HCl waste containing high dissolved metal concentrations, as well as unreacted ores/coke overblow. Depending on the original ore and processing conditions, varying Sc concentrations may be found in these waste streams. A small level of Sc (0.5%) in Al alloys in only 0.1% of the global annual Al market would result to an annual scandia (Sc_2O_3) need of ~350 tonnes[84] (~230 t Sc). Currently, the global supply of Sc is estimated to be between 10–15 tonnes per year only[223] and primary Sc deposits above 100 ppm are rarely reported.[84] It has been estimated that about 60% of the 4.5 million tons of pigment production world-wide is generated by the chlorine process.[121] The volume of aqueous acid waste of the chloride route as well as Sc concentrations will certainly depend on the operational conditions of the respective plant (e.g., type and grade of ore used, dimensions of scrubber, etc.). Nevertheless such wastes may contain sufficient Sc to meet even future demand.

Sc is commonly concentrated and purified by solvent extraction/precipitation.[226] For some elements, in particular the solvent extraction process step may contribute considerably to the overall environmental impact of the processing chain (e.g., up to one third in the case of neodymium oxide[228]). For Sc recovery, it has been demonstrated that a pre-enrichment is needed for sufficiently concentrating Sc for later selective extraction.[226] Here, nanofiltration (NF) can offer two crucial advantages: firstly, since it is based on a different separation principle, it may offer selectivity while, secondly, decreasing the volume to be extracted downstream, decreasing the environmental impact of the solvent extraction steps.[229] However, a severe limitation of NF is that in high ionic strength solutions satisfactory fluxes can only be achieved via high operational pressures, increasing operational costs.[172,230,231] Furthermore, only a very limited number of commercial membranes can withstand strongly acidic conditions (regularly found in hydrometallurgy).

LbL modified membranes are assembled by depositing several layers of oppositely charged polyelectrolytes (PE) on an ultrafiltration (UF) membrane. This technology allows tailoring of the membrane characteristics (porosity, selectivity, stability, etc.)[232–234] towards a target ion and application. This is achieved through selection of a suitable PE, varying the number of layers, and/or varying the coating method (e.g., the ionic strength, the pH).[232,235] LbL membranes often have a higher permeability during acidic filtration than conventional NF membranes. For instance, LbL membranes showed 16 times higher permeability in comparison to a commercial membrane (AS 3012, AMS, TelAviv, Israel) in P recovery from acidic leachates[236] with increased P yield.[235] In conse-

quence, the filtration units can be smaller, or a lower transmembrane pressure (TMP) can be applied, leading to a considerably lower operational (energy consumption) and capital costs.[235,236] A limitation to LbL membranes may be their instability in strong acids. So far, studies focused on stability in H_3PO_4[235,236] and acid stability in HCl was only shown by immersing the membrane in 1 M HCl.[214,232,237] No studies have been carried out post-filtration regarding element retention or flux behaviour, so that it remains unclear if sufficient acid stability can be achieved over the long term. Thus, this study is the first to apply LbL membranes in concentrated HCl matrixes for Sc recovery. LbL membranes were optimized with regards to their selectivity towards the target ion (Sc) as well as to their acid resistance by modifying coating parameters (number of layers, ionic strength) in model solutions. The best LbL membrane was applied for filtration of real TiO_2 wastes and compared to commercial membranes.

2.3 Experimental

2.3.1 Membranes

Polyethersulfone (PES) based hollow fibre membranes (type: UFCLE) provided by Pentair (Enschede, the Netherlands) were used as a support structure to prepare LbL membranes (see 2.3.2). The UF membrane had a molecular weight cut-off of 100 kDa and a pure water permeability of 1,100 L m^{-2} h^{-1} bar^{-1}. The membranes were potted in modules containing two fibres each. Each hollow fibre had an inner diameter of 0.8 mm, and a length of 300 mm. This resulted in a total membrane surface of 15 cm^2 per module. After potting, the bare membranes were rinsed with deionized water for at least 1 h. An acid resistant flat sheet membrane (Duracid KH) with a membrane area of 8 cm^2 was purchased from Suez (Ratingen, Germany). The Duracid membrane was cut into pieces of 100×30 mm and immersed in deionized water for 24 h. Compaction took place for at least 12 h in the test cell at 5 bar and a feed flow of 12 L h^{-1}.

2.3.2 Layer-by-layer modified membrane preparation

The application of the PE on the membranes was carried out using a custom-made set up which allowed dynamic coating.[232,236] The positively charged poly(diallyldimethylammonium chloride) (PDADMAC; MW = 400–500 kDa, 20 wt% in water) and the negatively charged poly(sodiumstyrenesulfonate) (PSS; MW = 1,000 kDa, 25 wt% in water) were purchased from Sigma-Aldrich (Buchs, Switzerland). The oppositely charged PE were diluted in an NaCl solution (0.05–1 M), and were alternately coated onto the membrane, starting with the positively charged PE, and always terminated by the PSS. The pH of the coating solution was neutral. Dead-end filtration was applied to concentrate the PE inside the lumen of the membrane. Each filtration cycle was carried out with the same duration and pressure to ensure equal amounts of PE retained in the lumen. After each coating cycle, the membrane was flushed with deionized water until a conductivity

of below 3 μS cm^{-1} was reached. The conductivity was measured using a GMH 3451 conductivity meter from Greisinger (Regenstauf, Germany).

2.3.3 Membrane filtration

A custom-made testing device was used for the filtration (see Annex). At a TMP of 5 bar a BVP-Z gear pump (Cole-Parmer, Wertheim, Germany) was used to establish the desired cross-flow velocity for operation in turbulent mode. Experiments were performed in batch circulation mode with the concentrate fed back into the feed vessel. The feed vessel was placed in an ice bath, maintaining the feed temperature at 0°C. Elemental retention was determined in cross-flow mode. At a TMP of 5 bars, the flow was 160 mL min^{-1}, resulting in a cross-flow velocity of 2.65 m s^{-1} and a Reynolds number of > 2,300 (thus at turbulent flow). Each LbL membrane modification was tested in triplicate.

2.3.4 Feed solutions

Model solutions consisted of 1 M HCl, 45,000 mg L^{-1} Fe (added as Fe(II)O × 7 H$_2$O, 99% purity, Sigma-Aldrich, Buchs, Switzerland) and 90 mg L^{-1} Sc (added as Sc$_2$(III)O$_3$, 99.9% purity, Sigma-Aldrich, Buchs, Switzerland). When needed, the pH of the model solution was adjusted using NaOH (98.5% purity, Sigma-Aldrich, Buchs, Switzerland). The pH was measured using a WTW inoLab Multi 9310 IDS pH-meter (Weilheim, Germany). In addition, both the optimized LbL membranes and the Duracid membrane were used for filtering a real TiO$_2$ acidic waste stream (see 2.4.2). The composition of the solution changed depending on the process as determined by elemental analysis (see Annex). For filtration, the acid waste was diluted at 1:5 (vol:vol) and the pH set to 1.5. Solids were separated by filtration (0.45 μm).

2.4 Results and discussion

2.4.1 Selective Sc recovery using layer-by-layer modified membranes

Ionic strength in the coating solution is known as a major parameter influencing the structure and morphology of the assembled layers. This is due to the fact that net charge neutrality of the PE can be attained either by oppositely charged repeat units of the counter PE (referred to as 'intrinsic charge compensation') or by salt counter ions (referred to as 'extrinsic charge compensation').[238] Extrinsic charge compensation by salt ions is expected to yield thicker multilayers, with individual chains having more mobility, resulting in less stable structures.[238] Here, high ionic strength during coating (1M NaCl) resulted in the highest Sc retention (64.3 ± 1.5%; Figure 2.1), whereas low ionic strength did not yield membranes with sufficient Sc retention (33.7 ± 1.9% at 0.05 M; Figure 2.1). Ionic strength did not influence Fe retention, remaining below 12.3% in all cases. The impact of the

applied NaCl concentrations on Sc retention as well as on stability is in accordance with Adusumilli et al.,[239] who showed a 10 times thicker PE film when the assembly was performed with 1 M NaCl compared to 0.05 M NaCl. Despite yielding the highest Sc retention, the high ionic strength did indeed result in instable membranes, underlined by the decrease in Sc retention after 60 min of filtration (30.6 ± 10.4%; Figure 2.1). It is known that the high ionic strength of the feed solution can irreversibly impact the structure of NF membranes.[240–242] During exposure of the LbL membranes to high ionic strength and/or acidic solutions, the intermolecular repulsion effects within the polymer chains can be lessened, leading to a more open and swollen structure.[240,243,244] Indeed, the intermediate (0.5 M) NaCl concentration appeared to be the best trade-off between sufficient initial Sc retention (53.5 ± 3.6%) and stability (45.7 ± 7.2 Sc retention after 60 min; Figure 2.1).
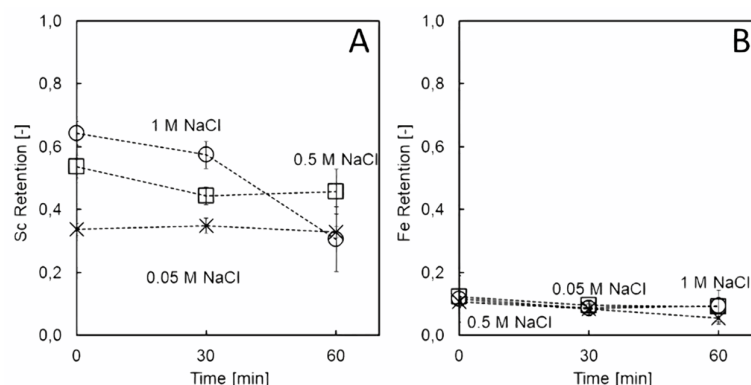
Figure 2.1 Sc (A) and Fe (B) retention by (PDADMAC/PSS)₃ in model solution as a function of coating condition

Additional bi-layers may result in improved membrane properties with regards to element retention as well as stability,[214,232,239] yet come at the price of requiring more time and chemicals for membrane preparation. Increasing the number of bi-layers in PDADMAC/PSS systems impacting filtration has been ascribed to the charge overcompensation of PDADMAC, leading to diffusion of the PE from top layers into lower layers.[214,245] Here, the addition of more than three bi-layers did not result in improved Sc retention, and the (PDADMAC/PSS)₃ system showed satisfactory acid stability (i.e., 45.7 ± 7.2% Sc retention after 60 min; Figure 2.2). The addition of more bi-layers only had a minor beneficial effect on Fe retention (minimal retention of 4.2 ± 1.3% with seven bi-layers, Figure 2.2), which is too little to justify additional preparatory work due to the low retention using three bilayers (12.3 ± 1.1%). The results are in line with previous studies that have shown already three bi-layers giving high magnesium retention and thus NF membrane properties.[214]
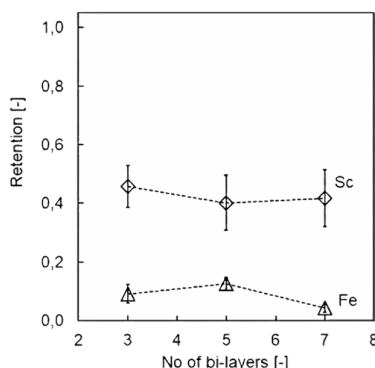
Figure 2.2 Sc and Fe retention after 60 min of model solution filtration for (PDADMAC/PSS)$_x$ membranes as a function of the number of bi-layers applied.

Acidity may influence both chemical (i.e., degradation) and physical (e.g., swelling, structural order, disintegration) integrity of the LbL membranes.[234] Regarding the application in hydrometallurgy in general and for TiO$_2$ wastes in particular, high resistivity towards acid is desirable. Considering that a solution with high ionic strength can diminish the electrostatic interaction of the PE, less stable membranes are expected in high acidic environments. Indeed, at low (0.1) pH, the (PDADMAC/PSS)$_3$ system was indicated to be insufficiently stable, underlined by decreased Sc retention before and after filtration (53.5 ± 3.6% to 45.7 ± 7.2%, Figure 2.3A and B). Adjusting the pH to 1.5 had a positive effect on Sc retention and membrane stability (63.3 ± 4.4% before to 64.6 ± 10.7% after 60 min of filtration; Figure 2.3A and B), while achieving high selectivity towards undesired Fe (14.4 ± 0.9% after filtration). Acid stability down to pH ≥ 1.5 constitutes an expansion of (PDADMAC/PSS)$_3$ systems that have previously been shown to be stable down to pH 2.5 (PDADMAC/PSS coated Si capillaries for chromatography).[237] Improving acid resistivity even further for other hydrometallurgical applications while conserving selectivity for the target ions remains the subject of future work. Certainly, increasing the number of bi-layers and modifying the coating conditions can still considerably improve acid resistivity (e.g., up to 3M HCl, which is considerably higher than previously reported[237,246], see Annex). Alternatively, in the future crosslinking of other PE may result in high acid resistivity, however, at the expense of more steps/chemicals necessary and potential loss of selectivity. Here, increasing the pH of the waste had an additional advantage, since some unwanted elements (impurities such as radioactive uranium (U) and thorium (Th)) already precipitate at this value, whereas most Sc (80%) remained in solution (see Annex). Therefore, acid resistivity towards pH 1.5 solutions was found sufficient for Sc recovery from TiO$_2$ wastes.
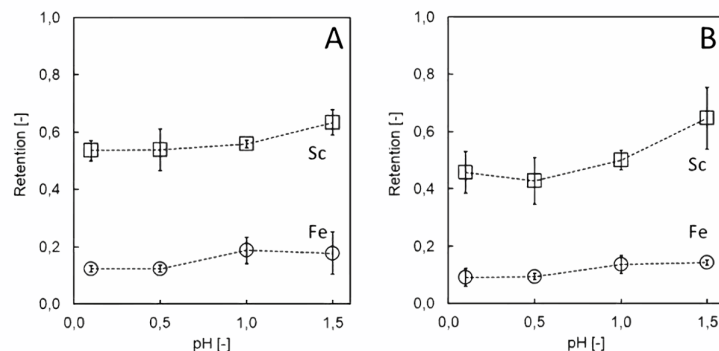
Figure 2.3 Acid stability in term of Sc and Fe retention as a function pH before (A) and after 60 min (B) of model solution filtration.

2.4.2   Scandium recovery from real wastes of the TiO$_2$ industry

Using real, complex aqueous waste from the TiO$_2$ industry confirmed the good Sc retention and selectivity towards major impurities (Fe). There was little effect of permeate recovery on Sc retention up to 60% permeate recovery, and Sc retention remained high (≥56%; Figure 2.4). After, retention decreased to 41%, only. The same trend was observed for Th, an impurity in the TiO$_2$ waste, although with higher initial retention of 81% (Figure 2.4). At high permeate recovery, the decrease in element retention can be partly ascribed to higher membrane-shielding effects and hence a decrease of the Donnan effect.[173,240,247] Next to these phenomena, the decreased flux led to a lower convective flow, favouring diffusive membrane transport. Initial flux values of 27 L m^{-2} h^{-1} were recorded, which decreased successively to 10 L m^{-2} h^{-1} at 70% permeate recovery. Since scaling or precipitation of metals is not likely in this acidic solution, the decrease in flux can probably be ascribed solely to an increasing osmotic pressure during permeate recovery. It should be noted that despite the high Th retention, overall Th concentrations were low due to pH adjustment (removing ~75% of dissolved Th prior filtration) so that Th was not concentrated above the initial value.
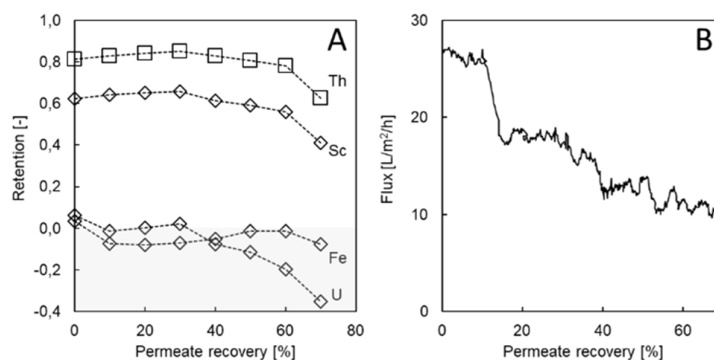
Figure 2.4 Elemental retention (A) and flux (B) as a function of permeate recovery in real acid waste.

Other impurities such as Fe and U were efficiently removed by LbL filtration, as underlined by the even negative retentions (Figure 2.4). Since no Fe or U are concentrated in the retentate, the Sc:Fe

40

ratio was shifted in an even more favourable direction. In previous studies, low U retention was observed for NF membranes and a decrease in pH led to lower retention values as well.[248,249] Other studies report a decreased influence of Donnan exclusion for anions such as chloride in a lower pH environment.[250] Thus, dielectric and steric exclusion play a major role in retention. Two other studies claim that large hydrated ions with a strong hydration shell are retained best.[251,252] This seems to apply to Sc and Th in the here presented experiments. In a study presented by Tansel et al. (2012), Fe^{2+} was categorized as a large hydrated ion but with a weak hydration shell, leading to lower retention values, which might also be the case for U.[251]

To benchmark the obtained membrane performance, a filtration experiment was conducted using a commercially available acid resistant Duracid membrane at 0% permeate recovery. The Duracid membrane achieved less Sc retention (50%) and retained more Fe (4%) and U (31%), whereas less Th was retained (69%). The results are in accordance with a previous study that assigned lower retention for monovalent, divalent, and trivalent ions to HCl used to acidify the feed solution using the same membrane.[229] Most importantly, it has to be noted that even at 0% permeate recovery, a flux of as little as 1 L m^{-2} h^{-1} was measured, which was 3% of the flux that was reached for the LbL membranes at the same conditions (Figure 2.4B). Thus, when aiming at an identical amount of permeate volume, a 28-fold membrane area or notable pressure increase would be needed. In conclusion, the LbL membranes used here offer advantages regarding not only selectivity but also lower operational costs and/or energy demand.

2.5   Conclusions

2.5.1   Nanofiltration as alternative separation for critical raw material recovery from acidic wastes

Here, first the separation of Sc from TiO_2 waste was demonstrated as a proof of principle. The Sc concentration found here (76–90 mg L^{-1}) qualify TiO_2 acid wastes as an ore.[84] Some ~2.5 to ~3 million m^3 of this waste would thus be sufficient to cover the entire projected future Sc demand, a volume that may in fact be available considering the ~4.5 million tons of pigment produced. This study adds to previous studies that have shown the potential of nanofiltration for recovery of critical raw material from acidic wastes. For instance, NF could be used for recovery of Fe and acid (HNO_3, HF) from spent pickling baths,[253] Zinc and Fe recovery from acidic electroplating effluents,[254] phosphorous recovery from acid leached sewage sludge,[173,255] or indium from acid leached photovoltaics,[229] to name a few.

Recovery of critical raw materials by nanofiltration in general offers the major advantages of relying on a different separation principle than conventional techniques (i.e., ion exchange, solvent extraction, precipitation) as well as generating concentrates depleted in impurities, beneficial for downstream processing by conventional techniques.[229] One challenge regarding the filtration of

strong acidic solutions is their corrosivity. Since LbL membranes operate at lower pressure ranges (here, 5 bar) but still reach high fluxes [here, up to 27 L m^{-2} h^{-1} in real wastes], the filtration units can be built out of corrosion resistant plastic parts. Though the proof of principle for LbL filtration of TiO$_2$ wastes was made here, a challenge for future research remains the acid resistivity and long-term stability[234] of the membranes themselves. Although acid resistivity can be improved to some extent by the addition of more layers or changed coating conditions (see Annex), some wastes may still remain inaccessible without pre-treatment.

3 Combination of nanofiltration and solvent extraction for scandium recovery
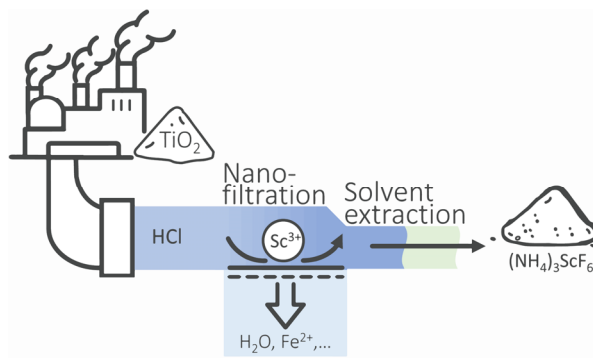
This chapter was published as

S. Hedwig†, B. Yagmurlu†, D. Huang, O. Von Arx, C. Dittrich, E. C. Constable, B. Friedrich, and M. Lenz, Nanofiltration-Enhanced Solvent Extraction of Scandium from TiO_2 acid waste, *ACS Sustainable Chem. Eng.*, **2022**, *10* (18), 6063-6071; DOI: 10.1021/acssuschemeng.2c01056
†Both authors contributed equally to the publication.

Contribution of Sebastian Hedwig: Conceptualization, Formal Analysis, Investigation, Methodology, Supervision, Validation, Visualization, Writing – original draft, Writing – review & editing.

3.1 Abstract

Scandium is a critical raw material with a technological potential to reduce transportation costs and CO_2 emissions. However, global supply and market adoption are crucially impaired by the lack of high-grade Sc ores and recovery strategies. A tandem nanofiltration solvent extraction route is demonstrated to enable effective Sc recovery from real-world acid waste from the chloride TiO_2 production route. The process involving several filtration stages, solvent extraction and precipitation was optimized, ultimately producing >97 % pure $(NH_4)_3ScF_6$.

3.2 Introduction

The intensifying climate crisis demands the transition of society to alternative technologies that can reduce anthropogenic greenhouse emissions to an environmentally acceptable level. The rare earth element (REE) scandium (Sc) offers opportunities for 'greening' the energy and transportation industries. For example, solid oxide fuel cells containing Sc can economically produce electricity from hydrogen and Sc is the most efficient dopant for aluminium alloys, allowing the production of ultra-light car bodies.[80,117] Minute amounts of Sc are sufficient for making aircraft Al alloys weldable and 3D printable, with up to 20% weight-saving for future aircraft construction.[256]

However, Sc has not been widely adopted by the industry due to limited market availability and astronomical prices (Sc_2O_3: 2'200 USD kg^{-1} in 2021).[103] Suppliers face a number of challenges with regard to Sc: reluctant customers, technologically demanding production processes and shortages of high-quality Sc ores. Due to its (potential) economic importance, which is impeded by a pronounced supply risk, Sc has been classified as a critical raw material (CRM) by the European Commission since 2017.[40,219] The European CRM initiative seeks for measures to remove supply bottlenecks for important commodities. One important strategy is to untap so far unused sources, such as industrial wastes. Although Sc rarely occurs naturally in concentrated ores, it is rather abundant in the Earth's crust (Sc: 22 ppm; Pb: 14 ppm). Overall, Sc is present in hundreds of commercial minerals and can be found in waste streams of mineral industrial processes.[83,125,133] White pigment (TiO_2) has a global production volume of 8,000,000 t·a^{-1}[257,258] with about half of the TiO_2 being produced by chloride route[126] in which TiO_2-rich ore is digested at high temperatures with elemental chlorine and coke. Volatile $TiCl_4$ is generated and can be condensed from the off-gases of the process. Afterwards, $TiCl_4$ is converted to pure TiO_2 and Cl_2, the latter being recycled. Chlorides of accompanying metals enter the scrubbing water, which eventually turns into a semi-concentrated HCl slurry containing unreacted ore, coal particles and numerous dissolved metals.[86,123] Among these, Sc is in the hundred ppm range, making TiO_2 acid waste a promising Sc resource.[256]

Solvent extraction (SX) is the most commonly used technique to separate and concentrate Sc from aqueous solutions.[125,135,147,226,259–261] The commonest extractants are organophosphorus compounds, such as di-(2-ethylhexyl)phosphoric acid (D2EHPA).[125,135,147,226,259,260] Nevertheless, ex-

traction of trace Sc from complex aqueous media remains technically challenging, requiring high aqueous to organic phase ratios, with the higher costs and emissions associated with large process volumes. In addition, co-extraction of impurities (e.g. Fe, Ti, Zr, Th, U, etc.) reduces the loading capacity and selectivity of the system and directly affects the final purity of the product.[117,262–264] Therefore, strategies for pre-concentration of Sc upstream to SX and reduction of impurities are urgently sought.

One possibility could involve membrane-based technologies such as nanofiltration (NF), which rely on other separation principles than SX.[256] NF membranes bear pores of 0.2-2 nm, corresponding to a molecular weight cut-off (MWCO) of 200 - 1000 Da. Separation of solutes during NF is based on size as well as electrostatic interactions in the case of dissolved ions. Typically, multivalent ions show high retention in NF, while monovalent species easily permeate. Recently, Remmen et al. demonstrated the potential of NF for Sc recovery from TiO_2 acid waste.[256] However, only diluted acid waste was tested and downstream processing was not considered.

Therefore, our study investigated the process engineering needed for Sc recovery from TiO_2 waste, using NF combined with SX, with a view to real-world future implementation. NF was examined using commercial membranes under relevant operating conditions, such as high pressure and with undiluted acid waste. A variety of commercially available acid-resistant NF membranes was tested to account for differences between fabrications and manufacturers. Eventually, NF was used to produce a Sc concentrate from the acid waste.

Sc SX was examined for both the acid waste and the NF concentrate. In this context, the benefits and limits of upstream NF prior to SX were investigated. Effects such as changes in co-extraction, Sc yield, need for post-treatment and plant dimensioning were considered, each being difficult to predict in advance. Ultimately, the overall process was evaluated in regard of implementation possibility for TiO_2 manufacturing via the chloride route.

3.3 Materials and Methods

3.3.1 Chemicals and materials

Acid waste was provided from a TiO_2 producer located in the Netherlands. All aqueous solutions were prepared using ultrapure water (>18 MΩ; Barnstead Smart2Pure water purification system, ThermoFisher Scientific, Switzerland). For pH adjustment NaOH solution (30 wt%) was used together with a pH-meter (inoLab Multi 9310 IDS, WTW, Germany). Suspended solids were removed by microfiltration using: 1) vacuum filtration in combination with glass fibre filters (0.4 μm, MN GF-5, Macherey-Nagel, Germany) or 2) decantation and gravity filtration with filtration bags (1 μm, Eurowater, Germany). Residual suspended particles were removed by ultrafiltration (MWCO 150 kDa, UP150, Microdyn-Nadir, Germany) (see 2.3.4).

3.3.2 Analytical methods

3.3.2.1 QqQ-ICP-MS

Samples were diluted with nitric acid (3%), using an autodilution system (Simprep, Teledyne Cetac Technologies, USA). Samples were analysed using triple quadrupole inductively coupled plasma mass spectrometry (QqQ-ICP-MS) as previously described.[256] The analysis was performed on an 8800 QqQ-ICP-MS system (Agilent, Basel, Switzerland) using general purpose operational settings. Quantification was performed via multi-element standards (0-50 ppb, seven points). To account for matrix effects ^{103}Rh was used as the internal standard. To quantify ^{23}Na$^+$, ^{52}Cr$^+$, ^{55}Mn$^+$, ^{56}Fe$^+$, ^{60}Ni$^+$, ^{66}Zn$^+$, ^{89}Y$^+$, ^{137}Ba$^+$, ^{139}La$^+$, ^{140}Ce$^+$, ^{141}Pr$^+$, ^{146}Nd$^+$, ^{147}Sm$^+$, ^{153}Eu$^+$, ^{157}Gd$^+$, ^{159}Tb$^+$, ^{163}Dy$^+$, ^{165}Ho$^+$, ^{166}Er$^+$, ^{169}Tm$^+$, ^{172}Yb$^+$, ^{208}Pb$^+$, ^{232}Th$^+$ and ^{238}U$^+$ the ICP-MS was operated in single quad mode using helium as a collision gas, whereas ^{24}Mg$^+$, ^{27}Al$^+$, ^{39}K$^+$, ^{45}Sc$^+$, ^{47}Ti$^+$, ^{51}V$^+$, and ^{90}Zr$^+$ were measured in triple quad mass-shift mode using O_2 as a reaction gas. ^{7}Li$^+$ concentration was determined using no-gas single quad mode.

3.3.3 Dead-end NF

For dead-end NF a HP4750 stirred cell (Sterlitech, USA, Figure S9.3, Annex) was used. Flat sheet membranes (Table S1, Annex) were cut into circular shapes and immersed for >20 h in ultrapure water. Afterwards, the membranes were inserted into the cell with the active side (14.6 cm^2) oriented toward the feed solution (100 mL per experiment). The cell was closed and the pressure was adjusted to 35 bar under continuous stirring (300 rpm). Unless otherwise described, filtration was carried out until 30 % permeate was recovered (determined by weight).

3.3.4 Cross-flow filtration

For cross-flow filtration (UF and NF) a modular filtration unit (MaxiMem, PS Prozesstechnik, Switzerland) was used (Figure S9.4, Annex). Experiments with flat sheet membranes (active area: 200 cm^2) were conducted at a cross-flow flux of 5 L min^{-1} and a temperature of 25 °C. Spiral wound elements (1812 type: 1.8" diameter, 12" length, 31 mil spacer, 0.32 m^2 active area) were used at a cross-flow flux of 10 L min^{-1} and a temperature of 25 °C. Ultrafiltration (UF) was conducted isobarically at 10 bar under flat sheet conditions. Prior to use, NF membranes were compacted at 10 bar over-night using ultrapure water.

3.3.5 SX

Solvent extraction tests were conducted in a glass beaker with a phase ratio of 1 (50 mL : 50 mL). Each organic phase was contacted with untreated acid waste and NF concentrate for 15 minutes to reach the equilibrium under mild stirring at room temperature. The selected organic phase was loaded with a phase ratio (volume of aqueous phase: volume of organic phase) of 7 for investiga-

tions on scrubbing and stripping behaviour. For investigation of loading and scrubbing dependency on Fe valency in the NF concentrate, iron metal (1.5 g L^{-1}) was added to reduce any Fe^{3+} to Fe^{2+}.

For scrubbing tests, HCl (37%, laboratory grade) was diluted with ultrapure water to the desired concentrations. Stripping solutions were prepared using reagent grade NH$_4$F. Extractants (D2EHPA, Cyanex 923, N1923 and tri-n-butyl phosphate (TBP)) were diluted with dearomatized kerosene (Exxsol D80, ExxonMobile, Germany). Aqueous and re-extraction solutions of the organic phases were sampled for the efficiency calculations.

The distribution ratio and the selectivity of the organic extractants are calculated according to the following equation:

$$D_x = \frac{C_x^{Org}}{C_x^{Aq}} \text{ and } \alpha_{x/y} = \frac{D_x}{D_y} \tag{3.1}$$

where; D_x is the distribution coefficient of element X, C_x is the concentration of element X in aqueous/organic phase, α is the extraction selectivity.

3.4 Results & Discussion

3.4.1 pH-adjustment / preparation of NF feed
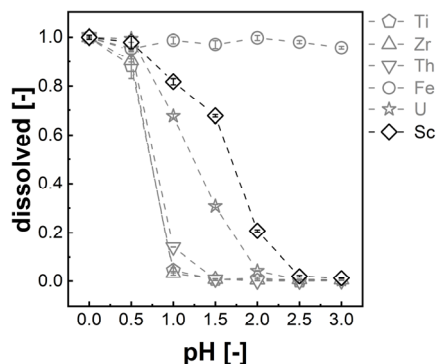
Figure 3.1 Dissolved elements in the acid waste during neutralisation with NaOH.

The acidic waste from the European TiO$_2$ production site contained suspended solids (mainly overblown coke and unprocessed ore) and numerous elements in widely varying concentrations. Some of the elements present were known to be problematic for Sc recovery via SX (e.g. Ti, Zr) or potentially hazardous to health and safety (naturally occurring radioactive material, NORM).[125] Ti can be retained in the solution or scrubbed out of the extractant during SX of the waste from the alternative sulfuric acid TiO$_2$ production process by adding H$_2$O$_2$ to facilitate formation of Ti peroxo sulfate complexes[226] although, this is not possible in the chlorine process in which Ti must be removed before SX.

Excellent separation of Sc from Ti, Zr and Th was achieved at pH 1 to 1.5 (Figure 3.1). Most of the Sc (82 ± 1% at pH 1; 68 ± 1% at pH 1.5) remained in solution, whilst the other metals precipitated

quantitatively (>99%). Adjusting the pH to 1.5 was considered as the best option, as the majority (69 ± 1%) of U also precipitated (Figure 3.1).

In general, Sc precipitation started at pH >1 and was completed at pH 2.5. For Ti, Zr and Th a steep drop in solubility was observed between pH 0.5 and 1 (Figure 3.1). Further, U precipitated slightly faster than Sc, starting at pH <1 and being >95% precipitated by pH 2 (Figure 3.1). In contrast, Fe remained completely dissolved within the range of pH 0 to 3 (Figure 3.1). The high solubility of Fe indicated the predominant presence of ferrous iron instead of ferric iron[265], as the latter precipitates at pH ≥3.

After pH adjustment, element concentrations in the supernatant were monitored over two weeks. Concentrations were mostly stable over time at different pH values, except near the inflection point of precipitation, where no plateau was reached even after two weeks. There, concentrations increased over time, presumably as a correction of over-precipitation due to local supersaturation.[266] At a pH of 1.5, an equilibration time of 48 hours after NaOH addition was found sufficient.

During S/L separation of the slurry (pH = 1.5), the precipitated hydroxides and oxides were only filtered with difficulty. With filter bags (1 μm sieve size), the filtrate was still turbid, whilst 0.4 μm filters rapidly clogged. The best procedure involved sedimentation of the precipitate (≈48 h) followed by decantation and bag filtration to give a clear solution. The solid fraction (approx. 32% v/v) was a moist gel.

Following microfiltration, residual particles were removed by UF to prevent scaling in subsequent processing. The microfiltrate was easily filterable, with losses determined by the dead volume of the filtration unit (≈200 mL). The UF permeate, obtained after the pre-treatment, is subsequently referred to as NF feed.

Only few studies of the precipitation behaviour of Sc and other elements contained in the acid waste of the TiO_2 chloride route have been reported. Most recently, Remmen et al. described precipitation trends at pH of 1.5 for different elements in the waste.[256] The precipitation trends at pH 1.5 presented here conform with those previously reported.[256] However, in our system more precipitation was observed (Sc: ~30%, Th: >99% and U: ~70% (here) vs. Sc: ~20%, Th: 80%, U: 40% (Remmen et al.)).[256] We assume this arises from the removal of microparticles by UF. Otherwise, pH values of incipient precipitation reported were extremely low for various elements compared to other literature.[267–270] Precipitation of Th and U is reported to occur between pH 5-7 from chloride media (1-2 for Th from sulfate media).[267] Sc reportedly precipitated at pH ≥3 in HCl.[270] Presumably, the high concentrations of Ti and Zr, whose hydroxides are known to be barely soluble even at a pH of <2, result in co-precipitation.[268]

Overall, the results show that the precipitation of elements in complex real solutions can deviate greatly from findings in model solutions. Although precipitation rates and solubility products are known for the pure compounds, effects such as sorption/coprecipitation and kinetic limitations in

complex mixtures make ab initio predictions of behaviour very difficult, making extensive testing inevitable when developing processes based on secondary resources.

3.4.2   NF-membrane screening
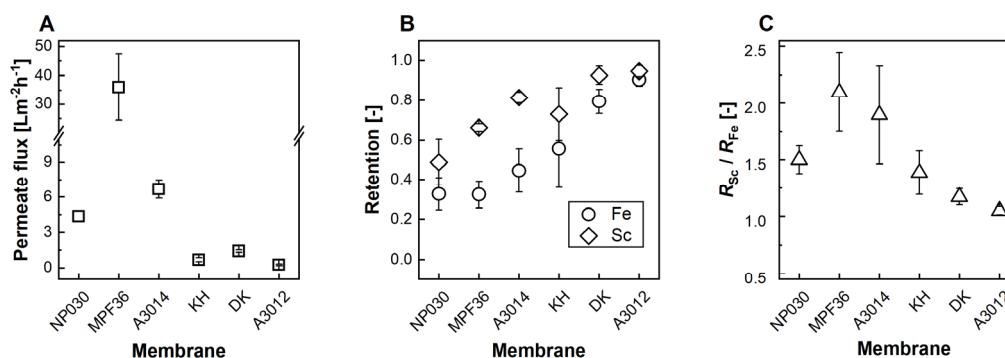
Figure 3.2 Permeate flux (A), element retention (B) and quotient of Sc over Fe retention (C) (dead-end filtration at 35 bar and 30 % permeate recovery).

Six potential NF-membrane candidates were compared in terms of: 1) permeate flux (Figure 3.2A), 2) element retention (mainly R_{Sc} and R_{Fe}; Figure 3.2B) and 3) Sc selectivity (expressed through R_{Sc} divided by R_{Fe}; Figure 3.2C) during filtration of the NF feed. The membrane showing the best performance of high permeate flux, and high R_{Sc}, while being permeable for competing elements, was A3014, with a permeate flux of 6.7 ±0.8 $Lm^{-2}h^{-1}$, an R_{Sc} of 0.81 ± 0.03 and a Sc over Fe selectivity of 1.9 ±0.4.

The tested membranes had permeate fluxes ranging from 0.25 $Lm^{-2}h^{-1}$ to 35 $Lm^{-2}h^{-1}$, in the sequence A3012 < KH < DK < NP030 < A3014 < MPF36 (Figure 3.2A), largely consistent with the MWCO reported by the manufacturers (Table S9.3, Annex), with tighter membranes (A3012, DK, KH) showing lower fluxes.

Sc retentions were between 0.49 – 0.95, in the order NP030 < MPF36 < KH < A3014 < DK < A3012 (Figure 3.2B). For Fe, retentions in the range of 0.32 - 0.90 were observed, following the order MPF36 ≈ NP030 < AMS3014 < KH < DK < A3012 (Figure 3.2B). Lastly in terms of Sc over Fe selectivity, a range of 1 (no selectivity) to 2 was found, following the order A3012 < DK < KH < NP030 < A3014 < MPF36 (Figure 3.2C).

While the MWCO were found to be helpful in explaining the trends, there were also exceptions, e.g. the loosest membrane (MPF36, MWCO: 1000 Da) showed the highest flux but not the lowest Sc retention. Instead, the NP030 (MWCO: 500 Da) retained the least Sc, while Fe retention appeared similar to the MPF36. The NP030 showed also a lower flux than the A3014 (MWCO: 400 Da), although being potentially looser.

Low element retention has already been reported for the NP030. Kose Mutlu et al. tested NP030 and the DK for REE recovery from fly ash leachate at low pH.[185] REE retentions were some eight times lower for NP030 in comparison to DK[185] and pH-dependent zeta-potential measurements

revealed considerably higher positive surface charges for DK, than for the polyether sulfone membrane NP030.[185] Hence, a potential Donnan rejection mechanism was less pronounced and element retention lower for NP030 than for other membranes.

For NF-based Sc recovery, only MPF36 and A3014 were suitable, as both exhibited good Sc over Fe selectivity and sufficient permeate fluxes. Of the two potential candidates, A3014 was selected for further process development, as a high R_{Sc}, crucial for low Sc losses, was considered more important than high permeate flux. However, MPF36 may represent an interesting choice, when yields are less important than filtration time and operation costs.

Remmen et al. developed layer-by-layer (LbL) assembled NF membranes, which showed a R_{Sc} of up to 0.60 compared to a R_{Fe} of >0.05 and high permeate flux (up to 28 Lm^{-2}h^{-1}) at just 5 bar.[256] Aside from NP030, all commercial membranes had higher R_{Sc}, but also higher R_{Fe} values. Therefore, more Sc could be recovered with commercial membranes, but at lower selectivity reaching maximally two times higher R_{Sc} (0.66 and 0.81) than R_{Fe} (0.32 and 0.44) for MPF36 and A3014, respectively. Further, the permeate fluxes were considerably lower compared to LbL membranes: 35 bar pressure were necessary for the MPF36 to reach 36 Lm^{-2}h^{-1}, while the second fastest membrane (A3014) reached only ~7 Lm^{-2}h^{-1}. However, the test conditions differed to those of Remmen et al., where the acid waste was diluted (1:5).[256] With the higher initial concentration of the feed, a correspondingly higher osmotic pressure had to be overcome and a higher operational pressure was inevitable.

3.4.3 NF process for acid waste concentration
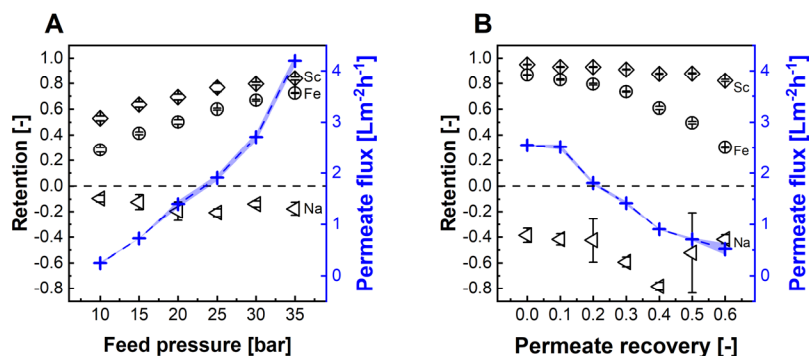
Figure 3.3 Element retention and permeate flux against the feed pressure at 0% permeate recovery (A) and element retention and permeate flux against the permeate recovery rate at 35 bar (B).

In cross-flow filtration mode with A3014, 35 bar (maximum feed pressure) was optimal in regard to permeate flux (4.2 ±0.1 Lm^{-2}h^{-1}) and R_{Sc} (0.84 ±0.01). For Sc selectivity, 1.2 times higher R_{Sc} than R_{Fe} was observed.

Increasing the feed pressure led to almost linear increase of the permeate flux from 0.25 ±0.02 Lm^{-2}h^{-1} (10 bar) to 4.2 ±0.1 Lm^{-2}h^{-1} (35 bar; Figure 3.3A). At the same time, R_{Sc} improved from 0.53 ±0.02 (10 bar) to 0.84 ±0.01 (35 bar; Figure 3.3A). In comparison, R_{Fe} started at 0.28 ±0.02 (10

bar) and rose to 0.72 ±0.01 (35 bar). Since R_{Fe} increased faster than R_{Sc}, the selectivity of Sc over Fe decreased from 1.9 (10 bar) to 1.2 (35 bar). In comparison to Sc and Fe, monovalent cations, such as Na$^+$, were well permeable, indicated by negative retentions throughout the experiments (Figure 3.3A). Element retentions rose with higher feed pressure due to the subordinate role of diffusive salt transport with simultaneous increase in water permeation.[173]

With regard to R_{Fe}, a discrepancy between crossflow (0.72) and dead end (0.44) filtration was observed, while R_{Sc} was similar (∼0.8) in both cases. Therefore, Sc over Fe selectivity was lower during crossflow tests. This is probably due to better compaction when using the cross-flow setup, explaining the higher retentions but also lower permeate flow in these tests.[271] On the other hand, higher concentration polarisation during dead-end filtration conjunct to stronger electrostatic repulsion for Sc^{3+} than for Fe^{2+} might have led to the deterioration of R_{Fe} while being less important for R_{Sc}.[256]

In terms of energy consumption, maintaining the same crossflow rate of 10 Lmin^{-1} at 35 bar required about 2.5 times more energy than at 10 bar.[272] However, the permeate flow at 35 bar increased in comparison 17 times, shortening the operation time and compensating the higher energy consumption at elevated pump load. Therefore, in this case concentrating can be considered more energy efficient at higher pressure.

Ultimately, from 2.0 L NF feed, 0.8 L NF concentrate was produced. Overall, 84 ±3% of the Sc and 58 ±2% of the Fe remained in solution (Table 3.1). The permeate recovery was stopped at around 60 % due to a low permeate flux (0.5 Lm^{-2}h^{-1}) decreased R_{Sc} (0.12) and a low residual concentrate volume, being insufficient to maintain a crossflow rate of 10 L min^{-1}.

The permeate flux decreased gradually from 2.5 ±0.1 Lm^{-2}h^{-1} to 0.5 ±0.1 Lm^{-2}h^{-1} (Figure 3.3B). In terms of element retentions, higher values were found than in the previous experiments. R_{Sc} decreased from 0.95 ±0.01 to 0.82 ±0.01 and Fe became notably more permeable with increasing concentration, with R_{Fe} starting at 0.87 ±0.01 and decreasing to 0.30 ±0.01 at 60 % permeate recovery. Therefore, the Sc over Fe selectivity improved from 1.1 to 2.7. Representative of monovalent ions, Na$^+$ showed very high permeability throughout the experiment, permeating against its concentration gradient (R_{Na} < -0.3).

During concentration, permeate fluxes and element retentions decreased due to the osmotic pressure increase, as reported before.[256] Interestingly, the Sc retention was less affected than e.g. the Fe retention. It is assumed that this was caused by concentration polarisation, being proportional to element feed concentration, and becoming even more prevalent as filtration progressed and concentrations increased.[273] Permeability, however is expected to be lower for Sc^{3+} than for Fe^{2+}, due to stronger Donnan exclusion. Hence, NF became more selective for Sc with ongoing progress of the operation.

Table 3.1 Volumes and elemental concentrations for different streams during the production NF concentrate and elemental NF yields and concentration ratios for comparison of NF concentrate with NF feed and initial waste.

		Initial waste	Microfiltrate	NF feed	NF concentrate	NF Yield	concentrate / initial waste	concentrate / NF feed
Volume	[L]	3.2	2.2	2.0	0.8		0.24	0.37
Sc	[mg L⁻¹]	41.1 ± 0.1	33.3 ± 0.5	28.9 ± 0.5	61 ± 2	0.84 ±0.03	1.5	2.1
Ti	[mg L⁻¹]	4540 ± 10	28.5 ± 0.6	5.1 ± 0.2	8.1 ± 0.4	0.64 ±0.04	0.002	1.6
Zr	[mg L⁻¹]	1170 ± 20	8.0 ± 0.3	0.12 ± 0.03	0.19 ± 0.02	0.63 ±0.17	0.0002	1.6
Al	[mg L⁻¹]	1730 ± 10	1611 ± 30	1430 ± 11	2950 ± 70	0.83 ±0.02	1.7	2.1
Fe	[mg L⁻¹]	17600 ± 200	17100 ± 100	15800 ± 200	23100 ± 600	0.58 ±0.02	1.3	1.5
Th	[mg L⁻¹]	79 ± 1	5.8 ± 0.2	2.9 ± 0.1	5.4 ± 0.01	0.74 ±0.03	0.07	1.9
U	[mg L⁻¹]	13.9 ± 0.2	0.29 ± 0.01	0.09 ± 0.01	0.10 ± 0.01	0.44 ±0.07	0.006	0.9
V	[mg L⁻¹]	1070 ± 20	930 ± 30	840 ± 20	1340 ± 40	0.64 ±0.02	1.3	1.6
Na	[mg L⁻¹]	150 ± 30	29000 ± 1000	26000 ± 300	15000 ± 400	0.28 ±0.01	100	0.6
Mn	[mg L⁻¹]	4600 ± 200	4600 ± 100	4400 ± 100	5500 ± 200	0.5 ±0.02	1.2	1.3

3.4.3.1 Solvent Extraction Behaviour
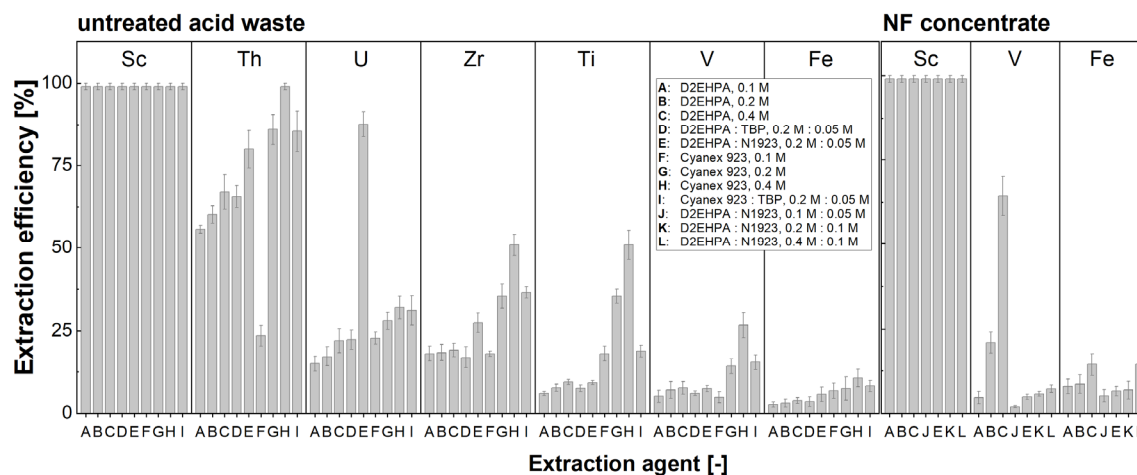
Figure 3.4 Organic screening for the optimization of the loading behaviour both from untreated acid waste and NF concentrate (impurities with < 10ppm concentration are not included).

Although various studies of the sulfate TiO₂ production route have been reported[147,226,274], limited information is available for SX processes on the chlorine TiO₂ production waste. D2EHPA, Cyanex 923 and synergistic mixtures of these organics worked best to recover Sc selectively from complex solutions from the sulfate process. Therefore, these extractants were tested with various concentrations in D80 kerosene to observe the selectivity, phase separation behaviour and the co-extraction levels of the impurities from untreated acid waste and NF concentrates (Figure 3.4).

All extractants performed similarly in Sc extraction, lowering the Sc concentration to < 1 ppm after extraction in all tests with untreated acid waste (Figure 3.4). Increasing the D2EHPA concentration did not significantly increase the co-extraction of impurities. While Ti, Zr, V and Fe co-extraction remained stable (Figure 3.4), extraction of radionuclides increased from 55% to 67% and 15% to 22% for Th and U, respectively. Unlike D2EHPA, increasing Cyanex 923 concentration (to 0.4 mol·L^{-1}) resulted in high co-extraction of Th (> 99%), Ti (~50%), Zr (~50%), V (30%) and Fe (10%). No synergistic effect of TBP with these extractants was observed. Co-extraction generally increased with synergistic addition of N1923 to D2EHPA, reaching 85% for Th and 31% for U. Increased NORM extraction was expected, as amines are widely used in commercial solvent extraction of radioactive elements.[275] Even though promising extraction efficiencies were found, the phase separation was problematic in all cases due to high transition metal loading.[146,276,277] Formation of an inseparable phase occurred in all extraction trials with slow separation behaviour, predicting high loss of the organic phase and processing problems in a larger scale continuous operation.

Extraction tests with the NF concentrate were carried out using the most promising extractants, D2EHPA and synergistic D2EHPA-N1923 couple. Similar to the untreated acid waste, Sc was completely extracted when using NF concentrate. However, high co-extraction was found with D2EHPA as the extractant. This was especially pronounced for higher D2EHPA concentration, reaching 65% for V and 14% for Fe at 0.4 mol·L^{-1} D2EHPA (Figure 3.4). It was previously reported that addition of N1923 can substantially improve Sc selectivity.[147,278,279] Here, addition of 0.05 mol·L^{-1} efficiently supressed V co-extraction and slightly decreased Fe loading (Figure 3.4). Sc selectivity over other elements increased during extraction with the synergistic D2EHPA-N1923 mixture (Table S9.4, Annex). Phases separated rapidly during extraction of the NF concentrate, making the process viable for larger scale operation.

Considering the loading capacity, selectivity towards Sc and the phase separation, the best extractant option was identified as 0.2 mol·L^{-1} D2EHPA with 0.05 mol·L^{-1} N1923 in D80 kerosene.

3.4.3.2 Scrubbing

After SX with the selected organic and a phase ratio of 7, Sc was enriched considerably (0.49 g·L^{-1}). Of the major impurities present in the NF concentrate, Fe (6.3 g·L^{-1}) and Al (16 mg·L^{-1}) were found in the organic phase. The trace impurities in NF concentrate, Ti, Zr and Th, were enriched in the organic phase after SX to 32 mg·L^{-1}, 25 mg·L^{-1} and 20 mg·L^{-1}, respectively.

HCl was preferred as the scrubbing solution due to strong interaction between Fe and Cl, and avoiding unwanted complex formations from other anions.

No Sc was scrubbed out from the organic phase (Table S9.5, Annex). With increasing HCl concentration Ti, Zr, Th, Al removal was only slightly improved, while highest Fe removal (89%) was obtained with 4 mol·L^{-1} HCl. Therefore, 4 mol·L^{-1} HCl was selected for scrubbing after SX, removing aside from Fe also 72%, 76%, 20% and 56% of Ti, Zr, Th and Al, respectively.

Although the majority of Fe in the NF concentrate was ferrous[265], a fraction oxidized to ferric spontaneously. Presumably, the ferric portion caused high Fe co-extraction, as the affinity of D2EHPA for Fe^{3+} is considerably higher than for Fe^{2+}. In order to suppress Fe co-extraction, iron metal was added to the NF concentrate, reducing Fe^{3+} to Fe^{2+} (equation 3.2).

$$2\ Fe^{3+} + Fe^{0}_{(s)} \rightarrow 3\ Fe^{2+} \tag{3.2}$$

Extraction from three post-treatments for the NF concentrate (original, reduced, reduced & acidified), were compared in terms of Fe co-extraction suppression capability.

Reduction of ferric iron resulted in a sharp drop of the co-extraction values: while 3.3 $g·L^{-1}$ Fe was co-extracted with the original NF concentrate, only 0.36 $g·L^{-1}$ Fe after reduction and 0.17 $g·L^{-1}$ Fe after reduction and acidification were extracted. Thus, reduction & optionally acidification enables complete Fe scrubbing during SX, requiring only few mixer-settler units.

3.4.3.3 Stripping

Although D2EHPA is a very effective extractant for Sc extraction, its strong bonding characteristics make Sc stripping from the organic phase challenging. Concentrated acids as well as strong alkali solutions have been used for stripping.[141] However, even highly concentrated acids, were relatively unsuccessfully, and concentrated NaOH solutions used instead.[142] Nevertheless, other problems arise from stripping of D2EHPA with NaOH: 1) loss of organic due to solubility of Na-D2EHPA in aqueous solutions, 2) separation issues with 3rd phase formation owing to solubility variations of the extractant in kerosene, 3) immediate precipitation of $Sc(OH)_3$ and clogging of the liquid flow in continuous operation.[277,280,281]

Therefore, NH_4F was selected as the stripping agent due to stable and strong complexation forming $(NH_4)_3ScF_6$. Here, quantitative (>99 %) Sc stripping was achieved (Table 3.2). The final product contained only traces of impurities, wherefore Sc accounted for ∼97 wt-% of the metals in the strip liquor (Table 3.2). Residual impurities could be removed via anti-solvent crystallisation, yielding pure $(NH_4)_3ScF_6$.[149] Calcination of this product gives easy access to ScF_3, which can be directly utilized in Al-Sc alloy production.[149] Therefore, high temperature processing to convert $Sc(OH)_3$ into Sc_2O_3 or treatment with gas phase HF to produce ScF_3 can be avoided.

Table 3.2 Compositions and flows of critical elements through the complete solvent extraction process from NF concentrate to strip liquor.

		Raffinate	Loaded Org.	Scrubbed Org.	Scrubbed Org. (Stage 3)	Stripped Org.	Strip Liquor
Sc	[mg L^{-1}]	n.d.	494 ± 7	492 ± 3	491 ± 4	n.d.	1468 ± 31
Ti	[mg L^{-1}]	2.7 ± 0.3	31.6 ± 1.8	9.8 ± 0.4	3.4 ± 0.08	n.d.	8.4 ± 1.2
Zr	[mg L^{-1}]	n.d.	2.4 ± 0.03	0.4 ± 0.02	0.2 ± 0.01	0.05 ± 0.02	0.5 ± 0.01
Al	[mg L^{-1}]	2912 ± 70	24.5 ± 0.8	7.4 ± 0.9	1.1 ± 0.06	0.3 ± 0.03	2.8 ± 0.05
Fe	[mg L^{-1}]	22968 ± 600	676 ± 28	38.4 ± 2.2	3.2 ± 0.1	n.d.	9.9 ± 1.0
Th	[mg L^{-1}]	1.4 ± 0.1	22 ± 1.1	15.4 ± 0.7	8.6 ± 0.7	1.5 ± 0.05	23.4 ± 2.9
U	[mg L^{-1}]	n.d.	0.09 ± 0.01	n.d.	n.d	n.d.	n.d.

3.4.4 Process flow scheme / integration into chloride route
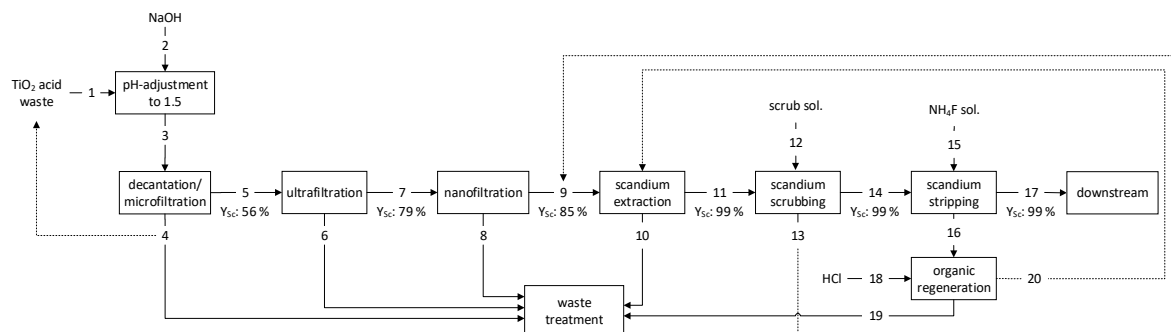
Figure 3.5: Block flow diagram of the tandem NF-SX process for Sc recovery from TiO$_2$ acid waste.

The proposed Sc recovery process comprises seven stages (Figure 3.5). From pH adjustment to NF, only sodium hydroxide, electrical power and re-usable filters/membranes, were required. NaOH, although expensive compared to lime/limestone, was needed to avoid high multivalent cations concentrations (e.g. Ca^{2+}) which would be enriched during NF due to high retentions, increasing the osmotic pressure of the feed, opposing the feasibility of the filtration. However, in view of the overall process (i.e. Sc recovery conjunct to chloride route TiO$_2$ production), NaOH might be available from upstream chlorine production via NaCl electrolysis, saving on transportation costs.[282]

In terms of Sc yields, the S/L separation (i.e. MF & UF) brought substantial losses (around 56%). Thus, despite the high yields (82%, four stages) following UF, the overall Sc yield was 36%. However, these could be mitigated by more efficient S/L of the hydroxide sludge, such as by the use of a filter press. Losses during lab-scale UF (stream 6) due to the dead volume of the filtration unit

would become negligible on a larger scale. Alternatively, streams 4 and 6 could be redirected into the original acid waste. This would reduce the amount of Sc discharge. Neutralisation followed by S/L separation, is currently used for acid waste treatment after chlorine TiO_2 production. Hence, NF feed could be produced by minor adjustment of the current treatment conditions.

During NF, most of the Sc (85 %) was preserved in the concentrate. The NF permeate (stream 8) is relatively diluted compared to the upstream media and could be re-used as scrubbing water in the gas washer of the TiO_2 production process. This would contribute to a zero liquid discharge approach and would keep NF related Sc losses in the system.

SX downstream to NF allowed for quantitative (99 %) Sc recovery from the concentrate. Due to excellent phase separation, no organic should be in the raffinate (stream 10). This Sc depleted solution could either be returned to the existing TiO_2 waste treatment process or could serve for further element recovery (e.g. V, Mn, other REE). The scrubbing effluent (stream 13) could be re-used for acidification of the NF concentrate once Fe^0 was added (Figure S9.5, Annex). Compared to the NF concentrate the throughput of stream 13 was rather low. Hence, combination of 13 and 9 would lead to negligible dilution but allow for waste mitigation and pH adjustment.

After Sc recovery via NF and SX, the Sc depleted solutions could be returned into the existing waste treatment route.

3.5 Conclusion

A combination of NF and SX has been applied to recover Sc from acid waste, originating from chloride-route TiO_2 production. The major findings were:

- pH adjustment 1-1.5 preserved Sc dissolved, precipitated challenging impurities (Ti, Zr, Th, U)

- AMS Nanopro A-3014 provided best trade-off between permeate flux, Sc retention & selectivity

- At most effective pressure of 35 bar, 60% of the volume and various bulk impurities (such as ~40% Fe, V, Mn) were removed, while 85% of Sc remained in the concentrate

- A mixture of D2EHPA and N1923 was most selective in SX

- Upstream removal of Ti, Zr, Th, U drastically increased Sc selectivity during SX

- NF prior to SX improved phase separation and reduced process volume

- Addition of Fe^0 suppressed Fe^{3+} coextraction and improved Fe scrubbing

- NH_4F was found as highly efficient stripping agent for Sc (purity >97%)

- Overall Sc recovery was 36% (six stages), which could be improved in the future by more efficient engineering of the MF & UF stages

The proposed process could be integrated into the waste disposal unit of a TiO_2 production plant without drastic plant changes and could be a step towards waste valorisation and effective resource use, enabling the production of a CRM with promising future potential.

This page is intentionally left blank.

4 Pilot scale scandium recovery from titania acid waste

This chapter was submitted as

Contribution of Sebastian Hedwig: Conceptualization, Formal Analysis, Investigation, Methodology, Supervision, Validation, Visualization, Writing – original draft.

4.1 Abstract

Scandium (Sc), declared a critical raw material in the European Union (EU), could face further supply issues as the EU depends almost entirely on imports from China, Russia and Ukraine.

In this study, a tandem nanofiltration-solvent extraction procedure for Sc recovery from titania (TiO_2) acid waste was piloted and then augmented by antisolvent crystallisation. The new process, comprising advanced filtration (hydroxide precipitation, micro-, ultra- and nanofiltration), solvent extraction and antisolvent crystallisation, was assessed in relation to material and energy inputs and benchmarked on ScF_3 production. From ~1 m³ of European acid waste containing traces of Sc (81 mg L⁻¹), ~13 g Sc (43% yield, nine stages) was recovered as $(NH_4)_3ScF_6$ with a purity of approximately 95%, demonstrating the technical feasibility of the approach. The production costs per kilogram of ScF_3 were lower than reported market prices, which underscores a competitive process at scale. Although a few technical bottlenecks (e.g. S/L separation and electricity consumption) need to be overcome, combining advanced filtration with solvent extraction and antisolvent crystallisation promises a future supply of this critical raw material from European secondary sources.

4.2 Introduction

Supply chains are the backbone of the economy. However, their resilience is increasingly challenged by social, environmental and geopolitical factors, potentially leading to disruption and, consequently, economic damage. Herein, critical raw materials (CRM) are a key factor, as they are economically important but at risk in supply. To identify and counteract raw material criticality, the European Union (EU) has launched a raw materials initiative, publishing a list of CRMs every three years since 2011.[40] The rare earth metal scandium (Sc) has been included on the list since 2017 because of its applications in high-strength aluminium alloys and high-efficiency fuel cells.[40,219] Used in aircraft engineering, up to 20% lighter airplanes could be built compared with today's standards.[256] Sc_2O_3 is vital for commercialised solid oxide fuel cells, which facilitates the direct conversion of hydrogen to electrical power.[90,256]

However, market acceptance has been low due to a severe lack of Sc supply and extremely high prices.[103] Until recently, the majority of the supply came from China (66%), with Russia (26%) and Ukraine (7%) as other suppliers.[41]

The underdevelopment of Sc production can be partially attributed to the scarcity of Sc ores. Sc has a low affinity to common ore-forming anions and, thus, is widely dispersed in the lithosphere.[105] Consequently, Sc recovery from secondary sources, where it is concentrated, is a compelling notion. One example of secondary sources is waste from the chloride route for white pigment (TiO_2) production. This two-stage process is responsible for 3–4 Mt a⁻¹ or approx. 50% of the global TiO_2 supply.[126] Rutile or titania-rich starting materials are converted into volatile $TiCl_4$ using Cl_2 and coke. After separation, $TiCl_4$ reacts with O_2 and pure TiO_2 is obtained, whereas Cl_2 is recycled. Impurities

accompanying the starting materials are washed out in the scrubber water.[121] These impurities contain HCl (approx. 15%), unreacted ore, coke, and a variety of metal chlorides. Sc has been reported to be present in the range of several hundred ppm.[121,283]

Some approaches have been developed to recover Sc. Conventionally, solvent extraction (SX) is used, followed by precipitation as a hydroxide or oxalate salt.[125,284] After calcination at temperatures in the range of 700–800 ºC, Sc_2O_3 is obtained.[108] The oxide is then converted to ScF_3 using hydrofluoric acid.[285] Afterwards, metallothermic reduction of ScF_3 is conducted to produce Sc metal or Al-Sc alloys.[285–287]

Remmen et al. presented nanofiltration (NF) using tailor-made layer-by-layer assembled membranes (LbL membranes) as a viable option, retaining most of the Sc while partially depleting impurities.[256]

We showed in our previous study that the combination of NF and SX can be successfully utilised to produce a strip liquor containing > 97% pure $(NH_4)_3ScF_6$ from genuine TiO_2 acid waste.[283] Peters et al. reported the further purification of such Sc strip liquors using antisolvent crystallisation (ASC) with ethanol to yield > 98.7% pure $(NH_4)_3ScF_6$.[288] It was also reported that the metals are usually present in the solid product in relative proportions that reflect their abundance in the strip liquor.[289] Furthermore, studies on the solubility of $(NH_4)_3ScF_6$ in NH_4F solutions and NH_4F-alcohol mixtures were published.[290] The ammonium metal fluorides of Fe and Al were shown to exhibit considerably lower solubilities than $(NH_4)_3ScF_6$, while $(NH_4)_3ZrF_7$ exhibited comparable solubility to $(NH_4)_3ScF_6$, in NH_4F-alcohol mixtures.[289] Further studies showed the importance of supersaturation control on the quality of the product crystals and that trade-off exists between product quality and productivity.[291]

However, a discrepancy was found between the dimensions of the prospected Sc recovery route and the volume of waste generated. Therefore, this study aimed to upscale the previously presented seven-stage NF-SX process by treating ~1 m^3 of real TiO_2 acid waste. In addition, the final solid product was synthesised, and the quality was enhanced by ASC. The newly developed procedure was assessed in terms of the material and energy costs required to produce 1 kg ScF_3 as the closest marketable product in the Sc supply chain.

4.3 Materials and Methods

4.3.1 Chemicals and materials

Acid waste was obtained from a TiO_2 producer in the Netherlands. NaOH solution (30% w/w) for pH adjustment was provided by Getec Park.Swiss, Switzerland.
HCl (37% w/w, laboratory grade, PANREAC QUIMICA S.L.U., Spain), NH_4F (reagent grade, Merck, Germany), D2EHPA (Lanxess, Germany), N1923 (HalloChem, China) and dearomatised kerosene

(Exxsol D80, ExxonMobile, Germany) were used for SX. Analytical-grade ethanol (99.95% v/v) for the ASC experiments was purchased from VWR, Sweden.

4.3.2 Analytical methods

4.3.2.1 Triple quadrupole inductively coupled plasma mass spectrometry (QqQ-ICP-MS)

Samples were diluted using nitric acid (3% w/w) and an autodilution system (Simprep, Teledyne Cetac Technologies, USA). Thereafter, they were analysed using QqQ-ICP-MS. The analysis was performed on an 8800 QqQ-ICP-MS system (Agilent, Switzerland) using general-purpose operational settings. Quantification was performed via multi-element standards (0-50 ppb, seven points). To account for matrix effects, ^{103}Rh was used as the internal standard. To quantify ^{23}Na$^+$, ^{52}Cr$^+$, ^{55}Mn$^+$, ^{56}Fe$^+$, ^{60}Ni$^+$, ^{66}Zn$^+$, ^{89}Y$^+$, ^{137}Ba$^+$, ^{139}La$^+$, ^{140}Ce$^+$, ^{141}Pr$^+$, ^{146}Nd$^+$, ^{147}Sm$^+$, ^{153}Eu$^+$, ^{157}Gd$^+$, ^{159}Tb$^+$, ^{163}Dy$^+$, ^{165}Ho$^+$, ^{166}Er$^+$, ^{169}Tm$^+$, ^{172}Yb$^+$, ^{208}Pb$^+$, ^{232}Th, and ^{238}U$^+$, the ICP-MS was operated in single-quad mode using helium as collision gas. Meanwhile, ^{24}Mg$^+$, ^{27}Al$^+$, ^{39}K$^+$, ^{45}Sc$^+$, ^{47}Ti$^+$, ^{51}V$^+$ and ^{90}Zr$^+$ were measured in triple-quad mass-shift mode using O$_2$ as a reaction gas. ^{7}Li$^+$ concentration was determined using no-gas single-quad mode.

4.3.2.2 Inductively coupled plasma optical emission spectrometry (ICP-OES)

Element concentrations in the ASC tests were analysed by ICP-OES (iCAP 7400, Thermo Fisher Scientific Inc., USA). Supernatant samples were withdrawn and filtered (0.2 μm, polypropylene syringe filters) prior to dilution. HNO$_3$ (3.45% v/v) was used for dilution.

4.3.2.3 Powder X-ray diffraction (XRD) and scanning electron microscopy (SEM)

Powder XRD spectra were recorded on a Siemens D5000 (Siemens AG, Germany) to examine the crystalline phases of the product. Micrographs were captured via SEM using a Philips/FEI-XL 30 series environmental scanning electron microscope (Philips, The Netherlands) to assess crystal size and morphology.

4.3.3 Neutralisation

An intermediate bulk container (IBC, 1 m^3 volume) was equipped with an agitator (SR6, Simix, Germany) and NaOH dosing pumps (Vantage 5000, Verder, Germany). An exhaust air connection (Figure S9.6, Annex) was used for pH adjustment. The pH and temperature were measured using an inline sensor (Aquastick, Thermo Fisher Scientific Inc., The Netherlands). Caustic soda (30% w/w, 150 L) was successively added to the acid waste (800 L) under stirring until pH 1.5 was reached. The reaction mixture (950 L) was stirred for 24 h before settling for 48 h.

4.3.4 Microfiltration (MF)

MF was carried out using a bag filtration unit (2-EF6-F, Eurowater, Germany; Figure S9.6, Annex) with two filtration bags (size 2, polypropylene, 1 μm nominal removal rate, 17 L volume). The filtration unit was fed by emptying the precipitation tank from top to bottom using a dip tube and a peri-

staltic pump (Vantage 5000, Verder, Germany) with a variable flow rate until the pressure reached 2 bar. Afterwards, pressurised air (4 bar) was applied to further dewater the filter cake. The filter bags were emptied periodically (after 8, 15, 20 and 23 h) and reused until the filtration of the batch was completed. In total, 700 L filtrate was separated from 250 L hydroxide sludge.

4.3.5   Ultrafiltration (UF) and NF

Both UF and NF were carried out in cross-flow operation mode using a modified filtration system (Osmo Inspector, Convergence, The Netherlands; Figure S9.6, Annex). For UF, 1812 spiral wound elements (UP150, Microdyn-Nadir, Germany, membrane area: 0.23 m^2, MWCO: 150 kDa) were used. For batch UF (500 L), a transmembrane pressure (TMP) of 5–20 bar was applied at a cross-flow rate of 8 L min^{-1} and T of 25 °C. The UF was stopped after 80% permeate recovery (400 L). A 2540 spiral wound element (NanoPro A-3014, AMS Technologies, Israel; membrane area: 1.6 m^2, MWCO: 400 Da) was used for NF. Prior to use, the module was compacted overnight by filtrating water (TMP: 15 bar, cross-flow rate: 8 L min^{-1}, T: 25 °C). NF was operated in batch mode, aiming for a permeate recovery of 60%. The TMP was kept constant at 35 bar at a cross-flow rate of 8 L min^{-1}. In total, 250 L was filtrated in five batches (50 L each) using the same membrane module without in-termediate washing (Figure 3). Approximately 100 L of dark green concentrate was obtained after NF. Equations for calculating the concentration factor (*X*), element (M) retention (R_M), permeate flux ($J_{permeate}$) and specific energy consumption (SEC) are given in Annex 9.3.

4.3.6   Solvent extraction

SX was conducted with NF concentrate (100 L) in continuous counter-current operation using 12 PVDF MEAB MSU-0.5 mixer-settler units (MEAB Chemie Technik GmbH, Germany) connected in series (Figure S9.7, Annex). The active mixer volume of the MSU-0.5 was 0.12 L, while the settler volume was 0.48 L with a loading surface area of 0.006 m^2. The number of stages in each process step (extraction, scrubbing and stripping) was determined by constructing the McCabe-Thile dia-grams. Therefore, the respective solutions in each step were contacted with the organic solution with different phase ratios to obtain the equilibrium loading, scrubbing and stripping curves (Figure 4.4). To minimise Fe co-extraction, Fe^0 (1.5 g per litre) was added to the NF concentrate in a separate tank, reducing any Fe^{3+} to Fe^{2+}. Afterwards, Sc was extracted using 0.2 mol·L^{-1} D2EHPA with 0.05 mol L^{-1} N1923 in D80 kerosene with a phase ratio of 4 (aqueous:organic). Co-extracted impurities in the loaded organic were scrubbed with HCl (4 mol L^{-1}) with a phase ratio of 0.1. The scrub liquor was recycled into the SX feed solution to eliminate Sc losses and control the pH for better Sc selectivity during SX. To remove entrained acid in the organic phase, which could lead to HF formation during stripping with NH$_4$F, scrubbed organic was washed with NaCl solution (2% w/w) with a phase ratio of 0.1. For Sc stripping, NH$_4$F solution (3 mol L^{-1}) was added to the washed organic with a phase ratio of 0.33, yielding an (NH$_4$)$_3$ScF$_6$ solution. Finally, the organic was made to

come in contact with HCl (2 mol L^{-1}) with a 0.1 phase ratio to recondition the stripped organic phase and neutralise deprotonated D2EHPA.

4.3.7   Antisolvent crystallisation

A strip liquor (pH= 5.74) after SX and stripping with NH$_4$F solution (3 mol L^{-1}) was used for the ASC tests. All tests were conducted in triplicate. To examine the Sc precipitation efficiency, ethanol (99.95%) was added all at once to aliquots of the strip liquor to reach final concentrations of 2, 4, 6, and 8 mol L^{-1}, which corresponded to ethanol:strip liquor volumetric ratios of approximately 0.13, 0.31, 0.54, and 0.88, respectively. In addition, the precipitation efficiency of the other elements was examined at an ethanol concentration of 8 mol L^{-1}. After ethanol addition, all suspensions were agitated at 500 rpm using a magnetic stirrer under ambient conditions for 1 h. The solid material obtained after crystallisation at 8 mol L^{-1} ethanol concentration was dried overnight under ambient conditions and used for further analysis.

4.4   Results and Discussion

4.4.1   Process flow scheme
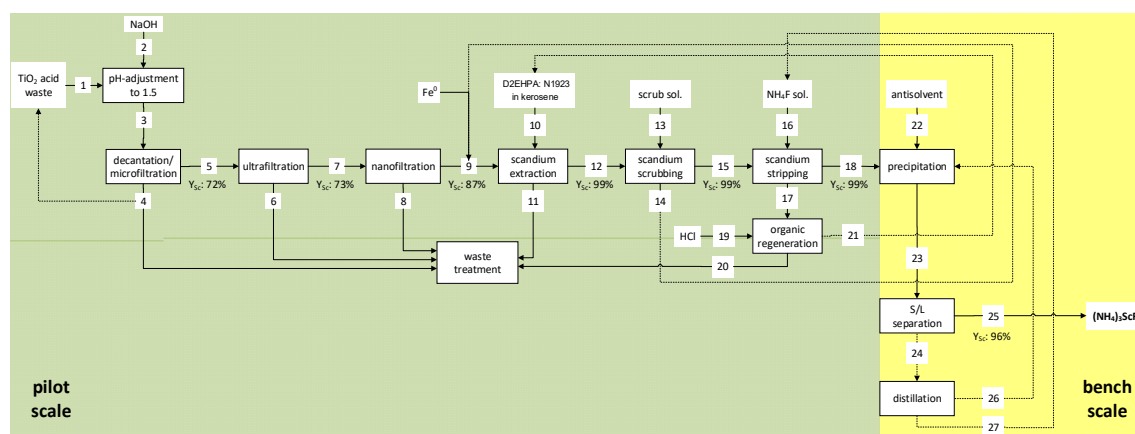
Figure 4.1 Block flow diagram of the scandium recovery process.

The process (Figure 4.1) was based on previous studies and comprised nine stages, excluding organic regeneration and final waste treatment.[283,288] The first four stages (pH adjustment to NF) are summarised under the term 'advanced filtration' (AF). Stages five to seven (Sc extraction, scrubbing and stripping) are named SX. The last two stages (precipitation and S/L separation) are summarised under ASC. While AF and SX were tested on a pilot scale, ASC was conducted on a bench scale to optimise the parameters for recovering Sc from the strip liquor (Figure 4.1).

Table 4.1 Mass balance of the Sc recovery process based on 100 L of NF concentrate. Stream numbers refer to the steps defined previously (details in Figure 4.1), with the key streams being the acid waste (1), the NF concentrate (9), the SX raffinate (11), the strip liquor (18) and the crystallised $(NH_4)_3ScF_6$ product (25).

Process step		pH-adjustment			Microfiltration		Ultrafiltration		Nanofiltration		Sc extraction			Sc scrubbing			Sc stripping			Precipitation & S/L Separation	
Stream No.		1	2	3	4	5	6	7	8	9	10	11	12	13	14	15	16	17	18	24	25
Volume [L]		357	67	424	112	313	63	250	150	100	25	100	25	2.5	2.5	25	10	25	10	10	0.01
Sc	Amount [g]	29 ± 1	-	-	8.5 ± 0.2	21 ± 1	6.1 ± 0.3	15 ± 1	1.9 ± 0.3	13.0 ± 0.4	-	0.10 ± 0.01	13 ± 1	-	0.005 ± 0.001	13 ± 1	-	0.10 ± 0.01	12.7 ± 0.4	0.500 ± 0.002	12.6 ± 0.16
	Yield* [-]	-	-	-	0.29	0.72	0.29	0.73	0.13	0.89	-	0.01	1.00	-	0.00	1.00	0.00	0.01	0.98	0.04	0.96
Ti	Amount [g]	1900 ± 50			1600 ± 50	200 ± 10	200 ± 10	1.1 ± 0.1	0.4 ± 0.1	0.6 ± 0.1	-	0.4 ± 0.1	0.03 ± 0.01	-	0.006 ± 0.001	0.020 ± 0.002	-	n.d.	0.1 ± 0.1	0.110 ± 0.003	0.00 ± 0.01
	Yield* [-]	-	-	-	0.89	0.11	>0.99	0.01	0.32	0.58	-	0.67	0.05	-	0.20	0.67	0.00	0.00	5.00	1.00	0.00
Fe	Amount [g]	11300 ± 300			2100 ± 100	9000 ± 500	1700 ± 50	6300 ± 100	3500 ± 200	2900 ± 100	-	2200 ± 200	64 ± 9	-	n.d.	1.4 ± 0.3	-	n.d.	0.17 ± 0.05	0.110 ± 0.001	0.02 ± 0.01
	Yield* [-]	-	-	-	0.19	0.81	0.29	0.7	0.55	0.46	-	0.76	0.02	-	0.00	0.02	0.00	0.00	0.12	0.85	0.15
Zr	Amount [g]	720 ± 30			740 ± 30	100 ± 5	89 ± 4	0.11 ± 0.01	0	0.11 ± 0.01	-	0.01 ± 0.01	0.12 ± 0.03	-	0.02 ± 0.01	0.11 ± 0.01	-	0.02 ± 0.01	0.09 ± 0.04	0.020 ± 0.001	0.080 ± 0.003
	Yield* [-]	-	-	-	0.88	0.12	>0.99	0.001	0	100	-	0.09	1.09	-	0.17	0.92	0.00	0.18	0.82	0.20	0.80
Th	Amount [g]	41 ± 1			39 ± 4	8 ± 1	5 ± 1	2 ± 1	0.03 ± 0.01	1.9 ± 0.2	-	0.2 ± 0.03	1.7 ± 0.4	-	0.05 ± 0.03	1.8 ± 0.5	-	0.2 ± 0.1	0.4 ± 0.1	0.020 ± 0.001	0.210 ± 0.006
	Yield* [-]	-	-	-	0.83	0.17	0.78	0.22	0.01	1.07	-	0.11	0.89	-	0.03	1.06	0.00	0.11	0.22	0.09	0.91
U	Amount [g]	9.3 ± 0.2			9 ± 1	1.2 ± 0.2	1.9 ± 0.2	0.97 ± 0.03	0.71 ± 0.02	0.24 ± 0.01	-	n.d.	0.20 ± 0.05	-	0.02 ± 0.01	0.19 ± 0.04	-	n.d.	0.18 ± 0.03	0.080 ± 0.005	0.150 ± 0.007
	Yield* [-]	-	-	-	0.88	0.12	0.22	0.78	0.73	0.24	-	0.00	0.83	-	0.10	0.95	0.00	0.00	0.95	0.36	0.64
V	Amount [g]	725 ± 8	-	-	160 ± 10	520 ± 20	110 ± 2	368 ± 7	193 ± 9	178 ± 5	-	140 ± 10	10 ± 2	-	9 ± 2	1.1 ± 0.3	-	0.3 ± 0.1	0.6 ± 0.1	0.280 ± 0.003	0.32 ± 0.01
	Yield* [-]	-	-	-	0.22	0.72	0.21	0.71	0.53	0.48	-	0.79	0.06	-	0.90	0.11	0.00	0.27	0.55	0.47	0.53
Al	Amount [g]	1710 ± 70			480 ± 60	1410 ± 70	280 ± 10	910 ± 40	192 ± 7	900 ± 40	-	710 ± 20	22 ± 3	-	21 ± 2	0.3 ± 0.1	-	0.2 ± 0.1	0.09 ± 0.02	0.40 ± 0.02	0.10 ± 0.05
	Yield* [-]	-	-	-	0.28	0.82	0.20	0.64	0.21	0.99	-	0.79	0.02	-	0.95	0.01	0.00	0.67	0.30	0.80	0.20

* Yield per stage was calculated based on inputs from the direct upstream.

From the acid waste (stream 1), 12.6 g of Sc (43%) was recovered in the form of $(NH_4)_3ScF_6$ (stream 25; Table 4.1). The total recovery yield after nine stages was higher than previously reported for bench scale tests (36%, six stages)[283], but still comparably lower than reported in other studies, such as Zhou et al. (68.6%)[260], Chen et al. (90.34%)[146], Zhou et al. (95%)[135,261]. Major losses occurred in the early stages of AF (streams 1 to 9) within this study. Approximately half of the Sc (∼14.6 g) was lost after pH adjustment, MF and UF (streams 1 to 7). In contrast, virtually no losses occurred during SX (streams 9 to 18) and just minute amounts of Sc were lost (0.4 g, 3%) during ASC (streams 18 to 25). Therefore, considering the stages from NF to ASC, ∼84% yield was achieved (six stages, streams 7 to 25). Moreover, with respect to the latest five stages only (SX to ASC, streams 9 to 25), ∼97% Sc yield was reached. Thus, while the yield of MF and UF leaves room for improvement, the yield of the other process stages was on par with the aforementioned studies.

4.4.2   Advanced filtration

4.4.2.1 Precipitation and removal of interfering metals
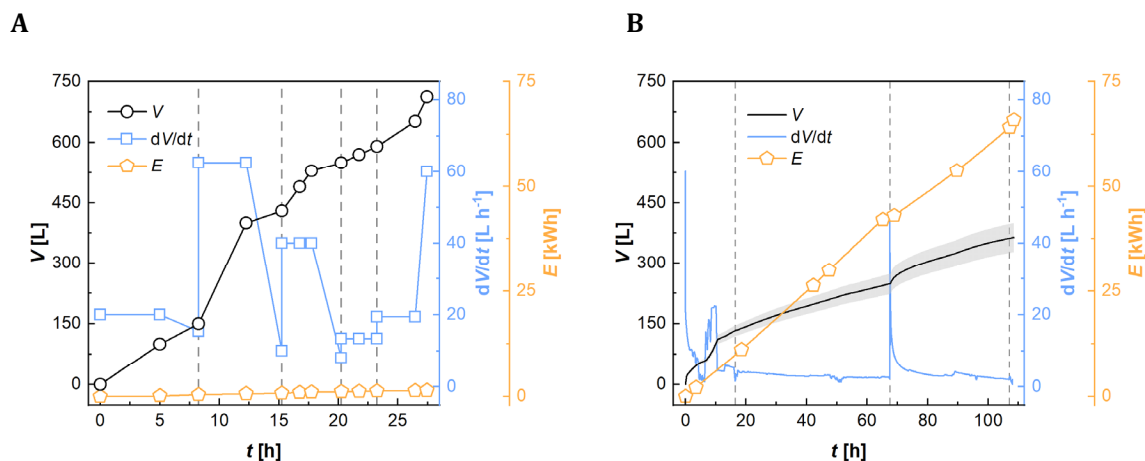
Figure 4.2 Volume of filtrate generated, flow rate and energy consumption during microfiltration (A) and ultrafiltration (B). The grey dashed lines indicate the exchange of filter bags/ultrafiltration membranes.

The received TiO_2 acid waste contained Sc (∼81 mg L^{-1}) and more than 30 other elements up to multiple grams per litre (Table 4.1). Some of these elements disturb SX but precipitate at pH 1.5, while the majority of Sc is preserved in the solution.[256,283]

After pH adjustment and MF, the majority of Sc (72%) remained in the filtrate (stream 5, Table 4.1). This result was higher than during the bench scale tests, where only 56% of the Sc was preserved.[283] Regarding the impurities, similar to the bench scale tests[283], with the hydroxide sludge (∼250 L, stream 4), interfering elements were effectively removed (Ti: 88%, Zr: 88%, Nb 88%, U: 88%, Th: 83%). S/L separation worked slightly better on the pilot scale, yielding 74% filtrate recovery in comparison to 69% during the bench-scale experiments.[283]

The ratio between sludge and bag filter volume changed disproportionately during upscaling. In the bench-scale tests, 1 L sludge was removed using a bag filter of 1.9 L volume (ratio of 0.53).[283] In the pilot phase, 250 L of sludge (stream 4) was separated using two bag filters of 17 L each (ratio of 7.4). As a result, the bag filters had to be emptied multiple times. The precipitate was allowed to settle for over 48 h, and the reactor was drained from top to bottom to prevent premature filter clogging. This strategy succeeded, as reflected in the initially higher filtration rates and longer operating intervals before the discharge of the filter cake than at the end of filtration (Figure 4.2A). However, the start-up phase (0–8 h) was exceptional, as the pump speed and immersion depth of the dip tube were not optimal, resulting in a low filtration rate and filter clogging after 150 L of filtrate was produced (Figure 4.2A).

Only a thickened sludge was obtained with no fully dewatered filter cake after MF. Therefore, the hygroscopic nature of the precipitated hydroxides impeded S/L separation. Flushing with pressurised air helped recover more filtrate but did not represent a satisfactory solution for continuous production. A plate filter press could help optimise the filtrate yield through higher compression and ease the procedure through automated discharge of the separated precipitate.[292]

The obtained filtrate was still partially turbid, being especially visible after filter exchange. This could be due to the use of extremely coarse filter bags, whereby the particle removal efficiency is usually low before the build-up of a filter cake. Felt bags with a nominal filter rating of 1 μm were used in this process. This means that particles of 1 μm and larger are retained but to an undefined percentage, as indicated by the manufacturer.[293,294] For future tests, filtration materials with 1 μm absolute rating (i.e. assured removal rate of > 99% for particulates of ≥ 1 μm) could achieve a better separation result.

SEC for MF was ∼2.1 kWh m^{-3} of filtrate (Figure 4.2A), similar to the SECs reported for the MF of slurries, such as using a rotating MF (4 kWh m^{-3}).[295]

Following MF, the filtrate was further clarified using UF. In this process, a 0.4 m^3 ultrafiltrate (stream 7) was obtained, containing 73% of the Sc from the 0.5 m^3 MF permeate (stream 5) (Table 4.1, Figure 4.2B). Multiple elements were effectively removed with the residual suspended particles, including Ti (> 99%), Zr (> 99%), Nb (> 99%) and Th (78%) (Table 4.1).

Directly after the deployment of new spiral wound elements, high filtration rates (40–60 L h^{-1}/170–260 L m^{-2} h^{-1}) were observed during UF. However, these rates decreased to < 10% of their initial value within 5 h of operation. Rinsing with diluted hydrochloric acid did not restore permeability (tested after 16 and 107 h). After ∼109 h, 80% permeate recovery was achieved, and UF was stopped because the feed had considerably thickened and the permeate flow had irreversibly decreased to below 2 L h^{-1}.

Owing to the low filtration rate (average 3.6 L h^{-1}/16 L m^{-2} h^{-1}), the SEC for permeate production was high, eventually reaching 165 kWh m^{-3}. Despite taking the challenging nature of the feed into account, the SEC appears to be at least an order of magnitude higher than the typical values report-

ed for UF.[296,297] Apparently, the spiral wound elements were rapidly clogged, which drastically affected their performance. Nevertheless, the UF was continued to provide feed for downstream NF experiments. This approach, however, was not cost-effective. High particle loading in the UF feed should be avoided through better S/L separation upstream of the UF to improve the operation. In this regard, employing a filter press (as used at the TiO$_2$ manufacturing facility) or drum centrifugation would be recommended.[298] In addition, different membrane designs could ease cleanability, allowing the recovery of lost permeability, thereby keeping the filtration rates high and increasing membrane lifespan. In this process, capillary or tubular membrane elements should be tested.[292,299] If the permeate flux is kept in the measured starting range of 170–260 L m^{-2} h^{-1}, the SEC can be reduced by up to 95%. The suggested changes for MF and UF should result in higher Sc yields (currently 53%, three stages), thereby boosting the overall process efficiency.

4.4.2.2 NF
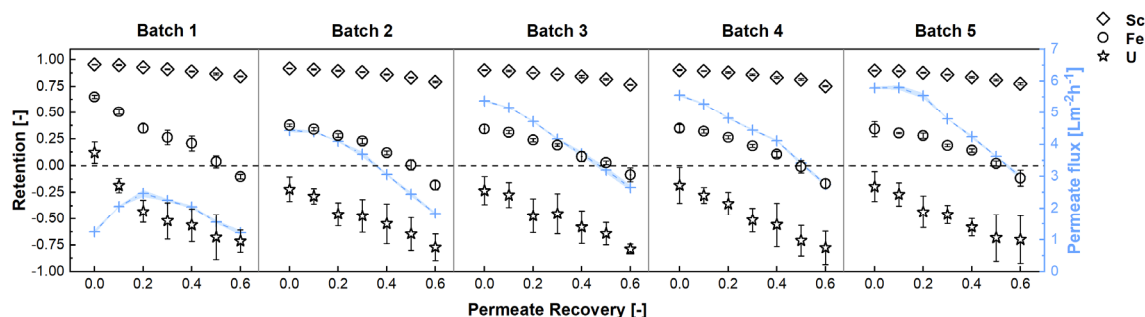
Figure 4.3 Element retentions and permeate fluxes during the five batches (each 50 L) of nanofiltration.

The pilot NF was based on bench-scale tests, aiming for 60% permeate recovery (i.e. a final concentration factor of 2.5 (Equation S1, Annex).[283] The targeted amount of NF concentrate (100 L) was set to allow downstream pilot SX. Thus, five batches of ultrafiltrate (50 L each) were concentrated with the same 2540 spiral wound membrane elements.

Sc retention during the pilot experiments was similar to that of the bench scale tests.[283] Starting at 0.96, a slight decrease to 0.85 after 2.5-fold concentration was observed in the first batch (Figure 4.3). Sc retention was slightly lower in batch two, with initial and final values of 0.92 and 0.79, respectively (Figure 4.3). The retention in batches three to five seemed to have reached constant values, being in each case initially 0.90 and 0.76 after 60% permeate recovery (Figure 4.3). The measured Sc retention over the whole NF and all batches combined was 0.90, leading to a total Sc recovery yield of 87% (stream 9, Table 4.1), which was slightly higher than that reported for the bench-scale tests (84%).[283] Overall, the Sc concentration was increased by a factor of ~2.2 (from 60 mg L^{-1} to 130 mg L^{-1}; Table 4.1).

Some impurities were successfully depleted by NF, such as Fe (-55%), V (-53%) or U (-73%) (Table 4.1). For instance, Fe retention was > 0.60 at the beginning of batch one and drastically decreased over the course of the NF, reaching negative values (Figure 4.3), that is, the permeate concentration

was higher than the concentration in the retentate. From batch two onwards, the initial Fe retention was < 0.40 and showed a falling trend during NF (Figure 4.3). The mean Fe retention over the entire NF stage was only ~20%. Overall, the Sc over Fe selectivity (i.e. the ratio of R_{Sc}/R_{Fe}) was exceptionally high, reaching a mean of 4.5, whereas the bench-scale test reached a maximum of 2.7.[283]

Apart from Fe, U retention was remarkably low and constantly negative throughout the NF, except for the very first recorded value in batch one. The extremely high U permeability was reflected in an average retention of -0.97 and a yield of only 24% in the NF concentrate. This behaviour was only matched by monovalent cations, such as Na+, reaching an average retention of -0.72 and a final yield of 29% in the NF concentrate. The U retention found is in line with the results of Remmen et al..[256] One explanation could be the speciation of U in chloride-rich acidic environments, that is, the presence of monovalent or uncharged complexes. This finding was confirmed by EXAFS measurements showing the presence of chloro-uranyl complexes, such as $UO_2(H_2O)_xCl^+$ and $UO_2(H_2O)_xCl_2$, at HCl concentrations of $\geq$ 4 mol L^{-1}.[300] For future recovery of U from complex streams, where co-extraction represents a challenge in SX, the aforementioned phenomenon in NF could be leveraged as a U pre-separation step.

A steady increase in permeate flow during Sc concentration was observed from batch one to batch five (Figure 4.3). Except for the first batch, the permeate flow started at its highest value and declined as the feed concentration advanced. However, the permeate flux in the first batch started low (1.25 ± 0.05 L m^{-2} h^{-1}), subsequently increased (2.5 ± 0.1 L m^{-2} h^{-1} at 20% permeate recovery) and then decreased again (1.22 ± 0.07 L m^{-2} h^{-1} at 60% permeate recovery) (Figure 4.3). This 'parabolic' behaviour was not previously observed in bench-scale tests. One explanation might be the five times larger membrane area in the pilot trials, which would have required a longer swelling time initially.[301]

During the bench-scale tests, membranes were only used once for the concentration experiments. As shown in this process, reusing was beneficial in terms of permeate flux and Sc selectivity over several impurities, such as Fe, V or U (Figure 4.3). The behaviour is in agreement with previous studies showing that acid soaking may result in higher permeability of polyethyleneimine-coated thin film composite membranes.[302,303] Although not disclosed, AMS patents suggest a comparable active layer in the NanoPro A-3014 membrane.[304,305] In addition, despite the higher permeate flux in batches three to five, no higher element retention was observed (Figure 4.3), indicating that the ion flux increased proportionally to the water flux (convective flow). Lopez et al. observed a similar behaviour when testing NF for rare earth element recovery from acidic solutions and interpreted it as a sign of increased pore size caused by degradation.[156] In contrast to the aforementioned study, an especially acid-resistant NF membrane was used in our study to withstand HCl exposure. Although partial membrane degradation cannot be excluded, the similarity of element retentions and permeate fluxes in batches three to five indicates the NanoPro A-3014's primary suitability for the

application (Figure 4.3). Therefore, the membrane can be further reused. Based on the results, longer membrane equilibration prior to NF should be considered for future Sc recovery.

The production of 2.5-fold concentrated acid waste through NF took 31 h (310 h m^{-3}). The increase in permeate flow rate (average batch one: 1.8 L m^{-2} h^{-1}; average batch five: 4.7 L m^{-2} h^{-1}) resulted in decreased operating time with each batch. Furthermore, the energy consumption rate was almost constant during the entire NF (1 kWh h^{-1}). Accordingly, the respective energy cost decreased with each batch due to the accelerating filtration rate. The mean SEC for concentrate production was 327 and 265 kWh m^{-3}, considering only the last three batches (both referring to concentrate volume). The key to the high energy demand of NF was the low permeate flux (max. 5.8 L m^{-2} h^{-1} at 35 bar TMP). The use of RO or NF with small membrane permeability has already been reported (e.g. in the field of acid purification).[172] However, SEC needs to be optimised to improve process profitability for future applications. In this process, highly permeable LbL- membranes could be of interest as soon as more stable products suitable for highly concentrated streams become commercially available.[256] The minimisation of the cross-flow rate could be an option in the case of the NanoPro A-3014. A reduction is possible as long as permeate flux and Sc retention are not impaired[306] and no scaling occurs (unlikely at pH 1.5). Moreover, the energy demand per membrane area can be decreased by further upscaling the system.[307] For example, a pump delivering 10 times the flow would consume proportionally more energy but could feed an 8040 element that has 15 times the membrane area of a 2540 element.[272,308,309] Consequently, SEC could be cut by a third. Furthermore, a smaller spacer (31 mil instead of 46 mil) could increase the membrane area per element, specifically by 25%, in the case of 8040 elements.[308] Finally, the implementation of energy recovery devices, such as Pelton turbines, could recover 30–40% of the total energy.[310,311] These adjustments could result in 70% savings in SEC.

In summary, the pilot NF performed better than the bench scale, recovering more Sc with better selectivity and demonstrating that membrane reuse does not only reduce investment costs but also improves Sc selectivity and operating speed. The high SEC calls for membrane and system optimisation, providing a starting point for future efforts.

4.4.3 Solvent extraction

A   **B**   **C**
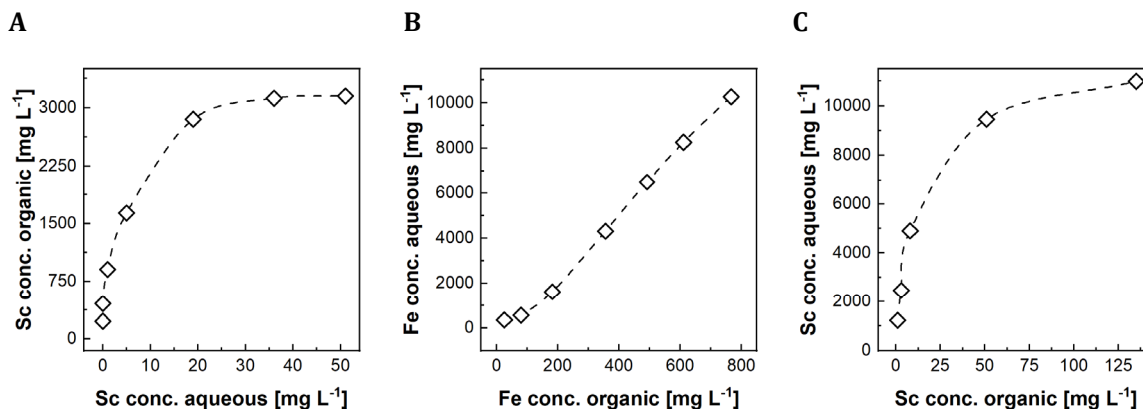
Figure 4.4 Equilibrium diagrams for loading (A), scrubbing (B) and stripping (C) of Sc using 0.2 mol L^{-1} D2EHPA with 0.05 mol L^{-1} N1923 in D80 kerosene at the bench scale.

Table 4.2 Average phase separation speed in each step of SX.

Process step	Separation Speed [m h^{-1}]
Extraction	3.4
Scrubbing	2.6
Washing	14.8
Stripping	10.8
Conditioning	3.9

As previously reported, a synergistic mixture of D2EHPA and N1923 reduces the co-extraction of impurities, such as V and Fe, in the SX circuit.[283] Based on this, 0.2 mol L^{-1} D2EHPA with 0.05 mol L^{-1} N1923 in D80 kerosene was used as the organic solution for the pilot testing. The equilibria for Sc loading, scrubbing and stripping were determined on a bench scale prior to the pilot experiments (Figure 4.4). A maximum loading of 3 g L^{-1} was observed during the laboratory investigations (Figure 4.4A). However, worse separation behaviour was observed beyond the Sc loading of 1.5 g L^{-1}. The organic started foaming, slowing down phase separation due to high Sc loading, which ultimately prevented continuous processing at this loading level. Therefore, Sc loading was chosen between 0.5–0.7 g L^{-1}, eliminating phase separation issues and yielding fast separation. Based on the equilibrium loading diagram, full Sc loading required two stages of extraction (Figure 4.4A).

In terms of scrubbing behaviour, using HCl (4 mol L^{-1}) in 3–4 scrubbing stages resulted in the effective removal of the co-extracted Fe from the loaded organic (Figure 4.4B). In addition, D2EHPA showed considerably higher affinity to Fe^{3+} than to Fe^{2+}, wherefore the addition of Fe^0 suppressed Fe co-extraction by reducing Fe^{3+}.[283] As such, Fe^0 was added to the NF concentrate before the loading stage. The scrub liquor (i.e. spent HCl after scrubbing) was recycled into the loading feed solution to eliminate Sc losses and lower the solution pH, thereby suppressing Fe^{2+} co-extraction.

Investigations on Sc stripping equilibrium (Figure 4.4C) confirmed the effectiveness of NH_4F (3 mol L^{-1}). Complete Sc stripping was achieved in most cases. However, the solubility limit of $(NH_4)_3ScF_6$ (~7.5 g L^{-1})[290] at Sc concentrations above 2 g L^{-1} was exceeded, leading to crystallisation. Since solid precipitate could harm the SX process by forming cruds and inseparable phases, causing organic losses, a final Sc concentration of 1.0–1.5 g L^{-1} was targeted for the strip liquor. Based on the equilibrium data, four stages of stripping were required for effective Sc stripping (Figure 4.4C).

The settling behaviour in each SX step was investigated, and the separation speeds of the aqueous and organic solutions were calculated (Table 4.2). In all cases, separation speeds exceeded 2 m h^{-1}, implying rapid, successful separations (Table 4.2). Moreover, both mixing modes (aqueous or organic phase as the dispersant) were tested. However, no impact on separation behaviour was observed. Generally, no phase separation problems occurred in the pilot SX tests.

The processing of the entire NF concentrate (100 L) lasted for 17 h. The pilot SX worked efficiently with only minute Sc losses, reaching a yield of ~98% (three stages) and a tenfold increase of Sc concentration in the strip liquor (~1.27 ± 0.04 g L^{-1}; stream 18, Table 4.1). Impurities in the product included V, Th, U and Fe (Table 4.1). Despite the removal of most Fe, minute amounts were still present in the strip liquor, probably due to the spontaneous oxidation of Fe^{2+} to Fe^{3+} during the continuous operation. To prevent this occurrence in the future, sealed mixer-separator units could be used instead of running the SX in an open atmosphere. Although only traces of Th and U were observed in the NF concentrate, they were almost inseparable from Sc in SX. Therefore, 75% of U and 21% of Th ended up in the strip liquor. Notably, the mass balance for Th after stripping did not add up, and 67% of the total extracted Th was neither measured in the stripped organic nor in the strip liquor. Insoluble Th complexes possibly formed after NH_4F addition and precipitated without being noticed in the pilot unit. In the case of V, co-extraction was well suppressed by the use of N1923 as co-extractant, leading to only 6% co-extraction (Table 1). In the scrubbing stage, 90% of the extracted V was removed (Table 4.1). The 0.3% (i.e. 0.6 g) initial V that was eventually stripped still made it a major impurity in the strip liquor due to its high starting concentration (Table 4.1). In total, approximately 90% Sc purity was reached, which was below par with the previously reported bench scale result of 97%.[283] Although the entire NF concentrate was processed, the SX process had probably not yet reached its equilibrium. Supposedly, higher purities can be attained in a longer continuous operation. During the pilot trials, the purity levels in the samples collected increased as the SX process continued.

4.4.4   Anti-solvent crystallisation

A

B

C
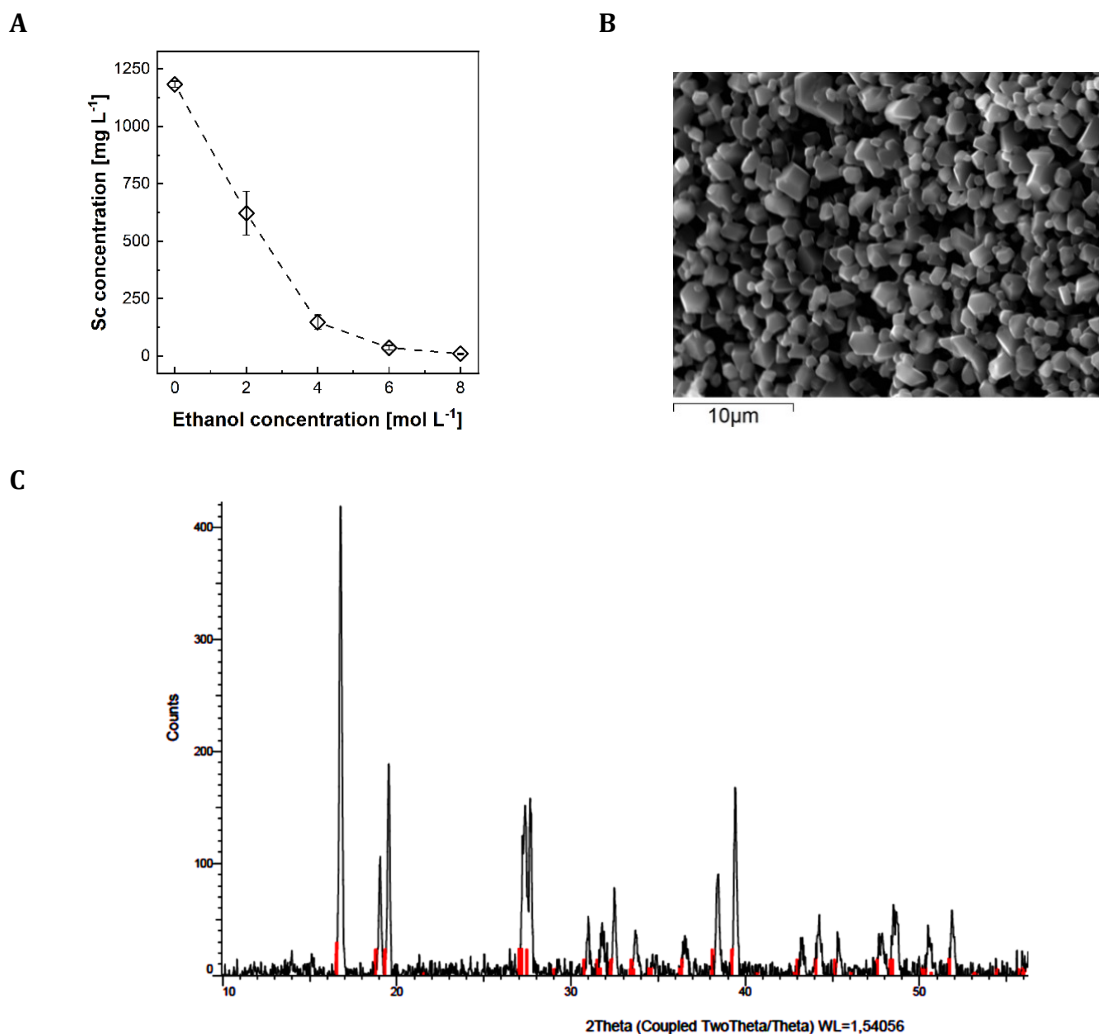
Figure 4.5 Solution concentration profile for Sc (A), SEM micrograph of the solid obtained at 8 mol L^{-1} ethanol (B) and XRD pattern of the solid product obtained at 8 mol L^{-1} (C). The red lines are the reference pattern for $(NH_4)_3ScF_6$ of monoclinic-structure PDF card 00-040-0595 (C).

Sc crystallisation started quickly after the addition of ethanol to the strip liquor. The amount of precipitated Sc asymptotically approached a scandium recovery of > 95 % with increasing ethanol concentration (Figure 4.5). A concentration of 8 mol L^{-1} appeared optimal to maximise Sc recovery with a yield of 96% (Table 4.1).

After instantaneous antisolvent addition (8 mol L^{-1}), discrete, regular-shaped crystals with an average size of approximately 1–2 μm were obtained, as seen in the SEM image (Figure 4.5B). The mean size and size distribution of the crystal product can be controlled by seeding and supersaturation control.[291] Powder XRD measurements identified the obtained solids as predominantly $(NH_4)_3ScF_6$ (PDF 00-040-0595; Figure 4.5C) The peaks of other ammonium metal fluorides, such as Zr, V, Al or Fe, which were present in the strip liquor could not be detected. This could indicate low concentrations in the solid material but may also be attributed to similar peak positions of most ammonium metal fluorides.

Element concentrations were also measured in the strip liquor before and after ASC with 8 mol L^{-1} ethanol (Table 4.1). Based on the results, the solid product's purity was determined to be 93.5% on a metal basis or 95.1% on the basis of ammonium metal fluorides (Table S9.6, Annex; assuming the formation of ammonium metal fluoride complexes for all impurities). Impurities could be incorporated into crystal lattices or adhere to the crystal surfaces without actually precipitating as ammonium metal fluorides. As reported previously, Ti tends to remain solubilised, most likely due to its stable titanyl ion (TiO^{2+}) in the solution.[289] Similar to their abundance in the strip liquor, the major impurities found in the solid product were V, Th and U (ordered by mass fraction; Table 4.1). Furthermore, minute amounts of Al and Zr are present in the solid (Table 4.1). Comparable to SX, the product purity after ASC was below par compared with the previously reported purities of ca. 99%.[288] As previously described, SX was probably further away from its equilibrium than during the bench scale tests, which also negatively affected the downstream ASC. Hence, the easiest solution would be to further optimise Sc selectivity upstream to ASC. This result could also be partly due to the lower initial Sc concentration in the strip liquor than previously reported.[288] Nonetheless, crystallisation in more stages, starting with a lower amount of antisolvent and better control of the supersaturation during crystallisation, could help increase the purity, potentially at the cost of total yield.[289,291,312] Moreover, purification of the product could be achieved through a combination of SX and ion exchange.[135,313]

In terms of ASC process design, the required ethanol amount of 0.88 L per litre strip liquor appeared high. However, the spent ethanol can be distilled and reused in ASC without deterioration of precipitation efficiency. In a previous study, methanol and ethanol recovered through simple distillation with alcohol purities of 75–85% (v/v) showed Sc recovery efficiencies > 97% when reused in ASC.[314] Furthermore, after antisolvent distillation, the spent aqueous solution, which was partially depleted in NH$_4$F, can be reused in the SX stripping stage with adequate make-up (Figure 4.1).

4.4.5 Process flows and production cost assessment

Table 4.3 Energy and material flows and costs to produce 1 kg of ScF$_3$.

Description		AF	SX	ASC	CAL	Total	Sum energy and material costs [€]
Acid waste	[kg]	13'198				13'198	-
Ethanol	[kg]			25		25	6-20
HCl 33%	[kg]		42			42	4-5
NaOH 30%	[kg]	3'160				3'160	230-253
NH$_4$F (3 mol L^{-1})	[kg]		36			36	4
Fe powder	[kg]		5.3			5.3	10-12
Water	[kg]		69			69	0.01
Electricity	[kWh]	2'426	3.7	1.1	0.9	2'432	119-136
Heat	[kWh]			576		576	12
Waste	[kg]	13'198	4'012	42		17'252	-
Total costs	[€]	350-389	18-22	18-31	0.04-0.05	386-442	386-442
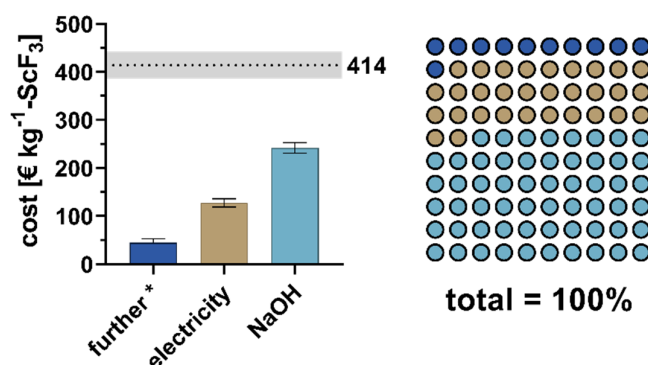
Figure 4.6 Costs for ScF$_3$ production. Bars indicate maximal/minimal assumptions for prices. Note that ethanol, HCl, NH$_4$F, Fe powder, water and heat combined contributed little (11%) to the overall cost and are summarised as 'further'.

The developed process was benchmarked based on the production of 1 kg ScF$_3$ as the marketable product closest to (NH$_4$)$_3$ScF$_6$. As previously reported, (NH$_4$)$_3$ScF$_6$ can be easily converted into ScF$_3$ by calcination.[149] Following previous studies, the conversion of 2.1 kg (NH$_4$)$_3$ScF$_6$ into 1 kg ScF$_3$ was considered with an input of 0.9 kWh electricity (Table 4.3).[315–317] Furthermore, for AF, filter materials, such as the organic phase in SX, were assumed to be fully reusable. For SX and ASC, 90% recyclability of NH$_4$F solution and antisolvent was assumed, respectively. The underlying prices used for assessment are given in Annex (Table S9.7, Annex).

The total input for the production of 1 kg ScF$_3$ from ~13,000 kg AW totalled to ~3,400 kg of materials and ~3,000 kWh of energy consumption (Table 4.3). The generated waste was ~17,300 kg. Giv-

en that the waste is a mix of hydroxides, it could be disposed of similarly to the TiO_2 plant waste treatment.

The total material and energy costs to produce 1 kg ScF_3 were ~414 ± 28 € (Table 4.3, Figure 4.6). United States Geological Survey (2022) reported a price (1–5 g lot size) of US\$216,000 (~216,000 €) per kilogram of ScF_3, which is assumed to be very high.[103] Prices on online portals (e.g. alibaba.com) range between ~721–1546 € kg[1] of ScF_3 (99–99.99% purity; Table S9.7, Annex). Hence, the production costs for ScF_3 determined in this study were considerably lower than the market prices reported.

Among all the process inputs, NaOH had the highest cost share (~58%; Figure 4.6), followed by electricity consumption (~31%; Figure 4.6). All further inputs contributed only 11% to the total costs (Figure 4.6). On the process level, the initial AF step had the major cost share (~89%; Table 4.3). Therefore, process optimisation should target the AF stage first. As previously described, a high optimisation potential for the energy consumption of AF is expected (savings of 95% for UF and 70% for NF). This could reduce the energy consumption by ~2000 kWh kg^{-1} of ScF_3, lowering the production cost by 25% or 110 € kg[-1]. The primary cost driver would still be neutralising with NaOH. The neutralisation, although assigned to the AF stage in this study, is already a part of waste treatment in TiO_2 production. Hence, the actual cost of pH adjustment in AF should be calculated as the difference between the cost for neutralisation with NaOH or with lime/limestone, similar to the current practice. Using $CaO/CaCO_3$ would not be an option in AF, as Ca^{2+} shows considerably higher retention than Na^+ in NF, thereby increasing the osmotic pressure and deteriorating filtration performance. Kapil et al. compared the neutralisation efficiency for different chemicals, revealing a 10% lower consumption of $CaCO_3$ compared with NaOH for reaching the same pH.[318] Thus, considering a slightly lower price per kilogram for limestone than for caustic soda, a treatment with NaOH is expected to cost roughly 20% more (Table S9.7, Annex). This means that the existing TiO_2 production already covers 80% of the neutralisation costs (i.e. ~200 € kg[-1] ScF_3) previously allocated to AF. Therefore, the additional neutralisation cost during AF is estimated to be 50 ± 5 € kg[-1] ScF_3.

In summary, the entire AF would realistically cost around 70 ± 30 € kg[-1] ScF_3, which is approximately 80% lower than the current pilot operation. In this scenario, a total material and energy cost for ScF_3 of 120 ± 40 € kg[-1] is conceivable. The overall process yield (43%, nine stages) could be improved, bearing the potential to cut the production cost in half. The Sc losses during the initial S/L separation (MF and UF) could be easily minimised by exchanging bag filtration with a filter press similar to that used in TiO_2 production.

4.5 Conclusion

This study demonstrated the feasibility of combining AF techniques, SX and ASC to obtain 95% pure $(NH_4)_3ScF_6$ as a close-to-market Sc product from a real TiO_2 acid waste. Major challenges during AF

included the low filtration rates because of small particle size and hygroscopicity of the precipitated hydroxides and the osmotic pressure of the feed. NF improved with the progression of the pilot tests, yielding higher permeate flux and Sc selectivity, which were interpreted as benefits of membrane equilibration. Overall, the process volume was reduced through NF by 60%, with 87% Sc yield and depletion of impurities such as Fe, V and U.

During pilot SX, high separation efficiency for Sc was observed with the previously published process.[283] Phase separation worked rapidly, and tertiary phases did not occur. However, the achieved purity still left room for improvement, calling for longer test runs that allow better process equilibration and a closed system to minimise spontaneous Fe oxidation. In total, a tenfold concentrated Sc liquor (98% yield, three stages) was produced, with minimal co-extraction of competing elements such as Fe or V.

Using strip liquor, the ASC tests indicated the addition of 0.88 v/v ethanol as the best option, delivering the highest Sc yield (96%).

The overall process has the potential to produce ScF_3 at competitive market prices from a European secondary source. Thus, the combination of AF-SX-ASC could boost the supply of Sc, mitigating possible policy-induced shortages in the future.

This page is intentionally left blank.

5 Polymer inclusion membranes for scandium recovery from titania acid waste
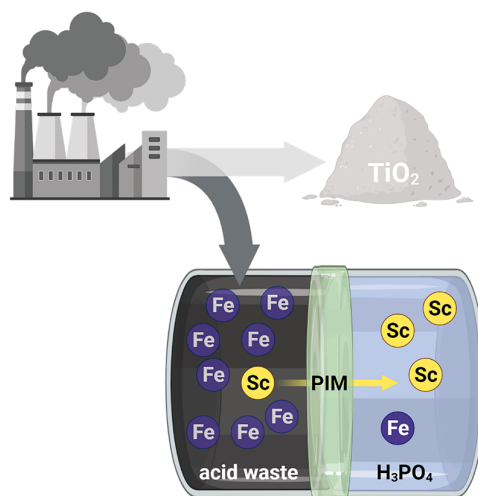
This chapter was published as

S. Hedwig, M. Kraus, M. Amrein, J. Stiehm, E.C. Constable, and M. Lenz, Recovery of scandium from acidic waste solutions by means of polymer inclusion membranes, *Hydrometallurgy* **2022**, *213*, 105916; DOI: 10.1016/j.hydromet.2022.105916

Contribution of Sebastian Hedwig: Conceptualization, Formal Analysis, Investigation, Methodology, Project administration, Supervision, Validation, Visualization, Writing – original draft, Writing – review & editing.

5.1 Abstract

Scandium is a raw material with properties that promise considerable potential for application in alloys to enable aviation fuel savings and as dopants for use in sustainable energy production using solid oxide fuel cells. Despite these attractive properties, scandium is rarely used due to its scarcity and unreliable supply. Therefore, new strategies for scandium recovery are of economic priority. In this study, polymer inclusion membranes (PIMs) consisting of PVDF-HFP, 2-NPOE and DEHPA, were optimised for selective scandium separation from real TiO_2 production waste. With the optimised system, more than 60% of the scandium was recovered with high selectivity, resulting in scandium mole fraction at more than two orders of magnitude higher in the receiving phase than in the original waste. This suggests PIMs may be an effective way to recover scandium from bulk waste, thus easing the scarcity and insecurity that currently limit its bulk application.

5.2 Introduction

In recent decades, many nations have been highly dependent on the import of raw materials, thus creating uncertainty in terms of supply security and price stability.[319] Consequently, a 'raw materials initiative' was launched by the European Union in 2008 to define measures to secure a sustainable and affordable raw material supply for the future.[40,219] One raw material that is considered particularly critical to the EU economy is the rare earth metal scandium (Sc).[40,219] Currently, Sc has two major potential applications: as an alloying metal for aluminium (Al) and as an essential component in solid oxide fuel cells (SOFCs). In aluminium alloys, Sc shows the highest reinforcement increase per atomic percent, making it the most efficient known additive in this regard.[80] In addition, Sc–Al alloys show improved corrosion resistance, fatigue behaviour and weldability. Specialised aerospace alloys such as Scalmalloy®, requiring just ~0.2% (w/w) of Sc, offer weight savings of up to 20% in aircraft.[256] To date, the majority of Sc (90% of annual global production) is used for scandia-stabilised zirconia, a solid electrolyte for SOFCs. This ceramic material exhibits considerably enhanced conductivity and lower operating temperatures than alternatives such as yttrium-stabilised zirconia.[91,320] Thus, the use of Sc can effectively lower operation costs and boost energy conversion efficiency.

Despite high demand, global Sc supply is relatively low (~15–25 t year^{-1} in 2021), resulting in high prices (~US\$4,370,000 t^{-1}; Table S9.8, Annex).[103,321] The average Sc concentration in the Earth's crust is estimated to be 22 ppm (25 g/t), which is comparable to cobalt (25 ppm).[102,322] However, there are no high-concentration primary sources for Sc due to lack of selective affinity for common ore-forming anions. Hence, Sc is found in low concentrations in over 100 minerals and is won only as a by-product of mining other elements.[323] Only very rarely have primary Sc deposits above 100 ppm been reported.[84]

Industrial waste, in particular from the production of white pigment (TiO_2), has been identified as a major secondary source of Sc, due to its ready availability, high volume and (relatively) high Sc concentration.[125,324] The major processes for TiO_2 production, namely the sulfate route and chloride route, account for an annual global production of ~3.7 Mt and 3.3 Mt, respectively.[126] The chloride route is claimed to be superior in terms of energy demand, labour-intensity and waste generation.[121,126] For this, high-grade TiO_2 (>85%) ores are converted into volatile $TiCl_4$ by reaction with coke and elemental chlorine at high temperature (900 – 1000 °C). After purification by fractional distillation of the $TiCl_4$ and reaction with oxygen, pure TiO_2 pigment is obtained.[121] A hydrochloric acid solution is generated as waste during such production. This contains unreacted ore, coke and dissolved metal chlorides and may have major elements such as Ti, Fe and Al and also traces of naturally occurring radionuclides and rare earth elements.[126,256] The Sc concentration in this acidic waste can be as high as 76 – 90 ppm, which is considerably higher than for bauxite leachates.[124,125,256,324] Currently, Sc is lost after neutralisation of the waste and deposition of a hydroxide cake. The production of one ton of TiO_2 generates approximately 0.2 t of filter cake.[124] Annually, the chloride route generates and disposes of ~0.7 Mt of dry waste containing up to 220 t of Sc.[325] To date, few routes for Sc recovery from TiO_2 waste have been investigated.[125,256,326,327] Recently, membrane-based processes using either nanofiltration[256] or polymer inclusion membranes (PIMs) have been proposed.[192,193,206]

Compared to conventional separation technologies such as distillation or solvent extraction (SX), membrane processes offer considerably lower energy and material/chemical consumption.[144,159,256] The role of membrane processes is becoming increasingly important, as they can reduce the energy consumption of large-scale industrial separation processes by up to 90 %.[159] The key to success for a given application is finding suitable membranes that provide high separation selectivity and high throughput/production rates, and there is steadily growing interest in the research and development of new and improved membranes. The PIMs comprise a class of membranes that allow for the selective extraction and transport of a target solute, such as metal ions, from a feed to a receiving phase. In principle, PIMs are dense, hydrophobic thin films that incorporate lipophilic ligands as extraction agents ('carriers'). When brought into contact with an aqueous solution containing metal ions (the feed phase), the carriers may complex these ions and extract them into the membrane phase. Subsequently, the PIM can release the extracted ions by exposure to an aqueous solution (receiving phase) capable of cleaving the previously formed carrier complexes, for example by protonation. These steps are similar to extraction and stripping in SX[139] or adsorption and elution using solvent impregnated resins.[137] In contrast to these conventional approaches, the two-dimensional shape of the PIMs allows single-stage uptake and release of metals. Therefore, the membrane is placed between the feed and the receiving phase. Metals can then be complexed and taken up on the feed side, diffused through the PIM and released on the

opposite side, regenerating the carrier. Thus, transmembrane metal transport is achieved (Figure 1.14).[153]

The development of PIMs can benefit from the knowledge gained on SX, especially concerning the efficiency and selectivity of organic extraction agents towards certain elements.[141]

Recently, Sharaf et al. reported the use of cellulose triacetate–based PIMs for the separation of Sc from five competing lanthanides in nitric acid media at pH 4.[206] The PIMs contained a mixture of mono-2-ethylhexyl (2-ethylhexyl)phosphonate (PC-88A) and decanoic acid as carriers. After optimisation of membrane composition and the receiving phase, they achieved 96.7% Sc transport across the membrane within 96 h of operation. Remarkably, almost no co-transport of competing metals in the model feed was observed.[206] Yoshida et al. (2019) reported amic acids as carriers for Sc transport across PIMs[192,193] and demonstrated excellent selectivity for Sc with respect to 11 different metals (including Y, Dy, Cr and Al), with only Fe(III) being co-transported. After 96 h, 94% Sc was recovered from sulfuric acid (pH 3), with only minor transport of competing metals, except for Fe(III), which was transported with 32% efficiency.[192,193]

Despite these promising approaches, all PIM studies to date have used artificial model solutions to study Sc recovery. These may have been over-simplified by using equimolar element concentrations, too high dilutions, or solutions in which only a limited number of elements were present and which did not model real waste compositions[256] in which Sc is present only in minute concentrations (mg L^{-1}) in a cocktail of major impurities (multiple g L^{-1}). In this study, PIMs were assessed for Sc extraction from real TiO_2 acid wastes. The PIM composition was first systematically optimised for efficiency, speed and selectivity of Sc extraction using a design of experiment (DoE) approach.[328,329] After identification of the most efficient receiving phase in extraction/elution experiments, the optimised PIMs were tested in transport experiments, including elevated temperature tests.

5.3 Materials and methods

5.3.1 Chemicals and solutions

Unless otherwise stated, all chemicals and solvents were purchased from Sigma-Aldrich (Switzerland) and used without further purification.

All aqueous solutions were prepared using ultrapure water (<18 MΩ; Barnstead Smart2Pure water purification system, ThermoFisher Scientific, Switzerland). Poly(vinylidene fluoride-co-hexafluoropropylene) (PVDF-HFP) as pellets, di-(2-ethylhexyl)phosphoric acid (DEHPA; 95%, Alfa Aesar, USA) and 2-nitrophenyl octyl ether (NPOE; 98%, Alfa Aesar, USA) were used for membrane casting . The three acids: H_3PO_4, H_2SO_4 and HCl in different concentrations were used as receiving solutions.

Elements were incorporated in model solutions based on those commonly present in industrial acid wastes (Mg, Al, Sc, Ti, V, Cr, Mn, Fe, Y, Zr, Nb, La, Ce, Dy, Yb).[256,283] Two solutions containing these elements in 0.1 mM or 1 mM concentrations with a pH of 1.5 were prepared. Model solution feeds were prepared from stock solutions of metal chlorides or oxides in hydrochloric acid (2 M). For pH adjustments a pH-meter (inoLab Multi 9310 IDS, WTW, Germany) was used.

The original acid waste came from the 'chloride route' of TiO_2 production and was provided by a manufacturer based in the Netherlands. Before the experiments, NaOH (98.5% purity) was added to adjust the pH to 1.5 and remove some of the impurities by precipitation (e.g. >99% Ti, 75% Th, 40% U; for details see Remmen et al., 2019 and Hedwig et al., 2022). After a settling period (48 h), the solids were removed by decantation and ultrafiltration (Molecular weight cut-off: 150 kDa, UP150, Microdyn-Nadir, Germany). Eventually a clear blue to green solution was obtained (for element concentrations see Table 5.5).

5.3.2 Membrane casting

The PIMs were cast using a solvent evaporation approach. PVDF-HFP, DEHPA and NPOE were dissolved in tetrahydrofuran by heating to reflux for 2 h, after which the solution was cooled to room temperature and an aliquot was poured into a glass ring (7.5 cm diameter) placed on a levelled float-glass table. The ring was covered with filter paper, and the solvent was allowed to evaporate overnight. Cast membranes were carefully peeled off the table. The membranes were weighed (KERN ABJ 320-4, Kern & Sohn, Germany), and their thickness was measured at five points using a micrometre screw gauge (Micromaster, 0-30 mm, TESA, Switzerland).

5.3.3 Extraction and elution experiments

For extraction and elution experiments, rectangular pieces (15 x 30 mm) were punched out of a PIM and fixed in 3D-printed polypropylene (PP) frames (Figure S9.8, Annex). The PIMs thus prepared were immersed in a feed solution (0.1 mM, 40 mL) and shaken at 300 rpm and 25°C in a thermo-shaker (IKA, KS 4000 i control, Germany) for 24 h. Afterwards, the PIMs were removed from the solution, dried with a paper tissue, fixed again in a PP frame and immersed in a receiving solution (40 mL; 300 rpm; 25°C). The loading capacity Q_M (i.e. the absolute amount of a metal M extracted per membrane; µmol g^{-1}), was determined after 24 h when the metal uptake had reached a plateau. Furthermore, χ_M (i.e. the mole fraction of a metal M among the extracted metals) and $J_{0,M}$ (i.e. the initial flux of a metal M; nmol m^{-2} s^{-1}) were calculated (for calculations see Annex). The latter was determined via the rate constant of the extraction k_{ex}, whereas for the elution, the rate constant was denoted as k_{el} (calculations in Annex). As a control test to account for equipment-related sorption, one set of triplicates was run without any PIM.

5.3.4 Transport experiments

Transport experiments were conducted using custom-made high-density polyethylene (HDPE) cells (Figure S9.8, Annex). Every cell consisted of two connectable half-cells, each holding 120 mL. The junction between them was circular (20 cm²). The PIMs were inserted between the half cells, which were then filled with feed and receiving solution. Cells were agitated at 300 rpm in a thermo-shaker, if not otherwise stated, at 25°C (IKA, KS 4000 i control, Germany).

5.3.5 Design of experiments

To find the optimal ratios of PVDF-HFP, DEHPA and NPOE while limiting the number of experiments, a DoE approach using STAVEX (AICOS Technologies AG, Switzerland) was used. Three response variables were defined to characterise an optimal PIM in terms of Sc extraction: 1) a high Sc loading capacity Q_{Sc}, 2) a high initial Sc extraction flux $J_{0,Sc}$ and 3) a high mole fraction of Sc among all extracted metals χ_{Sc}. The limits for the DoE were set as ω(PVDF-HFP) 25–95%, ω(DEHPA) 5–51% and ω(NPOE) 0–25%, respectively, where ω is the mass fraction of the corresponding constituent. The experimental plan was generated based on a D-optimal vertex-centroid design.[330] In total, 11 different compositions, distributed over the entire factor region, were specified by the software. The corresponding membranes were cast and used for extraction experiments (duplicate, 24 hours, 0.1 mM model feed). Based on the empirical data, the software fitted statistical models for each response variable, expressing how the response depends on the three influence factors. The p-values of the model parameters express the probability that a parameter has a significant influence on the response variable.

5.3.6 QqQ-ICP-MS analysis

The samples were diluted using 3% nitric acid using an autodilution system (Simprep, Teledyne Cetac Technologies, USA) and analysed using triple quadrupole (QqQ) inductively coupled plasma mass spectrometry (ICP-MS). The analysis was performed on an 8800 QqQ-ICP-MS system (Agilent, Basel, Switzerland) using general purpose operational settings. Quantification was performed via multi-element standards (0–50 µg L^{-1} (ppb), seven points). To account for matrix effects, ^{103}Rh was used as the internal standard. To quantify $^{23}Na^+$, $^{52}Cr^+$, $^{55}Mn^+$, $^{56}Fe^+$, $^{60}Ni^+$, $^{66}Zn^+$, $^{89}Y^+$, $^{137}Ba^+$, $^{139}La^+$, $^{140}Ce^+$, $^{141}Pr^+$, $^{146}Nd^+$, $^{147}Sm^+$, $^{153}Eu^+$, $^{157}Gd^+$, $^{159}Tb^+$, $^{163}Dy^+$, $^{165}Ho^+$, $^{166}Er^+$, $^{169}Tm^+$, $^{172}Yb^+$, $^{208}Pb^+$, $^{232}Th^+$ and $^{238}U^+$, the ICP-MS was operated in single quad mode using helium as a collision gas, whereas $^{24}Mg^+$, $^{27}Al^+$, $^{39}K^+$, $^{45}Sc^+$, $^{47}Ti^+$, $^{51}V^+$, $^{90}Zr^+$ and $^{93}Nb^+$ were measured in triple-quad mass-shift mode using O_2 as a reaction gas. The $^7Li^+$ concentration was determined using no-gas single-quad mode (for figures of merit, see Table S9.9, Annex).

5.4 Results

5.4.1 Optimisation of the membrane composition
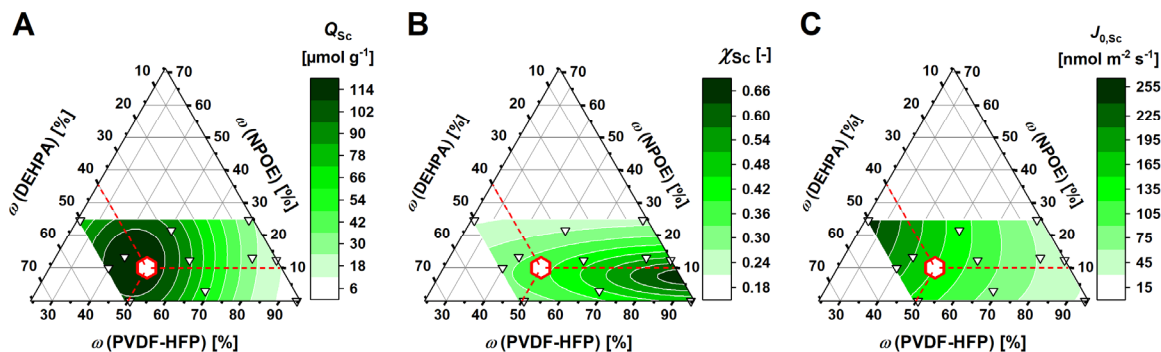
Figure 5.1 DoE models for Sc loading capacity (Q_{Sc}; A), the mole fraction of Sc among all extracted metals (χ_{Sc}; B) and the initial flux of Sc extraction ($J_{0,Sc}$; C), used for membrane composition optimisation. White triangles indicate cast PIMs for verification, whereas the red dashed lines intersect at the optimal compromise between the three parameters.

The optimisation approach was based solely on the extraction of metals from the feed into the PIM. In this regard, PIMs with a composition of 50/40/10 wt% PVDF-HFP/DEHPA/NPOE were found to provide the best compromise between Q_{Sc}, χ_{Sc} and $J_{0,Sc}$ while retaining structural integrity. At this optimal compromise composition, the statistical model predicted a Q_{Sc} of 117 ± 13 µmol g^{-1} (Figure 5.1A; Table 5.1), χ_{Sc} of 0.37 ± 0.04 (Figure 5.1B; Table 5.1) and $J_{0,Sc}$ of 150 ± 33 nmol m^{-2} s^{-1} (Figure 5.1C; Table 5.1), respectively. The experimental results were largely consistent with this prediction (Table 5.1). Overall, the models described the experimental results well, reflected by the R^2 values of 95.3% (Q_{Sc}), 95.7% (χ_{Sc}) and 90.6% ($J_{0,Sc}$) (Table S9.10, Annex). The composition of 50/40/10 wt% PVDF-HFP/DEHPA/NPOE is henceforth referred to as 'optimal polymer inclusion membrane' (optimal PIM).

The scandium loading capacity (Q_{Sc}) increased with declining ω(PVDF-HFP) and rising ω(DEHPA), with ω(NPOE) having no visible effect (Figure 5.1A). This stronger influence of ω(DEHPA) and ω(PVDF-HFP) compared to that of ω(NPOE) is also reflected by the non-significant p-values of the latter within the statistical model (Table S9.10, Annex). The optimal compromise PIM was already close to the best Q_{Sc} predicted at 45.8/42.6/11.7 wt% PVDF-HFP/DEHPA/NPOE (Figure 5.1A; Table 5.1).

Co-extraction of other metals occurred each time, illustrated by a value of χ_{Sc} <1 (Figure 5.1A; Table 5.1 and Table 5.2). When using the optimal PIM, the overall selectivity and capacity order was Sc > Zr > Yb > Dy > Y > Ti > Ce > La > Fe > Al > Nb > V > Mn > Mg > Cr (Table 5.2). The maximum χ_{Sc} was calculated for a PIM composed of 88.3/4.5/7.2 wt% PVDF-HFP/DEHPA/NPOE (Figure 5.1B). Here, all three factors were influential (Table S9.10, Annex).

With respect to $J_{0,Sc}$, a difference of one order of magnitude was calculated between the slowest and the fastest membranes (Figure 5.1C; Table 5.1). The highest flux was achieved at 25/50/25 wt%

PVDF-HFP/DEHPA/NPOE (Figure 5.1C; Table 5.1), which was at the maximum of the DEHPA factor range and at the minimum of the PVDF-HFP factor range, consequently being almost at the minimum of the NPOE factor range. Based on the p-values within the statistical model, it seems that $J_{0,Sc}$ depends mainly on the linear effects of ω(DEHPA) and ω(PVDF-HFP), with the p-value of ω(NPOE) and for higher-order effects (interactions, quadratic terms) being insignificant.

The PIMs with PVDF-HFP content lower than 50% were not useable, since they showed strong adhesivity and were too soft to be removed from the glass table without damage, leading to the above specification of the optimal compromise setting.

Table 5.1 Modelled and measured results of the DoE study on extraction tests with model feed (15 elements, each 0.1 mM).

Membrane composition			Modelled			Measured (%-predicted)[a]			
ω(PVDF-HFP) [%]	ω(DEHPA) [%]	ω(NPOE) [%]	Q_{Sc} (± 13) [µmol g^{-1}]	χ_{Sc} (± 0.04) [-]	$J_{0,Sc}$ (± 33) [nmol m^{-2} s^{-1}]	Q_{Sc} [µmol g^{-1}]	χ_{Sc} [-]	$J_{0,Sc}$ [nmol m^{-2} s^{-1}]	Sc extracted [%][b]
95	5	0	6	0.46	26	6 ± 7 (95)	0.07 ± 0.12 (15)	2 ± 1 (8)	3 ± 4
83	5	12	14	0.54	40	13 ± 7 (88)	0.50 ± 0.49 (93)	40 ± 11 (101)	8 ± 5
76	11	13	28	0.49	57	36 ± 5 (131)	0.55 ± 0.44 (111)	89 ± 20 (155)	16 ± 2
70	5	25	26	0.24	47	28 ± 7 (107)	0.25 ± 0.17 (103)	51 ± 12 (108)	14 ± 3
69	28	3	64	0.44	83	72 ± 5 (112)	0.45 ± 0.16 (103)	111 ± 25 (134)	32 ± 2
60	28	12	86	0.42	110	75 ± 4 (86)	0.40 ± 0.14 (95)	114 ± 25 (103)	37 ± 2
51	28	21	96	0.27	134	83 ± 7 (86)	0.27 ± 0.06 (99)	91 ± 34 (68)	29 ± 3
50	50	0	105	0.30	137	104 ± 6 (99)	0.29 ± 0.07 (99)	142 ± 51 (103)	44 ± 3
50	40	10	117	0.37	150	95 ± 8 (81)	0.29 ± 0.03 (78)	136 ± 17 (91)	48 ± 4
43	44	13	118	0.32	181	133 ± 21 (113)	0.31 ± 0.08 (96)	177 ± 27 (98)	38 ± 6
40	50	10	111	0.31	192	101 ± 7 (91)	0.33 ± 0.1 (105)	166 ± 68 (87)	58 ± 4
25	50	25	73	0.20	257	78 ± 1 (106)[c]	0.20 ± 0.03 (100)	283 ± 15 (110)	76 ± 1

a.   %-predicted = $\frac{\text{value (measured)}}{\text{value (modelled)}}$

b.   Sc extracted = $(1 - \frac{c_{24h}^{feed}}{c_0^{feed}}) \times 100\%$

c.   The membrane was cast twice as thick due to stability issues

Table 5.2 Mean Q_M, X_M and $J_{0,M}$ after 24 h extraction using the optimal PIM and model feed.

Element	c_0^{feed} [mmol L^{-1}]	c_{24}^{feed} [mmol L^{-1}]	Extracted [%][a]	Q_M [μmol g^{-1}]	X_M [-]	$J_{0,M}$ [nmol m^{-2} s^{-1}]
Sc	0.092 ± 0.001	0.048 ± 0.001	48 ± 4	95 ± 8	0.29 ± 0.03	140 ± 20
Zr	0.085 ± 0.002	0.066 ± 0.002	21 ± 2	39 ± 3	0.12 ± 0.01	70 ± 20
Yb	0.089 ± 0.001	0.073 ± 0.001	17 ± 2	32 ± 3	0.10 ± 0.01	61 ± 4
Dy	0.087 ± 0.002	0.075 ± 0.002	14 ± 1	26 ± 1	0.08 ± 0.01	52 ± 8
Y	0.085 ± 0.001	0.074 ± 0.001	13 ± 1	23 ± 1	0.07 ± 0.01	53 ± 9
Ti	0.097 ± 0.002	0.085 ± 0.002	11 ± 4	23 ± 9	0.07 ± 0.02	50 ± 30
Ce	0.086 ± 0.001	0.076 ± 0.001	11 ± 1	20 ± 2	0.06 ± 0.01	30 ± 10
La	0.060 ± 0.001	0.052 ± 0.001	12 ± 1	16 ± 1	0.05 ± 0.01	23 ± 7
Fe	0.052 ± 0.005	0.045 ± 0.005	13 ± 9	14 ± 9	0.04 ± 0.03	20 ± 30
Al	0.061 ± 0.004	0.055 ± 0.004	9 ± 4	11 ± 6	0.04 ± 0.01	7 ± 5
Nb	0.036 ± 0.001	0.030 ± 0.001	14 ± 2	10 ± 2	0.03 ± 0.01	40 ± 3
V	0.067 ± 0.003	0.064 ± 0.003	4 ± 2	6 ± 3	0.02 ± 0.01	40 ± 20
Mn	0.068 ± 0.002	0.065 ± 0.002	3 ± 2	5 ± 3	0.01 ± 0.01	15 ± 10
Mg	0.057 ± 0.003	0.055 ± 0.003	3 ± 2	4 ± 3	0.01 ± 0.01	8 ± 7
Cr	0.071 ± 0.002	0.070 ± 0.002	1 ± 1	1 ± 1	0.00 ± 0.01	14 ± 6

a. Extracted = $(1 - \frac{c_{24h}^{feed}}{c_0^{feed}}) \times 100\%$

5.4.2 Choice of receiving phase

Despite DEHPA having high selectivity for Sc extraction, the release from the membrane (elution) is challenging.[141,192] Therefore, three mineral acids in different concentrations were tested as the receiving phase for Sc recovery from loaded PIMs. The best receiving phase for Sc elution was phosphoric acid (7–12 M), eluting >97 ± 5% of Sc (Figure 5.2A).
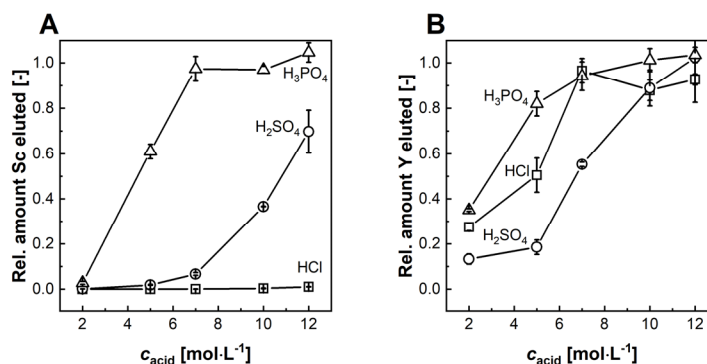
Figure 5.2 Relative eluted Sc (A) and Y (B) at different receiving phases.

Eluted Sc generally increased with higher acid concentration but was mostly dependent on the acid type (Figure 5.2A). Phosphoric acid eluted a minor fraction of Sc at lower concentrations (2.7 ± 0.7% for 2 M), while it became considerably more effective when higher concentrations were used (61 ± 3% for 5 M, quantitative for >7 M). This was different to other acids: no elution for Sc using hydrochloric acid was found even at high molarities (1.0 ± 0.4% for 12 M), and H_2SO_4 resulted in a maximum elution of only 70 ± 9% when the highest concentration (12 M) was used (Figure 5.2A). Furthermore, the membranes tended to be coloured yellow and red after contact with concentrated

hydrochloric acid and sulfuric acid, respectively, suggesting instability issues. However, some pre-liminary IR data pointed towards stability at room temperature when using 7 M H_3PO_4 (Figure S9.9, Annex). The stability of membranes for re-use applications in different acid media thus warrants further investigations.

Some co-extracted metals, such as the heavy rare earth elements, were easier to elute. Elution worked to some extent with all tested acids, as shown for Y (Figure 5.2B). Quantitative results were achieved using hydrochloric acid and phosphoric acid at concentrations ≥7 M and sulfuric acid at 12 M.

The lowest phosphoric acid concentration that still yielded quantitative Sc elution was 7 M H_3PO_4 (Figure 5.2A), and this was deemed the optimal receiving phase for transport experiments, despite some co-extracted metals (e.g. Y; 94 ± 6%).

5.4.3   Sc transport from model solutions

Table 5.3 Results after 24 h transport experiments using 7 M H_3PO_4 as receiving (elution) phase from 0.1 mM model feed.

Element	c_0^{feed} [mmol L^{-1}]	Feed	Membrane	Receiving phase	χ_M^{rec} [-]	k_{ex} [h^{-1}]	P [mm h^{-1}]	$J_{0,M}$ [nmol m^{-2} s^{-1}]
				Relative amount [%][a]				
Mg	0.12 ± 0.02	92 ± 7	0 ± 10	20 ± 10	0.02 ± 0.01	0.02 ± 0.01	1.3 ± 0.6	50 ± 30
Al	0.11 ± 0.01	34 ± 3	0 ± 20	90 ± 20	0.10 ± 0.01	0.03 ± 0.01	1.6 ± 0.6	60 ± 20
V	0.10 ± 0.01	1 ± 1	0 ± 20	100 ± 20	0.10 ± 0.01	0.19 ± 0.02	11.2 ± 0.7	320 ± 30
Cr	0.11 ± 0.01	78 ± 3	0 ± 5	26 ± 5	0.02 ± 0.01	0.01 ± 0.01	0.5 ± 0.3	10 ± 10
Mn	0.11 ± 0.01	60 ± 5	0 ± 20	40 ± 20	0.04 ± 0.01	0.02 ± 0.01	1.1 ± 0.2	30 ± 10
Fe	0.12 ± 0.01	41 ± 4	0 ± 20	60 ± 20	0.07 ± 0.01	0.09 ± 0.01	5.3 ± 0.3	180 ± 20
Sc	0.07 ± 0.01	12 ± 2	40 ± 7	48 ± 7	0.03 ± 0.01	0.20 ± 0.02	12 ± 1	260 ± 20
Ti	0.11 ± 0.01	31 ± 3	10 ± 20	50 ± 20	0.06 ± 0.01	0.14 ± 0.02	8.5 ± 0.8	270 ± 40
Y	0.11 ± 0.01	0 ± 20	0 ± 30	100 ± 20	0.11 ± 0.01	0.40 ± 0.05	24 ± 3	800 ± 90
Zr	0.08 ± 0.01	70 ± 20	20 ± 20	0 ± 10	0.00 ± 0.01	0.00 ± 0.02	0 ± 2	0 ± 30
Nb	0.06 ± 0.01	100 ± 30	0 ± 30	0 ± 10	0.00 ± 0.01	0.00 ± 0.02	0 ± 1	0 ± 20
La	0.11 ± 0.01	0 ± 1	0 ± 20	90 ± 20	0.10 ± 0.01	0.25 ± 0.03	15 ± 2	500 ± 100
Ce	0.11 ± 0.01	0 ± 1	0 ± 20	90 ± 20	0.10 ± 0.01	0.29 ± 0.03	17 ± 2	600 ± 100
Dy	0.15 ± 0.01	0 ± 1	0 ± 20	100 ± 20	0.15 ± 0.01	0.39 ± 0.05	23 ± 3	1000 ± 200
Yb	0.11 ± 0.01	0 ± 1	0 ± 20	100 ± 20	0.10 ± 0.01	0.44 ± 0.06	27 ± 4	870 ± 100

a.   Relative amount: Feed = $\frac{c_{24h}^{feed}}{c_0^{feed}}$ ×100%; Membrane = 100% - Feed - Receiving phase; Receiving phase = $\frac{c_{24h}^{rec}}{c_0^{feed}}$ ×100%

Table 5.4 Results after 24 h transport experiments using 7 M H_3PO_4 as receiving (elution) phase from 1 mM model feed.

Element	c_0^{feed} [mmol L^{-1}]	Feed	Membrane	Receiving phase	χ_M^{rec} [-]	k_{ex} [h^{-1}]	P [mm h^{-1}]	$J_{0,M}$ [nmol m^{-2} s^{-1}]
		Relative amount [%][a]						
Mg	0.9 ± 0.1	93 ± 6	7 ± 6	0 ± 2	0.00 ± 0.05	0.012 ± 0.006	0.7 ± 0.3	160 ± 80
Al	1.1 ± 0.1	94 ± 3	6 ± 4	0 ± 2	0.00 ± 0.04	0.006 ± 0.01	0.3 ± 0.6	110 ± 200
V	0.8 ± 0.1	93 ± 2	6 ± 2	1 ± 1	0.02 ± 0.02	0.008 ± 0.004	0.5 ± 0.2	110 ± 50
Cr	1.0 ± 0.1	96 ± 3	4 ± 3	0 ± 1	0.00 ± 0.02	0.004 ± 0.003	0.2 ± 0.2	60 ± 60
Mn	1.2 ± 0.1	95 ± 3	5 ± 3	0 ± 1	0.00 ± 0.02	0.00 ± 0.01	0.0 ± 0.5	0 ± 200
Fe	1.0 ± 0.1	88 ± 5	11 ± 6	1 ± 2	0.00 ± 0.02	0.010 ± 0.005	0.6 ± 0.3	150 ± 90
Sc	0.7 ± 0.1	9 ± 9	60 ± 10	33 ± 3	0.60 ± 0.06	0.17 ± 0.04	10 ± 3	2000 ± 500
Ti	0.6 ± 0.1	87 ± 8	6 ± 8	7 ± 3	0.03 ± 0.02	0.02 ± 0.01	1.3 ± 0.7	200 ± 100
Y	1.0 ± 0.1	92 ± 2	3 ± 2	5 ± 1	0.10 ± 0.02	0.011 ± 0.002	0.6 ± 0.1	170 ± 30
Zr	0.4 ± 0.1	90 ± 9	0 ± 9	10 ± 2	0.00 ± 0.01	0.01 ± 0.01	0.8 ± 0.7	80 ± 70
Nb	0.4 ± 0.1	100 ± 40	0 ± 40	2 ± 3	0.00 ± 0.01	0.00 ± 0.05	0 ± 3	0 ± 200
La	0.9 ± 0.1	97 ± 2	3 ± 2	0.8 ± 0.3	0.01 ± 0.01	0.006 ± 0.004	0.3 ± 0.3	80 ± 60
Ce	0.7 ± 0.1	97 ± 2	2 ± 2	1.1 ± 0.4	0.01 ± 0.01	0.004 ± 0.002	0.3 ± 0.1	50 ± 20
Dy	0.9 ± 0.1	95 ± 2	2 ± 2	3 ± 1	0.08 ± 0.01	0.005 ± 0.002	0.3 ± 0.1	70 ± 40
Yb	1.0 ± 0.1	90 ± 2	4 ± 3	6 ± 2	0.15 ± 0.02	0.011 ± 0.004	0.7 ± 0.3	170 ± 70

a.   Relative amount: Feed = $\frac{c_{24h}^{feed}}{c_0^{feed}} \times 100\%$; Membrane = 100% - Feed - Receiving phase; Receiving phase = $\frac{c_{24h}^{rec}}{c_0^{feed}} \times 100\%$

In transport experiments using 0.1 mM model solutions, Sc was efficiently transported into the membrane (91 ± 2%; Figure 5.3A). The fraction of Sc transported into the receiving phase was relatively high (48 ± 9%; Figure 3B); however, this was opposed by a poor selectivity. Scandium(III) was the metal ion of the third-lowest concentration in the receiving phase under these conditions (Figure 5.3B, Table 5.3). In contrast to Sc(III), Y(III) was twice as fast extracted and quantitatively transported into the receiving phase (Figure 5.3B, Table 5.3).

Using concentrated model solutions (1 mM), most Sc was transported into the membrane (Figure 5.3C; Table 5.4) and one third of the total Sc was eluted into the receiving phase both within 24 h (Figure 5.3D; Table 5.4). Selectivity for Sc was high, reaching the highest χ_{Sc} among the elements in the phosphoric acid after 24 h (Figure 5.3B; Table 5.4). Other metals in the receiving phase were Yb, Y, Dy and smaller traces of Ti, V, La and Ce (Table 5.4). Regarding the kinetics, the highest k_{ex} and $J_{0,M}$ were obtained for Sc, with $J_{0,Sc}$ being ten times higher than in the experiments with diluted model solutions (Figure 5.3A; Table 5.4). The increase in $J_{0,Sc}$, is in accordance with the linear proportionality of $J_{0,M}$ to c_0^{feed} (equation 4, Annex). Still, k_{ex} for Sc was around 17% lower than in experiments with 0.1 mM model solutions. Differences in the transport kinetics after the feed change were more sizable for other elements. Here, $J_{0,M}$ of co-transported metals were at least one order of magnitude lower than $J_{0,Sc}$ (Figure 5.3C and D; Table 5.4).

In terms of Sc elution, k_{el} (0.019 ±0.001 h^{-1}) was found to be 10 times lower than the corresponding k_{ex} (Figure 5.3C and D; Table 5.4). In contrast, for Y with a k_{el} of 0.04 ± 0.02 h^{-1}, the rate constant was around four times greater than the corresponding k_{ex} (Figure 5.3C and D; Table 5.4).
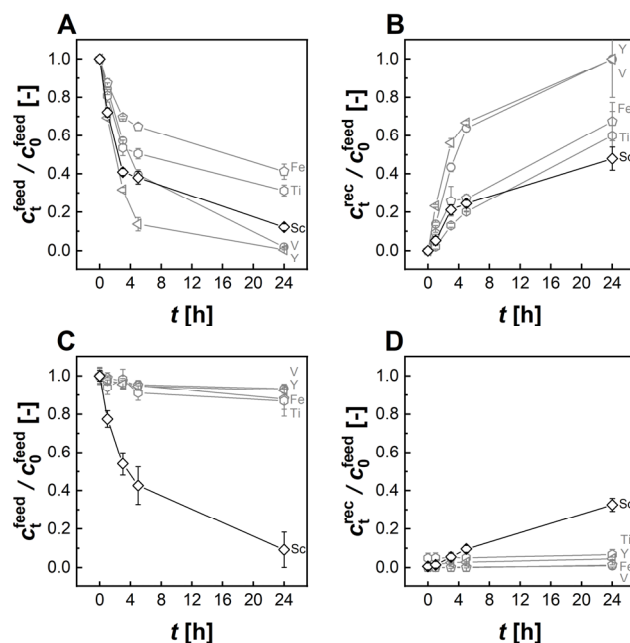
Figure 5.3 Extraction kinetics of transport experiments using 7 M H_3PO_4 as receiving phase from 0.1 mM (A, B) and 1 mM (C, D) multi-element feed with the concentration of the feed side (A,C) and the receiving side (B, D).

5.4.4   Sc transport from real acid waste

Scandium(III) was transported quantitatively (Figure 5.4C; Table 5.5) into the membrane when using real waste as a feed for the optimised PIM, making it the most extracted element among all elements measured (Figure 5.4C; Table 5.5). Only a few elements showed similarly high transport (Figure 5.4C; Table 5.5). Around one third of the Sc was eluted into the receiving phase within 24 h (Figure 5.4D; Table 5.5). Notably, χ_{Sc} increased by a factor of 600 from $(5.6 \pm 0.3) \times 10^{-4}$ in the feed to 0.34 ± 0.7 in the receiving phase (Table S9.11, Annex). In terms of co-transport, Th and Y were also significantly eluted into the receiving phase (Figure 5.4D; Table 5.5). However, because of their lower c_0^{feed}, Th and Y added little to the total amount of transported metal (χ_{Th}: 0.023 ± 0.004 and χ_Y: 0.04 ± 0.01; Figure 5.4B; Table S9.11, Annex). Instead, metals with high c_0^{feed} in the acid waste were associated with Sc in the receiving phase: V (χ_V: 0.34 ± 0.04), Fe (χ_{Fe}: 0.19 ± 0.04) and Al (χ_{Al}: 0.042 ± 0.007; Figure 5.4B; Table S9.11, Annex). All other metals had $\chi_M < 0.01$ (Figure 5.4B; Table S9.11, Annex).

In terms of kinetics, for Sc, a $J_{0,Sc}$ of 3500 ± 300 nmol m^{-2} s^{-1} was determined, along with a k_{ex} of 0.22 ± 0.02 h^{-1}. In comparison, for Th, a k_{ex} of 0.14 ± 0.02 h^{-1} but 25 times lower flux $J_{0,Th}$ with 140 ± 20 nmol m^{-2} s^{-1} was calculated. Yttrium(III) had a relatively lower rate constant k_{ex} of 0.03 ± 0.01 h^{-1} but a $J_{0,Y}$ of 160 ± 60 nmol m^{-2} s^{-1}, which was similar to Th, due to five times higher c_0^{feed} of Y (Table 5.5). As in the transport experiments using model feed, Sc elution was considerably slower than extraction by the membrane. A k_{el} of 0.015 ± 0.001 h^{-1} was found for Sc. For Th, a k_{el} of 0.012 ± 0.001 h^{-1}, and for Y, a k_{el} of 0.056 ± 0.005 h^{-1}, were determined.
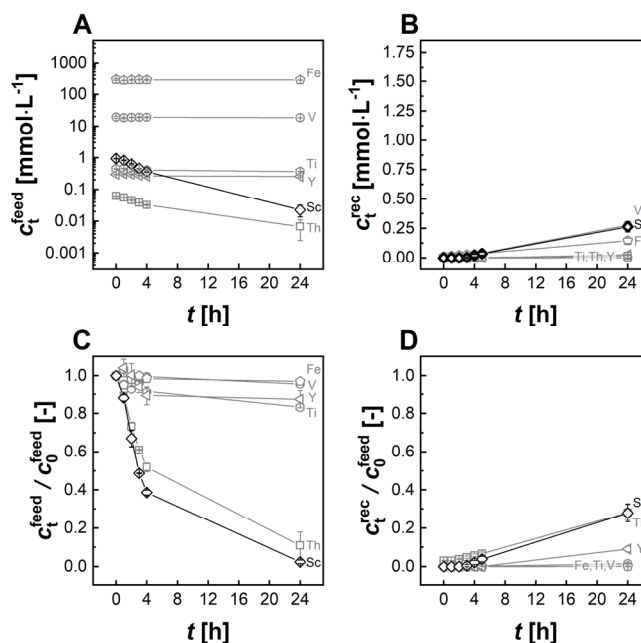
Figure 5.4 Recovery of Sc from real acid waste feed (A, C) into 7 M H_3PO_4 receiving phase (B, D) in terms of absolute concentrations (top) and relative amounts (bottom) at 25°C.

5.4.4.1 Influence of temperature
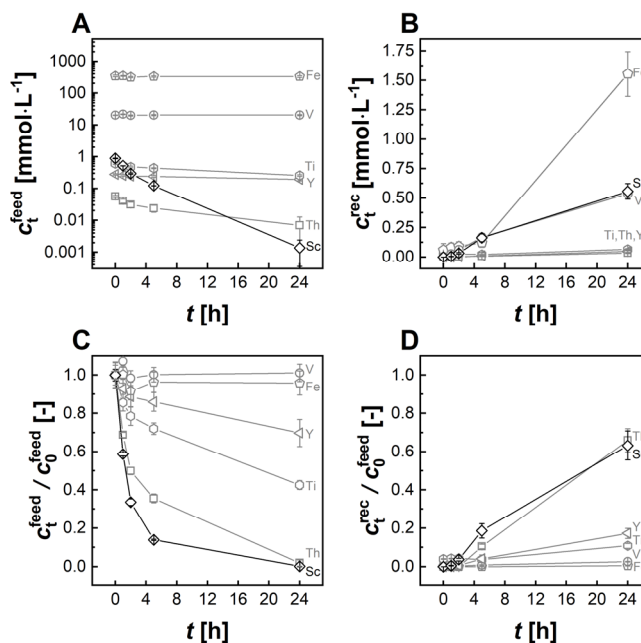
Figure 5.5 Recovery of Sc from real acid waste feed (A, C) into 7 M H_3PO_4 receiving phase (B, D) in terms of absolute concentrations (top) and relative amounts (bottom) at 60°C.

When the temperature was increased to 60°C, virtually all Sc was transported into the membrane (Figure 5.5A; Table 5.5). In comparison to the experiments at 25°C, more co-transport of other elements occurred (Figure 5.5A; Table 5.5). Sc transport was significantly more effective at higher temperature, with approx. twice as much Sc eluted into the receiving phase compared to room

temperature (Table 5.5). χ_{Sc} was relatively high in the receiving phase, with a value of 0.18 ± 0.02 (Table S9.12, Annex). Nevertheless, more co-transportation of other metals occurred (Figure 5.5; Table 5.5). Thorium and the heavy rare earth elements were particularly increased in the receiving phase (Table 5.5). However, as c_0^{feed} for these competing elements was substantially smaller than for Sc, their contribution to the total amount of transported substance was small (Figure 5.5B; Table 5.5). In absolute numbers, the most prevalent impurities transported were Fe and V, as already observed in the experiments at room temperature (Figure 5.5B; Table 5.5). Iron in particular showed a steep concentration gain, which began after ca. 5 h of operation. Hence, χ_{Fe} reached 0.5 ± 0.1 and χ_V was 0.18 ± 0.03 after 24 h in the receiving phase (Table S9.12, Annex). Extraction kinetics were increased by as much as a factor of 2.5 ($J_{0,Sc}$ = 8000 ± 100 nmol m^{-2} s^{-1}; k_{ex} = 0.54 ± 0.01 h^{-1}). For Sc elution, a k_{el} of 0.043 ±0.001 h^{-1} was determined, which was almost three times higher than in the 25°C experiments. In contrast, a k_{ex} of 0.34 ± 0.02 h^{-1} and a $J_{0,Th}$ of 310 ± 20 nmol m^{-2} s^{-1} were determined for Th. However, Th was slightly faster eluted than Sc, with a k_{el} of 0.046 ± 0.003 h^{-1}.

Table 5.5 Initial concentrations and relative elemental distribution after 24h of transport experiments using 7 M H$_3$PO$_4$ as receiving (elution) phase from real acid waste at 25°C and 60°C.

| Element | c_0^{feed} [mmol L^{-1}] | Relative amount [%][a] | | | | | |
| | | at 25°C | | | at 60°C | | |
		Feed	Membrane	Receiving phase	Feed	Membrane	Receiving phase
Li	0.26 ± 0.01	100 ± 20	0 ± 20	n.d.[b]	90 ± 20	10 ± 20	n.d.
Na	1190 ± 70	95 ± 5	5 ± 5	n.d.	99 ± 9	1 ± 9	n.d.
Al	100 ± 4	99 ± 4	1 ± 4	0.03 ± 0.01	100 ± 40	0 ± 40	0.1 ± 0.2
K	3.11 ± 0.1	95 ± 6	5 ± 6	n.d.	100 ± 7	0 ± 7	n.d.
Sc	0.94 ± 0.01	2 ± 1	70 ± 5	28 ± 5	0.2 ± 0.2	37 ± 8	63 ± 8
Ti	0.45 ± 0.01	83 ± 1	17 ± 1	0.2 ± 0.2	43 ± 3	47 ± 3	11 ± 2
V	19 ± 1	96 ± 5	3 ± 5	1.4 ± 0.1	100 ± 10	0 ± 10	2.6 ± 0.2
Cr	13 ± 1	97 ± 6	3 ± 6	n.d.	100 ± 30	0 ± 30	0.1 ± 0.2
Mn	66 ± 5	97 ± 6	3 ± 6	n.d.	95 ± 6	5 ± 6	0.04 ± 0.03
Fe	290 ± 20	97 ± 5	3 ± 5	0.05 ± 0.01	100 ± 7	0 ± 10	0.45 ± 0.06
Ni	0.82 ± 0.04	103 ± 1	0 ± 1	n.d.	96 ± 3	3 ± 3	1 ± 1
Zn	0.50 ± 0.01	107 ± 7	0 ± 8	3 ± 2	96 ± 8	4 ± 8	n.d.
Y	0.30 ± 0.01	87 ± 5	4 ± 5	9 ± 2	70 ± 8	13 ± 8	17 ± 3
Zr	0.11 ± 0.01	37 ± 2	62 ± 2	1 ± 1	28 ± 6	56 ± 7	16 ± 4
Nb	0.013 ± 0.001	33 ± 4	67 ± 4	n.d.	40 ± 4	49 ± 5	11 ± 2
Ba	0.73 ± 0.02	101 ± 3	0 ± 3	n.d.	100 ± 3	0 ± 3	0.9 ± 0.2
La	0.302 ± 0.002	101 ± 6	0 ± 6	n.d.	96 ± 2	4 ± 2	0.1 ± 0.3
Ce	0.77 ± 0.01	101 ± 4	0 ± 4	n.d.	94 ± 3	5 ± 3	0.7 ± 0.5
Pr	0.088 ± 0.001	101 ± 3	0 ± 3	n.d.	93 ± 2	6 ± 3	1.4 ± 0.5
Nd	0.312 ± 0.003	102 ± 3	0 ± 3	n.d.	91 ± 3	8 ± 3	1.8 ± 0.5
Sm	0.061 ± 0.002	100 ± 4	0 ± 4	n.d.	85 ± 5	9 ± 5	6.2 ± 0.9
Eu	0.010 ± 0.001	93 ± 3	7 ± 3	n.d.	84 ± 9	6 ± 9	10 ± 4
Gd	0.039 ± 0.001	94 ± 3	6 ± 3	n.d.	85 ± 5	5 ± 5	10 ± 2
Tb	0.007 ± 0.001	90 ± 3	10 ± 3	n.d.	80 ± 10	0 ± 20	17 ± 5
Dy	0.037 ± 0.001	89 ± 3	11 ± 3	n.d.	76 ± 4	5 ± 4	20 ± 3
Ho	0.008 ± 0.001	85 ± 4	15 ± 4	n.d.	78 ± 7	2 ± 7	20 ± 3
Er	0.023 ± 0.001	84 ± 5	16 ± 5	n.d.	73 ± 6	7 ± 6	21 ± 3
Tm	0.004 ± 0.001	82 ± 6	18 ± 6	n.d.	67 ± 6	9 ± 7	24 ± 3
Yb	0.027 ± 0.001	74 ± 8	20 ± 9	6 ± 3	67 ± 7	0 ± 7	34 ± 3
Lu	0.005 ± 0.001	70 ± 8	30 ± 8	n.d.	55 ± 7	18 ± 7	27 ± 3
Pb	0.144 ± 0.003	99 ± 3	1 ± 3	n.d.	94 ± 3	6 ± 4	n.d.
Th	0.063 ± 0.001	11 ± 8	61 ± 9	28 ± 5	2 ± 2	32 ± 7	66 ± 7
U	0.002 ± 0.001	82 ± 4	18 ± 4	n.d.	10 ± 30	90 ± 20	n.d.

a. Relative amount: Feed = $\frac{c_{24h}^{\text{feed}}}{c_0^{\text{feed}}}$ ×100%; Membrane = 100% - Feed - Receiving phase; Receiving phase = $\frac{c_{24h}^{\text{rec}}}{c_0^{\text{feed}}}$ ×100%

b. n.d. = not detected (< detection limit, see Annex)

5.5 Discussion

5.5.1 Optimisation of membrane / receiving phase

The membrane composition was optimised by means of an extraction/elution approach, optimising metal uptake into the membrane (extraction) and metal release from the membrane (elution) separately. For extraction, the optimal PIM was composed of 50/40/10 wt% PVDF-HFP/DEHPA/NPOE and harvested most Sc (Q_{Sc} = 95 ± 8 µmol g^{-1}) at a higher velocity ($J_{0,Sc}$ = 140 ± 20 nmol m^{-2} s^{-1}) and acceptable selectivity over other elements (χ_{Sc}= 0.29 ± 0.03). Ideally, all three parameters should be maximised, yet χ_{Sc} behaved oppositely to Q_{Sc} and $J_{0,Sc}$: while Q_{Sc} and $J_{0,Sc}$ increased with increasing DEHPA/decreasing polymer content of the membrane, χ_{Sc} did not. Since metal extraction is based on a chemical reaction between the carrier and the metal, higher carrier concentration can lead to higher reaction rates and a larger $J_{0,Sc}$. The Q_{Sc}, on the other hand, may benefit from increasing carrier concentration due to the higher number of binding sites available in the PIM. However, with more binding sites, more co-extraction may occur once the total capacity is sufficient to absorb not only the bulk of Sc but also metals with lower affinity for DEHPA. Furthermore, the reaction rates for the complexation of competing metals by DEHPA may benefit similarly to the complexation of Sc when the concentration of the carrier is increased. Together, these effects could explain the opposite influences of increasing DEHPA concentration on $J_{0,Sc}$, Q_{Sc} and χ_{Sc}. In this study, the optimal PIM was defined with respect to the maximum Sc yield at the expense of some selectivity. Once extracted and concentrated from the ppm level present in waste[256], selectivity can still be achieved during purification and refining, for example by liquid–liquid extraction and/or ion exchange.[125,141,331] However, according to the DoE results, PIM selectivity could be improved to some degree through the addition of NPOE in exchange for DEHPA. Generally, the role of the plasticiser is to weaken the interactions between the polymer chains, which in turn makes the membrane softer and more flexible. In addition, the carrier mobility within the PIM can be increased, which is important for metal transport through the membrane.[153] In this study, 5–10 wt% NPOE was found to improve Sc extraction selectivity. This was particularly pronounced in PIMs with lower DEHPA content. From the empirical model of the experimental results (see Annex), the membrane composition for the highest selectivity could be identified (88.3/4.5/7.2 wt% PVDF-HFP/DEHPA/NPOE). This could be advantageous for obtaining a purer Sc content in an earlier step (the receiving phase) of the processing chain. Due to the considerable Sc losses, however, it is doubtful whether this would be acceptable for Sc recovery applications. Rather, it may be an interesting option for Sc selective electrodes.[332]

Another part of the optimisation was the identification of a suitable receiving phase. Due to the high affinity of DEHPA for Sc, the stripping of the loaded DEHPA phase is known to be problematic in conventional SX, where strong bases are needed.[141] However, the metal transport across the PIM relies on a proton gradient from the receiving to the feed phase, working as a driving force for the

process.[153] For this reason, only acids were considered as receiving phases. Here, H_3PO_4 turned out to be an exceptional medium, reaching >97 ± 5% for the Sc elution. This is remarkable, because HCl and H_2SO_4 were found to be relatively ineffective for elution, as previously identified in convention-al SX studies using DEHPA.[333–335] We assume that the advantage of phosphoric acid is based on the thermodynamically favoured formation of Sc phosphate complexes over sulfate and chloride com-plexes in the receiving phase.[336] Due to their stability and low solubility products, Sc phosphates can be found naturally in mineral form (e.g. pretulite [$ScPO_4$] or kolbeckite [$ScPO_4·2H_2O$]).[336]

To the best of our knowledge, the recovery of Sc from a loaded organic DEHPA phase by means of phosphoric acid has not been reported, although the stripping potential of H_3PO_4 for uranium-loaded DEHPA has been described.[337] Although the results were obtained with DEHPA-containing PIMs, they may be to some extent transferable to conventional SX, making H_3PO_4 an alternative to alkaline stripping.[125,225] For example, the addition of lye can lead to saponification of DEHPA, which causes stronger emulsion/poorer phase separation in SX.[141,280,281] This can lead to consider-able extractant losses and eventually to the need to replace the organic phase.[141,280,281]

In comparison to co-extracted metals, Sc elution appears more challenging. On the one hand, this could be explained by the higher Lewis acidity of Sc and the stronger interaction between DEHPA and Sc, making the complex harder to cleave. On the other, it could also be a sign of different com-plexation of Sc and competing metals; the stoichiometry of the complex formed between lantha-nides and DEHPA in PIMs is reported to be 1:6, consistent with complexation by DEHPA dimers.[205,338] In those studies, H_2SO_4 (0.3–7 M) was found to be a satisfactory receiving phase for the transport of lanthanides (La, Gd, Yb). In the case of Sc, a recent study found a metal-to-DEHPA ratio of 1:2.5, implying monomeric complexation of DEHPA.[339] It is unclear whether DEHPA binds to Sc as a monomer or dimer in the PIM (Figure S9.10, Annex). Complexes of the monomer are ex-pected to be less affected by ligand substitution and more difficult to cleave.[340] This may explain why HCl and H_2SO_4 were suitable for the elution of Y, for example, but not of Sc.

5.5.2 Sc recovery from model solutions and real waste

From 1 mM model feed solutions, Sc transport was selective and fast, using the optimal PIM and receiving phase (Figure 5.3A and B, Table 5.4). In contrast, using the 0.1 mM model feed (Figure 5.3C and D, Table 5.3), no selectivity could be observed, and most metals were transported equally fast. This implies that the affinity of DEHPA for Sc is not exceptionally high among the tested ele-ments. It is unknown what exactly caused this change. One suggestion would be that different DEHPA-to-metal ratios may have led to this selectivity difference. In the case of the 1 mM feed, the ratio of DEHPA to metal was 2:5, while in the case of the 0.1 mM feed it was 12:5, considering dif-ferences in membrane thickness in the calculation. It is suggested that a lack of DEHPA compromis-es the formation of DEHPA-dimer complexes, or vice versa. Similarly, depending on the preferred coordination environment (1:3 or 1:6 metal:DEHPA)[205,338,339], the incorporation of a metal into the

DEHPA-PIM may be hindered or accelerated. In the case of Sc, k_{ex} in both transport experiments were almost similar (0.17 ± 0.04 and 0.20 ± 0.02 h^{-1}). For Y, in contrast, k_{ex} was found to increase by almost 40 times when having a higher DEHPA/metal ratio (from 0.011 ± 0.003 h^{-1} to 0.40 ± 0.05 h^{-1}). Thus, a certain concentration of the feed solution may be mandatory to allow the proposed 'kinetic discrimination' mechanism and selective recovery of Sc. However, for dilute solutions, the DEHPA content of the membrane may then be reduced to limit the transport of other metals, which is in line with the decrease in χ_{Sc} with increasing DEHPA membrane content in the DoE model.

In comparison to the model solutions, the industrial acid waste contained more than twice as many elements that were non-equimolar concentrated. These 33 elements were present from mg L^{-1} to multiple g L^{-1} scale, while Sc accounted for only around 42 mg L^{-1} (~1 mM; Table 5.5). Nevertheless, Sc was still transported almost quantitatively into the membrane, and almost a third of the initial Sc was transported across the membrane into the receiving phase (Figure 5.4; Table 5.5). Overall, a high selectivity was achieved, indicated by the increase of χ_{Sc} by a factor of 600 from the feed to receiving phase. Competing elements in terms of impurities co-transported were Y and Th. Although Th may generally be of occupational health and safety concern, here the final concentration was only 4.1 ± 0.7 ppm, which is below its average concentration in the Earth's crust (12 ppm).[341] Since the PIMs developed here could not discriminate between Th and Sc, downstream Th removal is necessary. This can be achieved by means of SX with neat tributyl phosphate[141] or by simple pH adjustment, as shown previously in the original waste used here. With respect to Ti, some transport into the membrane was observed, while no considerable amount reached the receiving phase within 24 h (Figure 5.4). While this underlined the successful separation of Ti and Sc with the PIM system, it also showed that Ti-rich feed solutions require pre-treatment as previously described.

Regarding the co-transport of major elements, satisfactory separation was achieved. In terms of Fe, only around 0.45% of the ca. 0.3 M Fe contained in the feed was transported into the receiving phase (Table 5.5). This suggested the presence of predominantly Fe(II), instead of Fe(III), as the former is poorly extracted by DEHPA only from chloride media[342] and the 'chloride route' TiO$_2$ production comprises strongly reducing conditions[343], favouring Fe(II). The low Fe co-transport observed here is in contrast to Sc SX studies, reaching high (>98%) Sc extraction at the cost of higher (e.g. 6.21%[344], 10%[333]) co-extraction of Fe. Similarly, ion exchange/solvent-impregnated resins found co-extraction of Fe[125], and our observations with PIMs represent a real advance in separation technology. For V, only 1.4% of the 20 mM were transported from the acid waste into the receiving phase (Table 5.5). Nevertheless, the two elements (V and Fe) account for more than 50% of the total elements in the receiving phase. Hence, further downstream removal/separation steps will be necessary to obtain a pure Sc product. It is possible that this may be achieved by selective precipitation either of Sc itself or impurities[264] In SX, such impurities could be removed after extraction by scrubbing/washing steps.[125,141]

However, regarding Sc elution from the loaded PIMs, there is room for improvement: whereas for SX, quantitative stripping from the loaded DEHPA phase appears achievable[125,141], maximally 63 ± 7% of the membrane-bound Sc was eluted into the receiving phase (Figure 5.5D).

Future implementation could involve scrubbing/washing steps instead of direct Sc elution to increase the selectivity of the process. As shown in Figure 5.2, HCl or H_2SO_4 may be options for impurity removal, as they were ineffective in Sc elution from the membranes.

A further improvement in PIM Sc recovery would be increased transport velocity, resulting in lower contact times and a lower footprint. Here, the system was heated up to 60°C, leading to twice as much Sc in the receiving phase after 24 h compared to the experiments at 25°C. The PIM process crucially relies on diffusion.[153,332] Based on Fick's law and the Stokes–Einstein equation for the diffusion coefficient, increasing the temperature is anticipated to have two effects: 1) directly, through the linear proportionality of the diffusion coefficient to temperature and 2) indirectly, by reducing the viscosity, which is inversely proportional to temperature. Higher temperatures result in greater movement of the solutes and simultaneously less resistance of the medium. The latter could be particularly important for the diffusion across the membrane and also within the receiving phase (7 M H_3PO_4 is about four times as viscous as water at 25°C[345]), facilitating the removal of transported Sc from the membrane surface.

The co-transport of other elements, such as Ti and Y was drastically increased (Figure 5.5C and D; Table 5.5). However, absolute concentrations of these metals were typically an order of magnitude lower than of Sc or showed only little elution, such as Ti (Figure 5.5A and B; Table 5.5). Thus, although 27 elements were found in the receiving phase, only two of them (Fe, V) accounted for 86% of all impurities (Table 5.5). Nevertheless, the increase of χ_{Sc} of over 300 times (from feed to receiving phase), underlined the selectivity for Sc.

All in all, these results suggest that the optimised system is a viable method for the extraction of Sc from industrial waste.

5.5.3   Comparison to previous PIM studies

The optimal PIM extraction conditions showed a high Sc flux of up to 44 times higher than in previous studies (Table 5.6). This is not due to the use of DEHPA but rather to the optimisation of experimental conditions. The initial Sc concentrations in the model solution and the acidic waste used for this study were 2–10 times higher than in other work, which increased the flux (Table 5.6; Equation S8, Annex). This study showed that PIMs can operate successfully even at pH < 2 and that a buffered solution is not necessarily required.

Table 5.6 Comparison of different studies, using PIMs for Sc recovery.

Carrier	$C_{0,Sc}^{feed}$ [mmol L⁻¹]	Feed solution	pH	$J_{0,Sc}$ [nmol m⁻² s⁻¹]	Sc transport-ed (24 h) [%]	Ref
benzoyltrifluoroacetone	0.5	0.1M CH₃COOH/CH₃COONa	6.1	690	-	[158]
2-thenoyltrifluoroacetone	0.5	0.1M CH₃COOH/CH₃COONa	6.1	610	-	[158]
2-furoyltrifluoroacetone	0.5	0.1M CH₃COOH/CH₃COONa	6.1	560	-	[158]
PC-88A & Versatic 10	0.1	0.1M HNO₃/NH₄NO₃	4.0	190	35–40	[206]
N-[N,N-di(2-ethylhexyl) aminocar-bonylmethyl]glycine	0.1	0.1M H₂SO₄/(NH₄)₂SO₄	3.0	380	35–40	[193]
N-[N,N-di(2-ethylhexyl)aminocarbonylmethyl] phenylalanine	0.1	0.1M H₂SO₄/(NH₄)₂SO₄	3.0	180	35–40	[193]
DEHPA	0.1	HCl (model solution)	1.5	260	48	This study
DEHPA	1	HCl (model solution)	1.5	2000	33	This study
DEHPA	1	HCl (TiO₂ acid waste, 25°C)	1.5	3500	28	This study
DEHPA	1	HCl (TiO₂ acid waste, 60°C)	1.5	8000	63	This study

Although it is mainly caused by higher initial concentrations, the possibility of drastically increasing the flux indicates that the potential of PIMs for Sc recovery has not yet been fully exploited and may be further optimised. It will be of interest to test streams with higher Sc concentrations for PIM-based Sc recovery in the future.

Another prerequisite for a functioning PIM system enabling metal transport is a functioning elution. As already described, Sc is notoriously difficult to cleave after complexation with phosphorus-based carriers. Yoshida et al. tested DEHPA as an extraction agent for Sc and excluded its use as a carrier for PIMs, as there were significant problems when trying to elute Sc with H₂SO₄.[192] Similarly, Sharaf et al. reported difficulties for elution when using PC-88A as a carrier.[206] In both studies, the carrier had to be changed/modified, to facilitate elution and successful Sc transport. By using H₃PO₄ as the receiving phase, we have demonstrated a way to use strong Sc complexing agents that are known to extract Sc even at very low pH. After 24 h, the transported Sc fractions in various transport experiments were of the same magnitude as in other studies (Table 5.6).[192,193,206]

5.5.4 Broader impact and implications for Sc recovery

In comparison to SX, PIMs reduce the amount of material needed by replacing the organic solvent phase with a thin polymer film, leading to the ecological footprint and costs arising from SX operation being mitigated.[346] This brings additional benefits by eliminating flammable solvents such as kerosene[125] during extraction. In our work, ca. 5 kg of membrane material was required to treat 1 m³ of acid waste. Based on estimated prices for ton quantities (see Annex), this translates into an investment of US$41 to recover Sc worth US$183 for a single cycle. Furthermore, PIMs can also be used in multiple cycles, and the surface-area-to-mass ratio can be further optimised. The energy demand for using PIMs does not differ considerably from that of SX or ion exchange, even though PIM Sc extraction worked best at 60°C.

5.6   Conclusions

Although PIMs have been developed and optimised for decades[153], they have few, if any, commercial applications for metal recovery. PIM experiments related to metal recovery on a laboratory scale deal primarily with model solutions or streams.[144] In this paper, we have shown for the first time that PIMs allow highly selective metal separation from real industrial waste as an alternative to conventional SX or ion-exchange approaches. Using waste containing some 30 metals, some of which were present at multiple g L^{-1} concentrations, minute amounts (mg L^{-1}) of Sc were separated with efficiency and selectivity.

6 Polymer inclusion membranes for scandium recovery: Reusability and improvement strategies

This chapter is in preparation for submission as

S. Hedwig[†], O. Von Arx[†], E. C. Constable, C. Housecroft and M. Lenz, Development of advanced membrane processes for scandium recovery from industrial waste.

[†]Both authors contributed equally to the publication.

Contribution of Sebastian Hedwig: Conceptualization, Formal Analysis, Investigation, Methodology, Project administration, Supervision, Validation, Visualization, Writing – original draft.

6.1 Abstract

Scandium (Sc) is a promising candidate among critical raw materials with high eco-innovation potential. The element possesses unique chemical properties rendering it vital for commercial solid oxide fuel cells and valuable for lightweight aircraft construction. A caveat, however, is its limited availability coupled with high market prices due to the lack of supply strategies. Following our previous concepts of applying membrane-based processes for the recovery of Sc, this study presents next steps towards the application of polymer inclusion membranes (PIMs) for Sc extraction from industrial waste. In this regard, different commercial organic extractants were examined on the base of the previously reported system. The reusability of the most promising membranes was investigated, together with underlying mechanisms of performance deterioration. Attempts were made to niellated some of the determined negative effects by means of membrane crosslinking. Finally, the PIM approach was complemented by nanofiltration to recover phosphoric acid, which was used for its high efficiency in Sc elution. Here, excellent purification results were achieved, wherefore the recyclability of the stream could be confirmed in subsequent transport experiments.

6.2 Introduction

The rare earth metal scandium has been declared a critical raw material (CRM) due to its crucial role for innovative applications but limited supply.[40,41,219] Currently, Sc is mainly used for solid oxide fuel cells (SOFCs) and in aluminium superalloys (e.g. Scalmalloy®).[81,91] SOFCs may support the transition to carbon-neutral energy generation, by enabling the production of electricity from the reaction of H_2 and O_2 to water.[89,90] Sc-Al alloys reconcile high-strength and weldability, posing an advantage over established durable Al-alloys (e.g. 2000 and 7000 series).[80] As <0.2% w/w of Sc considerably enhances material performance, Sc-Al alloys may find use in the transport sector, resp. wherever light-weight construction are important.[80] However, so far Sc is rarely used in the industry, due to its high price and its lack of supply.[103] Contrary to its production, the metal is relatively abundant in Earth's crust, being more common than e.g. lead.[102] Nonetheless, the metal is widely dissolved in the lithosphere and is rarely found concentrated.[103] While being an obstacle for primary production, this circumstance renders Sc recovery from secondary streams particularly attractive. Processes targeting the extraction of major components of ores, such as Al from bauxite or TiO_2 from ilmenite and rutile, leave Sc enriched behind in their corresponding by-products.[256,334] Hence, approaches targeting this Sc may start with higher initial concentrations than found naturally, while valorising otherwise landfilled wastes. Recently, membrane-based Sc recovery from TiO_2 acid waste has been presented, using e.g. nanofiltration (NF) or polymer inclusion membranes (PIMs).[256,283,347,348] NF was shown to allow for Sc concentration, while impurities can be depleted.[283,348] Therefore, the subsequent solvent extraction (SX) could be improved in regard of overall dimensioning, chemical use and achievable purity.[283] Alternatively to SX, PIMs can

extract Sc from the TiO_2 waste, by taking the Sc up into the membrane and eluting it into a receiving phase (RP).[347] Despite this principle has been proven for real acid waste, so far PIMs have been used in a single extraction cycle only.[347] Furthermore, Sc transport was never complete and reached maximally 60% at 60 °C.[347] Lastly, the receiving phase consisted of concentrated phosphoric acid, although phosphorous itself is also a CRM. Hence, the receiving phase itself calls for recovery strategies.[41,347]

Within this study, to improve Sc recovery, alternative carriers have been tested in addition to the previously examined di(2-ethylhexyl)phosphate (DEHPA). Furthermore, the most promising carriers, resp. membranes have been tested for reusability, within multiple extraction cycles. Based on the reports of Hoque et al., crosslinking has been applied to improve membrane stability.[197] Ultimately, NF has been used to recover the H_3PO_4 receiving phase and further concentrate Sc. The obtained phosphoric acid was reused for PIM-based Sc extraction.

6.3 Material and Methods

6.3.1 Chemicals and materials

The TiO_2 acid waste originated from a TiO_2 production site, located in the Netherlands, using the chloride route. Prior to use, the pH of the acid waste was adjusted to 1.5 using NaOH, followed by micro- and ultrafiltration for solid liquid separation. For further information see Hedwig et al. (2022).[283] Aqueous solutions were prepared using ultrapure water (arium comfort I water purification system, Sartorius, Germany). An HCl (pH 2) model feed was used, containing the following metals in 1 mM concentration: Mg, Al, Sc, V, Cr, Mn, Fe, Y, La, Ce, Dy and Yb. If not otherwise stated, 7 M H_3PO_4 was used as a receiving phase and TiO_2 acid waste was used as a feed phase (For element concentrations see Table S9.13, Annex). Chemicals were purchased commercially and used without further purification (Table 6.1).

Table 6.1 List of used commercial chemicals and solvents.

Substance	Abbreviation/Name	Source
Poly(vinylidene fluoride-co-hexafluoropropylene)	PVDF-HFP	Sigma-Aldrich
Polyethylene glycol dimethacrylate	PEG-DMA	Sigma-Aldrich
2-Nitrophenyl octyl ether	NPOE	Alfa Aesar
2,2-Dimethoxy-2-phenylacetophenone	DMPA	Sigma-Aldrich
Di-(2-ethylhexyl)phosphoric acid	DEHPA	Sigma-Aldrich, Alfa Aesar
2-Ethylhexyl hydrogen-2-ethylhexylphosphonate	PC-88A	TCI
Bis(2,4,4-trimethylpentyl)phosphinic acid	Cyanex 272	Sigma-Aldrich
Tributyl phosphate	TBP	Sigma-Aldrich
Trioctylphosphine oxide	TOPO	Sigma-Aldrich
Mixture of octyl- / hexylphosphine oxides	Cyanex 923	MEAB GmbH
Tetrahydrofuran	THF	Sigma-Aldrich
Phosphoric acid		Fluka
Nitric acid		Thermo Fisher Scientific
Periodic table mix 1		Sigma-Aldrich
Periodic table mix 2		Sigma-Aldrich
Periodic table mix 3		Sigma-Aldrich

6.3.2 Analytical methods

6.3.2.1 QqQ-ICP-MS

All samples were diluted with 3% HNO_3, using an auto-dilution system (Simprep Teledyne Cetac Technologies, USA). Metal concentrations were determined using an inductively coupled plasma triple quadrupole mass spectrometer (ICP-QqQ-MS, 8800 system, Agilent, Basel, Switzerland). General purpose operational settings were used. Multi-element standards (Sigma-Aldrich, Switzerland) were used for metal quantification (0-50 ppb range, 7 points calibration, $R^2 > 0.999$). ^{103}Rh was used as an internal standard to account for matrix effects. The quantification of ^{23}Na$^+$, ^{24}Mg$^+$, ^{44}Ca$^+$, ^{51}V$^+$, ^{52}Cr$^+$, ^{55}Mn$^+$, ^{60}Ni$^+$, ^{66}Zn$^+$, ^{89}Y$^+$, ^{90}Zr$^+$, ^{93}Nb$^+$, ^{137}Ba$^+$, ^{139}La$^+$, ^{140}Ce$^+$, ^{141}Pr$^+$, ^{146}Nd$^+$, ^{147}Sm$^+$, ^{153}Eu$^+$, ^{157}Gd$^+$, ^{159}Tb$^+$, ^{163}Dy$^+$, ^{165}Ho$^+$, ^{166}Er$^+$, ^{169}Tm$^+$, ^{172}Yb$^+$, ^{208}Pb$^+$, ^{232}Th$^+$ and ^{238}U$^+$ was performed in single quad mode with helium as a collision gas. To quantify ^{27}Al$^+$, ^{39}K$^+$, ^{45}Sc$^+$, ^{47}Ti$^+$ and ^{56}Fe$^+$, triple quad mass shift mode was chosen, using O_2 as a reaction gas, whereas no-gas single quad mode was used to determine the concentration of ^{7}Li$^+$.

6.3.2.2 ICP-OES

All samples were diluted with 3% HNO_3, using an auto-dilution system (Simprep Teledyne Cetac Technologies, USA). For the quantification of phosphorus, inductively coupled plasma optical emission spectrometry (ICP-OES) was used (Spectroblue FMS16, Ametek, USA). A single element standard was used (Sigma-Aldrich, Switzerland) for calibration (0-100 ppb range, 8 points calibration, $R^2 > 0.999$).

6.3.2.3 ATR-FTIR spectroscopy

IR spectra were measured using attenuated total reflectance Fourier-transform infrared spectroscopy (ATR-FTIR) in the mid-IR region (4000-650 cm^{-1}, 32 scans, spectral resolution 4 cm^{-1}) using a Cary 630 FTIR spectrometer (Agilent, Germany) with a room temperature detector, Deuterated L-alanine-doped TriGlycine Sulfate (DLaTGS) and a diamond attenuated total reflectance (ATR) module (Agilent, Germany).

6.3.2.4 µ-XRF spectroscopy

For analysis of elements within membranes, spatial resolved micro X-ray fluorescence (µXRF) measurements were conducted on a M4 Tornado system (Bruker, Germany). Membrane pieces were mapped under the following conditions: Rh microfocus X-ray tube, 50 kV accelerating voltage, 600 mA beam current, 25 mm distance between spots, 50 ms per pixel.

6.3.3 Membrane casting

6.3.3.1 General procedure

All polymer inclusion membranes were prepared using the solvent casting method: base materials were dissolved in THF (6 mL per 600 mg of materials) under reflux for 1 h. Aliquots of the solution were poured into glass rings (7.5 cm inner diameter), which were fixed to a levelled glass plate with silicone grease. The ring casts were covered with filter paper and an enclosure to allow for slow evaporation of the solvent overnight. The finished membranes were removed from the glass plate and stored in glass petri dishes. All membranes were weighed and measured in thickness. For the latter, five points across the membrane were measured with a micrometer screw gauge (Micromaster, 0-30 mm, TESA, Switzerland).

In general, PIMs weighing 600 mg were prepared, consisting of 50 wt% PVDF-HFP, 40 wt% of carrier and 10 wt% NPOE. Carriers that were investigated were PC-88A, Cyanex 272, TBP, TOPO and Cyanex 923 (Table 6.2).

Table 6.2 Composition of non-crosslinked PIMs

PIM	PVDF-HFP [wt%]	Carrier [wt%]	NPOE [wt%]
DEHPA	50	40	10
PC-88A	50	40	10
Cyanex 272	50	40	10
TBP	50	40	10
TOPO	50	40	10
Cyanex 923	50	40	10

6.3.3.2 Crosslinked membranes

Crosslinked PIMs were made following the procedure of Hoque et al..[197] Therefore, 46.4 wt% of a polymer blend, 40 wt% DEHPA or PC-88a, 10 wt% NPOE and 0.6 wt% DMPA were mixed. The polymer blend consisted of varying ratios of PVDF-HFP and PEG-DMA (Table 6.3). Crosslinked membranes were prepared by dissolving PVDF-HFP, the carrier and NPOE in THF as described before. Afterwards, the solution was allowed to cool to room temperature and PEG-DMA and DMPA (11 mg) were added. The solution was stirred for 30 min at room temperature and poured into prepared casts. After complete evaporation of the solvent the membranes were removed from the glass plate and exposed to UV light (375 nm) for 30 min.

Table 6.3 Composition of crosslinked PIMs. The 'polymer ratio' describes the ratio of PVDF-HFP compared to PEG-DMA.

PIM	PVDF-HFP [wt%]	PEG-DMA [wt%]	Carrier [wt%]	NPOE [wt%]	DMPA [wt%]	Polymer ratio [-]
DEHPA, CL 1:1	24.7	24.7	40	10	0.6	1:1
DEHPA, CL 7:3	34.6	14.8	40	10	0.6	7:3
PC-88A, CL 3:2	29.6	19.8	40	10	0.6	3:2
PC-88A, CL 7:3	34.6	14.8	40	10	0.6	7:3
PC-88A, CL 9:1	44.5	4.9	40	10	0.6	9:1

6.3.4 Transport experiments

For transport experiments, PIMs were mounted into tailor-made cells made of high-density poly-ethylene (HDPE), as previously described.[347] Assembled cells were closed and agitated (120 rpm) on a temperature controlled incubator shaker (KS 4000i, IKA, Germany).

6.3.4.1 Process parameters

The processes of metal extraction and re-extraction were assumed to follow first order kinetics. Therefore, the kinetic rate constant of the extraction of metals into a PIM (k_{ex}) was defined as:

$$\ln\left(\frac{c_t^{feed}}{c_0^{feed}}\right) = -k_{ex} \cdot t \tag{6.1}$$

The concentration of a metal in the feed at a given time (t) was described as c_t^{feed}. Therefore the initial concentration in the feed is c_0^{feed}. The rate constant, k_{ex}, describes the velocity of the metal extraction process. Correspondingly, the elution of metals from the PIM into the receiving solution was described as:

$$\ln\left(1 - \frac{c_t^{rec}}{c^{PIM}}\right) = -k_{el} \cdot t \tag{6.2}$$

with the rate constant, k_{el}, the concentration in the RP, c_t^{RP} and c^{PIM} the amount of the metal in the PIM.

The permeability (P) of a membrane can be calculated from k_{ex}, the volume (V) and the membrane area (A):

$$P = k_{ex} \cdot \frac{V}{A} \tag{6.3}$$

The molar fraction of a metal (χ_M) in the RP, as a measure for the selectivity of a PIM for a certain metal was calculated as follows:

$$\chi_M = \frac{n_M}{n_{tot}} \tag{6.4}$$

With the amount of a metal M (n_M) and the total amount of metals present in the solution (n_{tot}).

6.3.5   Nanofiltration

6.3.5.1 Process parameters

Important process parameters for nanofiltration are the retention (R), the selectivity (S) and the permeate flux (J). By comparing the concentration of a certain compound (i) in the permeate ($c_{P,i}$) and the feed ($c_{f,i}$) phase, the retention for this compound (R_i) can be calculated.[171]

$$R_i = 1 - \frac{c_{P,i}}{c_{f,i}} \tag{6.5}$$

The selectivity expresses the membrane's ability to discriminate between different components (i, j) of a mixture, by correlation of the concentrations of those components in the feed ($c_{f,i}$, $c_{f,j}$) and the permeate ($c_{P,i}$, $c_{P,j}$).[171]

$$S = \frac{c_{P,i}/c_{P,j}}{c_{f,i}/c_{f,j}} \tag{6.6}$$

The permeate flux of a membrane (J) can be calculated as follows:

$$J = \frac{V_P}{A \cdot \Delta t} \tag{6.7}$$

Whereas V_P describes the volume of permeate, Δt a time interval and A, the area of the membrane.[349]

The transmembrane pressure (TMP), can be calculated from the pressure of the feed (p_F), the pressure of the retentate (p_R) and the pressure of the permeate (p_p):

$$\text{TMP} = \frac{p_F + p_R}{2} - p_P \tag{6.8}$$

The used cross-flow filtration unit was only equipped with one pressure gauge prior to the membrane module. Due to the small system dimensions, p_R is estimated to be approximately equal to p_F (i.e. no pressure drop along the module). Furthermore the p_p is expected to be drastically lower than p_F, wherefore it is estimated to be zero. Following equation 6.5, TMP is estimated to be approximately equal to p_F.

6.3.5.2 Cross-flow operation

Nanofiltration was performed in cross-flow operation mode (8 L min⁻¹) on a MaxiMem filtration system (PS Prozesstechnik GmbH, Switzerland) using a NanoPro A-3014 acid-stable spiral-wound membrane element (1812, 31 mil spacer, 0.25 m² membrane area, AMS technologies, Israel). As a feed solution spent receiving phase from PIM experiments was used (metal concentrations shown in Table 6.4).

Table 6.4 Concentration of elements in the used receiving phase used for NF experiments.

Element	Concentration [mmol L^{-1}]
Na	4.9×10^{-1}
Mg	3.8×10^{-3}
Sc	1.4×10^{0}
Ti	2.5×10^{-2}
V	6.4×10^{-1}
Cr	5.3×10^{-3}
Mn	3.1×10^{-2}
Fe	2.0×10^{0}
Ni	4.0×10^{-3}
Zn	6.6×10^{-3}
Y	2.6×10^{-3}
Ba	2.0×10^{-4}
Ce	3.0×10^{-4}
Dy	1.5×10^{-3}
Yb	3.4×10^{-3}
Th	3.6×10^{-4}

6.3.5.2.1 Pressure dependence

Starting at 10 bar, the pressure was increased until 35 bar in 5 bar steps. Therefore, spent RP was used as a feed (2 L, 2.675 kg) under continuous retentate recirculation. At each pressure step, samples (1 mL) of permeate and retentate were taken after 15 min, 30 min and 45 min.

6.3.5.2.2 Permeate recovery

Permeate was continuously recovered using spent RP (2 L, 2.679 kg) as a feed at 35 bar (p_F). Samples (1 mL) were taken from permeate and retentate to the beginning and after every 10% recovery, until 60% recovery was reached. Achieved recovery rate was determined by monitoring the permeate weight with a balance.

6.3.5.3 Titration

Concentrations of H_3PO_4 (PA) were determined twice by titration with NaOH (0.1 M). All solutions were diluted (1:50) and titrated up to the second half-equivalence point. Consumption of NaOH for reaching the first equivalence point was derived from the titration curves (tangent method). The concentration of H_3PO_4 in solution was calculated as follows:

$$c_{PA} = \frac{c_{NaOH} \cdot V_{NaOH}}{V_{PA}}$$

(6.9)

6.4 Results & Discussion

6.4.1 Carriers for Sc transport

In regard of the previously reported procedure for Sc recovery using PIMs, the corresponding optimal membrane, consisting of 50/40/10 wt% PVDF-HFP/DEHPA/NPOE, is henceforth described as the 'benchmark PIM' or short 'benchmark'. In this study, further commercially available carriers with Sc affinity were examined for PIM-based Sc extraction from TiO_2 acid waste in comparison to DEHPA (Figure 6.1).[144,339,350]
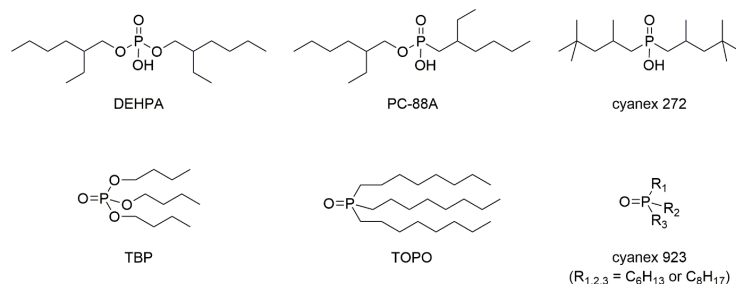
Figure 6.1 Chemical structures of carriers used in this study.

PIMs with alternative carriers were analogue to the benchmark membrane, whereas simply the mass fraction of DEHPA was substituted. After casting, all membranes were used in transport experiments at room temperature, with TiO_2 acid waste as the feed and 7 M H_3PO_4 as the RP. The PIM specimens were compared in regard of: 1) Sc transport into the membrane, 2) Sc transport into the RP, 3) the obtained mole fraction of Sc in the RP after 24 h and 4) the rate constant for the Sc transport into the membrane (Figure 6.2).

Figure 6.2 Amount of Sc transported into the membrane and transported into the RP relative to the total amount of Sc in the feed (A). Rate constants of the Sc transport into the membrane and mole fraction of Sc in the RP after 24 h (B).

Cyanex 272, TBP, TOPO and Cyanex 923 did not facilitate efficient Sc transport. Rate constants of extraction and χ_{Sc} in the RP were considerably lower compared to DEHPA and PC-88A. Moreover, Sc was only partially transported into the membrane, resp. in case of TBP virtually all Sc remained in the feed. However, PIMs with PC-88A, outperformed the benchmark PIM in regard of extraction speed (k_{ex} = 0.104 h^{-1}), while offering high selectivity (χ_{Sc} = 0.32). Additionally, 92% of the total Sc was extracted and 85% was transported into the RP. In all tests, the benchmark PIM performed worse than in the previous study, considering rel. Sc transport into the membrane and RP and extraction speed.[347] However, the absolute amount of Sc transported was similar, and the selectivity was superior. Possibly, this was caused by differences in the acid waste composition (Table S9.13, Annex). Concerning PC-88A, Yoshida et al. reported before its advantages as a highly Sc-selective carrier in PIMs. However, as they used H_2SO_4 as a RP, a modifier (versatic acid) was necessary to

107

allow for Sc elution and transport.[206] Although, all carriers used in this study showed some chemical similarity, the measured Sc transport velocity, selectivity and overall efficiency deviated significantly (Figure 6.2). The Sc selectivity, expressed as χ_{Sc}, decreased in the order DEHPA > PC-88A > Cyanex 272. The rate constant and transport of Sc decreased in the order PC-88A > DEHPA > Cyanex 272 (Figure 6.2). In part, the observed trends can be explained through the Pearson's Hard-Soft-Acid-Base theory (HSAB).[351] Sc^{3+} can be considered a hard Lewis-acid, due to its high charge and small ionic radius.[351,352] Structurally, in the series DEHPA, PC-88A, Cyanex 272, TOPO/Cyanex 923, alkoxy substituents of the central phosphine oxide are getting increasingly replaced by alkyl chains. Thus, the carriers' hardness, resp. the hardness of the corresponding bases, decreases in the same order. According to the HSAB principle, Sc^{3+} should show the highest affinity to hard bases, being the corresponding anions of DEHPA. Hence, the highest selectivity was found for PIMs based on DEHPA. On the other hand, the higher affinity comes along with increased stability of Sc-DEHPA complexes, impairing the release of Sc and thus the underlying transport mechanism in the PIM. Here, PC-88A is assumed to provide a better balance between affinity and stability. While X_{Sc} was only slightly below the experiments with DEHPA-PIMs, higher rate constant and almost complete Sc transport into the RP was observed. Ultimately, the three additional carriers, Cyanex 272, TOPO and Cyanex 923 were assumed being too soft bases, wherefore the affinity for Sc^{3+} was insufficient. Moreover, under the strongly acidic conditions, the neutral extractants could be protonated, resulting in cationic-carrier species.[141] This could become hindering for the extraction of Sc, which appears to be well extractable as cationic species under the present conditions, as indicated by its affinity for cation exchanging extractants.

6.4.2 Reusability studies

As DEHPA and PC-88A containing PIMs were successful in a single Sc transport cycle, reusability of these membranes was further investigated.

Regardless of the temperature, with every reuse of DEHPA-based PIMs, overall performance (k_{ex}, χ_{Sc}, amount transported) considerably decreased (Figure 6.3).
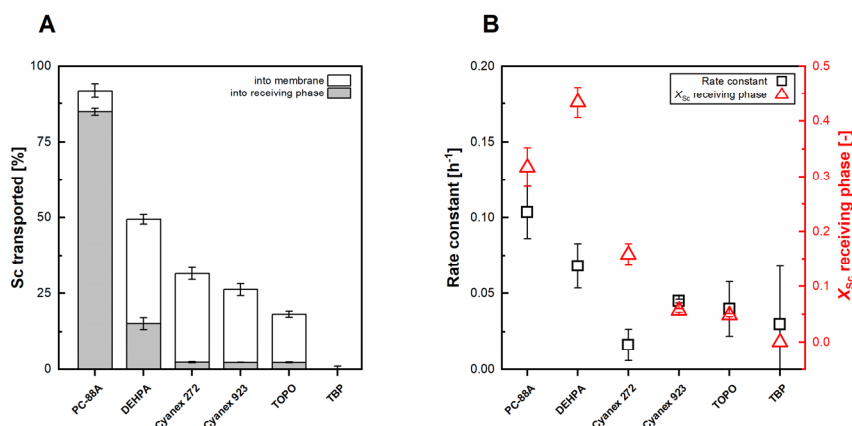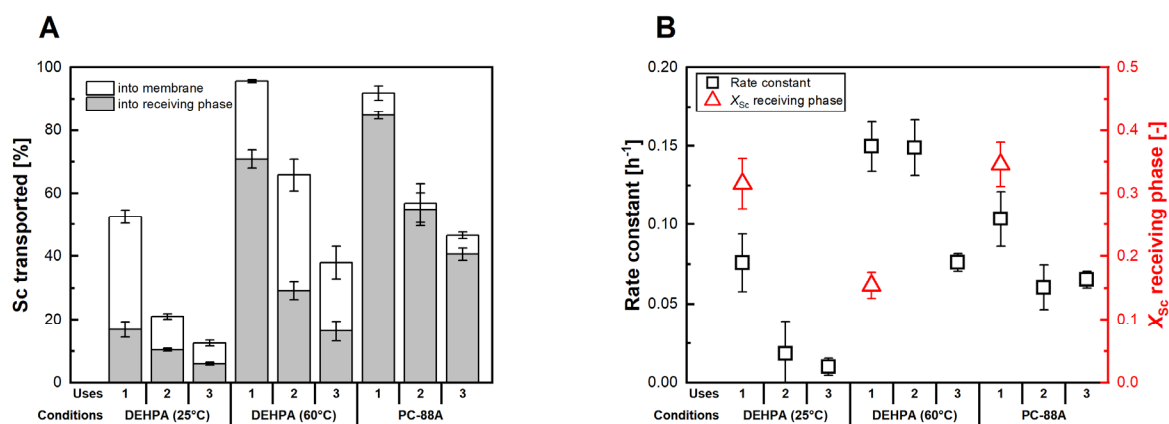
Figure 6.3 Amount of Sc transported into the membrane and transported into the RP relative to the total amount of Sc in the feed (A). Rate constants of the Sc transport into the membrane and mole fraction of Sc in the RP after 24 h (B).

Furthermore, membrane appearance visibly changed during reuse, turning from slightly transparent and colourless to brownish and untransparent (Figure 6.4). Eventually, a salty crust covered the feed side of the membrane.
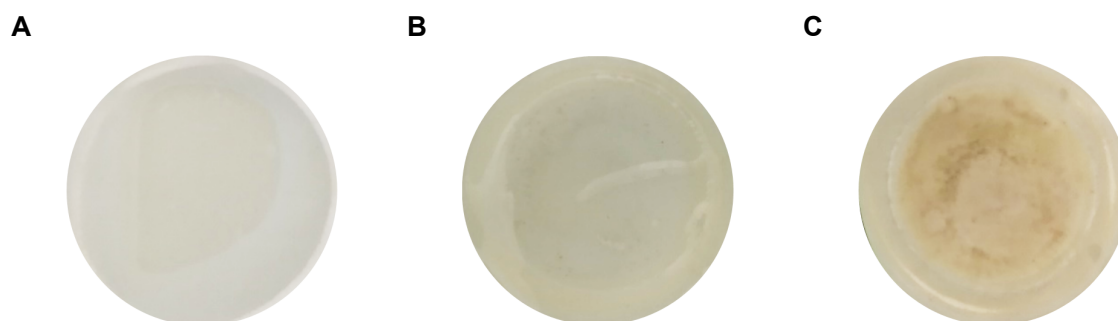
Figure 6.4: Comparison of benchmark PIM before (A), after single time (B) and after three-time use (C) for Sc recovery at 60 °C.

Based on ICP-MS results, the salt contained mainly Fe. Changes of the composition of the membrane were examined using µ-XRF and ATR-FTIR analyses. Principally, a loss of efficiency can be caused by leaching of plasticiser and carrier (i.e. NPOE and DEHPA) into the aqueous phases.[190] Hence, with every reuse the PIM would be increasingly depleted in DEHPA.

A qualitative µ-XRF analysis of benchmark PIMs, suggested DEHPA depletion and metal (e.g. Sc and Fe) enrichment (Figure 6.5). During the analysis, the contacted surfaces of three differently often used specimens were compared with their still pristine edges. After image processing, the corresponding element content to every pixel was expressed as a different colour and in adjusted brightness, according to its concentration (Figure 6.5). This was used as an estimate for the respective element concentration in the membrane. Notably, the peak for Sc was derived from its theoretical position in the XRF spectrum due to overlap with energetic bands of other elements.[353] Hence, the analyses showed higher background noise for Sc, limiting the possible interpretation.

In the unused membrane no Fe and Sc was found. Phosphorous on the other hand was uniformly distributed within the PIM. After the first use at 60 °C, the contacted centre and the pristine edge were visually separated through a darker line, where the O-ring compressed the membrane during the experiment. While Sc enrichment and P depletion could not be confirmed after a single use, Fe indeed seemed to accumulate in or on the membrane. This could be explained through the affinity of DEHPA for Fe^{3+}, or also indicate the deposition of $FePO_4$ on the membrane.[142] After three uses, the µ-XRF results clearly showed a decrease in P concentration, even though the PIM had contact to phosphoric acid. Hence, under the assumption only DEHPA contributed to the phosphorous content of the membrane, some carrier was lost during membrane reuse (Figure 6.5).

	Sc		Fe		P	
	Centre	edge	Centre	edge	centre	edge
Pristine						
1×, 60 °C						
3×, 60 °C						
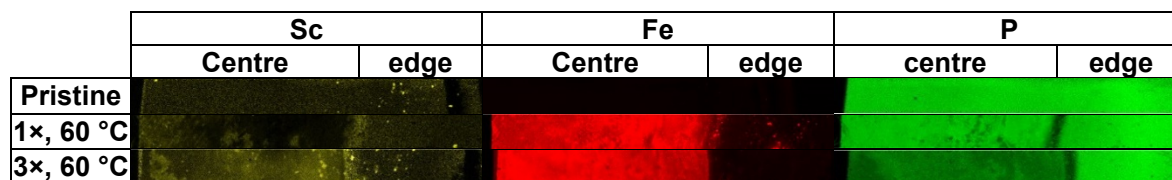
Figure 6.5 µ-XRF measurements of Sc, Fe, and P in the benchmark PIM before and after single, resp. three-times use at 60 °C. The labels 'centre' and 'edge' indicate the respective areas of membrane that were exposed to the feed and RP, resp. not exposed.

The chemical composition of the membrane was investigated further using FTIR spectroscopy. When comparing FTIR spectra of used and pristine PIMs, broader and additional bands can be observed after use, such as those indicating metal complexation at around 1060 cm^{-1}.[339] Nonetheless, the most prominent band of DEHPA (P-O-C, P-O-H stretching vibration, at 1016 cm^{-1}) was also well visible in all PIM spectra and thus used as a proxy for the DEHPA content of the membrane.[354,355] Comparing DEHPA-PIMs used at room temperature, even three-times reuse led only to minute decrease of the DEHPA stretching vibration (Figure 6.6). Therefore, DEHPA appeared to be preserved in the PIM. On the contrary, when used three-times at 60 °C the band at 1016 cm^{-1} appeared considerably less intensive, supporting losses of DEHPA as assumed after µ-XRF analysis.
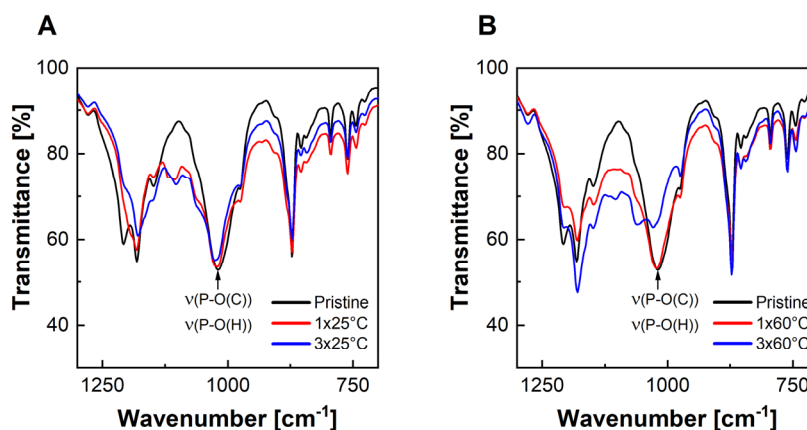
Figure 6.6 Sections of ATR-FTIR spectra recorded from DEHPA PIMs during reusing experiment at room temperature (A) and at 60°C (B).

PC-88A-containing PIMs were only tested and reused at room temperature, due to their already high performance. However, also these PIMs showed considerably deteriorating Sc transport in terms of speed, selectivity and total amount with membrane reuse. FTIR measurements, suggest also here the loss of some carrier, but broadening of relevant bands after membrane use impaired the interpretation. Aside of carrier losses, metal accumulation in the membrane could also contribute to the deterioration of PIM performance. In that regard, complexes could precipitate within the PIM and bind carrier, which would no longer be available for metal transport across the membrane. Overall, the results indicate considerable constraints for the long-term use of PIMs in the designed process.

6.4.3 PIM crosslinking

In order to improve PIM stability and carrier preservation within the membrane, the concept of crosslinking (CL) was applied. Therefore, a part of the polymer was replaced with a crosslinker (PEG-DMA). Initially, polymer ratios from 1:1 up to 9:1 (PVDF-HFP:PEG-DMA) were targeted (Table 6.3).

However, with increasing amount of crosslinking polymer, the structural integrity of the membranes decreased. Hence, DEHPA membranes with a polymer ratio of 1:1 and PC-88A PIMs with a ratio of 3:2 were omitted. Following the best conditions for 'standard' DEHPA and PC-88A PIMs, crosslinked DEHPA PIMs (ratio 7:3) were examined at 60°C, whereas the PC-88A crosslinked membranes (ratio 7:3 and 9:1) were examined at room temperature (Figure 6.7).
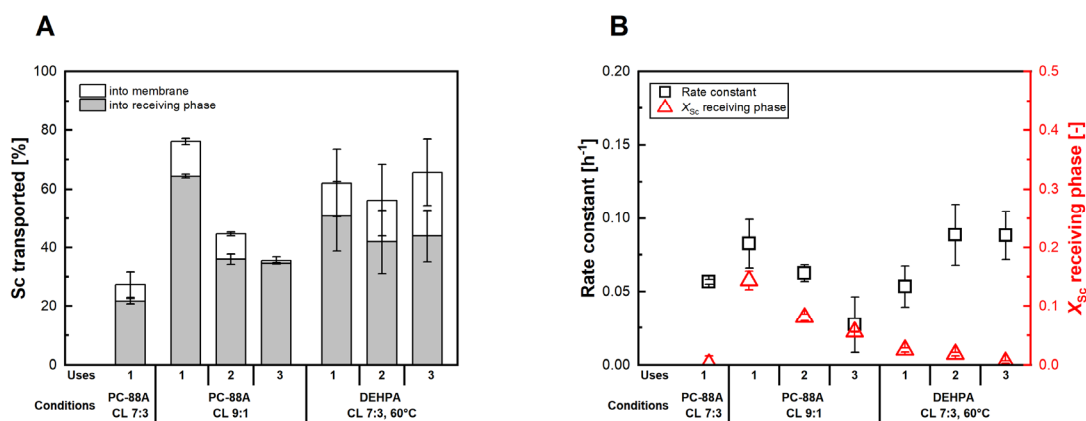
Figure 6.7 Comparison of crosslinked PIMs. Amount of Sc transported into the membrane and transported into the RP relative to the total amount of Sc in the feed (A). Rate constants of the Sc transport into the membrane and mole fraction of Sc in the RP after 24 h (B).

In terms of Sc transport, all crosslinked membranes performed worse compared in single-use experiments to their non-crosslinked equivalents (Figure 6.7). With decreasing polymer ratio, the Sc transport deteriorated. Therefore, only PIMs with highest polymer ratio were considered for reusing experiments.

In direct comparison, the crosslinked DEHPA membranes appeared to underperform during the first transport cycle but yielded more constant Sc transport with reuse (Figure 6.7). While this appears beneficial, the caveat was a considerably worse selectivity than reported before.[347] Probably, the increased PEG content increased the PIM permeability for impurities, undermining the selectivity of the carrier. Nonetheless, this result shows, that crosslinking DEHPA PIMs could improve Sc extraction from TiO_2 acid waste in the long run, due to better reusability.

In comparison, crosslinked PIMs with PC-88A did not show any benefit relatively to their respective 'standard' equivalents (Figure 6.7). Principally, deterioration followed a similar trend as observed for the not-crosslinked membrane. However, the crosslinked PC-88A membrane performed inferior to the standard version in every considered aspect.

All membranes of this study were compared in regard of their ability to transport Sc into the receiving phase (Figure 6.8). Except for the benchmark PIM at room temperature, in all experiments ≥ 50% of the total Sc was transported into the RP within 24 h. During the second and third reuse in case of the 'standard' membranes downward trends were clearly observed. The crosslinked PC-88A membrane, however, showed little difference between the second and third run, although transporting considerably less after the first run. In case of the crosslinked DEHPA PIM (7:3 ratio), almost constant performance was observed, wherefore it became the membrane transporting the most Sc during the third run (Figure 6.8).
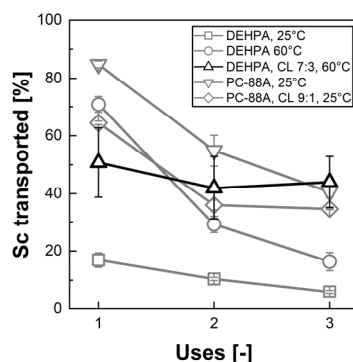
Figure 6.8 Comparison of Sc transported into the receiving phase for different reusing experiments.

O'Bryan et al. previously reported, that crosslinking can improve the stability of a PIM.[201] Based on the results with PC-88A and DEHPA PIMs, this could explain the improved reusability. Apparently, more research is needed to understand the deterioration mechanisms and to show long-term reusability. Nonetheless, crosslinking poses a promising approach to further tune PIM-based element recovery.[347]

6.4.4 Tandem PIM-NF for receiving phase reuse

Despite the advantages shown for PIM-based Sc recovery, the use of 7 M H_3PO_4, calls for recovery strategies on itself, as also P is considered a CRM. In the past, nanofiltration was thoroughly studied for phosphoric acid purification.[172] Hence, this principle was applied on the RP, using spent acid

from PIM-based Sc recovery experiments. Initially, the influence of the pressure was examined. Here, the permeate flux increased with the TMP, which was expected due to the proportionality of TMP and water flux (Figure 6.9).[356] At the same time, P retention stayed almost constant, while Sc retention slightly increased with rising pressure (96.3% at 10 bar; 98.0% at 35 bar). This can be explained by an enhancement of convective P-transport, which does not seem to be the case with Sc.[235] Notably, during filtration, the feed turned increasingly turbid, due to entrapment of air within the viscous liquid, partially impairing the flux measurement.[345] As the highest permeate flux and Sc retention was observed at maximum TMP (35 bar was the upper limit of the filtration system.), this pressure was chosen for H_3PO_4 recovery. During the recovery experiment, R_{Sc} was constant at 97.9 ± 0.3%, while the average R_P was 2 ± 1% (Figure 6.9). The permeate flux remained mostly constant at 2.3 ± 0.2 L m^{-2} h^{-1} over the entire filtration.
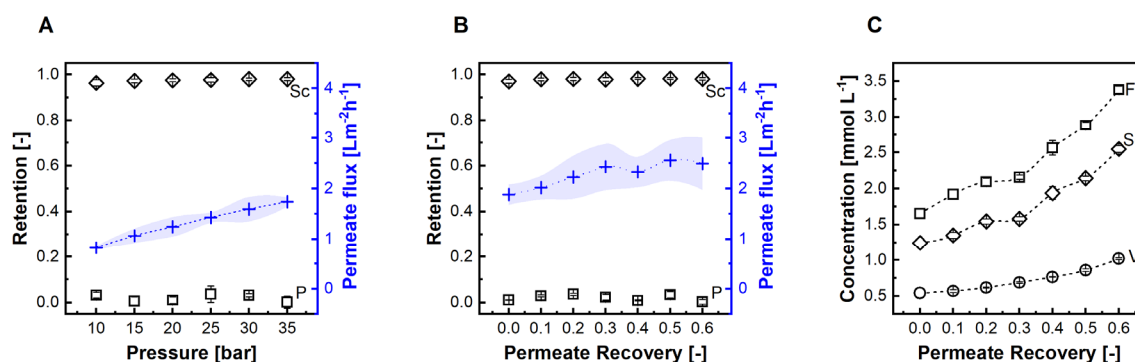
Figure 6.9 Pressure dependence on the retention of Sc and P and permeate flux (A). R_{Sc} R_P, and permeate flux (B) and Sc, V, Fe concentration development in the retentate (C) during the permeate recovery experiment.

Due to limited amount of spent RP, a maximum of 60% permeate recovery was possible with the filtration setup to maintain a turbulent cross-flow rate. However, the results suggest the possibility of at least some more H_3PO_4 recovery without significantly impairing permeate flux or purity. In fact, concentrations of metals were approximately two orders of magnitude higher in the retentate (~mM range) compared to the permeate, while H_3PO_4 concentration (~7 M) was unchanged (Table 6.5). Ultimately, metal retentions were more than twice as high in the retentate at the end of the experiment compared to the feed (Table 6.5). Hence, NF showed overall a promising potential for combination with the developed PIM system and for future application.

Table 6.5 Retention and concentration of Sc, V, Fe and H_3PO_4 in the feed, permeate and retentate (H_3PO_4 determined by titration).

Species	Retention [%]	Feed [mol L^{-1}]	Permeate [mol L^{-1}]	Retentate [mol L^{-1}]
Sc	98	1.34×10^{-3}	6.65×10^{-5}	2.81×10^{-3}
V	97	6.44×10^{-4}	3.15×10^{-5}	1.13×10^{-3}
Fe	98	1.95×10^{-3}	8.49×10^{-5}	3.85×10^{-3}
H_3PO_4	0.5	7.1 ± 0.1	7.2 ± 0.1	7.2 ± 0.1

Although the concentrations of phosphoric acid and impurities in the recovered NF permeate were confirmed by ICP-MS and titration, the obtained solution was used in a final PIM transport experi-

ment to confirm its reusability. Here, Sc transport at 60 °C with the benchmark PIM, was directly compared with pristine and recycled RP. Very comparable results were found (Table 6.6). If at all, recycled RP was even slightly superior to fresh H_3PO_4 (Table 6.6).

Table 6.6 Comparison of pristine and NF-treated H_3PO_4 in a transport experiment (60 °C) using benchmark PIMs.

Receiving phase	k_{ex} [h^{-1}]	χ_{Sc}	Sc extracted [%]	Sc in RP [%]
H_3PO_4, 7 M, pristine	0.15 ± 0.02	0.09 ± 0.01	96 ± 0.5	71 ± 3
H_3PO_4, 7 M, recycled	0.19 ± 0.01	0.13 ± 0.01	98 ± 0.5	80 ± 5

Therefore, the reusability of the RP after work-up through NF can be confirmed. This strategy would not only allow to save on costs for fresh H_3PO_4, but also prevents wasting the CRM phosphorous. In addition, NF can effectively concentrate Sc from the RP. Potentially, if driven further, the solubility limit could be reached, allowing to easily separate a crude Sc product.[263,264] When compared to the previous NF-SX approaches, tandem PIM-SX simplifies the process engineering for Sc recovery considerably.[256,283] In view of the NF, the spent RP is still a concentrated solution, but it contains mainly H_3PO_4 and only minute amounts of dissolved metals, making it far less complex than the TiO_2 waste. Furthermore, the stream is not chloride-rich, allowing the use of standard materials for high-pressure filtration, such as 316 L or other stainless-steel alloys. On the downside, NF requires time and energy, driving the OPEX of the recovery procedure. More advanced NF membranes can certainly be a benefit for future tandem PIM-NF application. This could be for instance lbl-membranes.[235,357] Overall, the results suggest this combination as advantageous for Sc recovery.

6.5 Conclusion

Previously, we reported on PIMs for the extraction of Sc from TiO_2 acid waste.[347] Within the current study, alternative carriers and the reusability of PIMs and H_3PO_4 as a receiving phase for Sc, were examined. Therefore, five additional phosphorous-based carriers were selected and tested analogue to the already reported DEHPA. Of all tested compounds PC-88A showed the highest performance (transport speed, Sc selectivity and overall transported quantity). In terms of PIM reusability, specimens of the two most successful membranes, containing PC-88A or DEHPA, were used in three consecutive transport experiments. In each scenario considerably deteriorating Sc transport was observed with increasing number of reuses. As a potential solution, PIMs were crosslinked with PEG-DMA using the method reported by Hoque et al..[197] Crosslinked membranes showed inferior Sc transport properties, but might be advantageous for prolonged PIM use according to the results. This effect appeared to be the strongest for DEHP-based crosslinked membranes, but further investigations are needed for ultimate confirmation. Nonetheless, more insight is needed to understand the underlying principles of deterioration. Using µXRF and ATR-FTIR methods in this study, the depletion of carrier and the enrichment of metal salts within the membrane appear likely. Lastly, the reuse of spent RP after work-up with NF was investigated. In this regard, excellent

separation of impurities and H_3PO_4 was found, suggesting NF as a promising addition to PIM-based Sc recovery.

This study showed consequent steps to the implementation of PIM-based Sc recovery in a real-world scenario. The challenges and solution strategies described could well extend to other processes using metal extractants such as SX, solvent-impregnated resins or various types of liquid membranes. For instance, the combination of the two complementary membrane processes PIM transport and NF has yielded synergies that could also apply to the aforementioned processes. Ultimately, the results may enable alternative membrane-based hydrometallurgy and pave the way for its future application.

This page is intentionally left blank.

7 Conclusion

7.1 Summary of the research work

The presented work dealt with the recovery of the critical raw material scandium from industrial acid waste by means of advanced membrane processes. In this regard, two complementary strategies have been pursued: nanofiltration for Sc concentration (Chapter 2, 3 and 4) and polymer inclusion membranes for direct selective Sc separation (Chapter 5 and 6).

Chapter 2 dealt with the first tests on nanofiltration for Sc recovery from industrial TiO_2 acid waste. For this purpose so-called layer-by-layer assembled membranes (lbl-membranes) were made and examined on their potential for Sc recovery under challenging conditions. For making lbl-membranes, negatively charged hollow-fibre polyether sulfone ultrafiltration membranes were coated alternatingly with polycations and polyanions. In this study the effects of coating conditions, number of bi-layers, and pH on Sc and Fe retention were investigated in depth, using model solutions. The most promising membrane was coated in the presence of 0.5 M NaCl with three bi-layers of PDADMAC/PSS and the optimal pH was 1.5. Both was used for Sc recovery from real acid waste. During filtration of the acid waste (diluted 1:5, pH 1.5), high selectivity for Sc over impurities such as Fe and U was observed. Sc retention started at > 60% and decreased only slightly during permeate recovery (70% total recovery rate). In contrast, Fe and U were not retained at the beginning and increasingly permeated against their concentration gradient (i.e. showed negative retentions). The permeate flux was remarkably high for NF and reached 27 L m^{-2} h^{-1} at 5 bar feed pressure. For comparison a commercial membrane (Duracid, GE, USA) was operated under the same conditions. Thereby, only 1 L m^{-2} h^{-1} was measured, whereas lower Sc retention (50%) was observed. At the same time Fe retention was slightly higher (4%). Therefore, the novel membrane was more water-permeable, while offering higher selectivity for Sc over Fe than the commercial membrane. Overall the results suggested lbl-NF-membranes as a viable option to concentrate Sc, while depleting impurities contained in the TiO_2 acid waste.

Chapter 3 dealt with the elaboration of a novel route for Sc by-production by means of NF and SX. The starting material of the study was industrial acid waste from a European TiO_2 production site. Initially, effects of pH on element solubility were studied. Quantitative precipitation of several impurities (Ti, Th, Zr, U) was observed at pH of 1.0-1.5 while keeping most of Sc dissolved (> 60%). Unlike in the previous study (Chapter 2), solid-liquid separation was augmented by ultrafiltration, which further improved removal of the above-mentioned precipitated elements. Using the prepared solution, isobaric dead-end filtration tests with six commercial nanofiltration membranes (see Annex 9.2) were conducted. Based on permeate flux, total Sc retention and Sc over Fe selectivity, the most promising membranes were the SelRO MPF-36 (Koch Separation Solutions, USA) and the NanoPro A-3014 (AMS Technologies, Israel). Because the A-3014 offered considerably higher Sc

retention, it was selected for further investigations, although the MPF-36 offered far higher permeate flux. In cross-flow filtration mode, pressure dependence (10-35 bar) and permeate recovery tests were conducted. With increasing pressure, an asymptotic increase in Sc and Fe retention was observed. The permeate flux rose especially between 30 and 35 bar, wherefore the latter was chosen as operating pressure for permeate recovery. Using ~2.0 L of pre-treated acid waste, 60% permeate was recovered. Due to high retention (82-95%) most of Sc (84%) was preserved in the obtained concentrate (0.8 L). Impurities, such as Fe, were effectively depleted (-42%) as retentions steeply fell with progressing permeate recovery. Both, the initial acid waste and the NF concentrate were subjected to SX investigations. Here nine different organic extractants, resp. mixtures of these, were benchmarked on their capability of selectively extracting Sc. In this regard, SX of the untreated acid waste appeared challenging due to the high content of impurities (e.g. Ti, Zr, Th, U). Notably, after NF treatment these issues did not occur in SX, most likely due to the pH adjustment and impurity removal stage. While every tested extractant or combination thereof extracted Sc virtually completely, a synergetic mixture of D2EHPA and the primary amine N1923 (0.1 M : 0.05 M) yielded the highest selectivity. Additionally, it was found that oxidation of Fe^{2+} can lead to higher coextraction of Fe. Hence, by addition of Fe^0, coextraction of Fe was successfully suppressed. After SX, subsequent scrubbing with HCl (4 M) removed most residual coextracted elements (mainly V and Fe). Eventually, the loaded and scrubbed organic phase was stripped with NH_4F solution yielding > 97% pure Sc strip liquor (measured on metal base). Ultimately, the entire seven stage process was discussed and analysed in regard of its integration potential into the existing TiO_2 manufacturing process.

Chapter 4 dealt with the scale-up of the previously developed NF-SX Sc recovery process for TiO_2 acid waste. For this purpose a pilot unit was constructed, comprising a reactor for pH-adjustment, a bag filtration unit for sludge removal, and a modified reverse osmosis unit for ultra- and nanofiltration (Figure S9.6, Annex). The SX pilot consisted of 12 PVDF mixer-settler units (MEAB MSU-0.5, MEAB Chemie Technik GmbH, Germany), which were connected in series (Figure S9.7, Annex). In total, 800 L of acid waste from a European TiO_2 production site was treated in the pH adjustment stage, using 150 L NaOH (30%, w/w) to reach a pH of 1.5. After 24 h reaction and 48 h settling time, the slurry was filtered, yielding 250 L of wet hydroxide sludge and 700 L of filtrate. Of this, ca. 70% (500 L) was freed from residual particles by ultrafiltration. Approximately 400 L of clear ultrafiltrate was obtained, while the residual 100 L had turned into a gel due to the high sludge content. The related drop in efficiency led to the abortion of the ultrafiltration. Thereby, the residue was discarded. Eventually, Sc concentration by means of NF (NanoPro A-3014, AMS Technologies, Israel) was examined batchwise (five times, 50 L each). At a permeate recovery rate of 60%, high retention of Sc was found throughout the batches (90% on average). Therefore, the Sc yield of the NF stage was 87%. By comparison, the average retention of Fe in NF was only around 20%, resulting in a depletion of approximately 55% of the initial Fe. Likewise, 53% of V and 73% of U were removed

by NF. All these impurities showed a decreasing retention trend per batch, but also globally from batch 1-5. From batch to batch, the permeate flux remarkably improved, especially after the first. Thus, NF was 260% faster (average values) in the last run compared to the initial batch. Thus, with ongoing operation the NF became considerably more efficient measured on Sc selectivity and permeate flux. A total of 100 L NF concentrate was produced and used for pilot SX. Almost perfect Sc yield was achieved over all three stages involved in 'SX' (~98%, combined value of extraction, scrubbing, stripping). However, although coextraction of impurities was mostly suppressed or later resolved in scrubbing stage as described previously (Chapter 3), the overall purity in the strip-liquor was inferior to the previous study (90% instead of 97%). It is believed, that the SX had not yet reached its equilibrium, deteriorating the selectivity. Still, 12.7 g of Sc were extracted from the NF concentrate. Subsequent to SX, conditions for antisolvent crystallisation were examined. Here, the addition of 8 M EtOH was found optimal, due to the highest yield of Sc (96%). The purity of the final product was determined at 93% on metal basis, resp. 95% on ammonium-fluoride complex basis. Ultimately, material and energy flows of the entire process were evaluated in comparison to ScF_3 as the closest commercial product. Overall, these process costs were found to be below market value of ScF_3. However, the costs for NaOH and energy in NF were particularly high, contributing considerably to the total OPEX. Viable options to decrease the OPEX costs were presented and discussed, leading to the estimation, that roughly 80% of the cost could be saved with available options. In conclusion, the pilot experiments suggest the applicability of NF for the recovery of Sc in combination with SX and antisolvent crystallisation.

Chapter 5 dealt with the development of a process based on polymer inclusion membranes for the Sc recovery from real TiO_2 acid waste. A design of experiments study was carried out to systematically determine the optimal membrane composition of DEHPA, NPOE and PVDF-HFP with respect to Sc extraction. Based on Sc loading capacity, selectivity, extraction rate, and structural integrity, the optimal compromise was found at a ratio of 50/40/10% w/w (PVDF-HFP/DEHPA/NPOE). Subsequently, receiving phases were examined. Here, different concentrations of HCl, H_2SO_4 and H_3PO_4 were tested. In regard of HCl, no concentration allowed for Sc elution. Using H_2SO_4, elution of Sc started at ~5 M but even at 12 M Sc only ~70% was recovered from the membrane, while material degradation was already observable. In contrast, H_3PO_4 was remarkably effective, eluting some Sc already at ~2 M and reaching full elution at ~7 M. Therefore, H_3PO_4 (7 M) was deemed the optimal receiving phase for Sc. At the same time, yttrium was eluted by any of the tested receiving phases. Based on the optimised PIM and receiving phase, Sc transport was investigated on model solutions containing 15 elements commonly present in titania chloride-route acid waste. Here, concentration of all elements was 0.1 mM in one model solution and 1 mM in a second solution. In both cases, Sc transport into the membrane reached approx. 90% after 24 h. Elution within the same time was relatively slower, whereas the fractions of the total Sc reaching the receiving phase were ~50% (0.1 mM model feed) and ~33% (1 mM model feed) respectively. The two experiments differed consid-

erably in terms of Sc transport selectivity: when the diluted feed was used, the mole fraction of Sc reached only 0.03 in the receiving phase, while it was 0.60 in case of the 1 mM feed. The reason for this behaviour could not be clarified. However, it was hypothesised, that it might have been caused by different carrier to element ratios. Here it was stated that an excess of carrier would favour carrier-dimerization, which is known as preferred arrangement for some elements, such as most lanthanides. As in other studies Sc was preferably coordinated by DEHPA-monomers, this was assumed leading to the observed selectivity differences. Nevertheless, in virtue of the more selective, hence successful, transport of Sc in case of the more concentrated solution, the developed PIM system was used for transport experiments with real acid waste. Therefore, pre-treated acid waste was used, as already before during NF-SX studies (Chapters 3 and 4). The developed system was able to transport virtually all Sc from the acid waste into the membrane within 24 h. At the same time ~28% reached the receiving phase with high selectivity, indicated by a Sc mole fraction of 0.34, compared to 0.00056 in the feed (increase of > 600). Moreover, after the transport experiment, mainly two elements (Fe and V) were still associated with Sc in the receiving phase, demonstrating a considerable simplification of the matrix. Ultimately, a transport experiment at 60 °C was carried out with real acid waste. Here, Sc was transported outstandingly fast, with > 80% of Sc being extracted from the feed after 4 h. Within 24 h ~63% of the Sc was found in the receiving phase. Although the co-transport of impurities increased, selectivity for Sc was still high as indicated by a 300-times higher Sc mole fraction in the receiving phase compared to the feed. The majority (86 %) of impurities in the receiving phase consisted still of V and Fe. Membrane degradation was briefly examined using FTIR-spectroscopy, whereas spectra recorded before and after use at 60 °C indicated virtually no changes in the composition. The results from transport experiments were compared to other liquid membrane/PIM studies for Sc extraction. Principally, similar trends in terms of total transported Sc fraction were found. However, with respect to the Sc flux, up to 44 times higher values were found in this study, which was assumed a result of the initially higher Sc concentrations, but also due to the use of heat. In conclusion, the developed PIM system appeared to be suitable for Sc recovery from real acid waste.

Chapter 6 deepened the knowledge of the polymer inclusion membrane-based approach of Sc recovery from titania acid waste. The previously designed procedure (Chapter 5) was reviewed with regard to the choice of extractant, the reusability of PIMs, the effects of membrane crosslinking and the addition of NF to recycle the spent receiving phase. When comparing different carriers, DEHPA was found the most selective extractant, but not the most effective. Instead PC-88A showed outstanding Sc transport capability, transporting as much as 85% of the total Sc into the receiving phase, where the mole fraction of Sc reached 0.32 on measured metal base. The previously developed PIMs based on DEHPA were only competitive in terms of transport quantity, when operated at 60 °C. While comparable results to the previous study were found at 60 °C, at room temperature transport was worse. It is believed that this may have been a result of different acid waste composi-

tions. Triple reuse was tested with DEHPA and PC-88A containing membranes using real acid waste. Here, DEHPA membranes were tested at room temperature and 60 °C, while PC-88A containing membranes were examined only at room temperature. Throughout the tests, considerably deteriorating extraction performances were observed with ongoing reuse number. Searching for causes, µXRF- and ATR-FTIR analyses were carried out. These revealed a decreasing carrier content of the PIMs, while metals from the acid waste increasingly enriched in the membranes. Here, intending to improve the membranes, crosslinking using PEG-DMA was tested. Generally, this approach appeared to be counterproductive for Sc transport with respect to transport rates, selectivity and total transported amount. Furthermore, the attempted crosslinking of PC-88A containing PIMs offered no benefits over the 'standard' equivalent. In regard of DEHPA PIMs however, more consistent reusability was observed within three cycles of Sc recovery. Although the selectivity suffered, this experiment may give a promising outlook for future experiments to improve the stability and applicability of PIMs in real hydrometallurgical scenarios. Ultimately, the recycling of the receiving phase by means of NF was demonstrated. In this regard, a NanoPro A-3014 membrane (AMS Technologies, Israel) was used to treat spent receiving phase from various combined PIM experiments. After investigating the effect of pressure on element retentions and permeate flux, 35 bar (the limit of the system) was chosen for a permeate recovery experiment. Overall, excellent separation of Sc from the spent RP was achieved using NF. While Sc retention remained over the entire pressure range above 95%, P retention at maximum reached only 3.6%. On the downside, the permeate flux was generally low, reaching maximally 1.7 L m^{-2} h^{-1} in pressure tests. Most likely this was due to the relatively high acid concentration of the feed, increasing its osmotic pressure. During permeate recovery 60% of H$_3$PO$_4$ was recovered. Notably, this amount was limited by the available spent receiving phase, whereas based on the observations higher permeate recovery potential was anticipated. This conclusion was based on the observed stable and unimpaired filtration performance during the experiment. During permeate recovery, the means of permeate flux, Sc recovery and P retention were R_{Sc} = 97.9 ± 0.3%, R_P = 2 ± 1% and J = 2.3 ± 0.2 L m^{-2} h^{-1}, respectively. The recycled H$_3$PO$_4$ was analysed using ICP-MS and titration, revealing an acid concentration of 7.2 M and metal concentrations in the order of 10^{-5} M in the final product. The latter was two orders of magnitude lower compared to the untreated H$_3$PO$_4$. Thus, for a final confirmation of the reusability, the purified receiving phase was used for a Sc transport experiment with DEHPA-based PIMs and real acid waste at 60 °C. A control with pristine H$_3$PO$_4$ was run in parallel. Here no significant difference was found between the two, wherefore the overall reusability was seen confirmed. This series of follow-up tests on PIMs for Sc recovery elucidated strengths and weaknesses of the PIM approach.

7.2 Discussion

The presented work aimed to develop membrane technologies for the recovery of Sc from a complex secondary stream. In this regard, the thesis had a highly application-oriented focus. Part of the research on NF for Sc recovery, were investigations on novel lbl-membranes compared to commercial products. Given the stated advantages of lbl membranes over commercial membranes, it might be surprising that the latter ended up being used for more intensive testing and upscaling. Nonetheless, the work on lbl-membranes brought fundamental insights into the use of NF for Sc recovery from acidic chloride waste. At first, there was a considerable lack of knowledge, wherefore neither materials for suitable membranes nor for the filtration conditions were known. Through systematic screening, it was possible to identify the UFCLE(PDADMAC/PSS)$_3$ as a suitable lbl-membrane, which seemed to work well at a pH of 1.5. Under these conditions, it was for the first time demonstrated that NF has a chance as a tool for Sc separation. One of the most promising observations was, that at an average Sc retention of ~60%, some impurities (e.g. Fe and U) permeated even against their concentration gradient. This suggested that the ion selectivity of lbl-NF-membranes can indeed be exploited to enrich Sc in the retentate/concentrate, while simplifying the matrix composition. Furthermore, the system seemed to be clearly superior to a compared commercial membrane, by offering a substantially higher permeate flux, as well as better Sc retention, and selectivity. Eventually, the operation at low pressures (5 bar) would allow for the use of cheap acid resistant plastic components during construction of a filtration plant. Nevertheless, there were still some caveats to the use of lbl-membranes. In the presented study, only diluted acid waste was used. This was in part due to stability concerns, as layers from PSS/PDADMAC were known to disintegrate in contact with electrolyte solutions.[214,358] In fact, after exposure to 1 M HCl, deterioration of the retention capabilities of the chosen membrane was observed (Figure S9.2, Annex). A thicker layer seemed to help, but long-term stability especially when exposed to concentrated acid waste was uncertain, at least with the combination of polyelectrolytes (Figure S9.2, Annex). Furthermore, a five times higher concentration, would have led to a considerable increase of the osmotic pressure of the feed. The prepared hollow-fibre membranes, however, were limited in regards of their maximum operation pressure (< 10 bar). In the case of pre-dilution of the acid waste, the purpose of NF to re-concentrate Sc may also be questioned, especially if it cannot be guaranteed that all Sc is retained during NF. Lastly, as the membranes were custom-made, upscaling of their production would have posed an additional challenge. Relatively simple changes and additions, such as using stronger polyelectrolytes and more pressure-resistant/thicker substrates (e.g. ceramic UF membranes) or automated coating units, could potentially address some of these aspects.[214,357] However, due to their drawbacks and considering the projected pilot operation, commercially available membranes were deemed the more mature and reliable option in the frame of this thesis. In comparison to the lbl-membrane tests, the combination of TFC NF-membranes and concentrated acid

waste negatively impacted permeate flow rates and pressure requirements for the filtration. Still, some of the 'looser' NF-membranes (MWCO > 300 kDa) proved useful for the recovery approach. High Sc retentions (> 90%) allowed its preservation. At the same time, permeation of impurities, such as Fe, increased during permeate recovery, leading to their depletion. As demonstrated during pilot experiments, this effect increased with membrane reuse, potentially due to better equilibration. Thus, the choice of the commercial NanoPro A-3014 can be considered a suitable example to demonstrate the application of NF for Sc recovery from TiO_2 acid waste. Although it cannot be conclusively determined whether or not the concerns about the lbl membranes would have manifested themselves, the results of Chapters 3 and 4 suggest that the choice of commercial membrane was appropriate in terms of the desired demonstration of NF applicability at laboratory and pilot scale. Based on initially described technological obstacles (see section 1.6) the applicability of NF and the proposed process route for Sc recovery can be reviewed. Overall, it was demonstrated, that the aggressive HCl waste can be handled by the selected means, in small and in large scale. Most of the related issues (e.g. high acidity, suspended solids, NORM) were solved by pH adjustment and S/L separation. On the other hand, these two stages were probably also the least optimised, comprising substantial Sc losses and high time and labour intensity. However, both stages are already part of the existing wastewater treatment process during TiO_2 production. Thus, their applicability can be seen as granted and process adaption would only mean a change of the target pH. Moreover higher yields seem likely on the full-scale plant. After pre-treatment, the solution remained highly concentrated, which, however, did not pose a problem for the used NF membrane. With regard to process engineering on the other hand, material incompatibility was found for parts made of stainless steel (1.4404), due to the high chloride content. Corrosion-resistant alloys, such as 'Super Duplex' (1.4410) or Hastelloy® C-276 (2.4819) appeared suitable throughout. On the other hand, considering the investment costs, it would be desirable to omit these alloys. As a workaround, to provide pressure and corrosion resistance a common option in the chemical industry would be the use of lining.[359] From this perspective, NF application is considered viable.

The applicability can be reviewed further with respect to Sc separation from a complex matrix, the compatibility of NF with surrounding processes, and the scalability. Overall, substantial amounts of Sc were recovered from the secondary stream (43%, 9 stages, Figure 4.1). Certainly, SX was a key stage, removing the majority of impurities and enriching Sc by a factor of ten. Nevertheless, upstream treatment was beneficial for SX, resulting in lower coextraction of impurities and better phase separation (NF concentrate vs. untreated acid waste). With respect to NF, the process volume reduction by 60%, the ~2.2-fold concentration of Sc, and the depletion of impurities (Fe, V, U, etc.) was considered advantageous for Sc recovery. Of particular note is the complementary separation effect of NF observed for U. Uranium permeated to high degree against its concentration gradient, resulting in the removal of more than 70%, while in SX, no separation was possible. As thorium in contrast showed high retention, NF could pose a method to separate these two elements in the fu-

ture. Further, benefits for TiO_2 production could arise, such as lower water consumption by reusing the NF permeate as gas scrubbing water and lower freight if the process acid were sold to waste recyclers. Given that other tri- and tetravalent elements, such as Al^{3+}, Ti^{4+}, and Th^{4+}, have exhibited comparable or even higher retentions, the use of NF could be extended to the recovery of these elements as well as to the recovery of REEs. Regarding the scalability, no disadvantages were observed when treating 125 times more volume with a ~5 times larger membrane. In fact, NF appeared to perform better (higher R_{Sc}, higher Sc over Fe selectivity, higher permeate flux) when operated for longer and on larger scale. This can becomes especially evident when comparing the initial dead-end filtration test (Figure 3.2), to the larger lab scale tests (Figure 3.3), to the final pilot experiments (Figure 4.3). In terms of overall process scalability, SX was found to perform initially worse during pilot experiments, which indicated the need for longer operation and equilibration after upscaling. However, one caveat of NF was the energy consumption, which could result in cost that outweigh the described advantages. It should be repeated that, as outlined in Chapter 4, the specific energy consumption estimated from the pilot experiments was not realistic. Full scale units are operated far more energy efficient, which with respect to the observed scalability of NF, seems a logical step to improve the overall applicability. In practice, zero-liquid-discharge methods already utilise high-pressure reverse osmosis systems (up to 300 bar) to concentrate brine (100-250 g L^{-1}), which consumes considerably less energy (~5 kWh m^{-3} vs. ~265 kWh m^{-3} measured here).[360] Therefore, if such processes can be employed to avoid disposal costs and to recover water, the energy consumption will most likely be no argument against the applicability of NF for the recovery of valuable elements. From another perspective, the availability of renewable energy sources could make the cost of energy less of a factor in the future.[361] If this were to happen, the low material footprint of NF could make it a highly recommendable addition to a wide range of existing extraction processes. In the meantime, improvements through engineering or in the field of highly permeable NF-membranes, such as those achieved through the lbl-approach or advanced materials like MXenes[152] may increase the popularity of NF for hydrometallurgical tasks.

In summary, the presented results suggest the potential of NF for element recovery from complex acidic streams. NF provided complementary separation when compared to established processes, while also removing a sizable portion of the process volume and certain impurities. Additionally, the pilot study demonstrated that NF became increasingly effective with longer operation and on larger scales. The overall work successfully developed the NF approach from non-existent to pilot scale, achieving the defined goal of enhancing its technology readiness level.

With respect to PIMs, a similarly application-oriented approach was taken as before in the development of the NF method. In parallel to this work, multiple studies about PIMs for Sc recovery were published. These studies presented novel carriers to extract Sc from diluted model solutions.[192,193,206] As PIMs are a membrane-based approach to mimic SX, it was assumed the development of a PIM process for TiO_2 acid waste could leverage the knowledge already gained on SX

(Chapter 3). Hence, to avoid screening of multiple extractants without information on the functionality of the surrounding membrane system DEHPA was fixed as the carrier for PIMs, while the composition of the membrane and the receiving phase were optimised. After completing this, tests with alternative carriers to DEHPA were conducted, revealing PC-88A as an attractive option (Chapter 6). This alternative was already reported before for Sc recovery using PIMs, however limited elution made the addition of co-extractants necessary.[206] As the optimised system presented here allowed for substitution of the carrier, while achieving fast transport, this could indicate a general suitability of some parameters. For instance, the polymer and plasticiser content as well as H_3PO_4 as receiving phase, could represent a useful starting point for further PIM-based Sc/element recovery. In regard of the applicability of PIMs on the aggressive and complex TiO_2 acid waste, the developed system, showed some chemical resistance and high Sc selectivity. Nevertheless, reusing the membranes posed a challenge, that has not yet been solved (Chapter 6). Remarkably, FTIR-analyses suggested, that even after a single use at 60 °C, the composition of the base materials did not change considerably. Instead, enrichment of metals, respectively salts, was observed already after the first transport cycle. Here, probably the use of phosphoric acid led to precipitation issues, because phosphates, such as vivianite ($Fe_3[PO_4]_2 \cdot 8\ H_2O$) and strengite ($Fe[PO_4] \cdot 2\ H_2O$) are known for their low solubilities also at acidic pH.[362] So far, it has not been attempted to 'clean' the PIMs prior to reuse, although this might help restoring the membrane's initial extraction capacities. Potentially, other mineral acids or descaling agents commonly used for membranes could be tested for this.[363] Instead of membrane cleaning, efforts have been made to find a solution that prevents carrier leaching during PIM use, which was particularly evident after use at 60 °C. According to Hoque et al. crosslinking could be one such option.[197] Here, the suitability of this approach in its current form was still limited due to the selectivity losses identified. Moreover, only one combination seemed to improve reusability. It is possible that other crosslinking agents/strategies may provide the desired leap in reusability, but further research is certainly needed. Aside of optimisation attempts on PIMs and the surrounding system, the combination of PIMs and NF has been targeted. This allowed to effectively separate Sc as described in Chapters 2-4 but allowed working with a fairly simpler matrix. Thus, the tandem PIM-NF could become an interesting solution, whereas complex matrices are exchanged by a PIM process which does not need pressure but only agitation.

Overall, the work on PIMs, revealed a remarkable potential of the technology for the extraction of metals from real waste streams. If the reusability can be improved, the process might be well suited for recovery of Sc from TiO_2 acid waste. Beyond the specific application presented, this work could encourage others to test PIMs under harsh conditions to eventually develop the technology into a mature hydrometallurgical process.

To conclude, the studies conducted in this thesis, especially aimed to improve the technological readiness level of membrane-based element recovery.[364] Thus, the NF approach was brought from experimental proof of concept (Chapters 2 and 3), to cubic metre pilot scale, and demonstration in

relevant environment (Chapter 4).[364] The relevance of the implementation of NF for the recovery of Sc was confirmed, both on lab and pilot scale by downstream SX studies conducted by B. Yagmur-lu (Chapters 3 and 4). In light of PIMs, a proof of principle succeeded in relevant environment (Chapters 5 and 6). A need for further optimisation was identified before the system can be brought to a higher level of maturity. Finally, the combination of PIMs and NF has proven useful (Chapter 6).

7.3   Broader implications and recommendations for future research

This thesis aimed to explore strategies for achieving a sustainable raw material supply. Moreover, by addressing the valorisation of waste, parts of this work could contribute to the transition to a circular economy.[365] Membrane-based processes were demonstrated to be a viable solution for treating challenging secondary streams with a small material footprint and relying mainly on energy input. Hence, it is believed, that a complete transition to renewable energy – as planned for a truly circular economy – could promote and benefit from membrane-based hydrometallurgy. Even if the challenge of energy supply can be solved by renewables, the supply of resources will always be linked to sorting technologies that can reduce the entropy of a stream until a pure material is obtained.[366] In this regard, increasingly entropic products and secondary streams, pose a challenge, if not a risk, to the implementation of a circular economy.[367] The current lack of recycling can largely be attributed to problems in waste separation.[75,367] While this work focused on membrane-based processes designed for hydrometallurgical tasks and the separation of ions, their scope is limited to such wastes. Nevertheless, the extensive study of membrane processes on the TiO$_2$ acid waste in this work may serve as an encouragement for zero-liquid-discharge approaches to tackle challenging process waters.

In terms of future research for NF, the stability of highly water-permeable membranes, particularly those of the lbl-type, in harsh environments should be addressed. Crosslinking of the coated bi-layers or the use of stronger polyelectrolytes, such as polyallylamine, could be potential solutions.[357,368] Additionally, the NF process could be improved with more pressure-resistant membranes and filtration units to better compensate for the high osmotic pressure of the concentrated acid waste, leading to higher permeate flow and recovery rates and potentially reducing energy consumption (as discussed in Chapter 3). It may also be worthwhile to test operation of NF in diafiltration mode, allowing for impurities to be washed out of the Sc concentrate.

Regarding PIMs, further testing of crosslinking with more aliphatic/hydrophobic crosslinkers should be conducted to explore their potential. Additionally, the preparation of fixed-site carrier membranes, achieved by covalently binding the carrier to the polymer, could improve stability.[369] Despite its significant potential, the PIM strategy remains underexplored, leaving ample room for creativity. The immobilisation of an organic SX phase in a 2D shape opens up new possibilities, such as the production of tubular membranes to increase the surface area per volume and enable the construction of a counter-current plug-flow reactor/contactor. A more far-fetched idea could be to

employ several PIMs containing different carriers for different elements in series, creating a segmented setup similar to a bowel where different nutrients are adsorbed in different segments. By means of this concept, multiple elements could be recovered from the same waste stream in a single run, ideally.

This page is intentionally left blank.

8 References

[1] B. A. Kipfer, *Encyclopedic Dictionary of Archaeology*, Springer International Publishing; Imprint Springer, Cham, **2021**.

[2] United Nations, Department of Economic and Social Affairs, Population Division, *World Population Prospects 2022*, Online, **2022**.

[3] Gapminder.org, "Gapminder population dataset version 7, based on data by Angus Maddison improved by CLIO INFRA.", can be found under https://www.gapminder.org/data/documentation/gd003/, **2022**.

[4] K. Klein Goldewijk, A. Beusen, J. Doelman, E. Stehfest, *New anthropogenic land use estimates for the Holocene; HYDE 3.2*, **2016**.

[5] C. Lascelles, *A short history of the world*, Crux Publishing, **2011**.

[6] T. Wiedmann, M. Lenzen, L. T. Keyßer, J. K. Steinberger, *Nat Commun* **2020**, *11*, 3107.

[7] L. Chancel, *Nat Sustain* **2022**, *5*, 931.

[8] J. Hickel, D. W. O'Neill, A. L. Fanning, H. Zoomkawala, *Lancet Planet Health* **2022**, *6*, e342-e349.

[9] F. Krausmann, C. Lauk, W. Haas, D. Wiedenhofer, *Glob Environ Change* **2018**, *52*, 131.

[10] J. Syvitski, J. R. Ángel, Y. Saito, I. Overeem, C. J. Vörösmarty, H. Wang, D. Olago, *Nat Rev Earth Environ* **2022**, *3*, 179.

[11] C. Soriano, *GeologicaActa* **2020**.

[12] A. G. Brown, S. Tooth, R. C. Chiverrell, J. Rose, D. S. G. Thomas, J. Wainwright, J. E. Bullard, V. R. Thorndycraft, R. Aalto, P. Downs, *Earth Surf. Process. Landforms* **2013**, *38*, 431.

[13] V. Rull, *Quaternary* **2018**, *1*, 24.

[14] J. Zalasiewicz, C. N. Waters, E. C. Ellis, M. J. Head, D. Vidas, W. Steffen, J. A. Thomas, E. Horn, C. P. Summerhayes, R. Leinfelder et al., *Earth's Future* **2021**, *9*.

[15] J. Zalasiewicz, M. Williams, W. Steffen, P. Crutzen, *Environ Sci Technol* **2010**, *44*, 2228.

[16] J. Zalasiewicz, C. N. Waters, C. P. Summerhayes, A. P. Wolfe, A. D. Barnosky, A. Cearreta, P. Crutzen, E. Ellis, I. J. Fairchild, A. Gałuszka et al., *Anthropocene* **2017**, *19*, 55.

[17] S. H. M. Butchart, M. Walpole, B. Collen, A. van Strien, J. P. W. Scharlemann, R. E. A. Almond, J. E. M. Baillie, B. Bomhard, C. Brown, J. Bruno et al., *Science* **2010**, *328*, 1164.

[18] H. M. Pereira, L. M. Navarro, I. S. Martins, *Annu. Rev. Environ. Resour.* **2012**, *37*, 25.

[19] W. Steffen, K. Richardson, J. Rockström, S. E. Cornell, I. Fetzer, E. M. Bennett, R. Biggs, S. R. Carpenter, W. de Vries, C. A. de Wit et al., *Science* **2015**, *347*, 1259855.

[20] W. J. Ripple, C. Wolf, J. W. Gregg, K. Levin, J. Rockström, T. M. Newsome, M. G. Betts, S. Huq, B. E. Law, L. Kemp et al., *BioScience* **2022**, *72*, 1149.

[21] International Resource Panel, Stefan Bringezu, Anu Ramaswami, Heinz Schandl, Meghan O'Brien, Rylie Pelton, Jean Acquatella, Elias T. Ayuk, Anthony Shun Fung Chiu, Robert Flanegin

et al., *Global Resources Outlook 2019. Natural Resources for the Future We Want*, United Nations, New York, **2020**.

[22]   D. H. Meadows, Meadows Dennis L., J. Randers, W. W. Behrens, *The limits of growth; a report for the Club of Rome's project on the predicament of mankind*, New York, Universe Books [1973], **1972**.

[23]   T. W. Murphy, *Nat. Phys.* **2022**, *18*, 844.

[24]   G. Herrington, *Journal of Industrial Ecology* **2021**, *25*, 614.

[25]   J. Rockström, W. Steffen, K. Noone, A. Persson, F. S. Chapin, E. F. Lambin, T. M. Lenton, M. Scheffer, C. Folke, H. J. Schellnhuber et al., *Nature* **2009**, *461*, 472.

[26]   United Nations, *Transforming our World: the 2030 Agenda for Sustainable Development. Working Papers*, **2015**.

[27]   United Nations, "Sustainable development goals. Communications material", can be found under https://www.un.org/sustainabledevelopment/news/communications-material/, **2019**.

[28]   L. McNeill, *Transitioning to Responsible Consumption and Production*, MDPI Books, [S.l.], **2020**.

[29]   International Resource Panel, *Managing and Conserving the Natural Resource Base for Sustained Economic and Social Development*, **2014**.

[30]   International Resource Panel, "Global material flows database", can be found under https://www.resourcepanel.org/global-material-flows-database, **2021**.

[31]   H. Schandl, Fischer-Kowalski Marina, J. West, S. Giljum, M. Dittrich, N. Eisenmenger, A. Geschke, M. Lieber, H. Wieland, A. Schaffartzik, *Global material flows and resource productivity. An Assessment Study of the UNEP International Resource Panel.*, Paris, **2016**.

[32]   M. Lenzen, A. Geschke, J. West, J. Fry, A. Malik, S. Giljum, L. Milà i Canals, P. Piñero, S. Lutter, T. Wiedmann et al., *Nat Sustain* **2022**, *5*, 157.

[33]   S. Bringezu, A. Ramaswami, H. Schandl, M. O'Brien, R. Pelton, J. Acquatella, E. T. Ayuk, A. S. F. Chiu, R. Flanegin, J. Fry et al., *Assessing global resource use: A systems approach to resource efficiency and pollution reduction*, Paris, **2017**.

[34]   International Resource Panel, *Sustainable Trade in Resources. Global Material Flows, Circularity and Trade*, **2020**.

[35]   S. Bringezu, *Resources* **2015**, *4*, 25.

[36]   International Resource Panel, *Decoupling natural resource use and environmental impacts from economic growth*, Kenya, UNEP, **2011**.

[37]   European Statistical Office (eurostat), "National accounts aggregates by industry (up to NACE A*64). NAMA_10_A64", can be found under https://ec.europa.eu/eurostat/databrowser/bookmark/b074416b-1cc5-494b-a559-2a0ede62e361?lang=en, **2022**.

[38]   M. Henckens, E. C. van Ierland, P. Driessen, E. Worrell, *Resources Policy* **2016**, *49*, 102.

[39]   G. A. Blengini, M. Grohol, *Methodology for establishing the EU list of critical raw materials. Guidelines*, Publications Office of the European Union, Luxembourg, **2017**.

[40]   European Commission, *Critical Raw Materials Resilience: Charting a Path towards Greater Security and Sustainability. COM/2020/474 final*, Brussels, Belgium, **2020**.

[41]   G. A. Blengini, C. E. L. Latunussa, U. Eynard, C. Torres de Matos, D. Wittmer, K. Georgitzikis, C. Pavel, S. Carrara, L. Mancini, M. Unguru et al., *Study on the EU's list of critical raw materials (2020)*, Publications Office of the European Union, Luxembourg, **2020**.

[42]   European Commission, *The Raw Materials Initiative — meeting our critical needs for growth and jobs in Europe*, Brussels, Belgium, **2008**.

[43]   Council of the European Union, *Regulation (EC) No 1893/2006 of the European Parliament and of the Council of 20 December 2006 Establishing the Statistical Classification of Economic Activities Nace Revision 2 and Amending Council Regulation (EEC) No 3037/90 As Well As Certain EC Regulations on Specic Statistical Domains."*, Brussels, Belgium, **2006**.

[44]   M. A. Thomas, *Eur J Dev Res* **2010**, *22*, 31.

[45]   I. McLean, A. McMillan, *The concise Oxford dictionary of politics*, Oxford University Press, [Oxford], **2009-**.

[46]   N. T. Nassar, S. M. Fortier, *Methodology and technical input for the 2021 review and revision of the U.S. Critical Minerals List: U.S. Geological Survey Open-File Report 2021–1045*, Reston, VA, **2021**.

[47]   H. Hatayama, K. Tahara, *Mater. Trans.* **2015**, *56*, 229.

[48]   P. Andersson, *The Extractive Industries and Society* **2020**, *7*, 127.

[49]   S. Kalantzakos, *The International Spectator* **2020**, *55*, 1.

[50]   International Energy Agency, *The Role of Critical Minerals in Clean Energy Transitions*, **2021**.

[51]   K. Hund, D. La Porta, T. P. Fabregas, T. Laing, J. Drexhage, others, *World Bank* **2020**, *73*.

[52]   A. Marín, D. Goya, *Environmental Innovation and Societal Transitions* **2021**, *41*, 86.

[53]   C. Ludwig, S. Valdivia, *Progress Towards The Resource Revolution*, World Resources Forum, Villigen PSI and St. Gallen, Switzerland, **2019**.

[54]   *Inclusive Green Growth*, The World Bank, **2012**.

[55]   *Towards Green Growth: Monitoring Progress*, OECD, **2011**.

[56]   OECD, *Sustainable Manufacturing and Eco-Innovation*, Paris, **2009**.

[57]   A. Sarkar, *EJSD* **2013**, *2*.

[58]   L. J. Belmonte-Ureña, J. A. Plaza-Úbeda, D. Vazquez-Brust, N. Yakovleva, *Ecological Economics* **2021**, *185*, 107050.

[59]   H. Dai, X. Xie, Y. Xie, J. Liu, T. Masui, *Applied Energy* **2016**, *162*, 435.

[60]   L. Rini, J. J. Schouteten, I. Faber, K.-B. Bechtold, F. J. A. Perez-Cueto, X. Gellynck, H. de Steur, *Sustainability* **2023**, *15*, 306.

[61]   D. Tilman, M. Clark, *Nature* **2014**, *515*, 518.

[62]   M. Krzywonos, K. Piwowar-Sulej, *Foods* **2022**, *11*.

[63]   J. Hickel, G. Kallis, *New Political Economy* **2020**, *25*, 469.

[64]   T. Parrique, J. Barth, F. Briens, C. Kerschner, A. Kraus-Polk, A. Kuokkanen, J. H. Spangenberg, *Decoupling debunked: Evidence and arguments against green growth as a sole strategy for sustainability*, Brussels, Belgium, **2019**.

[65]   T. Vadén, V. Lähde, A. Majava, P. Järvensivu, T. Toivanen, E. Hakala, J. T. Eronen, *Environ Sci Policy* **2020**, *112*, 236.

[66]   T. Vadén, V. Lähde, A. Majava, P. Järvensivu, T. Toivanen, J. T. Eronen, *Environmental Politics* **2021**, *30*, 462.

[67]   V. Moreau, F. Vuille, *Applied Energy* **2018**, *215*, 54.

[68]   J. S. Vandeventer, C. Cattaneo, C. Zografos, *Ecological Economics* **2019**, *156*, 272.

[69]   A. Tukker, *J. Clean. Prod.* **2015**, *97*, 76.

[70]   I. A. Ortega Alvarado, I. N. Pettersen, T. Berker, *Circ.Econ.Sust.* **2022**.

[71]   ING Economics Department, *Rethinking finance in a circular economy. Financial implications of circular business models.*, Online, **2015**.

[72]   FinanCE, *Money makes the world go round. (and will it help to make the economy circular as well?)*, The Netherlands, **2016**.

[73]   European Commission, *A new Circular Economy Action Plan. For a cleaner and more competitive Europe*, Brussels, Belgium, **2020**.

[74]   T. Bauwens, *Resources, Conservation and Recycling* **2021**, *175*, 105852.

[75]   Circle Economy, *The circularity gap report 2023*, Amsterdam, **2023**.

[76]   C. T. Horovitz, *Scandium Its Occurrence, Chemistry Physics, Metallurgy, Biology and Technology. Its Occurrence, Chemistry, Physics, Metallurgy, Biology and Technology*, Elsevier Science, Oxford, **1975**.

[77]   E. C. Constable, *Dalton Trans* **2019**, *48*, 9408.

[78]   N. G. Connelly, *Nomenclature of inorganic chemistry. IUPAC recommendations 2005*, Royal Society of Chemistry Publishing; IUPAC, Cambridge, **op. 2005**.

[79]   S. Cotton, *Lanthanide and Actinide Chemistry*, John Wiley & Sons, Ltd, Chichester, UK, **2006**.

[80]   Z. Ahmad, *JOM* **2003**, *55*, 35.

[81]   M. Awd, J. Tenkamp, M. Hirtler, S. Siddique, M. Bambach, F. Walther, *Materials (Basel)* **2017**, *11*.

[82]   J. Røyset, N. Ryum, *International Materials Reviews* **2005**, *50*, 19.

[83]   Ş. Kaya, C. Dittrich, S. Stopic, B. Friedrich, *Metals* **2017**, *7*, 557.

[84]   S. Reid, J. Tam, M. Yang, G. Azimi, *Sci. Rep.* **2017**, *7*, 15252.

[85]   A. Vafadar, F. Guzzomi, A. Rassau, K. Hayward, *Applied Sciences* **2021**, *11*, 1213.

[86]   B. Yagmurlu, B. Orberger, C. Dittrich, G. Croisé, R. Scharfenberg, E. Balomenos, D. Panias, E. Mikeli, C. Maier, R. Schneider et al., *Sustainable Supply of Scandium for the EU Industries from Liquid Iron Chloride Based TiO$_2$ Plants*, **2021**.

[87]   T. Dorin, M. Ramajayam, A. Vahid, T. Langan in *Fundamentals of Aluminium Metallurgy*, Elsevier, **2018**, pp. 439–494.

[88]   R. P. Narayanan, L.-C. Ma, N. K. Kazantzis, M. H. Emmert, *ACS Sustainable Chem. Eng.* **2018**, *6*, 5333.

[89]   Y. Mizutani, K. Hisada, K. Ukai, H. Sumi, M. Yokoyama, Y. Nakamura, O. Yamamoto, *Journal of Alloys and Compounds* **2006**, *408-412*, 518.

[90]   K. Ukai, M. Yokoyama, J. Shimano, Y. Mizutani, O. Yamamoto in *Ceramic Transactions Series* (Eds.: D. Jiang, Y. Zeng, M. Singh, J. Heinrich), John Wiley & Sons, Inc, Hoboken, NJ, USA, **2010**, pp. 185–190.

[91]   J. J. Spivey, D. A. Berry, D. Shekhawat, *Fuel cells: technologies for fuel processing*, Elsevier professional, s.l., **2011**.

[92]   V. Kharton, F. Marques, A. Atkinson, *Solid State Ionics* **2004**, *174*, 135.

[93]   J. W. Fergus, *Journal of Power Sources* **2006**, *162*, 30.

[94]   M. C. Williams, S. D. Vora, G. Jesionowski, *ECS Trans.* **2020**, *96*, 1.

[95]   S. J. McPhail, L. Leto, C. Boigues-Muñoz, *The yellow pages of SOFC technology. International status of SOFC deployment 2012-2013*, ENEA, Rome, **2013**.

[96]   O. Corigliano, L. Pagnotta, P. Fragiacomo, *Sustainability* **2022**, *14*, 15276.

[97]   Bloom Energy, *2021 Sustainability Report. Solutions for a Decarbonized Future*, San Jose, USA, **2022**.

[98]   A. Ballantine, "Everything You Need to Know About Solid Oxide Fuel Cells", can be found under https://www.bloomenergy.com/blog/everything-you-need-to-know-about-solid-oxide-fuel-cells/, **2019**.

[99]   S. Hardman, A. Chandan, R. Steinberger-Wilckens, *Journal of Power Sources* **2015**, *287*, 297.

[100]   B. Dziurdzia, Z. Magonski, H. Jankowski, *IOP Conf. Ser.: Mater. Sci. Eng.* **2016**, *104*, 12020.

[101]   A. Yuksekdag, B. Kose-Mutlu, A. F. Siddiqui, M. R. Wiesner, I. Koyuncu, *Chemosphere* **2022**, *293*, 133620.

[102]   D. R. Lide (Ed.) *CRC handbook of chemistry and physics. A ready-reference book of chemical and physical data*, CRC Press, Boca Raton, **2004**.

[103]   D. J. Cordier, *USGS Mineral Commodity Summary: Scandium*, **2022**.

[104]   K. J. Schulz, J. H. DeYoung, R. R. Seal, D. C. Bradley, *Critical mineral resources of the United States—Economic and environmental geology and prospects for future supply. Professional Paper 1802*, Reston, VA, **2017**.

[105]   J. Gambogi in *Minerals Yearbook*, *I* (Ed.: U.S. Geological Survey), U.S. Government Publishing Office, Reston, VA, **2018**.

[106] M. Huleatt, *Australian resource reviews: Scandium 2019*, Geoscience Australia, **2019**.

[107] Z. Wang, M. Y. H. Li, Z.-R. R. Liu, M.-F. Zhou, *Ore Geol. Rev.* **2021**, *128*, 103906.

[108] X. Shaoquan, L. Suqing, *Hydrometallurgy* **1996**, *42*, 337.

[109] M. C. Gentzmann, Freie Universität Berlin, **2023**.

[110] A. Ghosh, S. Dhiman, A. Gupta, R. Jain, *Environments* **2023**, *10*, 8.

[111] A. E. Williams-Jones, O. V. Vasyukova, *Economic Geology* **2018**, *113*, 973.

[112] C. M. Beland, A. E. Williams-Jones, *Chemical Geology* **2023**, *615*, 121223.

[113] Ionic Rare Earths, "Project: Makuutu Uganda (Earning up to 60%)", can be found under https://ionicre.com.au/makuutu-uganda/, **2023**.

[114] J. Hokka, T. Halkoaho, *3D modelling and mineral resource estimation of the Kiviniemi scandium deposit, Eastern Finland*, Geological Survey of Finland, Eastern Finland, **2016**.

[115] M. C. Gentzmann, K. Schraut, C. Vogel, H.-E. Gäbler, T. Huthwelker, C. Adam, *Applied Geochemistry* **2021**, *126*, 104898.

[116] M. Chen, T. E. Graedel, *J. Clean. Prod.* **2015**, *91*, 337.

[117] A. B. Botelho Junior, D. Espinosa, J. Vaughan, J. Tenório, *Miner. Eng.* **2021**, *172*, 107148.

[118] N. C. G. Silveira, M. L. F. Martins, A. C. S. Bezerra, F. G. S. Araújo, *Sustainability* **2021**, *13*, 12741.

[119] E. Mukiza, L. Zhang, X. Liu, N. Zhang, *Resources, Conservation and Recycling* **2019**, *141*, 187.

[120] R. M. Rivera, B. Ulenaers, G. Ounoughene, K. Binnemans, T. van Gerven, *Miner. Eng.* **2018**, *119*, 82.

[121] M. J. Gázquez, J. P. Bolívar, R. Garcia-Tenorio, F. Vaca, *Mater. Sci. Appl.* **2014**, *05*, 441.

[122] J. Gambogi, *USGS Minerals Information: Titanium and titanium dioxide*, **2023**.

[123] M. J. Gázquez, J. P. Bolívar, R. Garcia-Tenorio, F. Vaca, *Mater. Sci. Appl.* **2014**, *05*, 441.

[124] U. Förstner, W. Salomons, P. Mader, *Heavy Metals*, Springer Berlin Heidelberg, Berlin, Heidelberg, **1995**.

[125] W. Wang, Y. Pranolo, C. Y. Cheng, *Hydrometallurgy* **2011**, *108*, 100.

[126] C. Perks, G. Mudd, *Ore Geol. Rev.* **2019**, *107*, 629.

[127] S. Broek (Ed.) *The minerals, metals & materials series*, Springer Nature Switzerland, Cham, **2023**.

[128] L. D. Lash, J. R. Ross, *JOM* **1961**, *13*, 555.

[129] F. Faraji, A. Alizadeh, F. Rashchi, N. Mostoufi, *Reviews in Chemical Engineering* **2022**, *38*, 113.

[130] A. V. Boyarintsev, H. Y. Aung, S. I. Stepanov, A. A. Shoustikov, P. I. Ivanov, V. G. Giganov, *ACS Omega* **2022**, *7*, 259.

[131] K. Hatzilyberis, T. Lymperopoulou, L.-A. Tsakanika, K.-M. Ochsenkühn, P. Georgiou, N. Defteraios, F. Tsopelas, M. Ochsenkühn-Petropoulou, *Minerals* **2018**, *8*, 79.

[132] M. C. Gentzmann, A. Paul, J. Serrano, C. Adam, *Journal of Geochemical Exploration* **2022**, *240*, 107041.

[133]   G. Alkan, B. Yagmurlu, S. Cakmakoglu, T. Hertel, Ş. Kaya, L. Gronen, S. Stopic, B. Friedrich, *Sci. Rep.* **2018**, *8*, 5676.

[134]   S. L. Liu, *Advanced Materials Research* **2012**, *548*, 305.

[135]   J. Zhou, S. Ning, J. Meng, S. Zhang, W. Zhang, S. Wang, Y. Chen, X. Wang, Y. Wei, *J. Rare Earths* **2020**.

[136]   B. Onghena, K. Binnemans, *Ind. Eng. Chem. Res.* **2015**, *54*, 1887.

[137]   S. Batra, A. Awasthi, M. Iqbal, D. Datta, *Reviews in Chemical Engineering* **2022**, *38*, 209.

[138]   A. M. Reyes, G. Abrenica, G. Nazari in *The minerals, metals & materials series* (Ed.: S. Broek), Springer Nature Switzerland, Cham, **2023**, pp. 1181–1189.

[139]   J. L. Cortina, M. Aguilar Sanjuán, *Solvent extraction and liquid membranes. Fundamentals and applications in new materials*, CRC Press, Boca Raton, **2008**.

[140]   A. M. Wilson, P. J. Bailey, P. A. Tasker, J. R. Turkington, R. A. Grant, J. B. Love, *Chem Soc Rev* **2014**, *43*, 123.

[141]   W. Wang, C. Y. Cheng, *J. Chem. Technol. Biotechnol.* **2011**, *86*, 1237.

[142]   W. Wang, Y. Pranolo, C. Y. Cheng, *Sep. Purif. Technol.* **2013**, *108*, 96.

[143]   E. C. Constable, *Coordination Chemistry Reviews* **1985**, *62*, 131.

[144]   M. I. G. Almeida, R. W. Cattrall, S. D. Kolev, *J. Membr. Sci.* **2012**, *415-416*, 9.

[145]   S. Schrödle, W. Wachter, R. Buchner, G. Hefter, *Inorg Chem* **2008**, *47*, 8619.

[146]   Y. Chen, S. Ma, S. Ning, Y. Zhong, X. Wang, T. Fujita, Y. Wei, *Journal of Environmental Chemical Engineering* **2021**, *9*, 106226.

[147]   D. Zou, H. Li, J. Chen, D. Li, *Hydrometallurgy* **2020**, *197*, 105463.

[148]   D. Zou, Y. Deng, J. Chen, D. Li, *J. Rare Earths* **2022**, *40*, 1499.

[149]   Ş. Kaya, E. Peters, K. Forsberg, C. Dittrich, S. Stopic, B. Friedrich, *Metals* **2018**, *8*, 767.

[150]   E. Peters, *Recovery of Scandium using Antisolvent Crystallization in the Valorization of Scandium-containing Waste Streams*, KTH Royal Institute of Technology, Stockholm, **2022**.

[151]   L. Chen, Y. Wu, H. Dong, M. Meng, C. Li, Y. Yan, J. Chen, *Sep. Purif. Technol.* **2018**, *197*, 70.

[152]   S. Hong, F. Al Marzooqi, J. K. El-Demellawi, N. Al Marzooqi, H. A. Arafat, H. N. Alshareef, *ACS Materials Lett.* **2023**, *5*, 341.

[153]   L. Nghiem, P. Mornane, I. Potter, J. Perera, R. Cattrall, S. Kolev, *J. Membr. Sci.* **2006**, *281*, 7.

[154]   J.-M. Arana Juve, F. M. S. Christensen, Y. Wang, Z. Wei, *Chemical Engineering Journal* **2022**, *435*, 134857.

[155]   Y.-S. Zimmermann, C. Niewersch, M. Lenz, Z. Z. Kül, P. F.-X. Corvini, A. Schäffer, T. Wintgens, *Environ Sci Technol* **2014**, *48*, 13412.

[156]   J. López, M. Reig, O. Gibert, E. Torres, C. Ayora, J. L. Cortina, *Desalination* **2018**, *430*, 33.

[157]   A. Bashiri, A. Nikzad, R. Maleki, M. Asadnia, A. Razmjou, *Membranes (Basel)* **2022**, *12*.

[158]   M. Sugiura, M. Kikkawa, S. Urita, *J. Membr. Sci.* **1989**, *42*, 47.

[159]   D. S. Sholl, R. P. Lively, *Nature* **2016**, *532*, 435.

[160] P. Eriksson, *Environ. Prog.* **1988**, *7*, 58.

[161] W. J. Koros, Y. H. Ma, T. Shimidzu, *Pure and Applied Chemistry* **1996**, *68*, 1479.

[162] E. Drioli, L. Giorno (Eds.) *Springer eBook Collection*, Springer, Berlin, Heidelberg, **2019**.

[163] V. V. Bhaskar, N. J. Kaleekkal, *emergent mater.* **2022**, *5*, 1373.

[164] H. Shimura, *Polym J* **2022**, *54*, 767.

[165] A. W. Mohammad, Y. H. Teow, W. L. Ang, Y. T. Chung, D. L. Oatley-Radcliffe, N. Hilal, *Desalination* **2015**, *356*, 226.

[166] A. Yaroshchuk, M. L. Bruening, E. Zholkovskiy, *Advances in Colloid and Interface Science* **2019**, *268*, 39.

[167] T. Melin, R. Rautenbach, *Membranverfahren. Grundlagen der Modul- und Anlagenauslegung*, Springer, Berlin, Heidelberg, **2004**.

[168] R. Wang, S. Lin, *J. Membr. Sci.* **2021**, *620*, 118809.

[169] Y. Roy, D. M. Warsinger, J. H. Lienhard, *Desalination* **2017**, *420*, 241.

[170] D. Lu, Z. Yao, L. Jiao, M. Waheed, Z. Sun, L. Zhang, *Advanced Membranes* **2022**, *2*, 100032.

[171] T. Melin, *Membranverfahren*. *Grundlagen der Modul- und Anlagenauslegung*, Springer-Verlag Berlin Heidelberg, [New York], **2007**.

[172] M. P. González, R. Navarro, I. Saucedo, M. Avila, J. Revilla, C. Bouchard, *Desalination* **2002**, *147*, 315.

[173] T. Schütte, C. Niewersch, T. Wintgens, S. Yüce, *J. Membr. Sci.* **2015**, *480*, 74.

[174] Y.-A. Boussouga, H. Than, A. I. Schäfer, *Sci Total Environ* **2022**, *829*, 154287.

[175] F. Léniz-Pizarro, C. Liu, A. Colburn, I. C. Escobar, D. Bhattacharyya, *J. Membr. Sci.* **2021**, *620*.

[176] J. Fang, B. Deng, *J. Membr. Sci.* **2014**, *453*, 42.

[177] N. S. Suhalim, N. Kasim, E. Mahmoudi, I. J. Shamsudin, A. W. Mohammad, F. Mohamed Zuki, N. L.-A. Jamari, *Nanomaterials (Basel)* **2022**, *12*.

[178] Q. Li, M. Elimelech, *Environ Sci Technol* **2004**, *38*, 4683.

[179] S. K. Nayak, K. Dutta, J. M. Gohil (Eds.) *Advancement in Polymer-Based Membranes for Water Remediation*, Elsevier, San Diego, **2022**.

[180] C. Bhattacharjee, V. K. Saxena, S. Dutta, *Chemical Engineering Communications* **2020**, *207*, 413.

[181] Z. Cao, *J. Membr. Sci.* **2001**, *185*, 157.

[182] C. H. Tan, O. Lefebvre, J. Zhang, H. Y. Ng, S. L. Ong in *Membrane Technology and Environmental Applications* (Eds.: T. C. Zhang, R. Y. Surampalli, S. Vigneswaran, R. D. Tyagi, S. Leong Ong, C. M. Kao), American Society of Civil Engineers, Reston, VA, **2012**, pp. 298–330.

[183] N. N. R. Ahmad, W. L. Ang, Y. H. Teow, A. W. Mohammad, N. Hilal, *Journal of Water Process Engineering* **2022**, *45*, 102478.

[184] J. López, O. Gibert, J. L. Cortina, *Chemical Engineering Journal* **2021**, *405*, 127015.

[185]   B. Kose Mutlu, B. Cantoni, A. Turolla, M. Antonelli, H. Hsu-Kim, M. R. Wiesner, *Chemical Engineering Journal* **2018**, *349*, 309.

[186]   Z. Zhao, S. Feng, C. Xiao, J. Luo, W. Song, Y. Wan, S. Li, *Sep. Purif. Technol.* **2022**, *289*, 120748.

[187]   J. Way, R. D. Noble, T. M. Flynn, E. Sloan, *J. Membr. Sci.* **1982**, *12*, 239.

[188]   C. Tang, M. L. Bruening, *Journal of Polymer Science* **2020**, *58*, 2831.

[189]   M. Aguilar, J. L. Cortina, *Solvent Extraction and Liquid Membranes*, CRC Press, **2008**.

[190]   D. Wang, R. W. Cattrall, J. Li, M. I. G. Almeida, G. W. Stevens, S. D. Kolev, *J. Membr. Sci.* **2017**, *542*, 272.

[191]   Y. Y. N. Bonggotgetsakul, R. W. Cattrall, S. D. Kolev, *J. Membr. Sci.* **2016**, *514*, 274.

[192]   W. Yoshida, F. Kubota, Y. Baba, S. D. Kolev, M. Goto, *ACS Omega* **2019**, *4*, 21122.

[193]   W. Yoshida, Y. Baba, F. Kubota, S. D. Kolev, M. Goto, *J. Membr. Sci.* **2019**, *572*, 291.

[194]   V. T. Phuong, A. Lazzeri, *Composites Part A: Applied Science and Manufacturing* **2012**, *43*, 2256.

[195]   Z. Li, J. Fu, X. Zhou, S. Gui, L. Wei, H. Yang, H. Li, X. Guo, *Adv Sci (Weinh)* **2023**, e2201718.

[196]   N. Gama, R. Santos, B. Godinho, R. Silva, A. Ferreira, *J Polym Environ* **2019**, *27*, 1294.

[197]   B. Hoque, M. I. G. Almeida, R. W. Cattrall, T. G. Gopakumar, S. D. Kolev, *J. Membr. Sci.* **2019**, *589*, 117256.

[198]   G. Salazaralvarez, A. Bautistaflores, E. Desanmiguel, M. Muhammed, J. Degyves, *J. Membr. Sci.* **2005**, *250*, 247.

[199]   H. Matsuoka, M. Aizawa, S. Suzuki, *J. Membr. Sci.* **1980**, *7*, 11.

[200]   Y. Cho, C. Xu, R. W. Cattrall, S. D. Kolev, *J. Membr. Sci.* **2011**, *367*, 85.

[201]   Y. O'Bryan, Y. B. Truong, R. W. Cattrall, I. L. Kyratzis, S. D. Kolev, *J. Membr. Sci.* **2017**, *529*, 55.

[202]   M. I. G. S. Almeida, R. W. Cattrall, S. D. Kolev, *Anal. Chim. Acta* **2017**, *987*, 1.

[203]   S. D. Kolev, M. I. G. Almeida, R. W. Cattrall in *Handbook of Smart Materials in Analytical Chemistry* (Eds.: M. de La Guardia, F. A. Esteve-Turrillas), John Wiley & Sons, Ltd, Chichester, UK, **2019**, pp. 439–461.

[204]   R. Jha, M. D. Rao, A. Meshram, H. R. Verma, K. K. Singh, *Journal of Cleaner Production* **2020**, *265*, 121621.

[205]   C. F. Croft, M. I. G. Almeida, R. W. Cattrall, S. D. Kolev, *J. Membr. Sci.* **2018**, *545*, 259.

[206]   M. Sharaf, W. Yoshida, F. Kubota, S. D. Kolev, M. Goto, *RSC Adv.* **2018**, *8*, 8631.

[207]   V. Gold, *The IUPAC Compendium of Chemical Terminology*, International Union of Pure and Applied Chemistry (IUPAC), Research Triangle Park, NC, **2019**.

[208]   "Production of Scandium compounds and Scandium Aluminum alloys from European metallurgical by-products. SCALE project", can be found under https://cordis.europa.eu/project/id/730105, **2021**.

[209]   M. G. Buonomenna, *RSC Adv.* **2013**, *3*, 5694.

[210]   J. López, M. Reig, O. Gibert, J. L. Cortina, *Sep. Purif. Technol.* **2019**, *226*, 267.

[211] M. Alemrajabi, J. Ricknell, S. Samak, R. Rodriguez Varela, J. Martinez, F. Hedman, K. Forsberg, Å. C. Rasmuson, *Ind. Eng. Chem. Res.* **2022**, *61*, 18475.

[212] M. C. Amaral, L. B. Grossi, R. L. Ramos, B. C. Ricci, L. H. Andrade, *Desalination* **2018**, *440*, 111.

[213] M. Contreras, M. J. Gázquez, S. M. Pérez-Moreno, M. Romero, J. P. Bolívar, *Waste Biomass Valor* **2016**, *7*, 899.

[214] D. Menne, RWTH Aachen University, **2017**.

[215] N. T. Nassar, T. E. Graedel, E. M. Harper, *Sci Adv* **2015**, *1*, e1400180.

[216] W. R. Stahel, *Nature* **2016**, *531*, 435.

[217] K. Binnemans, P. T. Jones, B. Blanpain, T. van Gerven, Y. Pontikes, *J. Clean. Prod.* **2015**, *99*, 17.

[218] T. Hennebel, N. Boon, S. Maes, M. Lenz, *N Biotechnol* **2015**, *32*, 121.

[219] European Commission, *on the 2017 list of Critical Raw Materials for the EU. COM(2017) 490 final*, Brussels, Belgium, **2017**.

[220] C. R. Borra, B. Blanpain, Y. Pontikes, K. Binnemans, T. van Gerven, *J. Sustain. Metall.* **2016**, *2*, 365.

[221] É. Ujaczki, V. Feigl, M. Molnár, P. Cusack, T. Curtin, R. Courtney, L. O'Donoghue, P. Davris, C. Hugi, M. W. Evangelou et al., *J. Chem. Technol. Biotechnol.* **2018**, *93*, 2498.

[222] G. Alkan, B. Yagmurlu, L. Gronen, C. Dittrich, Y. Ma, S. Stopic, B. Friedrich, *Hydrometallurgy* **2019**, *185*, 266.

[223] U.S. Geological Survey, *Mineral Commodity Summaries*, **2019**.

[224] G. Buxbaum, G. Pfaff, *Industrial inorganic pigments*, Wiley-VCH, Weinheim, **2010**.

[225] Y. Li, Q. Li, G. Zhang, L. Zeng, Z. Cao, W. Guan, L. Wang, *Hydrometallurgy* **2018**, *178*, 1.

[226] H. Qiu, M. Wang, Y. Xie, J. Song, T. Huang, X.-M. Li, T. He, *Process Safety and Environmental Protection* **2019**, *121*, 118.

[227] S. Middlemas, Z. Z. Fang, P. Fan, *J. Clean. Prod.* **2015**, *89*, 137.

[228] E. Vahidi, F. Zhao, *J Environ Manage* **2017**, *203*, 255.

[229] Y.-S. Zimmermann, C. Niewersch, M. Lenz, Z. Z. Kül, P. F.-X. Corvini, A. Schäffer, T. Wintgens, *Environ Sci Technol* **2014**, *48*, 13412.

[230] A. Agrawal, K. K. Sahu, *J Hazard Mater* **2009**, *171*, 61.

[231] M. Regel-Rosocka, *J Hazard Mater* **2010**, *177*, 57.

[232] D. Menne, J. Kamp, J. Erik Wong, M. Wessling, *J. Membr. Sci.* **2016**, *499*, 396.

[233] J. de Grooth, R. Oborný, J. Potreck, K. Nijmeijer, W. M. de Vos, *J. Membr. Sci.* **2015**, *475*, 311.

[234] J. de Grooth, B. Haakmeester, C. Wever, J. Potreck, W. M. de Vos, K. Nijmeijer, *J. Membr. Sci.* **2015**, *489*, 153.

[235] L. Paltrinieri, K. Remmen, B. Müller, L. Chu, J. Köser, T. Wintgens, M. Wessling, L. C. de Smet, E. J. Sudhölter, *J. Membr. Sci.* **2019**, *587*, 117162.

[236] K. Remmen, B. Müller, J. Köser, M. Wessling, T. Wintgens, *J. Membr. Sci.* **2019**, *582*, 254.

[237] R. Nehmé, C. Perrin, H. Cottet, M.-D. Blanchin, H. Fabre, *J Chromatogr A* **2011**, *1218*, 3537.

[238]   J. B. Schlenoff, H. Ly, M. Li, *J Am Chem Soc* **1998**, *120*, 7626.

[239]   M. Adusumilli, M. L. Bruening, *Langmuir* **2009**, *25*, 7478.

[240]   W. Cheng, C. Liu, T. Tong, R. Epsztein, M. Sun, R. Verduzco, J. Ma, M. Elimelech, *J. Membr. Sci.* **2018**, *559*, 98.

[241]   G. Bargeman, J. B. Westerink, O. Guerra Miguez, M. Wessling, *Sep. Purif. Technol.* **2014**, *134*, 46.

[242]   C. Liu, L. Shi, R. Wang, *Reactive and Functional Polymers* **2015**, *86*, 154.

[243]   A. A. Antipov, G. B. Sukhorukov, H. Möhwald, *Langmuir* **2003**, *19*, 2444.

[244]   L. Ouyang, R. Malaisamy, M. L. Bruening, *J. Membr. Sci.* **2008**, *310*, 76.

[245]   C. Porcel, P. Lavalle, G. Decher, B. Senger, J.-C. Voegel, P. Schaaf, *Langmuir* **2007**, *23*, 1898.

[246]   D. Menne, C. Üzüm, A. Koppelmann, J. E. Wong, C. van Foeken, F. Borre, L. Dähne, T. Laakso, A. Pihlajamäki, M. Wessling, *J. Membr. Sci.* **2016**, *520*, 924.

[247]   A. R. Guastalli, J. Labanda, J. Llorens, *Desalination* **2009**, *243*, 218.

[248]   M. Ghasemi Torkabad, A. R. Keshtkar, S. J. Safdari, *Progress in Nuclear Energy* **2017**, *94*, 93.

[249]   M. Ghasemi Torkabad, A. R. Keshtkar, S. J. Safdari, *Hydrometallurgy* **2018**, *178*, 106.

[250]   R. Epsztein, E. Shaulsky, N. Dizge, D. M. Warsinger, M. Elimelech, *Environ Sci Technol* **2018**, *52*, 4108.

[251]   B. Tansel, *Sep. Purif. Technol.* **2012**, *86*, 119.

[252]   B. Tansel, J. Sager, T. Rector, J. Garland, R. F. Strayer, L. Levine, M. Roberts, M. Hummerick, J. Bauer, *Sep. Purif. Technol.* **2006**, *51*, 40.

[253]   K. M. Forsberg, Å. C. Rasmuson, *Miner. Eng.* **2007**, *20*, 950.

[254]   A. G. Boricha, Z. Murthy, *Sep. Purif. Technol.* **2009**, *65*, 282.

[255]   C. Blöcher, C. Niewersch, T. Melin, *Water Res* **2012**, *46*, 2009.

[256]   K. Remmen, R. Schäfer, S. Hedwig, T. Wintgens, M. Wessling, M. Lenz, *Environ. Sci.: Water Res. Technol.* **2019**, *5*, 1683.

[257]   J. Gambogi, *USGS Minerals Information: Titanium and titanium dioxide*, **2021**.

[258]   W. Zhang, Z. Zhu, C. Y. Cheng, *Hydrometallurgy* **2011**, *108*, 177.

[259]   A. D. Salman, T. Juzsakova, S. Mohsen, T. A. Abdullah, P.-C. Le, V. Sebestyen, B. Sluser, I. Cretescu, *Materials* **2022**, *15*, 2376.

[260]   J. Zhou, S. Ma, Y. Chen, S. Ning, Y. Wei, T. Fujita, *Hydrometallurgy* **2021**, *204*, 105724.

[261]   J. Zhou, Q. Yu, Y. Huang, J. Meng, Y. Chen, S. Ning, X. Wang, Y. Wei, X. Yin, J. Liang, *Hydrometallurgy* **2020**, *195*, 105398.

[262]   A. L. Smirnov, S. M. Titova, V. N. Rychkov, G. M. Bunkov, V. S. Semenishchev, E. V. Kirillov, N. N. Poponin, I. A. Svirsky, *J. Radioanal. Nucl. Chem.* **2017**, *312*, 277.

[263]   B. Yagmurlu, G. Alkan, B. Xakalashe, C. Schier, L. Gronen, I. Koiwa, C. Dittrich, B. Friedrich, *Sci. Rep.* **2019**, *9*, 11803.

[264]   B. Yagmurlu, C. Dittrich, B. Friedrich, *J. Sustain. Metall.* **2017**, *3*, 90.

[265] European Commission, *Reference Document on Best Available Techniques for the Manufacture of Large Volume Inorganic Chemicals - Solids and Others industry*, **2007**, Seville, Spain.

[266] E. R. Rene, *Sustainable Heavy Metal Remediation. Volume 1: Principles and Processes Environmental Chemistry for a Sustainable World Ser, v.8*, **2017**, Springer International Publishing, Cham, can be found under

https://ebookcentral.proquest.com/lib/kxp/detail.action?docID=4924231, pp. 101–120.

[267] A. C. García, M. Latifi, A. Amini, J. Chaouki, *Metals* **2020**, *10*, 1524.

[268] M. Svandova, P. Raschman, G. Sucik, A. Dorakova, A. Fedorockova **2015**, *21*, 247.

[269] J. F. Blais, Z. Djedidi, R. B. Cheikh, R. D. Tyagi, G. Mercier, *Pract. Period. Hazard. Toxic Radioact. Waste Manage.* **2008**, *12*, 135.

[270] B. Yagmurlu, C. Dittrich, B. Friedrich, *Metals* **2018**, *8*, 314.

[271] Y. A. Hussain, M. H. Al-Saleh, S. S. Ar-Ratrout, *Desalination* **2013**, *328*, 17.

[272] Wanner Engineering, Inc., *G03 Series Datasheet*, **2021**.

[273] Y. Mdemagh, A. Hafiane, E. Ferjani, *4open* **2018**, *1*, 5.

[274] Q. Lei, D. He, K. Zhou, X. Zhang, C. Peng, W. Chen, *J. Rare Earths* **2021**, *39*, 1126.

[275] N. T. Hung, B. Le Thuan, T. C. Thanh, M. Watanabe, D. van Khoai, N. T. Thuy, H. Nhuan, P. Q. Minh, T. H. Mai, N. van Tung et al., *Hydrometallurgy* **2020**, *198*, 105506.

[276] B. Gupta, A. Deep, P. Malik, S. N. Tandon, *Solvent Extraction and Ion Exchange* **2002**, *20*, 81.

[277] E. V. Yurtov, N. M. Murashova, *Theor Found Chem Eng* **2007**, *41*, 737.

[278] B. Yagmurlu, C. Dittrich, B. Friedrich, *Innovative scandium refining processes from secondary raw materials.*, **2018**.

[279] B. Yagmurlu, C. Dittrich, P. Davris, E. Balomenos, A. Pilichou, D. Panias, B. Friedrich, *Recovery of scandium from bauxite residue via solvent extraction.*, Online, **2020**.

[280] D. Wang, Y. Li, J. Wu, G. Xu, *Solvent Extraction and Ion Exchange* **1996**, *14*, 585.

[281] M. Sun, S. Liu, Y. Zhang, M. Liu, X. Yi, J. Hu, *Journal of Molecular Liquids* **2019**, *280*, 252.

[282] K. Li, Q. Fan, H. Chuai, H. Liu, S. Zhang, X. Ma, *Trans. Tianjin Univ.* **2021**, *27*, 202.

[283] S. Hedwig, B. Yagmurlu, D. Huang, O. von Arx, C. Dittrich, E. C. Constable, B. Friedrich, M. Lenz, *ACS Sustainable Chem. Eng.* **2022**, *10*, 6063.

[284] R. C. Vickery, *J. Chem. Soc.* **1955**, 245.

[285] A. M. Martinez, K. S. Osen, H. Gudbrandsen, C. Sommerseth, Z. Wang, O. Darell in *The minerals, metals & materials series* (Ed.: O. Martin), Springer International Publishing, Cham, **2018**, pp. 1559–1564.

[286] B. P. Kulikov, V. N. Baranov, A. I. Bezrukikh, V. B. Deev, M. M. Motkov, *Metallurgist* **2018**, *61*, 1115.

[287] M. Harata, T. Nakamura, H. Yakushiji, T. H. Okabe, *Mineral Processing and Extractive Metallurgy* **2008**, *117*, 95.

[288] E. M. Peters, Ş. Kaya, C. Dittrich, K. Forsberg, *J. Sustain. Metall.* **2019**, *5*, 48.

[289] E. M. Peters, C. Dittrich, B. Yagmurlu, K. Forsberg in *The minerals, metals & materials series* (Eds.: G. Azimi, K. Forsberg, T. Ouchi, H. Kim, S. Alam, A. A. Baba), Springer International Publishing, Cham, **2020**, pp. 177–189.

[290] E. M. Peters, M. Svärd, K. Forsberg, *Sep. Purif. Technol.* **2020**, *252*, 117449.

[291] E. M. Peters, M. Svärd, K. Forsberg, *CrystEngComm* **2022**, *24*, 2851.

[292] K. J. Howe, A. Marwah, K.-P. Chiu, S. S. Adham, *Water Res* **2007**, *41*, 3842.

[293] H. Gasper (Ed.) *Handbuch der industriellen Fest/Flüssig-Filtration*, Wiley-VCH, Weinheim, **2000**.

[294] Eaton Corporation, *Filtration + Separation* **2020**, *57*, 20.

[295] K. Meschke, V. Herdegen, T. Aubel, E. Janneck, J.-U. Repke, *Journal of Environmental Chemical Engineering* **2015**, *3*, 2848.

[296] J. Chamberland, D. Mercier-Bouchard, I. Dussault-Chouinard, S. Benoit, A. Doyen, M. Britten, Y. Pouliot, *Foods* **2019**, *8*.

[297] G. N. Vatai, D. M. Krstic, A. K. Koris, I. L. Gáspár, M. N. Tekic, *Desalination and Water Treatment* **2009**, *3*, 162.

[298] W. A. Crocker, *Journal of the Water Pollution Control Federation* **1982**, *54*, 1417.

[299] J. C. Crittenden, R. Rhodes Trussell, D. W. Hand, K. J. Howe, G. Tchobanoglous, *MWH\2019s Water treatment. Principles and design*, John Wiley and Sons, Hoboken, N.J., **2012**.

[300] P. G. Allen, J. J. Bucher, D. K. Shuh, N. M. Edelstein, T. Reich, *Inorg Chem* **1997**, *36*, 4676.

[301] J. Lavania, N. K. Rastogi, M. Balaraman, S. Rangaswamy, *ACS Omega* **2021**, *6*, 27052.

[302] Y. Zhang, Y. Wan, Y. Li, G. Pan, H. Yu, W. Du, H. Shi, C. Wu, Y. Liu, *J. Membr. Sci.* **2021**, *635*, 119472.

[303] G. Bargeman, *Sep. Purif. Technol.* **2021**, *279*, 119725.

[304] M. Perry, V. Ginzburg, B. Ginzburg, P. Lapido, EP2387445 (A2), **2010**.

[305] K. P. Lee, J. Zheng, G. Bargeman, A. J. Kemperman, N. E. Benes, *J. Membr. Sci.* **2015**, *478*, 75.

[306] Y. Roy, M. H. Sharqawy, J. H. Lienhard, *J. Membr. Sci.* **2015**, *493*, 360.

[307] Y. Okamoto, J. H. Lienhard, *Desalination* **2019**, *470*, 114064.

[308] AMS Technologies Ltd., *Datasheet AMS NanoPro A-3014*, **2022**.

[309] Wanner Engineering, Inc., *G35 Series Datasheet*, **2021**.

[310] W. Wilson, A. Gruendisch, I. Calder-Potts, *Desalination* **1987**, *65*, 231.

[311] V. G. Gude, *Desalination and Water Treatment* **2011**, *36*, 239.

[312] H. S. Demirel, M. Svärd, D. Uysal, Ö. M. Doğan, B. Z. Uysal, K. Forsberg, *Sep. Purif. Technol.* **2022**, *286*, 120473.

[313] Y. Chen, S. Ning, Y. Zhong, Z. Li, J. Wang, L. Chen, X. Yin, T. Fujita, Y. Wei, *Sep. Purif. Technol.* **2023**, *305*, 122499.

[314] E. M. Peters, Ş. Kaya, M. Svärd, K. Forsberg, *Recovery of alcohol after anti-solvent precipitation of (NH₄)₃ScF₆ from NH₄F strip liquors*, Cape Town, South Africa, **2021**.

[315] S. J. Lindsay, *Light Metals 2011*, Springer International Publishing, Cham, **2016**.

[316] A. Profaiser, W. Saw, G. J. Nathan, P. Ingenhoven, *Processes* **2022**, *10*, 1070.

[317] M. Krähenbühl, B. Etter, K. M. Udert, *Sci Total Environ* **2016**, *542*, 1155.

[318] N. Kapil, K. G. Bhattacharyya, *Appl Water Sci* **2017**, *7*, 2209.

[319] P. Fröhlich, T. Lorenz, G. Martin, B. Brett, M. Bertau, *Angew. Chem. Int. Ed.* **2017**, *56*, 2544.

[320] K. Binnemans, P. T. Jones, T. Müller, L. Yurramendi, *J. Sustain. Metall.* **2018**, *4*, 126.

[321] Shanghai Metals Market, "Scandium metal, USD/kg", can be found under https://www.metal.com/Rare-Earth-Metals/202104090004, **2022**.

[322] J. P. Sykes, J. P. Wright, A. Trench, P. Miller, *Appl. Earth Sci.* **2016**, *125*, 21.

[323] U.S. Geological Survey, *Mineral commodity summaries 2020*, Reston, VA, **2020**.

[324] J. Vind, A. Malfliet, C. Bonomi, P. Paiste, I. E. Sajó, B. Blanpain, A. H. Tkaczyk, V. Vassiliadou, D. Panias, *Miner. Eng.* **2018**, *123*, 35.

[325] M. Hoffmann, E. Vaszita, É. Ujaczki, l. Fekete-Kertész, M. Molnár, V. Feigl, C. Adam, *SCALE Deliverable D6.1 European inventory of Scandium containing by-products*, **2019**.

[326] C. J. Hartley, W. W. Hazen, D. R. Baughman, C. M. A. Bemelmans, P. F. Belits, T. J. Lanyk, B. F. Porter, L. Liao, J. Mcallister, M. S. Y. Yang, US2014193317 (A1), **2014**.

[327] R. J. Feuling, US5049363 (A), **1989**.

[328] J. Antony, *Design of Experiments for Engineers and Scientists*, Elsevier, Amsterdam, **2014**.

[329] A. Dean, D. Voss, D. Draguljić, *Design and analysis of experiments*, Springer, New York, **2017**.

[330] A. C. Atkinson, B. Bogacka, A. Zhigljavski (Eds.) *Nonconvex optimization and its applications*, *Vol. 51*, Kluwer Acad. Publ, Dordrecht, **2001**.

[331] D. Avdibegović, W. Zhang, J. Xu, M. Regadío, R. Koivula, K. Binnemans, *Sep. Purif. Technol.* **2019**, *215*, 81.

[332] M. I. G. S. Almeida, R. W. Cattrall, S. D. Kolev, *Anal. Chim. Acta* **2017**, *987*, 1.

[333] A. Ditze, K. Kongolo, *Hydrometallurgy* **1997**, *44*, 179.

[334] M. Ochsenkühn-Petropulu, T. Lyberopulu, G. Parissakis, *Anal. Chim. Acta* **1995**, *315*, 231.

[335] L. Pei, L. Wang, G. Yu, *J. Rare Earths* **2011**, *29*, 7.

[336] S. A. Wood, I. M. Samson, *Ore Geol. Rev.* **2006**, *28*, 57.

[337] S. Khorfan, J. Stas, M. Kassem, *J. Radioanal. Nucl. Chem.* **1998**, *238*, 145.

[338] E. A. Nagul, C. F. Croft, R. W. Cattrall, S. D. Kolev, *J. Membr. Sci.* **2019**, *588*, 117208.

[339] S. Das, S. S. Behera, B. M. Murmu, R. K. Mohapatra, D. Mandal, R. Samantray, P. K. Parhi, G. Senanayake, *Sep. Purif. Technol.* **2018**, *202*, 248.

[340] B. Gajda, M. B. Bogacki, *Physicochem. Probl. Miner. Process.* **2007**, *41*, 145.

[341] J. S. Herring in *Encyclopedia of Sustainability Science and Technology* (Ed.: R. A. Meyers), Springer New York, New York, NY, **2012**, pp. 11201–11219.

[342] M. Bartkowska, M. Regel-Rosocka, J. Szymanowski, *Physicochem. Probl. Miner. Process.* **2002**, *36*, 217.

[343]   H. Bordbar, H. Abedini, A. A. Yousefi, *Trans. Nonferrous Met. Soc. China* **2018**, *28*, 2114.

[344]   L.-K. Gao, B. Rao, H.-X. Dai, Z. Hong, H.-Y. Xie, *J. Chem. Eng. Japan / JCEJ* **2019**, *52*, 822.

[345]   A. A. Shaltout, R. Seoudi, E. A. El-Ashkar, K. A. Eid, *Analytical Letters* **2008**, *41*, 3034.

[346]   E. Vahidi, F. Zhao in *REWAS 2016* (Eds.: R. E. Kirchain, B. Blanpain, C. Meskers, E. Olivetti, D. Apelian, J. Howarter, A. Kvithyld, B. Mishra, N. R. Neelameggham, J. Spangenberger), Springer International Publishing, Cham, **2016**, pp. 113–120.

[347]   S. Hedwig, M. Kraus, M. Amrein, J. Stiehm, E. C. Constable, M. Lenz, *Hydrometallurgy* **2022**, *213*, 105916.

[348]   S. Hedwig, B. Yagmurlu, E. M. Peters, V. Misev, D. Hengevoss, C. Dittrich, K. Forsberg, E. C. Constable, M. Lenz, *ACS Sustainable Chem. Eng.* **2023**, *11*, 5883.

[349]   S. Kertész, Z. László, Z. Horváth, C. Hodúr, *Desalination* **2008**, *221*, 303.

[350]   N. K. Batchu, T. Vander Hoogerstraete, D. Banerjee, K. Binnemans, *RSC Adv.* **2017**, *7*, 45351.

[351]   R. G. Pearson, *J Am Chem Soc* **1985**, *107*, 6801.

[352]   P. W. Atkins, M. E. Hagerman, D. F. Shriver, *Inorganic chemistry*, Oxford Univ. Press, Oxford, **2010**.

[353]   S. Flude, M. Haschke, M. Storey, *Mineral Mag* **2017**, *81*, 923.

[354]   C. I. Sainz-Diaz, H. Klocker, R. Marr, H.-J. Bart, *Hydrometallurgy* **1996**, *42*, 1.

[355]   M. Hesse, H. Meier, B. Zeeh, *Spektroskopische Methoden in der organischen Chemie*, Thieme, Stuttgart, New York, **2005**.

[356]   J. Kamcev, B. D. Freeman in *Encyclopedia of Polymeric Nanomaterials* (Eds.: S. Kobayashi, K. Müllen), Springer Berlin Heidelberg; Springer, Berlin, Heidelberg, **2019**, pp. 1–9.

[357]   K. Remmen, RWTH Aachen University, **2020**.

[358]   C. Gao, S. Leporatti, S. Moya, E. Donath, H. Möhwald, *Chemistry* **2003**, *9*, 915.

[359]   V. B. Møller, K. Dam-Johansen, S. M. Frankær, S. Kiil, *J Coat Technol Res* **2017**, *14*, 279.

[360]   D. M. Davenport, A. Deshmukh, J. R. Werber, M. Elimelech, *Environ. Sci. Technol. Lett.* **2018**, *5*, 467.

[361]   E. C. Constable (Ed.) *Transitioning to sustainability series*, *volume 7*, MDPI, Basel, **2022**.

[362]   T. Iwama, C. Du, S. Koizumi, X. Gao, S. Ueda, S. Kitamura, *ISIJ Int.* **2020**, *60*, 400.

[363]   W. Yu, Di Song, W. Chen, H. Yang, *Water Res* **2020**, *183*, 115985.

[364]   European Commission, *HORIZON 2020 – work programme 2016-2017, General Annexes. G. Technology readiness levels (TRL)*, Luxembourg, **2014**.

[365]   Y. Kalmykova, M. Sadagopan, L. Rosado, *Resources, Conservation and Recycling* **2018**, *135*, 190.

[366]   R. Kümmel, *Entropy* **2016**, *18*, 75.

[367]   J. Martinez-Alier, *Local Environment* **2022**, *27*, 1182.

[368]   C. Qiu, S. Qi, C. Y. Tang, *J. Membr. Sci.* **2011**, *381*, 74.

[369]   Y. Li, S. Wang, G. He, H. Wu, F. Pan, Z. Jiang, *Chem Soc Rev* **2015**, *44*, 103.

This page is intentionally left blank.

9 Annex

9.1 Supporting information for Chapter 2

9.1.1 Elemental analysis

The concentrations of Fe and Mg were analysed in triplicate using Inductively Coupled Plasma Optical Emission Spectroscopy (ICP-OES) (Spectroblue SOP, Spectro Analytical Instruments, Kleve, Germany) using standard conditions (power of 1,400 W, coolant flow: 13 L min^{-1}, auxiliary flow: 1 L min^{-1}, nebulizer flow: 0.75 L min^{-1}). All other elements were measured using triple quadrupole Inductively Coupled Plasma Mass Spectrometry (qqq-ICP-MS) on an Agilent 8800 series machine (Agilent, Basel, Switzerland) using general-purpose operational settings. Quantification was performed via multi-element standards (Sigma- Aldrich). Rh was used as internal standard to account for matrix effects. Chloride concentrations were analysed using ion chromatography (IC). The IC consisted of a Dionex 2100 system, equipped with an online eluent generator, a self-regenerating suppressor, a guard and analytical column (AG17-C and AS17-C, 2 mm) (all Dionex, Olten, Switzerland). Chloride was separated from other ions using a hydroxide gradient and quantified by conductivity detection.

Table S9.1 Elemental concentration in the acid waste solution

Element	Concentration [mg L^{-1}]	Removal at pH 1.5 precipitation [%]
Sc	76 - 90	~20
Ni	22 - 84	0
U	20 - 23	~40
Th	102 - 133	~75
Ti	3 906 - 4 228	100
Na	447 - 1 182	-
Al	6 124 - 7 722	0
Ca	667 - 839	-
Fe	39 374 - 45 160	0
K	401 - 631	-
Cl	153 150 - 180 000	-

Table S9.2 Elemental concentration in the retentate after pH adjustment, dilution and filtration (60% permeate recovery).

Element	Concentration [mg L^{-1}]
Sc	23
U	5
Th	93
Fe	8 070

9.1.2 Filtration set-up
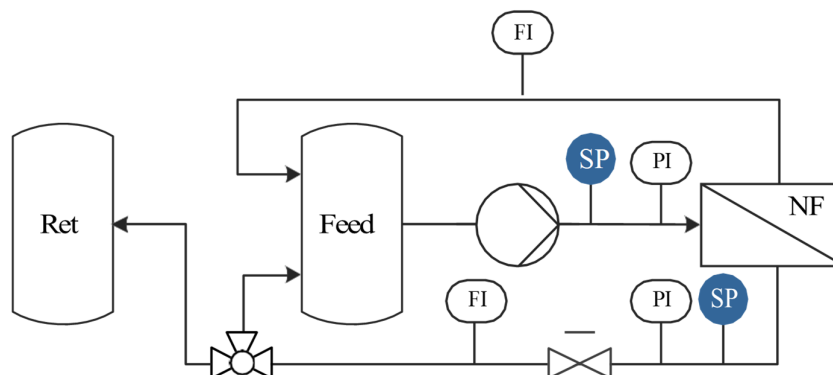
Figure S9.1 Flow chart of the custom-made filtration unit used for the experiments with flowmeters (Fl), pressure meters (Pl) and nanofiltration membrane (NF)

9.1.3 Stability towards higher HCl concentrations

Magnesium retention was used as an indicator of membrane acid stability. For this, 0.5 mM Mg was dissolved in deionized water. Mg retention was determined in cross-flow mode (5 bars of trans-membrane pressure, TMP) using 0.5 mM Mg solution. The flow was 160 mL/min, resulting in a cross-flow velocity of 2.65 m s^{-1} and a Reynolds number > 2,300 (thus a turbulent flow). HCl (32 wt%; Roth, Switzerland) was diluted in deionized water to 1 M, 2 M and 3 M, respectively, and Mg (as Mg_2SO_4 heptahydrate, ≥ 99%, Sigma-Aldrich) added to a final concentration of 0.5 mM.
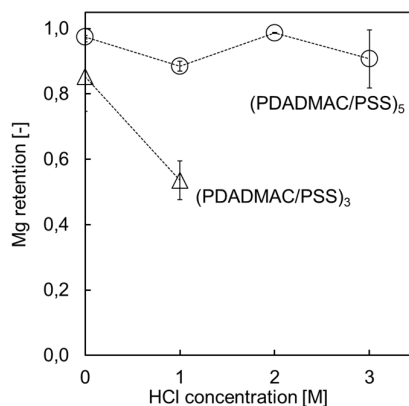
Figure S9.2 Acid stability in terms of Mg retention as a function of HCl concentration using 3 or 5 bi-layers systems. Coating was done at a higher (1 M NaCl) ionic strength.

9.2 Supporting information for Chapter 3

Table S9.3 Description and selected properties of the used NF membranes.

Manufacturer	Membrane	Abbreviation	pH-range [-]	MWCO [-]	Salt retention [-]	Clean water permeability [Lm^{-2}h^{-1}bar^{-1}]
AMS Technologies	NanoPro A-3012	A3012	0-12	200	≥0.96 (MgSO$_4$)	>2
AMS Technologies	NanoPro A-3014	A3014	0-12	400	≥0.92 (MgSO$_4$)	>2
Koch Separation Solutions	SelRO MPF-36	MPF36	1-13	1000	0.1 (NaCl)	>6
Microdyn-Nadir	NP030	NP030	0-14	500	>0.8 (Na$_2$SO$_4$)	>1
GE Osmonics / SUEZ	GE DK	DK	2-10	150-300	0.98 (MgSO$_4$)	>5
GE Osmonics / SUEZ	GE KH	KH	0-10	150-300	0.96 (MgSO$_4$)	2

1. Pressurised N$_2$ bottle (200 bar)
2. Pressure regulator
3. Sterlitech HP4750 filtration cell
4. Magnetic stirrer
5. Permeate collection vessel
6. Balance
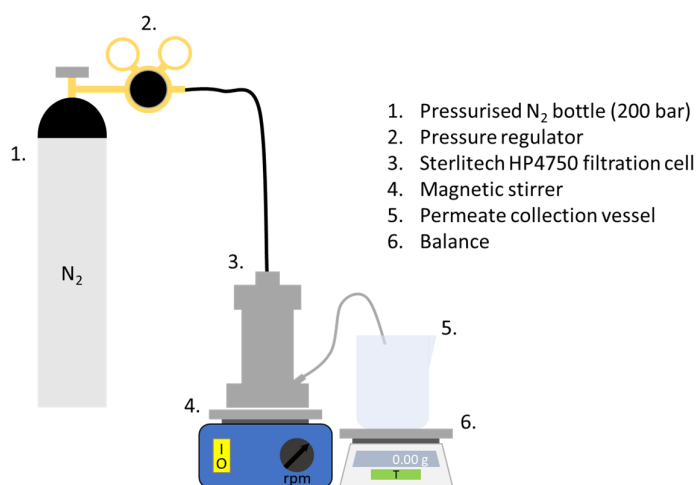
Figure S9.3 Schematic setup used for the dead-end nanofiltration.
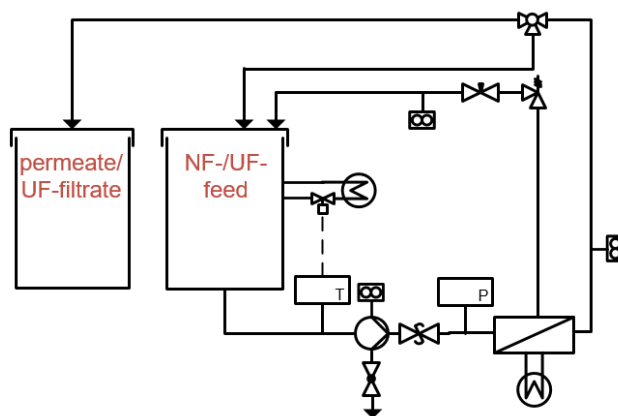
Figure S9.4 P&I diagram of the modular filtration unit (MaxiMem, PS Prozesstechnik, Switzerland).
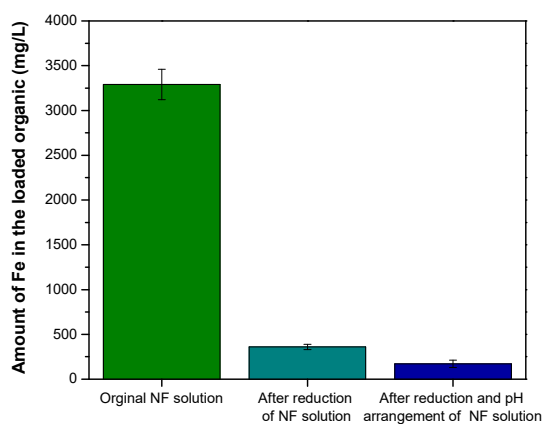
Figure S9.5 Comparison of the loading efficiencies during solvent extraction from NF retentate, reduced NF retentate and reduced and acidified NF retentate

Table S9.4 Comparison of the Sc selectivity of the organic reagents against major impurities (Al, Fe, V and Mn)

D2EHPA	N1923	$\alpha_{Sc/Al}$	$\alpha_{Sc/Fe}$	$\alpha_{Sc/V}$	$\alpha_{Sc/Mn}$
0.1 M	-	2559	839	1502	2671
0.2 M	-	1161	764	272	1542
0.4 M	-	118	431	40	961
0.1 M	0.05 M	1901	1341	3654	13003
0.2 M	0.05 M	1643	1036	1446	10868
0.2 M	0.1 M	1554	997	1193	4289
0.4 M	0.1 M	1455	426	929	1363

Table S9.5 Impurity scrubbing efficiencies of 4, 5 and 6 M HCl from the loaded D2EHPA+N1923 in D80 organic solution.

Scrubbing Solution	Sc (%)	Fe (%)	Ti (%)	Zr (%)	Th (%)	Al (%)
4 M HCl	< 1	89	72	76	20	56
5 M HCl	< 1	78	81	80	20	63
6 M HCl	< 1	77	84	84	15	63

9.3 Supporting information for Chapter 4

9.3.1 Advanced Filtration

9.3.1.1 Calculations

The dimensionless concentration factor (X) was calculated as follows:

$$X = \frac{V_{\text{feed}}}{V_{\text{concentrate}}} \tag{S1}$$

with the feed volume (V_{feed}) and concentrate volume ($V_{\text{concentrate}}$).

The dimensionless retention (R_{M}) of an element (M) in NF was calculated as follows:

$$R_{\text{M}} = 1 - \frac{c_{\text{M,permeate}}}{c_{\text{M,feed}}} \tag{S2}$$

with the concentration of an element in the permeate ($c_{\text{M,permeate}}$) and in the feed ($c_{\text{M,feed}}$).

The permeate flux (J_{permeate}) in L m^{-2} h^{-1} was calculated as follows:

$$J_{\text{permeate}} = \frac{V_{\text{permeate}}}{A_{\text{membrane}} \cdot t} \tag{S3}$$

with the permeate volume (V_{permeate}) in litre, the time in hours (t) and membrane area in m^2 (A_{membrane}).

The specific energy consumption (SEC) in kWh m^{-3} was calculated as follows:

$$\text{SEC} = \frac{W_{\text{electric}}}{V_{\text{product}}} = \frac{P_{\text{electric}} \cdot t}{V_{\text{product}}} \tag{S4}$$

with the electric work W_{electric} in kWh and the product volume (V_{product}) in m^3.

9.3.1.2 Overview pilot plant

A
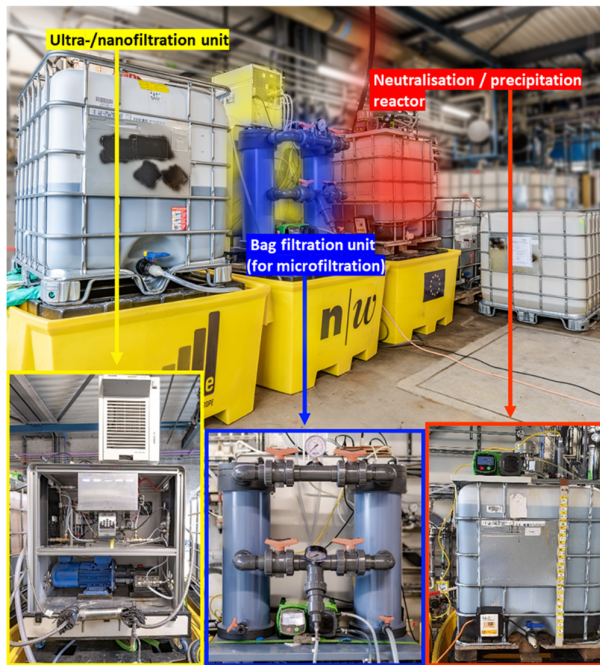
B
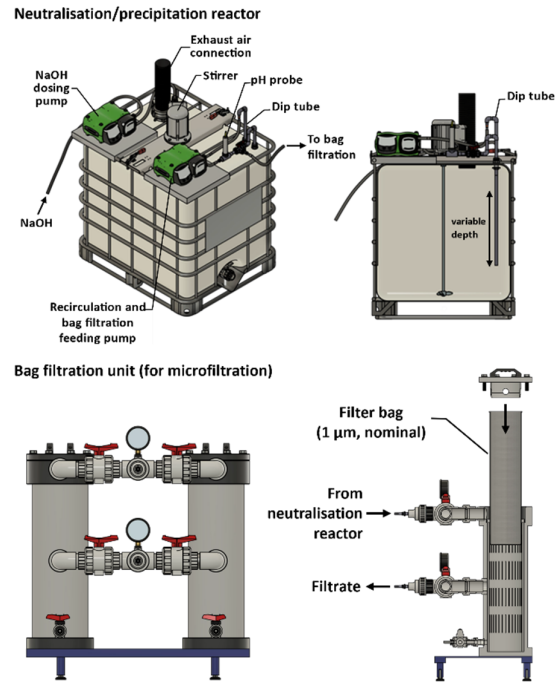
C

Ultra-/nanofiltration unit
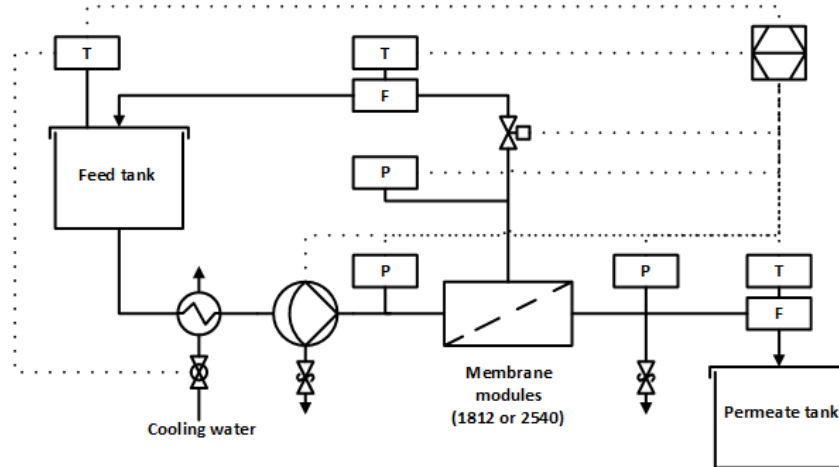
 Figure S9.6 Overview of the advanced filtration pilot unit (A), including computer aided design drawings of the neutralisation reactor and the bag filtration unit (B) and a piping and instrumentation diagram of the ultra- and nanofiltration unit (C).

9.3.2 Solvent extraction

9.3.2.1 Overview pilot plant
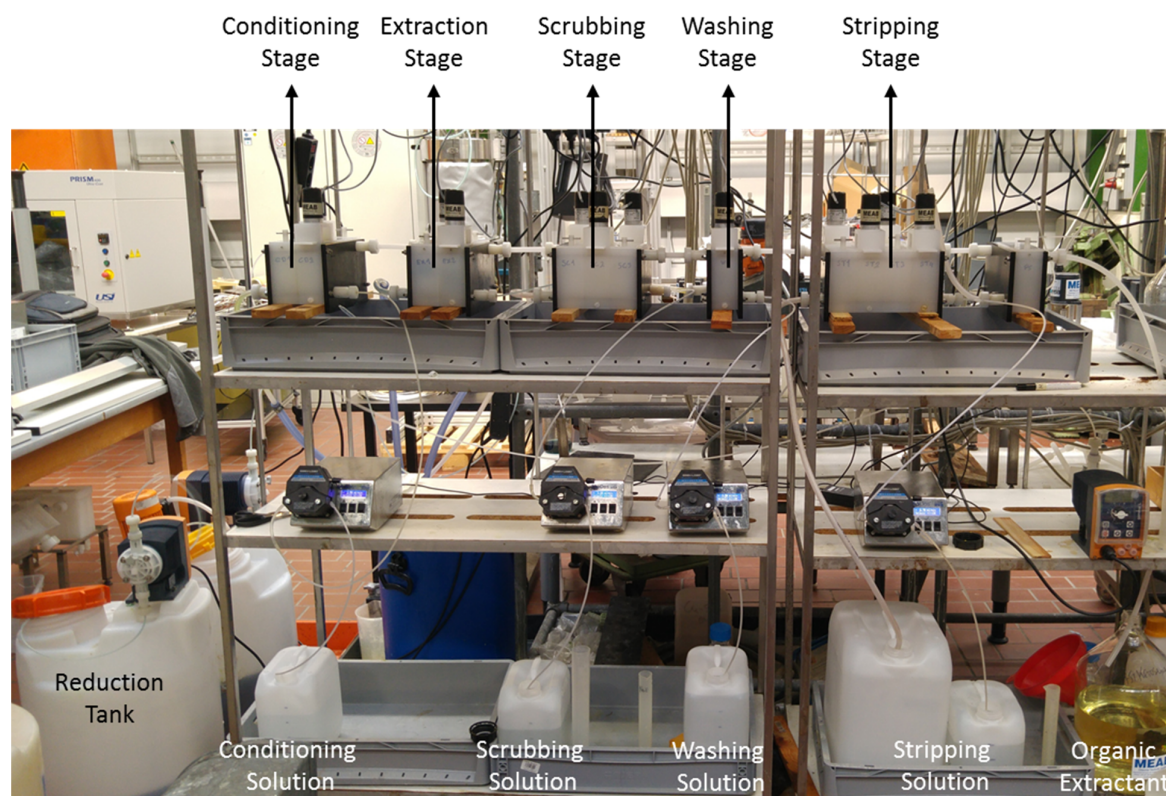
Figure S9.7 Overview of the solvent extraction pilot unit.

9.3.3 Anti-solvent crystallization

Table S9.6 Amounts of metals in the strip liquor (10 L) before and after precipitation. Precipitated amounts were calculated as the difference between 'before ASC' and after ('in solution'). Purities were calculated as the mass fraction of Sc, resp. $(NH_4)_3ScF_6$ in the total amount of metal, resp. $(NH_4)_xM^{y+}F_{(x+y)}$. Values are averages of triplicates with their associated standard deviations.

|		Before ASC	In solution	Precipitated	As $(NH_4)_xM^{y+}F_{(x+y)}$
Sc	**Amount [g]**	13.09	0.5 ± 0.002	12.6 ± 0.16	59.64
	Yield* [-]		0.04 ± 0.01	0.96 ± 0.01	
Ti	**Amount [g]**	0.11	0.11 ± 0.003	0 ± 0.01	0.00
	Yield* [-]		1 ± 0.04	0 ± 0.04	
Fe	**Amount [g]**	0.13	0.11 ± 0.001	0.02 ± 0.01	0.08
	Yield* [-]		0.85 ± 0.02	0.15 ± 0.02	
Zr	**Amount [g]**	0.10	0.02 ± 0.0005	0.08 ± 0.003	0.24
	Yield* [-]		0.2 ± 0.01	0.8 ± 0.01	
Th	**Amount [g]**	0.23	0.02 ± 0.001	0.21 ± 0.006	0.35
	Yield* [-]		0.09 ± 0.01	0.91 ± 0.01	
U	**Amount [g]**	0.23	0.08 ± 0.005	0.15 ± 0.007	0.29
	Yield* [-]		0.36 ± 0.03	0.64 ± 0.03	
V	**Amount [g]**	0.60	0.28 ± 0.003	0.32 ± 0.01	1.37
	Yield* [-]		0.47 ± 0.01	0.53 ± 0.01	
Al	**Amount [g]**	0.47	0.4 ± 0.02	0.1 ± 0.05	0.72
	Yield* [-]		0.8 ± 0.04	0.2 ± 0.04	
Purity (%)		87.5		93.47	95.12

9.3.4   Process flows and production cost assessment

Table S9.7 Energy and material flows to produce 1 kg ScF$_3$ by AF, SX, ASC and CAL. Specific energy and material costs.

Stream	Specific costs	Source
ScF$_3$ (99-99.99%)	721 – 1546 € kg^{-1}	https://www.alibaba.com/product-detail/Rare-earth-99-99-99-Scandi-um_1600274929720.html?spm=a2700.galleryofferlist.normal_offer.d_title.7d1f4b99lzMQrZ&s=p
Ethanol	0.25 – 0.80 € kg^{-1}	alibaba.com
HCl 33%	0.09- 0.12 € kg^{-1}	Industrial partner
NaOH 30%	0.073 –0.08 € kg^{-1}	Industrial partner
NH$_4$F	1.04 € kg^{-1}	lanxess.com, alibaba.com https://www.alibaba.com/product-detail/Professional-export-factory-direct-sales-Ammonium_1600572543550.html
Fe powder	1.91-2.27 € kg^{-1}	https://www.alibaba.com/product-detail/China-Factory-Bulk-High-Pure-Atom-ized_62526820923.html?spm=a2700.galleryofferlist.normal_offer.d_title.75d2561aspiX4N&s=p
Water	0.180 € m^{-3}	Industrial partner
NH$_4$F 3 mol L^{-1}	0.12 € kg^{-1}	
Electricity	0.049– 0.056 € kWh^{-1}	ec.europa.eu/eurostat/databrowser/view/NRG_PC_205__custom_1114276/default/table?lang=en
Heat	0.02 € kWh^{-1}	Industrial partner
CaCO$_3$	0.062 – 0.073 € kg^{-1}	https://www.alibaba.com/product-detail/White-Powder-Caco3-Powder-Calcium-Car-bonate_10000003295317.html?spm=a2700.galleryofferlist.normal_offer.d_image.3fb42725fIcYLj

9.4 Supporting information for Chapter 5

9.4.1 Membrane material cost estimation

Table S9.8 Prices for different compounds (based on the largest quantities offered).

Compound	Price [$ t^{-1}] (lot size)	Source (28.01.2022)
Sc, metal	4'367'330* (1 kg)	https://www.metal.com/Rare-Earth-Metals/202104090004
Sc_2O_3	921'234 (1 kg)	https://www.metal.com/Rare-Earth-Oxides/202104090003
PVDF-HFP	15'000 (estimation based on 1 t PVDF)	https://www.alibaba.com/product-detail/PVDF-powder-Lithium-Battery-coating-adhesive_60792409905.html?spm=a2700.details.0.0.689a3ac3X3lUnr
	570'000 (0.1 kg)	https://www.sigmaaldrich.com/catalog/product/aldrich/427160?lang=en&region=US
NPOE	3'000 (1 kg)	https://www.lookchem.com/product_Benzene-1-nitro-2--octyloxy--/2046562.html
	2'985'500 (0.1 kg)	https://www.manchesterorganics.com/V17568
DEHPA	1'100 (1 t)	https://www.alibaba.com/product-detail/Di-2-ethylhexyl-phosphoric-Acid-d2ehpa_60557475088.html?spm=a2700.galleryofferlist.normal_offer.d_title.5da56389LsA0M9
H_3PO_4 (85 %)	800 (1 t)	https://www.jinhetec.com/phosphoric-acid-food-grade/58419452.html
Kerosene (ρ= 0.8 g cm^3)	660 (1 gal)	https://www.eia.gov/dnav/pet/hist/LeafHandler.ashx?n=PET&s=EMA_EPPK_PWG_NUS_DPG&f=M

*Scandium prices stated are highly variable, see USGS scandium commodity profile (https://pubs.usgs.gov/periodicals/mcs2020/mcs2020-scandium.pdf)

9.4.1.1 Cost per membrane weight

Composition: 50/40/10 %w/w $\equiv$ 0.5 / 0.4 / 0.1 kg PVDF-HFP / DEHPA / NPOE

Calculation:

Position	Cost
PVDF-HFP	0.5 kg × 15 $ kg^{-1} = 7.5 $
DEHPA	0.4 kg × 1.1 $ kg^{-1} = 0.44 $
NPOE	0.1 kg × 3 $ kg^{-1} = 0.3 $
Total	$\equiv$ 8.24 $ kg^{-1}

9.4.1.2 Cost per m^3 of acid waste

Batch size: 0.12 L acid waste

Membrane weight: 0.6 g

Initial Sc concentration acid waste: 42 mg L^{-1}

Description	Calculation
Required membrane material	1000 L × 0.6 g / 0.12 L = 5 kg
Membrane material cost	5 kg × 8.24 $ kg^{-1} = 41.2 $
Maximum Sc recovery benefit	42 mg L^{-1} × 1'000 L × 4'367'330 $ t^{-1} ≈ 183.43 $

9.4.1.3 Equipment

A

B

values in mm

Figure S9.8 Explosion plan and dimensioning of the used diffusion chamber system (A) the extraction / re-extraction thin film holding frame (B). All dimensions are in mm.

9.4.2 Analytics

Table S9.9 Exemplary sensitivity, goodness of fit (R^2), LOD and LOQ of an elemental analysis via ICP-MS.

Element	Sensitivity [cps ppb^{-1}]	R^2 [-]	LOD [ppb]	LOQ [ppb]
Li	9166	1.000	0.022	0.072
Na	350	0.999	16.941	56.470
Al	7126	1.000	1.089	3.630
K	5656	0.996	7.597	25.322
Sc	8459	1.000	0.031	0.104
Ti	667	0.998	0.099	0.331
V	19662	1.000	0.012	0.041
Cr	4349	1.000	0.120	0.400
Mn	1627	1.000	0.075	0.250
Fe	3379	1.000	0.780	2.599
Ni	1220	1.000	0.044	0.146
Zn	447	1.000	0.127	0.422
Y	3647	0.999	0.007	0.022
Zr	11012	1.000	0.090	0.299
Nb	21171	0.999	0.075	0.249
Ba	1061	1.000	0.030	0.101
La	16701	1.000	0.010	0.035
Ce	21789	1.000	0.013	0.043
Pr	20702	0.999	0.005	0.016
Nd	3873	1.000	0.004	0.012
Sm	3331	0.999	0.002	0.005
Eu	13977	1.000	0.006	0.019
Gd	7002	0.999	0.007	0.022
Tb	36335	0.999	0.003	0.011
Dy	8678	0.999	0.008	0.025
Ho	35959	1.000	0.005	0.017
Er	13036	1.000	0.007	0.022
Tm	45916	0.999	0.004	0.012
Yb	10100	0.999	0.007	0.023
Lu	21536	1.000	0.003	0.011
Pb	44776	1.000	0.079	0.262
Th	48253	0.998	0.033	0.110
U	55468	1.000	0.005	0.018

9.4.3 Calculations

9.4.3.1 Kinetics

The kinetics of the metal extraction and re-extraction processes were assumed to be first order. The metal extraction can be described by:

$$\ln\left(\frac{c_t^{\text{feed}}}{c_0^{\text{feed}}}\right) = -k_{\text{ex}} \cdot t \tag{S5}$$

where t is the time in hours, c_t^{feed} is the concentration of a metal ion in the feed solution at time t, while c_0^{feed} is its initial concentration in the feed. k_{ex} is the kinetic rate constant of the extraction into the PIM. The re-extraction can be described through:

$$\ln\left(1-\frac{c_t^{rec}}{c^{PIM}}\right) = -k_{el} \cdot t \tag{S6}$$

where c_t^{rec} is the concentration of a metal ion in the receiving solution, c^{PIM} is its concentration in the membrane (i.e. taken up during the extraction step) and k_{el} is the kinetic rate constant of the elution. Furthermore, the permeability can be calculated as:

$$P = k_{ex} \cdot \frac{V}{A} \tag{S7}$$

with the volume V and the membrane area A. Through the permeability the initial extraction flux (dimension nmol m^{-2} s^{-1}) of a metal (M) can be determined:

$$J_{0,M} = c_0^{feed} \cdot P \tag{S8}$$

9.4.4   Design of experiment models

The DoE models considered three factors (ω(PVDF-HFP), ω(DEHPA), ω(NPOE)) also including the interactions between them and the quadratic terms. Hence, the parametric model equations can be generally expressed according to equation (S9):

$$f(x,y,z)=c_0+c_1\times x+c_2\times y+c_3\times z+c_4\times x\times y+c_5\times x\times z+c_6\times y\times z+c_7\times x^2+c_8\times y^2+c_9\times z^2 \tag{S9}$$

Here, x stands for ω(PVDF-HFP), y for ω(DEHPA) and z for ω(NPOE). Furthermore, $c_0 - c_9$ represent parametric constants, which are estimated based on a least squares fit of the experimental data, considering the mixture restrictions (i.e., that the factors sum up to 100%). Additionally, the used software seeks for better descriptions of the results by means of simple transformations of the response variables. In case of this study such an adjustment was used for Q(Sc) and X(Sc). Therefore follows, with reference to equation (S9):

$$Q_{Sc} = e^{f(x,y,z)} \tag{S10}$$

$$X_{Sc} = \sqrt{\frac{1}{-f(x,y,z)}} \tag{S11}$$

$$J_{0,Sc} = f(x,y,z) \tag{S12}$$

The estimated parameters and the corresponding R^2 values as expressions for the goodness of fits for Q_{Sc}, X_{Sc} and $J_{0,Sc}$ are enlisted in table 3. Please note that the p-values are based upon coded parameters, i.e., standardized to a range of 0 to 1 each, 0 corresponding to the minimum factor value,

1 to the maximum one. This ensures that all factors are weighed equally, considering their respective factor range. P-values within the fitted model are statistically significant if their value is < 0.05.

Table S9.10 Model parameters (c_0-c_9) with corresponding p-values and Pearson R^2 values for Q_{Sc}, X_{Sc} and $J_{0,Sc}$.

Parameter	Associated factor	Q_{Sc}		X_{Sc}		$J_{0,Sc}$	
		value	p-value	value	p-value	value	p-value
c_0	const.	4.467	1.602E-07	-5.7464	0.0003664	110.9796	0.0022
c_1	ω(PVDF-HFP)	-0.0148	6.669E-05	0.1084	0.0003123	-1.3464	0.0016
c_2	ω(DEHPA)	0.0287	7.349E-05	-0.0593	0.0081863	2.2541	0.0032
c_3	ω(NPOE)	0.0076129	0.2543	-0.3911	0.0004294	1.4744	0.2188
c_4	ω(PVDF-HFP) × ω(DEHPA)	0.000648	0.0032387	-0.0001067	0.8639	-0.015	0.5224
c_5	ω(PVDF-HFP) × ω(NPOE)	0.0004175	0.1123	0.0096454	0.0020898	-0.007	0.8633
c_6	ω(DEHPA) × ω(NPOE)	-0.0001938	0.545	0.0105	0.0018944	0.0547	0.3495
c_7	$(\omega$(PVDF-HFP)$)^2$	-0.0001929	0.0005015	-0.0009748	0.0049896	0.0042	0.3753
c_8	$(\omega$(DEHPA)$)^2$	-0.0006582	0.0061023	-0.002236	0.0282	0.0039	0.8841
c_9	$(\omega$(NPOE)$)^2$	-0.0007913	0.2894	-0.0349	0.0005727	-0.0441	0.7252
R^2 [%]		95.3		95.7		90.6	

9.4.5 Transport experiments

Table S9.11 Elemental concentrations and mean mole fractions of measured elements in real acid waste feed and receiving phase for room temperature transport experiments.

Element	c [mmol L^{-1}]	χ_M^{feed} [-]	χ_M^{rec} [-]	$\chi_M^{rec}/\chi_M^{feed}$ [-]
Li	0.26 ± 0.01	(1.5 ±0.1) ×10^{-4}	(0.0 ±0.0) ×10^0	0.0
Na	1190 ± 70	(7.0 ±0.6) ×10^{-1}	(0.0 ±0.0) ×10^0	0.0
Al	100 ± 4	(6.0 ±0.4) ×10^{-2}	(4.2 ±0.7) ×10^{-2}	0.7
K	3.1 ± 0.1	(1.9 ±0.1) ×10^{-3}	(0.0 ±0.0) ×10^0	0.0
Sc	0.94 ± 0.01	(5.6 ±0.3) ×10^{-4}	(3.4 ±0.7) ×10^{-1}	601.8
Ti	0.45 ± 0.01	(2.6 ±0.2) ×10^{-4}	(1.2 ±0.8) ×10^{-3}	4.6
V	19 ± 1	(1.2 ±0.1) ×10^{-2}	(3.5 ±0.4) ×10^{-1}	30.8
Cr	13 ± 1	(7.8 ±0.7) ×10^{-3}	(0.0 ±0.0) ×10^0	0.0
Mn	66 ± 5	(3.9 ±0.4) ×10^{-2}	(0.0 ±0.0) ×10^0	0.0
Fe	290 ± 20	(1.7 ±0.1) ×10^{-1}	(1.9 ±0.4) ×10^{-1}	1.1
Ni	0.82 ± 0.04	(4.9 ±0.4) ×10^{-4}	(0.0 ±0.0) ×10^0	0.0
Zn	0.5 ± 0.01	(3.0 ±0.2) ×10^{-4}	(1.7 ±0.9) ×10^{-2}	58.2
Y	0.298 ± 0.005	(1.8 ±0.1) ×10^{-4}	(3.5 ±0.7) ×10^{-2}	195.4
Zr	0.108 ± 0.001	(6.4 ±0.4) ×10^{-5}	(1.0 ±0.1) ×10^{-3}	14.9
Nb	0.013 ± 0.001	(7.6 ±0.8) ×10^{-6}	(0.0 ±0.0) ×10^0	0.0
Ba	0.73 ± 0.02	(4.4 ±0.3) ×10^{-4}	(0.0 ±0.0) ×10^0	0.0
La	0.302 ± 0.002	(1.8 ±0.1) ×10^{-4}	(0.0 ±0.0) ×10^0	0.0
Ce	0.771 ± 0.006	(4.6 ±0.3) ×10^{-4}	(0.0 ±0.0) ×10^0	0.0
Pr	0.088 ± 0.001	(5.2 ±0.3) ×10^{-5}	(0.0 ±0.0) ×10^0	0.0
Nd	0.312 ± 0.003	(1.9 ±0.1) ×10^{-4}	(0.0 ±0.0) ×10^0	0.0
Sm	0.061 ± 0.002	(3.6 ±0.2) ×10^{-5}	(0.0 ±0.0) ×10^0	0.0
Eu	0.0101 ± 0.0001	(6.0 ±0.3) ×10^{-6}	(0.0 ±0.0) ×10^0	0.0
Gd	0.039 ± 0.001	(2.3 ±0.1) ×10^{-5}	(0.0 ±0.0) ×10^0	0.0
Tb	0.0067 ± 0.0002	(4.0 ±0.2) ×10^{-6}	(0.0 ±0.0) ×10^0	0.0
Dy	0.037 ± 0.001	(2.2 ±0.1) ×10^{-5}	(0.0 ±0.0) ×10^0	0.0
Ho	0.0077 ± 0.0001	(4.6 ±0.3) ×10^{-6}	(0.0 ±0.0) ×10^0	0.0
Er	0.023 ± 0.001	(1.4 ±0.1) ×10^{-6}	(0.0 ±0.0) ×10^0	0.0
Tm	0.004 ± 0.0001	(2.4 ±0.2) ×10^{-6}	(0.0 ±0.0) ×10^0	0.0
Yb	0.0274 ± 0.0003	(1.6 ±0.1) ×10^{-6}	(2.3 ±0.9) ×10^{-3}	138.5
Lu	0.0046 ± 0.0001	(2.7 ±0.2) ×10^{-6}	(0.0 ±0.0) ×10^0	0.0
Pb	0.144 ± 0.003	(8.5 ±0.5) ×10^{-5}	(0.0 ±0.0) ×10^0	0.0
Th	0.063 ± 0.001	(3.7 ±0.2) ×10^{-5}	(2.3 ±0.4) ×10^{-2}	605.5
U	0.00222 ± 0.00002	(1.3 ±0.1) ×10^{-7}	(0.0 ±0.0) ×10^0	0.0

Table S9.12 Mean mole fractions of measured elements in real acid waste feed and receiving phase for 60 °C temperature transport experiments.

| Element	χ_M^{feed} [-]	χ_M^{rec} [-]	$\chi_M^{rec}/\chi_M^{feed}$ [-]
Li	$(1.4 \pm 0.2) \times 10^{-4}$	$(0.0 \pm 0.0) \times 10^{0}$	0.0
Na	$(6.5 \pm 0.8) \times 10^{-1}$	$(0.0 \pm 0.0) \times 10^{0}$	0.0
Al	$(5.9 \pm 0.4) \times 10^{-2}$	$(3.4 \pm 0.3) \times 10^{-2}$	0.6
K	$(1.4 \pm 0.1) \times 10^{-3}$	$(0.0 \pm 0.3) \times 10^{0}$	0.0
Sc	$(5.5 \pm 0.6) \times 10^{-4}$	$(1.8 \pm 0.4) \times 10^{-1}$	335.2
Ti	$(3.8 \pm 0.5) \times 10^{-4}$	$(2.2 \pm 0.1) \times 10^{-2}$	58.5
V	$(1.3 \pm 0.1) \times 10^{-2}$	$(1.8 \pm 0.3) \times 10^{-1}$	13.9
Cr	$(9.2 \pm 0.3) \times 10^{-3}$	$(5 \pm 7) \times 10^{-3}$	0.5
Mn	$(5.0 \pm 0.7) \times 10^{-2}$	$(1.2 \pm 0.7) \times 10^{-2}$	0.2
Fe	$(2.1 \pm 0.3) \times 10^{-1}$	$(5 \pm 1) \times 10^{-1}$	2.4
Ni	$(4.6 \pm 0.5) \times 10^{-4}$	$(2 \pm 2) \times 10^{-3}$	4.6
Zn	$(1.0 \pm 0.2) \times 10^{-4}$	$(0.0 \pm 0.0) \times 10^{0}$	0.0
Y	$(1.7 \pm 0.2) \times 10^{-4}$	$(1.6 \pm 0.3) \times 10^{-2}$	91.7
Zr	$(9.7 \pm 0.1) \times 10^{-5}$	$(8 \pm 2) \times 10^{-3}$	83.8
Nb	$(3.6 \pm 0.4) \times 10^{-5}$	$(2.1 \pm 0.5) \times 10^{-3}$	57.6
Ba	$(4.0 \pm 0.4) \times 10^{-4}$	$(1.8 \pm 0.4) \times 10^{-3}$	4.6
La	$(1.7 \pm 0.2) \times 10^{-4}$	$(1 \pm 2) \times 10^{-4}$	0.7
Ce	$(4.5 \pm 0.5) \times 10^{-4}$	$(2 \pm 1) \times 10^{-3}$	3.7
Pr	$(5.0 \pm 0.5) \times 10^{-5}$	$(4 \pm 1) \times 10^{-4}$	7.6
Nd	$(1.7 \pm 0.2) \times 10^{-4}$	$(1.6 \pm 0.5) \times 10^{-3}$	9.6
Sm	$(3.4 \pm 0.4) \times 10^{-5}$	$(1.1 \pm 0.2) \times 10^{-3}$	32.9
Eu	$(5.6 \pm 0.6) \times 10^{-6}$	$(3.0 \pm 0.2) \times 10^{-4}$	52.6
Gd	$(2.1 \pm 0.2) \times 10^{-5}$	$(1.2 \pm 0.3) \times 10^{-3}$	55.0
Tb	$(3.6 \pm 0.4) \times 10^{-6}$	$(3.3 \pm 0.2) \times 10^{-4}$	91.6
Dy	$(2.0 \pm 0.2) \times 10^{-5}$	$(2.1 \pm 0.1) \times 10^{-3}$	103.4
Ho	$(4.0 \pm 0.4) \times 10^{-6}$	$(4.1 \pm 0.2) \times 10^{-4}$	103.9
Er	$(1.2 \pm 0.2) \times 10^{-5}$	$(1.4 \pm 0.3) \times 10^{-3}$	109.6
Tm	$(2.1 \pm 0.3) \times 10^{-6}$	$(2.6 \pm 0.5) \times 10^{-4}$	128.5
Yb	$(1.4 \pm 0.2) \times 10^{-5}$	$(2.5 \pm 0.4) \times 10^{-3}$	177.7
Lu	$(2.6 \pm 0.3) \times 10^{-6}$	$(3.8 \pm 0.6) \times 10^{-4}$	145.9
Pb	$(7.8 \pm 0.8) \times 10^{-5}$	$(0.0 \pm 0.0) \times 10^{0}$	0.0
Th	$(3.5 \pm 0.5) \times 10^{-5}$	$(1.2 \pm 0.2) \times 10^{-2}$	334.8
U	$(3.1 \pm 0.4) \times 10^{-7}$	$(0.0 \pm 0.0) \times 10^{0}$	0.0

A **B**
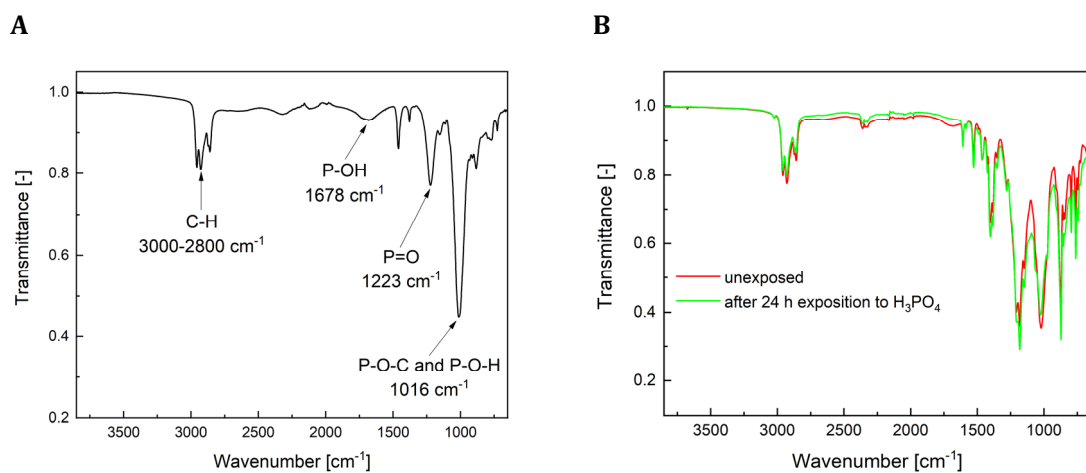
Figure S9.9 FTIR spectra of pure DEHPA (A) and the two superimposed FTIR spectra of an unexposed and a membrane after 24 h exposition to 7M H_3PO_4 in a transport experiment (B).
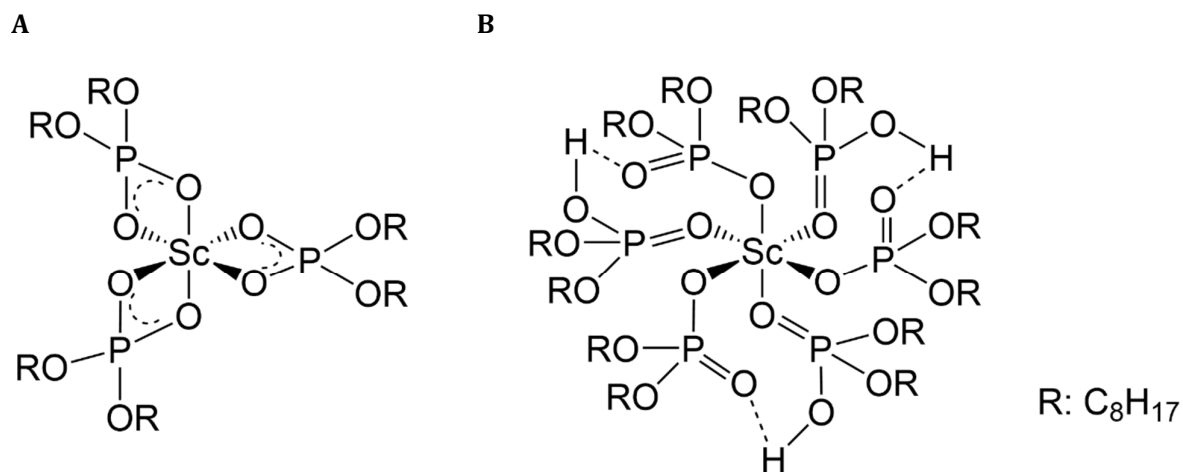
A **B**

Figure S9.10 Proposed complexes of Sc with A) monomer DEHPA and B) dimeric DEHPA.

9.5 Supporting information for Chapter 6

9.5.1 Composition of the acid waste

Table S9.13 Molar concentrations of elements in the TiO$_2$ acid waste used in the previous study[347] compared to the current study.

Element	Acid waste concentration [mmol L^{-1}]		Relative change[1]
	Old	New	
Li	$(2.8 \pm 0.2) \times 10^{-1}$	$(3.4 \pm 0.2) \times 10^{-1}$	+24%
Na	$(1.2 \pm 0.1) \times 10^{3}$	$(1.5 \pm 0.1) \times 10^{3}$	+31%
Mg	$(3.9 \pm 0.3) \times 10^{1}$	$(8.0 \pm 0.2) \times 10^{1}$	+104%
Al	$(8.1 \pm 1.0) \times 10^{1}$	$(1.3 \pm 0.1) \times 10^{2}$	+66%
K	$(2.4 \pm 0.2) \times 10^{0}$	$(3.1 \pm 0.5) \times 10^{0}$	+27%
Ca	$(1.3 \pm 0.2) \times 10^{0}$	$(3.8 \pm 0.4) \times 10^{0}$	+180%
Sc	$(8.3 \pm 0.3) \times 10^{-1}$	$(1.3 \pm 0.1) \times 10^{0}$	+61%
Ti	$(3.4 \pm 0.1) \times 10^{-1}$	$(2.5 \pm 1.1) \times 10^{-2}$	-92%
V	$(1.9 \pm 0.1) \times 10^{1}$	$(3.1 \pm 0.1) \times 10^{1}$	+62%
Cr	$(1.4 \pm 0.1) \times 10^{1}$	$(1.9 \pm 0.1) \times 10^{1}$	+43%
Mn	$(6.7 \pm 0.5) \times 10^{1}$	$(9.3 \pm 0.2) \times 10^{1}$	+41%
Fe	$(2.9 \pm 0.2) \times 10^{2}$	$(4.7 \pm 0.2) \times 10^{2}$	+61%
Ni	$(8.1 \pm 0.4) \times 10^{-1}$	$(1.2 \pm 0.1) \times 10^{0}$	+44%
Zn	$(4.7 \pm 0.3) \times 10^{-1}$	$(4.9 \pm 0.1) \times 10^{-1}$	+3%
Y	$(2.6 \pm 0.1) \times 10^{-1}$	$(3.4 \pm 0.1) \times 10^{-1}$	+33%
Zr	$(6.9 \pm 0.3) \times 10^{-2}$	$(1.4 \pm 0.6) \times 10^{-3}$	-79%
Nb	$(1.3 \pm 0.2) \times 10^{-2}$	$(2.1 \pm 1.1) \times 10^{-3}$	-84%
Ba	$(6.7 \pm 0.3) \times 10^{-1}$	$(1.0 \pm 0.1) \times 10^{0}$	+53%
La	$(2.5 \pm 0.1) \times 10^{-1}$	$(4.0 \pm 0.1) \times 10^{-1}$	+58%
Ce	$(6.5 \pm 0.3) \times 10^{-1}$	$(9.7 \pm 0.3) \times 10^{-1}$	+50%
Pr	$(7.4 \pm 0.3) \times 10^{-2}$	$(1.1 \pm 0.1) \times 10^{-1}$	+53%
Nd	$(2.7 \pm 0.1) \times 10^{-1}$	$(3.9 \pm 0.1) \times 10^{-1}$	+47%
Sm	$(4.9 \pm 0.3) \times 10^{-2}$	$(7.0 \pm 0.2) \times 10^{-2}$	+42%
Eu	$(7.9 \pm 0.5) \times 10^{-3}$	$(9.8 \pm 0.3) \times 10^{-3}$	+23%
Gd	$(3.3 \pm 0.2) \times 10^{-2}$	$(4.7 \pm 0.2) \times 10^{-2}$	+46%
Tb	$(4.9 \pm 0.2) \times 10^{-3}$	$(6.1 \pm 1.1) \times 10^{-3}$	+24%
Dy	$(3.1 \pm 0.2) \times 10^{-2}$	$(4.1 \pm 0.1) \times 10^{-2}$	+33%
Ho	$(5.8 \pm 0.3) \times 10^{-3}$	$(7.8 \pm 0.2) \times 10^{-3}$	+34%
Er	$(1.9 \pm 0.1) \times 10^{-2}$	$(2.5 \pm 0.2) \times 10^{-2}$	+29%
Tm	$(2.9 \pm 0.2) \times 10^{-3}$	$(3.8 \pm 0.1) \times 10^{-3}$	+31%
Yb	$(2.2 \pm 0.1) \times 10^{-2}$	$(3.1 \pm 0.1) \times 10^{-2}$	+40%
Lu	$(3.4 \pm 0.2) \times 10^{-3}$	$(4.6 \pm 0.1) \times 10^{-3}$	+33%
Pb	$(1.3 \pm 0.1) \times 10^{-1}$	$(1.8 \pm 0.1) \times 10^{-1}$	+40%
Th	$(5.0 \pm 0.4) \times 10^{-2}$	$(4.3 \pm 0.2) \times 10^{-2}$	-15%
U	$(4.7 \pm 0.3) \times 10^{-4}$	$(1.7 \pm 0.1) \times 10^{-2}$	+3520%

[1]Relative change = c(new)/c(old) - 1

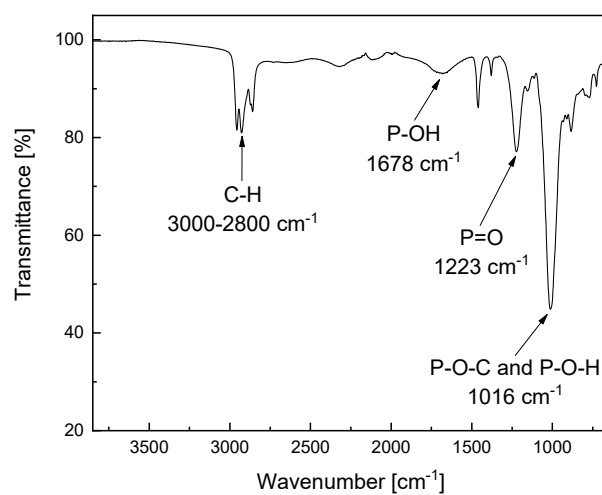### 9.5.2 FTIR-Spectra of reference compounds

Figure S9.11 FTIR spectrum of DEHPA.

This page is intentionally left blank.

List of publications

Research articles

1. K. Remmen†, R. Schäfer†, **S. Hedwig**, T. Wintgens, M. Wessling, and M. Lenz, Layer-by-layer membrane modification allows scandium recovery by nanofiltration, *Environ. Sci.: Water Res. Technol.*, 2019, **5**, 1683-1688; DOI: 10.1039/C9EW00509A

2. **S. Hedwig**†, B. Yagmurlu†, D. Huang, O. Von Arx, C. Dittrich, E. C. Constable, B. Friedrich, and M. Lenz, Nanofiltration-Enhanced Solvent Extraction of Scandium from TiO_2 acid waste, *ACS Sustainable Chem. Eng.*, **2022**, *10* (18), 6063-6071; DOI: 10.1021/acssuschemeng.2c01056

3. **S. Hedwig**, M. Kraus, M. Amrein, J. Stiehm, E.C. Constable, and M. Lenz, Recovery of scandium from acidic waste solutions by means of polymer inclusion membranes, *Hydrometallurgy* **2022**, *213*, 105916; DOI: 10.1016/j.hydromet.2022.105916

4. A. Potysz, A. Pędziwiatr, **S. Hedwig**, and M. Lenz, Rapid metal mobilisation through litter, water and bioweathering as the legacy of historical copper smelting, *J. Geochem. Explor.*, **2019**, *206*, 106364; DOI: 10.1016/j.gexplo.2019.106364

5. A. Potysz, A. Pędziwiatr, **S. Hedwig**, and M. Lenz, Bioleaching and toxicity of metallurgical wastes, *J. Environ. Chem. Eng.*, **2020**, *8*, 104450; DOI: 10.1016/j.jece.2020.104450

6. Y. Liu, **S. Hedwig**, A. Schäffer, M. Lenz, and M. Martinez, Sulfur Amino Acid Status Controls Selenium Methylation in *Pseudomonas tolaasii*: Identification of a Novel Metabolite from Promiscuous Enzyme Reactions, *Appl. Environ. Microbiol.*, **2021**, *87*, e0010421;DOI: 10.1128/AEM.00104-21

7. F. Schmidt†, M. Amrein†, **S. Hedwig**, M. Kober-Czerny, A. Paracchino, V. Holappa, R. Suhonen, A. Schäffer, E. C. Constable, H. J. Snaith, and M. Lenz, Organic solvent free PbI_2 recycling from perovskite solar cells using hot water, *J. Haz. Mat.*, **2023**, *447*, 130829; DOI: 10.1016/j.jhazmat.2023.130829

8. **S. Hedwig**†, B. Yagmurlu†, E. M. Peters, V. Misev, D. Hengevoss, C. Dittrich, K. Forsberg, E. C. Constable, and M. Lenz, From trace to pure: pilot scale scandium recovery from TiO_2 acid waste, *ACS Sustainable Chem. Eng.*, **2023**, *11* (15), 5883-5894; DOI: 10.1021/acssuschemeng.2c06979

9. I. Fekete-Kertész, T. Stirling, E. Vaszita, Z. Berkl, É. Farkas, **S. Hedwig**, K. Remmen, M. Lenz, M. Molnár, and V. Feigl, Ecotoxicity attenuation by acid-resistant nanofiltration in scandium recovery from TiO_2 production waste, *Heliyon*, **2023**, *9* (4), e15512, DOI: 10.1016/j.heliyon.2023.e15512.

†These authors contributed equally

Contribution to conferences

1. **S. Hedwig**, K. Remmen, T. Wintgens, E. C. Constable, and M. Lenz, Resource recovery from TiO$_2$ production acid waste by means of nanofiltration, *ICCE2019: International conference on chemistry and the environment 2019,* Thessaloniki, Greece, 16-20 June, **2019**, oral presentation.

2. **S. Hedwig**, K. Remmen, T. Wintgens, E. C. Constable, and M. Lenz, Selective Scandium recovery from complex wastes by nanofiltration, *Goldschmidt2019*, Barcelona, Spain, 18-23 August, **2019**, oral presentation.

3. **S. Hedwig**, E. C. Constable, and M. Lenz, Membrane based scandium extraction from industrial waste, *Goldschmidt Virtual2020*, online, 21-26 June, **2020**, oral presentation.

4. **S. Hedwig**, K. Remmen, E. C. Constable, and M. Lenz, Towards the first recovery of scandium from waste acid: pilot-scale nanofiltration, *ERES2020: European Rare Earth Resources*, online, 6-9 October, **2020**, oral presentation.

5. **S. Hedwig**, M. Kraus, J. Stiehm, E.C. Constable, and M. Lenz, Polymer inclusion membranes offer selective scandium extraction from white pigment acid waste, *ICOM2020: International conference on membranes & membrane processes 2020*, Online, 7-11 December, **2020**, oral presentation.